Université Fédérale
Toulouse Midi-Pyrénées

THÈSE

En vue de l'obtention du

DOCTORAT DE L'UNIVERSITÉ DE TOULOUSE

Délivré par :

Université Toulouse 3 Paul Sabatier (UT3 Paul Sabatier)

Présentée et soutenue par :
Guanghua JIN

le jeudi 24 septembre 2015

Titre :

Coordination Chemistry and Catalysis at Iron:
From Non-Innocent Ligands to CO_2 Transformation

École doctorale et discipline ou spécialité :
ED SDM : Chimie organométallique de coordination - CO 043

Unité de recherche :
Laboratoire de Chimie de Coordination LCC - CNRS

Directeur/trice(s) de Thèse :

Sébastien Bontemps, Chargé de Recherche CNRS (co-Directeur de thèse)
Sylviane Sabo-Etienne, Directrice de Recherche CNRS (Directrice de thèse)

Jury :
Fabien Delpech, Professeur, LPCNO, Université Paul Sabatier - Toulouse III (Président)
Elsie Alessandra Quadrelli, Directrice de Recherche CNRS, LCOMS, Villeurbanne (Rapportrice)
Ally Aukauloo, Professeur, Université Paris - Sud (Rapporteur)
Parisa Mehrkhodavandi, Professeur, University of British Columbia, Canada
Sébastien Bontemps, LCC - CNRS, Toulouse
Sylviane Sabo-Etienne, LCC - CNRS, Toulouse

Université Fédérale
Toulouse Midi-Pyrénées

THÈSE

En vue de l'obtention du

DOCTORAT DE L'UNIVERSITÉ DE TOULOUSE

Délivré par :

Université Toulouse 3 Paul Sabatier (UT3 Paul Sabatier)

Présentée et soutenue par :
Guanghua JIN

le jeudi 24 septembre 2015

Titre :

Coordination Chemistry and Catalysis at Iron:
From Non-Innocent Ligands to CO_2 Transformation

École doctorale et discipline ou spécialité :
ED SDM : Chimie organométallique de coordination - CO 043

Unité de recherche :
Laboratoire de Chimie de Coordination LCC - CNRS

Directeur/trice(s) de Thèse :

Sébastien Bontemps, Chargé de Recherche CNRS (co-Directeur de thèse)
Sylviane Sabo-Etienne, Directrice de Recherche CNRS (Directrice de thèse)

Jury :
Fabien Delpech, Professeur, LPCNO, Université Paul Sabatier - Toulouse III (Président)
Elsie Alessandra Quadrelli, Directrice de Recherche CNRS, LCOMS, Villeurbanne (Rapportrice)
Ally Aukauloo, Professeur, Université Paris - Sud (Rapporteur)
Parisa Mehrkhodavandi, Professeur, University of British Columbia, Canada
Sébastien Bontemps, LCC - CNRS, Toulouse
Sylviane Sabo-Etienne, LCC - CNRS, Toulouse

Acknowledgement

I would like to thank the jury members Dr. Alessandra Quadrelli and Dr. Ally Aukoloo for accepting to act as Reviewers for my thesis, Prof. Parisa Mehrkhodavandi and Prof. Fabien Delpech for accepting to examine my Ph.D study.

I would like to give my special appreciation to my supervisor Dr. Sylviane Sabo-Etienne, first for accepting me in the team and second for her endless guidance, patience, support and motivation, and additionally for her enthusiastic interest in new results. I also would like to thank for her kindness and mother-like attitude beyond as a supervisor. I really like the Christmas parties organized by her, and the gifts given by her after any long time conference she took part in. I also would like to thank my co-supervisor Dr. Sébastien Bontemps for his guidance and vast knowledge during priceless scientific discussions, support and encouragement during my Ph.D study. I am very happy to have a chance to work with him, because his American style humor always makes the Lab work lively and easy.

I would like to thank Dr. Gilles Alcaraz and Dr. Mary Grellier for their kind help in the lab as well as the help during daily life. I benefited a lot from them, not only the knowledge in chemistry, but also the attitude to work. I also would like to thank Dr. Laure Vendier, Dr. Jean-Claude Daran and Dr. Rémy Brousses for the X-ray data collection; Dr. Yannick Coppel and Dr. Christian Bijani for NMR experiments and for their valuable scientific discussions; Dr. Francis Lacassin and Dr. David Paryl for NMR training; Dr. Alain Moreau for elemental analyses; and all the others who indeed help me to finish my Ph.D smoothly.

My special thanks to my lab-mate Katie Smart, who never stops helping and encouraging me; to my friend Nuria Romero, who is the “lucky girl” of my reactions; to my friends Weili Wang, Jin Wang, Gunnar Werncke and Uta Baddack, Emmanuel Puig and Tugce Ayvali, who always make me feel at home in France and also for their endless encouragement and motivation throughout my Ph.D studies. It would be impossible to finish this challenging road without these valuable people. I appreciate their presence, friendship and amusement.

All current and former Equipe O members, Emmanuelle Mothes-Martin, Chris Wallis, Gaetan Benac-Lestrille, Audrey Cassen, Charly Faradji, Alain Eschlimann, Marion Beguerie, Carlos Pinheiro, Yannick Escudié and Alexandre Mau, together with the visitors we were lucky enough to host throughout the world, Cynthia Cuevas Chavez, Julio Zamora Moreno, Tatsuro Annaka, Vicky Corona, Prof. Alan Goldman and Prof. Christian Limberg for their scientific discussions and also good friendship.

Many thanks also to the colleagues from other groups of LCC, Marlene, Mahmoud, Yohan, Si, Emilie, Kais, Lucas, Quentin, Chen, Yin, Zhong, Mirko, Jérémy, Pascal, Roberto and so on for having amusement and pleasant moments in the last three years.

Thanks to all CNRS employees for their smiling faces every day and endless help.

China Scholarship Council (CSC) and ANR (Programme blanc “IRONHYC” ANR-12) are also acknowledged for financial support.

The last but not the least, my special appreciation and great thankfulness are dedicated to my mum Tingyun, my dad Tieshan, my brother Zhenghua and my girlfriend Yandi for their love, patience, unconditional support and motivation.

Contents

List of abbreviations

Acac	acetylacetone
Ar	aromatic
atm	atmosphere
BPPF	1’1-bis(diphenylphosphino)ferrocene
COD	cyclooctadiene
COT	cyclooctatriene
DBU	1,8-diazabicyclo[5.4.0]-undec-7-ene
dcpe	1,2-bis(cyclohexylphophino)ethane
depe	1,2-bis(diethylphosphino)ethane
DFT	density functional theory
diphos	1,2-bis(phenylphosphino)ethane
dipp	diisopropylphenyl
DMF	dimethylformamide
dmpe	1,2-bis(dimethylphosphino)ethane
dppe	1,2-bis(phenylphosphino)ethane
EA	elemental analysis
Et_2O	diethyl ether
Et	ethyl
EtNCS	isothiocyanate
eq.	equivalent
GPE	glycidylphenylether
HBpin	pinacolborane
HBcat	catecholborane
HS	high spin
HSPhSH	1,2-benzenedithiol
HRMS	High Resolution Mass Spectrometry
^{i}Pr	isopropyl
LiHBEt3	Lithium triethylborohydride
LS	low spin
MAO	methylaluminoxane
Me	methyl
MeCy	methylcyclohexane
MD’M	methyl-bis(trimethylsilyloxy)silicon
MMAO	methylaluminoxane
$(^{n}Bu)_4NI$	alkylammonium iodide
NP	(2-picolyl)diphenylphosphine
NPN	bis(2-picoly)phenylphosphine
NTs	N-tosyl
OTf	trifluoromethanesulfonate
PDI	bis(imino)prydine

Ph	phenyl
PPh_3	triphenylphosphine
$PhBP^{CH2Cy}_3$	tris(methylcyclohexylphosphino)phenylborate
PO	propyloxide
PP_3	tris(2-(diphenylphosphino)phenyl)phosphine
[PPN]Cl	bis(triphenylphosphino)iminium chloride
THF	tetrahydrofuran
TON	turnover number
^{t}Bu	tertiary butyl
TBAB	tetrabutylammonium
TBDMS	tert-butyldimethylsilyl
TIPS	triisopropylsilyl
TMDS	1,1,4,4-tetramethyldisiloxane
TMS	trimethylsilyl
[Tptm]H	tris(2-pyridylthio)methane
Xs	excess
9-BBN	9-borabicyclo[3.3.1]nonane

General introduction

General introduction

Nowadays, the consumption of global energy has increased tremendously because of a growing world population and intensified industrialization. In this context, the development of energy saving and new energy producing processes affords the most important solution to meet the energy needs in the long term, and catalysis is one of the pivotal technologies. However, the dominant catalysts are based on precious metals, such as Ru, Rh, or Pd, for both academic and industrial applications. Concerning price and sustainability of the catalysts, iron thus appears to be a metal of choice because it is inexpensive, abundant and rather non-toxic.

In this context, we focused on iron chemistry with two approaches. On one hand, the field of metal complexes bearing non-innocent ligands has attracted an increasing interest in the coordination chemistry community due to their potential catalytic properties. Substrates can be activated by both the metal center and the ligand allowing catalysis without changing the oxidation state of the metal center. On another hand, the field of CO_2 transformation is also very attractive to benefit from this abundant molecule as a C1 source to replace fossil resources. However, its high thermodynamic stability is a challenge for its functionalization under mild conditions. In the last decade, CO_2 has been transformed into HCOOH, CO, CH_3OH, CH_2O and CH_4. By adding an amine to a mediated-reduction of CO_2, the access to formamides and methylamines has been achieved. These processes pave the way to multicomponent transformations of CO_2 to generate more complex and valuable molecules, but the scope of CO_2 functionalization is still restricted to the formation of C-N bonds. Therefore, the first iron-based catalytic system was investigated for the transformation of CO_2 into a large variety of compounds under mild conditions.

The study “Coordination chemistry and catalysis at iron: from non-innocent ligands to CO_2 transformation” was performed at the “*Laboratoire de Chimie de Coordination du CNRS*” in Toulouse, France, in the team “*Architecture Organométallique et Catalyse*” under the supervision of Sylviane Sabo-Etienne and Sébastien Bontemps. The dissertation is composed of five chapters.

The first chapter is a bibliographic study concerning the chemistry of iron complexes involved in the two domains we selected: the combination of iron with non-innocent ligands leading to highly active catalysts, and the use of iron complexes for CO_2 transformations, involving stoichiometric and catalytic activation of CO_2.

In chapter 2, we have selected phosphine ligands bearing picolyl fragments which could favor a non-innocent behavior. By a careful control of the experimental conditions, a family of mono- and dimeric iron complexes has been isolated and the non-innocent behavior of the ligand has been observed. The combination of several techniques: X-ray diffraction, NMR (in solution and in the solid state), EPR, Mössbauer and infrared spectroscopy allows to characterize both diamagnetic and paramagnetic complexes.

In chapter 3, the iron-catalyzed CO_2 reductive functionalization is presented. A one-pot two-step strategy has been implemented under mild conditions. Our efforts to optimize the first iron-catalyzed CO_2 reduction step to afford selectively a bis(boryl)acetal compound will be detailed. This intermediate has then been used as a reactive and versatile source of methylene in functionalization reactions, leading to a large scope of value-added organic compounds.

In chapter 4, general remarks, conclusions and perspectives of the present work are described.

Chapter 5 is dedicated to the experimental part of this manuscript.

Chapter 1

Chapter 1

Bibliography

1. Introduction

A literature introduction entitled "Coordination chemistry and catalysis at iron: From non-innocent ligands to CO_2 transformation" is provided in this chapter. The interest of choosing iron is presented in section 1.1; the combination of iron with non-innocent ligands, including catalytic applications, are described in section 1.2; the utilization of iron complexes in CO_2 transformation, including stoichiometric and catalytic reactions, are reported in section 1.3.

1.1 Why iron?

The worldwide demand for precious metals such as Ru, Rh, Pd and Pt, is increasing rapidly due to their catalytic properties for academic and industrial applications.[1] However, limited natural reserves and environmental concerns are important parameters that need to be taken into account when exploring metal-catalyzed processes.[2] New strategies need to focus on both enhancing catalytic activities and using earth-abundant metals. Iron is the second abundant metal on earth (4.7 wt%). It is inexpensive (Figure 1[3]) and rather non-toxic by comparison to other metals. Iron thus appears as an ideal metal for molecular catalysis.[4–6]

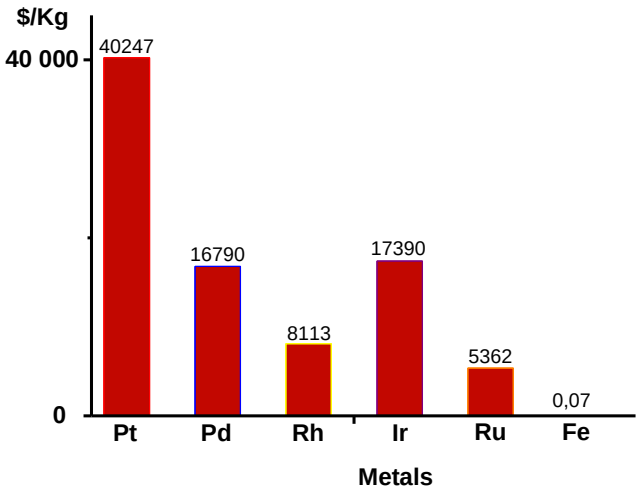

Figure 1. Price of precious metals versus iron, average from 2000 to 2015

In nature, the family of hydrogenases features iron active sites. These enzymes are playing a key role in the reversible oxidation of molecular hydrogen,[7] and are significantly more efficient than the electrochemical production of H_2 catalyzed by precious metal-based catalysts described in the literature.[8] In addition, iron is also present in other natural processes. For example, nitrogenase enzymes, responsible for biological nitrogen fixation, also feature iron active sites.[9,

[10, 11] In the industry, the iron-based Haber-Bosch process is employed to produce ammonia, the main precursor to fertilizers.

Despite the unique advantages of iron, its utilization remains relatively unexplored in the field of catalysis by comparison to other transition metals. Two main features hampering studies on iron-based complexes are the difficulties in controlling the oxidation state of the metal center, and limited in-depth NMR investigation caused by the paramagnetic properties of many complexes. Nonetheless, iron-based complexes in catalysis have been increasingly scrutinized, and very interesting catalytic properties have recently been described.[12–20]

1.2 Iron with non-innocent ligands

Selecting the nature of metal centers is only part of the synthetic strategy for the construction of complexes; careful choice of ligands is also vital for potential applications of the complexes. Normally, the utilization of ligands is thought to only stabilize the active metal centers, and to tune their reactivity by modifying their steric and electronic features. Most of the time, the ligands play a spectator role in catalytic systems. However, the so called “non-innocent ligands” can participate as a cooperative function with the metal centers for homogeneous catalytic applications.[21–28] Iron complexes bearing non-innocent ligands have been emerging in catalytic processes and are drawing more and more attention.[20,29,30]

A general overview of different non-innocent ligands is provided in this chapter as well as a more detailed analysis on the role of non-innocent ligands attached to iron in the field of catalysis.

1.2.1 Non-innocent ligand and non-innocent behavior

In the 1960s, the term “non-innocent” was introduced into chemistry for complexes with unclear oxidation state. When the location of electrons either on the central metal atom or on the ligand is well defined, the corresponding ligand is called innocent ligand, while to the contrary is non-innocent ligand.[31] As shown in Figure 2, the coordination of a non-innocent ligand to a transition metal center is described by the resonance forms **I** ↔ **II** ↔ **III** of various weight. Such non-innocent ligands are able to oxidize or reduce by one or more electrons, and serve as an electron reservoir. In this sense, this type of non-innocent ligand is redefined as “redox non-innocent ligand”.

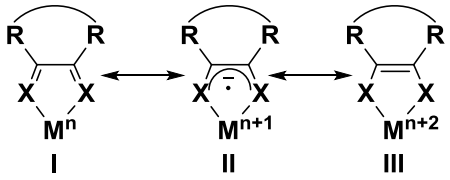

Figure 2. Transition metal complexes containing non-innocent ligands (X = NR, O or S)

Through detailed spectroscopic and theoretical investigations, including but not limited to, X-ray crystallography, magnetic susceptibility measurements, cyclic voltammetry, UV-vis, NMR, EPR, Mössbauer spectroscopy and density functional theoretical (DFT) calculations, it is possible to make an unambiguous assignment of the electronic structure of transition metal complexes containing redox non-innocent ligands.[23,32–35] Different properties and reactivity are also expected for the distinct isomers of M^nL^0 (**I**), $M^{n+1}L^{-1}$ (**II**) and $M^{n+2}L^{-2}$ (**III**) (Figure 2).

"Cooperative non-innocent ligand" is the second type of non-innocent ligands. This type of ligands plays a prominent role together with the metal center for the reactivity of the complexes. They participate directly in the reaction with elementary bond-making and bond-breaking steps and undergo reversible chemical transformations.[21,36] The metal center also holds its intrinsic reactivity, and takes part in the reaction as a binding site to bring substrates together. To be more specific, cooperative non-innocent ligands can be divided into outer-sphere and inner-sphere cooperating functions.

The outer-sphere cooperating bifunctional behavior was investigated by Noyori and co-workers with a diamine ruthenium complex as pre-catalyst for the hydrogenation of simple ketones.[37–39] The ketone substrate binds to the Ru-amino hydride complex **1** in the second coordination sphere via the hydridic Ru-$H^{\delta-}$ and protic N-$H^{\delta+}$ groups, leading to the corresponding alcohol and the Ru-amido complex **3**. The amido ligand in complexes **3** and **4** plays a role in the heterolytic splitting of H_2 to regenerate the Ru-amino hydride complex **1**. In this bifunctional reaction mechanism (Scheme 1), the amino ligand acts as a cooperating ligand, participating directly in the N-H bond activation (making/breaking) reactions to close the catalytic cycle. The ruthenium center supplies a vacant site for the generation of the Ru-σ-H_2 bond and ultimately restoration of the Ru-H bond.

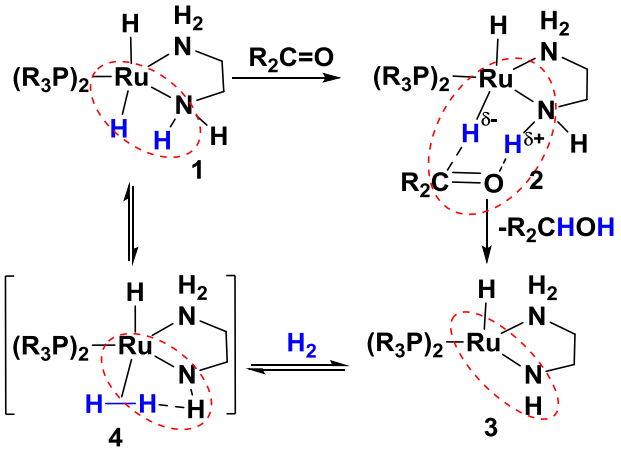

Scheme 1.Outer-sphere cooperative mechanism for the Noyori system

The inner-sphere cooperating function was studied by Milstein and co-workers.[40] The bifunctional behavior is based on aromatization-dearomatization processes on the ligand. An example is displayed in Scheme 2: in the key step, the dearomatized complex **5** activates the water molecule through H-OH bond breaking by cooperation between the metal center and the ligand, forming the aromatized hydroxo complex **6**.[41] Complex **6** can react with another equivalent of water evolving H_2 and forming the dihydroxo complex **7**. Irradiating **7** releases the hydrogen peroxide by reductive elimination and the Ru^0 intermediate **8**. **8** further converts to **5** by intra-migration of a proton from the methylene arm of the phosphorus side to the ruthenium center, in order to generate a hydride ligand together with dearomatization of the pyridine ring. The ligand and the metal cooperate in a synergistic manner.

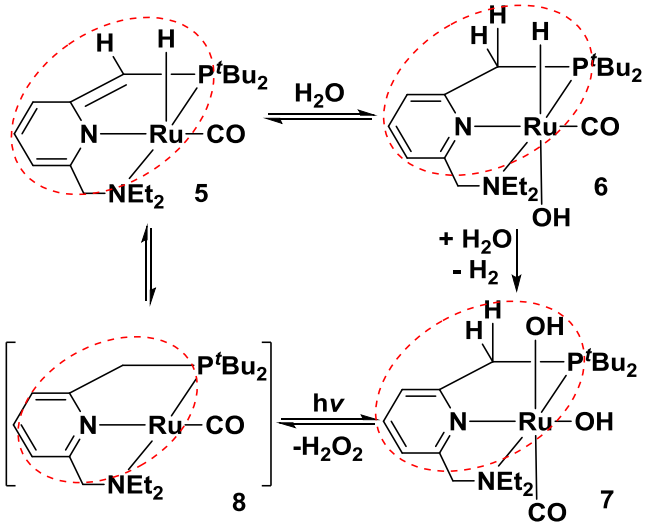

Scheme 2. Inner-sphere cooperative mechanism for the Milstein system

Nowadays, the number of non-innocent ligands has expanded and they are defined as redox (by electrons accepting/donating) and cooperative (by bonds making/breaking) ligands.

1.2.2 Non-innocent ligands with iron in catalysis

The properties of non-innocent ligands allow them together with metal centers to be involved in vital multi-electron catalytic transformations, and in direct activation reactions undergoing reversible chemical transformations.[25–27,42] Generally speaking, two main strategies can be distinguished when using non-innocent ligands containing iron pre-catalysts.

The redox non-innocent ligands are able to function as electron-reservoirs in catalysis (Scheme 3).[25,43,44] When an active redox non-innocent ligand temporarily stores (or releases) the additional electrons, multiple electrons (typically two) are transferred between the metal center and the substrates via either oxidative addition or reductive elimination. Such a catalytic process successfully avoids the possibility of uncommon oxidation states on the metal and thus enables more efficiency.

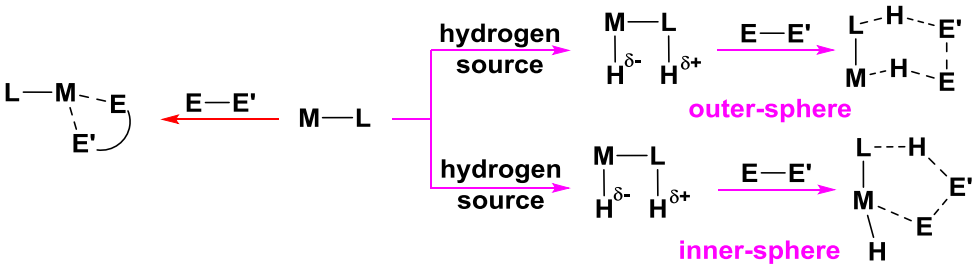

Scheme 3.Two general strategies of “non-innocent” utilization in catalysis

The cooperating non-innocent ligands supply an outer-sphere or inner-sphere catalytic mode (Scheme 3).[21,24,25,30,40,45] The outer-sphere metal-ligand bifunctional cooperation behavior starts from metal complexes containing hydride ligands and acidic hydrogen atoms, which normally is the result of heterolytic H_2 cleavage. The inner-sphere bifunctional cooperation behavior undergoes reversible structural changes in the processes of substrate activation and product formation. Notably, cooperating bifunctional catalysis undergoes reversible structural changes of the ligands without formal changes in the metal oxidation state.

1.2.2.1 Redox non-innocent ligands

A list of ligands has been investigated and showed redox non-innocent behavior upon coordination, such as dioxolenes,[46] dithiolenes,[47] amidophenoxides,[48] bipyridines,[49] cyanoacetylide,[50] bis- and mono- iminopyridines[51–53] and so on.[54] Among these, the bis- and

mono- (imino)pryidines based iron complexes have gained more attention because of their successful utilization as pre-catalysts.[20,29,55] Different types of catalytic reactions using these iron complexes are presented here.

1.2.2.1.1 Polymerization, oligomerization and cyclization (C-C coupling)

The first successful application of homogeneous iron catalysts bearing non-innocent ligands for ethylene polymerization was reported by Brookhart and co-workers in 1998.[56] Bis(imino)pyridines played an important role in the catalytic cycle by supplying electron storage capacity with high active iron pre-catalysts **9** (Figure 3). In the presence of modified methylaluminoxane (MMAO), a turnover frequency greater than 10^7 h^{-1} was achieved at 60 °C and 40 atm. ethylene. Even higher turnover frequency ($2X10^8$ h^{-1}) was obtained at 90 °C, as well as high selectivity (> 99 %) for oligomerization of ethylene to linear α-olefins.[57] Gibson and co-workers reported the same processes using similar iron-based pre-catalysts in the presence of methylaluminoxane (MAO),[58, 59] and observed high activities at room temperature and low ethylene pressure (1 atm.).

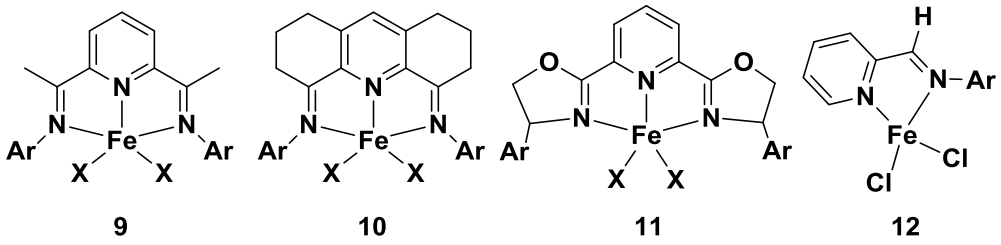

Figure 3. Redox non-innocent bis(imino)pyridine and mono-iminopyridine iron pre-catalysts

Later on, Chirik and co-workers developed a polymerization system which allowed to get rid of MMAO or MAO and used single-component iron catalysts.[60,61] The bis(imino)pyridine containing iron catalysts **9** were modified by using alkyl groups instead of halides coordinated to the iron centers. These complexes proved to be highly active and generated the final polymers with higher molecular weight and lower polydispersity compared with the MMAO (or MAO) activated catalysts.

The utilization of the iron pre-catalysts **9** (X = N_2) was also applied to intramolecular cyclization of dienes and enynes via either [2π + 2π] cycloaddition or hydrogen-mediated method that benefited from the unique electronic structure of the iron complexes.[62,63] Intermolecular [2π + 2π] cycloaddition between butadiene and ethylene to form vinylcyclobutane catalyzed by **9** was achieved in good yields.[64] A series of structurally characterized iron metallacycles **10** (X = N_2),

revealed the existence of several intermediates in hydrogenative cyclization and cycloaddition reactions. Combination of computational and experimental data suggested a monoreduced bis(imino)pyridine radical anion throughout the catalytic cycle, and the resulting Fe(I)-Fe(III) cycle was responsible for C-C bond formation.[65]

The mono(imino)pyridine supported iron pre-catalysts **12** were utilized in stereo- and regioselective C-C coupling of α-olefins to dienes,[66] and stereoselective polymerization of dienes.[67] The mono(imino)pyridine containing complexes, which featured the redox-active behavior of the bis(imino)pyridines, provided one more available coordination site on iron for dienes and thus allowed the control of compounds' geometry.

1.2.2.1.2 C-E bonds formation (E = H, B, Si, C)

The bis(imino)pyridine iron complexes were also successfully applied to olefin hydrogenation catalysis (Scheme 4, eq 1, E = H).[68,69] The catalytic process operates under mild conditions, with low catalyst loading (as low as 0.3 mol%) and low pressure of H_2 (1-4 atm.). A variety of olefins were hydrogenated efficiently, including amino- and oxygen-substituted olefins, with high conversion (> 99 %) and efficient catalytic turnover.

The pre-catalyst **9** (X = N_2) was not only active for olefin hydrogenation, but also for hydrosilylation (eq 1, E = SiR_3).[68] Both primary ($PhSiH_3$) and secondary (Ph_2SiH_2) silanes were efficient silylation reagents, generating rapidly anti-Markovnikov addition products over the course of minutes at room temperature. The reactions with $PhSiH_3$ were much faster than the corresponding reactions with Ph_2SiH_2, and the relative rates of hydrosilylation were similar to those of hydrogenation. Hydrosilylation of aldehydes and ketones was performed by using the alkyl iron pre-catalyst **9** (X = Alkyl),[70] and **11** containing bis(oxazoline)pyridine ligands (eq 2).[71] Both types of pre-catalysts exhibited broad functional group tolerance and high activities at room temperature with nearly 100 % conversions.

Tandem C-H activation/arylation to generate C-C bonds from unactivated arenes with aryl bromides was catalyzed by **9** (X = Br) (eq 3).[72] Experimental data and mechanistic investigation suggested that the system operated via a Fe-based inner-sphere C-H activation that allowed electron transfer from both the ligand and the substrates.

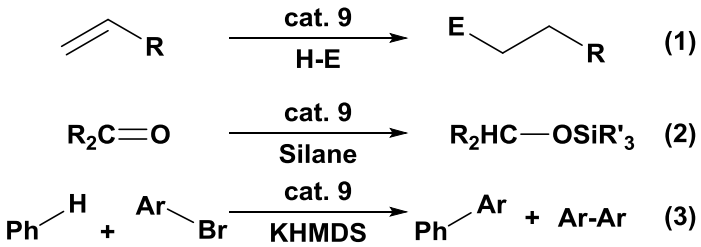

Scheme 4. C-E bond generation catalyzed by bis(imino)pyridine iron complexes **9** (X = N_2 or Br), (H-E = H_2 or silanes)

The dimeric complex [Fe(PDI)]$_2$(μ_2-N_2) (PDI = bis(imino)prydidine),[73] the dimeric form of complex **9** (X = N_2), was a highly active catalyst for regioselective olefin hydrosilylation,[12] and commercial tertiary silanes (R_3SiH) were rather active reagents for this catalytic system. Nearly 100 % conversion of olefins and equimolar quantity of final products were observed under mild conditions. In addition, complete hydrosilylation of the methyl-capped polyether with one equivalent of $(Me_3SiO)_2MeSiH$ (MD'M) (Scheme 5, eq 4), as well as cross-linked silicone polymers resulting from two commercial silicone fluids, SilForce SL6100 and SilForce SL6020 (Momentive Performance Materials, Waterford, NY) (eq 5), were observed with the dimeric iron catalyzed system instead of the industrial platinum catalysts.

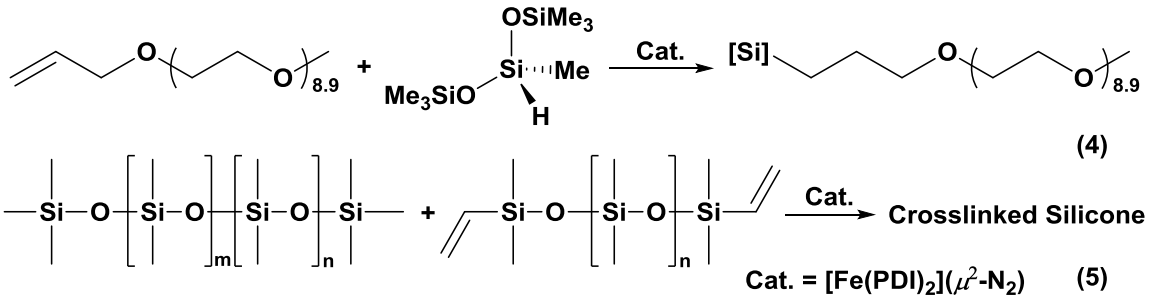

Scheme 5. Dimeric complex [Fe(PDI)]$_2$(μ^2-N_2) catalyzed hydrosilylation of an allyl polyether, and cross-linking of SL6020 and SL6100

The mono(imino)pyridine iron pre-catalysts **12** was also successful for the catalytic generation of carbon-boron[74] and carbon-silicon[75] bonds (Scheme 6). Apart from the modification on the iminopyridine ligand, the hydroboration catalytic system was similar to the previously used for C-C bond coupling reactions.[66,67] Optimized results gave up to 92 % isolated yields and good chemo-, regio-, and stereo-selectivity. Pinacolborane was chosen as a boron source and selectivity for the linear products was preferred over the branched, while (*E*)-stereoselectivity was achieved for both. The hydrosilylation catalytic system, relying on a well-defined iron

complex as pre-catalyst, afforded allylsilanes in high selectivity, with regio- and stereo-selectivity control on diene hydrosilylation, and thus avoiding the addition of other reducing agents such as activated magnesium and so on.

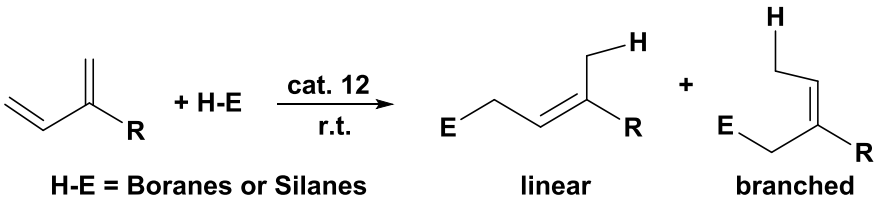

Scheme 6. Hydroboration and hydrosilylation of 1,4-dienes catalyzed by **12**

1.2.2.2 Cooperative non-innocent ligands

Three types of cooperative non-innocent ligands are presented here.[45] The first two types listed in sections 1.2.2.2.1 and 1.2.2.2.2 exhibit an outer-sphere cooperating mode (Noyori type[39]), and the inner-sphere cooperating mode (Milstein type[40]) is described in section 1.2.2.2.3.

Several special systems are not described here. For example, a multiproton-responsive iron complex bearing a NNN ligand (NNN = 2,6-bis(5-tert-butyl-1H-pyrazol-3-yl)pyridine) for N-N bond cleavage of hydrazines[76] and an uncommon metal-ligand cooperation behavior of a PPP-Ni complex (PPP^- = $P[2\text{-}P^iPr_2\text{-}C_6H_4]_2^-$).[77] They were not considered because they are either stoichiometric or not involving iron.[78] PNP-Fe complexes (PNP = 4,5-bis(diphenylphosphino)-acridine or 4,5-bis(diphenylphosphino)-9H-acridine-10-ide) for alkyne hydrogenation are also ignored as there is no evidence for the non-innocent behavior yet.[79]

1.2.2.2.1 Tetradentate diiminodiphosphine or diaminodiphosphine (PNNP)

Morris and co-workers prepared iron-based catalytic systems for asymmetric hydrogenation of polar double bonds (ketones and ketimines).[80] Three types of iron pre-catalysts **13**-**15**, bearing a family of tetradentate ligands (PNNP), proved to be highly active and enantioselective in the presence of a base as catalyst activator (Figure 4). Alcohol was necessary in the system because it was used as either solvent or hydrogen source for the catalytic cycle. Dihydrogen was also a possible hydrogen source, but the efficiency was not comparable with that of using alcohol even when raising the temperature up to 70 °C and pressure up to 25 atm..[81–83]

The (5,5,5-PNNP)iron pre-catalysts (**14** and **15**)[81,82,84,85] revealed huge improvement compared to the (6,5,6-PNNP)iron pre-catalysts (**13**), with almost 200 times higher turnover frequencies.[86–89] The steric and electronic structure of the substituents on both the phosphorus[90] and the

diaminebackbone[86] of the PNNP ligands influenced the catalytic activity. When the substituents on phosphorus were modified from Ph to Et to ^{i}Pr to Cy, the activity of the complexes and the enantioselectivity decreased from Ph to Et, and no activity was observed for the complexes with ^{i}Pr or Cy groups on the phosphorus. Steric effects on the diamine backbone in the pre-catalysts showed that more bulky substituents ((R,R)-dpen and (R,R)-dpen-OMe backbone) were more active and selective than less bulky substituents (diaminocyclohexane- and ethylenediamine).

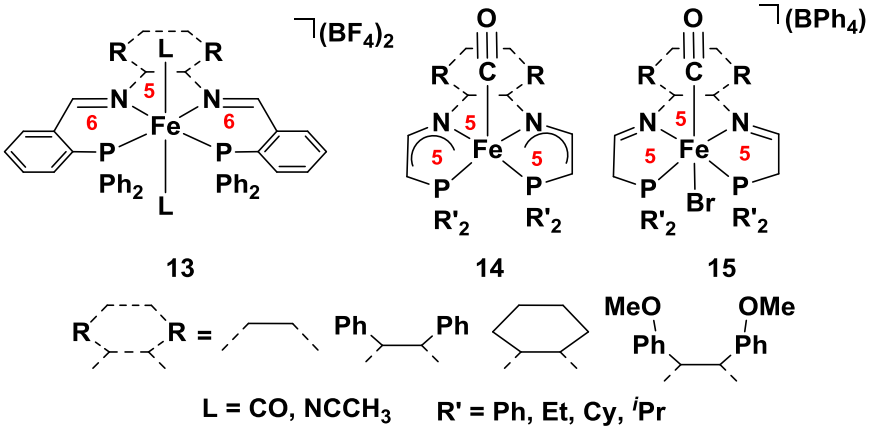

Figure 4. Three types of iron pre-catalysts bearing tetradentate ligands (PNNP), (6,5,6) and (5,5,5) stand for the sizes of the rings that the PNNP ligand makes with iron

Understanding of the catalyst activation process was gained through both experimental and computational studies.[83,87,91–93] As shown in Scheme 7, partial reduction of the PNNP tetradentate ligand in complex **16** with base was the key parameter, which generated the active catalytic species **17** with amido and eneamido moieties. The catalyst was then converted into an intermediate with a H-Fe-N-H moiety (in complex **18**), which hydrogenated the substrate in a bifunctional step-wise outer-sphere process.

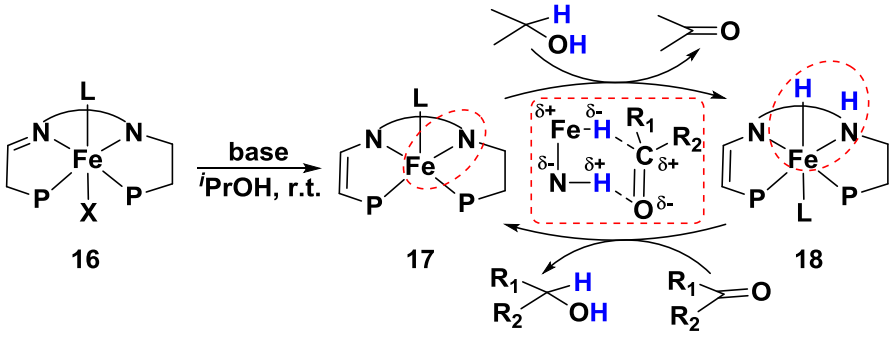

Scheme 7. Proposed catalytic cycle involving pre-catalyst **16**

1.2.2.2.2 Cyclopentadienone iron derivatives

The first iron-based cooperative non-innocent ligand was utilized for the reduction of ketones to alcohols in 2007.[94,95] The well-defined iron catalyst **22** was efficient to hydrogenate ketones under mild conditions with high chemoselectivity with up to 91 % isolated yield (Scheme 8). The cyclopentadienone iron complex **19** was an efficient catalyst for the reductive amination of alkyl aldehydes and amines,[96] and hydrogenation of CO_2 and bicarbonate under remarkably low H_2 pressures (1-5 atm.) with a turnover number of 447.[97] In fact, the truly active catalyst in both reductive hydrogenation and amination systems was **22**. The active catalyst **22** was generated in situ via two different pathways: in pathway **A**, the intermediate complex **20** featuring a vacant site at the iron center was formed by adding trimethylamine N-oxide (Me_3NO) to complex **19**, releasing trimethylamine and CO_2. **20** reacted with H_2 to form complex **22** retaining the H-Fe/O-H active moieties; while in pathway B, the reaction of complex **19** with the base evolved CO_2 and formed an anion intermediate **21**, which reacted with H_2O to give the active iron hydride alcohol complex **22**. The involvement of these species in the CO_2 hydrogenation process will be treated in section 1.3.2.2.

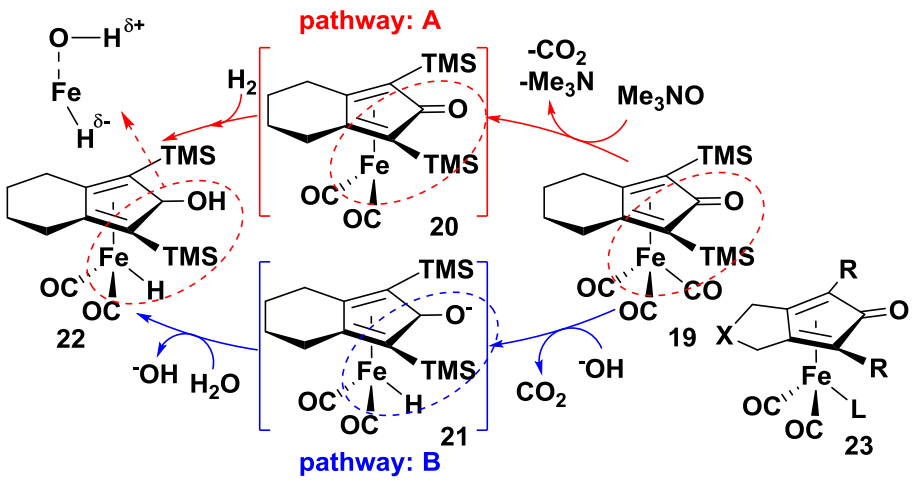

Scheme 8. Well-defined iron complex **22** used for bifunctional catalysis (metal-ligand cooperation) and two pathways to generate **22** from **19**

The scope of this type of cooperative ligands has been largely expanded in 2013.[98] As shown in Scheme 8, in the complex structure **23**, the functional group R can be replaced by trimethylsilyl (TMS), trisopropylsilyl (TIPS), tert-butyldimethylsilyl (TBDMS) and phenyl (Ph), group X can be CH_2, O, $C(CO_2Et)_2$ and N-tosyl (NTs), while group L stands for CO and CH_3CN, respectively. All of these iron complexes were efficient pre-catalysts for reductive amination of ketones with amines (Scheme 9). Computational studies revealed that the corresponding cyclopentadienone

iron alcohol complexes (containing the H-Fe/O-H moieties), the key features for these bifunctional cooperating catalysts, were generated via pathway **A**.

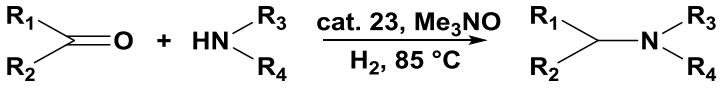

Scheme 9. Reductive amination of ketones with amines catalyzed by bifunctional iron catalysts

1.2.2.2.3 Tridentate 2,6-(methylenephosphino)pyridines (PNP)

A series of complexes featuring tridentate ligands based on central pyridine (PNL) have generated the inner-sphere cooperative concept for a non-innocent behavior in substrate activation reactions.[40,41,99] The metal-ligand cooperation involved dearomatization/aromatization of the pyridine caused by deprotonation/protonation of the benzylic arm of the ligands.[30,40,100,101] The non-innocent behavior of this type of ligands has been successfully utilized in the field of homogeneous catalysis with various transition metals.[36,78] The coordination chemistry of the ligands with iron has been investigated by Milstein,[102] Chirik[103] and Goldman,[104] independently, but to date, only Milstein and co-workers explored the cooperative behavior of PNP-Fe pre-catalysts **24**-**26** (Figure 5) for the hydrogenation of CO_2, ketones, esters and aldehydes.[105–109]

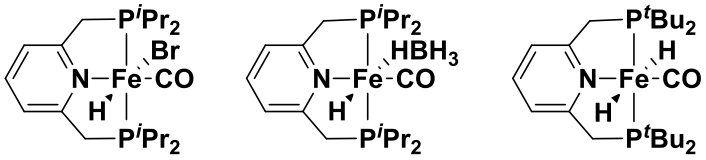

Figure 5. PNP-Fe pre-catalysts **24**-**26** used in hydrogenation of CO_2, ketones, esters and aldehydes

The well-defined complex [FeBr(H)(CO)(PNP-^{i}Pr$_2$)] **24** (Figure 5) was very active for the catalytic hydrogenation of ketones to alcohols in the presence of a base under mild conditions.[106] A turnover number of up to 1880 was observed when using 4.1 atmospheric pressure of H_2 at ambient temperature. Preliminary investigation showed that catalytic hydrogenation was facilitated only in an alcoholic solvent, ethanol giving the highest activity with a yield of 94 %. A remarkable improvement was obtained by using [Fe(BH_4)(H)(PNP-^{i}Pr$_2$)] **25** instead of **24**.[107] The base was no longer necessary and a slight increase on turnover number (1980) was observed.

Hydrogenation of esters to alcohols catalyzed by iron-based complexes was never reported before the use of complex [Fe(H)$_2$(CO)(PNP-^{t}Bu$_2$)] **26**.[108] Complex **26** was an efficient pre-catalyst for the selective hydrogenation of trifluoroacetic esters into the corresponding alcohols. The catalytic process took place under 5-25 atmospheric pressure of H_2 at 40 °C, and generated the products in good to quantitative yields. All these PNP-Fe complexes were also employed for the hydrogenation of aldehydes and exhibited high efficiency with a turnover number of 4000 for a large scope of substrates.[109] In addition, catalyst loading for all the hydrogenation reactions mentioned above was low (maximum 1 mol% and minimum 0.025 mol%). CO_2 hydrogenation catalyzed by complex **24** will be discussed in section 1.3.[105]

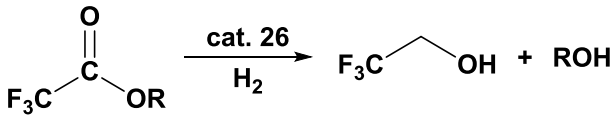

Scheme 10. Hydrogenation of trifluoroacetic esters to alcohols catalyzed by iron pre-catalyst [Fe(H)$_2$(CO)(PNP-^{t}Bu$_2$)] **26**

NMR spectroscopic as well as theoretical investigations on stoichiometric reactions gave mechanistic insights on these catalytic hydrogenation processes, and proved the intermediacy of dearomatized/aromatized intermediates.[105–108] A general mechanism, shown in Scheme 11, fits with all the PNP-Fe catalyzed hydrogenation reactions known until now. The carbonyl carbon atom of the ketone (aldehyde or ester) directly attacked the iron hydride moiety of **26** via C=O insertion into the Fe-H bond giving the corresponding intermediate complex **27**. Addition of base led to elimination of the final compound R_2CH-OH and formed the dearomatized intermediate **28**. Addition of H_2 to **28** regenerated the aromatized complex **26** via metal-ligand cooperation.

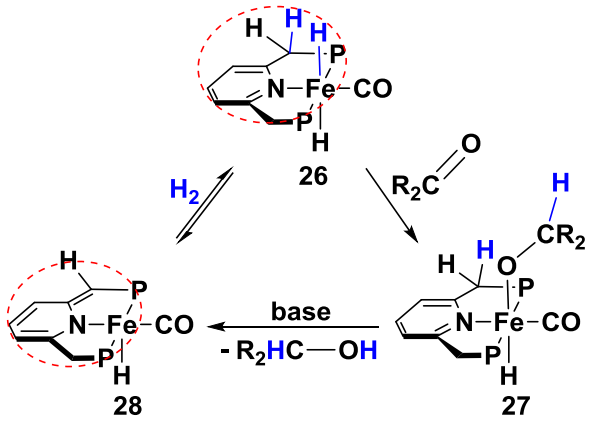

Scheme 11. Proposed mechanism for hydrogenation reactions (R_2C=O: ketones, aldehydes or esters)

The synthesis and dearomatization/aromatization behavior of PNN-Fe complexes (PNN = tridentate bipyridine-phosphine, Figure 6) have been studied recently,[100, 110] and such complexes were used as pre-catalysts for alkene hydroboration with pinacolborane.[111] These pre-catalysts showed pretty good catalytic efficiency under mild conditions, but there was no evidence for dearomatized/aromatized intermediates during the process. A bifunctional redox non-innocent mechanism seemed to be possible based on experimental and computational investigations.[30,101]

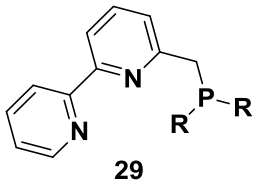

29

Figure 6. Tridentate phosphine-bipyridine (PNN) ligands

1.2.3 Summary

From the examples presented above, the combination of iron with non-innocent ligands has led to remarkable, highly active, environmental benign and versatile catalysts. The new catalytic reactions involve the activation of a large scope of substrates such as olefins, arenes, aldehydes, ketones, esters, and CO_2. The utilization of iron pre-catalysts featuring cooperative ligands led to unusual bond activation processes with no formal change in the iron oxidation state. It thus appears highly desirable to expand the number of iron complexes bearing a pyridine-based cooperative non-innocent ligand, and to study their reactivity.

1.3 Iron complexes in CO_2 transformation

CO2 is an attractive source of caron to replace fossil resoures, because it is rather non-toxic when compared to other C1 sources and it is abundant on earth.[112] Functionalization under mild conditions is a challenge because of its high thermodynamic stability.[113–116] While this field is rapidly growing, the use of inexpensive, abundant and environmentally friendly iron-containing complexes as catalysts remains rather unexplored.[117,118]

A compact summary of CO_2 transformation with homogeneous iron-based catalysts is provided here as an introduction. Selected examples afford a general overview about the development of CO_2 utilization as C_1 source catalyzed by iron.

1.3.1 Stoichiometric reactions between CO_2 and iron complexes

CO_2 features a carbon atom at the highest oxidation state, which explains its high thermodynamically stability. In this sense, CO_2 is an "inert" molecule. In order to really use it as a source of carbon, "how to make it reactive" is of importance.

In this context, the reaction of $[Fe(CO_2)(depe)_2]$ with methyl iodide or methyl triflate at room temperature giving the corresponding carbonyl iron complex $[FeX(CO)(depe)_2]X$ (X = I or OTf),[119] proved the coordination of CO_2 to iron was of importance as a basic pattern to make it "reactive".[120]

The coordination chemistry of CO_2 toward iron centers is presented in this section together with insertion, disproportionation and functionalization reactions.

1.3.1.1 Coordination chemistry of CO_2 to iron complexes

CO_2 coordination chemistry toward transition metal complexes has been studied to understand the different activation modes of this "inert" molecule.[121–125] The CO_2 molecule displays a linear (O-C-O angle of 180°) and centrosymmetric structure. The carbon atom exhibits a Lewis acid character while the two oxygen atoms are weak Lewis bases due to the difference in electronegativity between the carbon and oxygen atoms. The CO_2 ground state can be further described by two $4e^-$-3 centers O-C-O π bonds (Scheme 12).

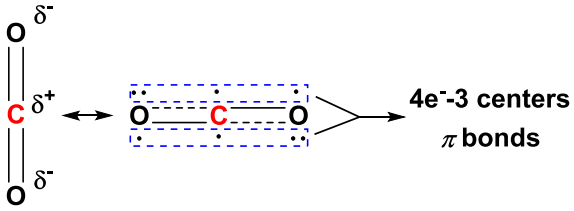

Scheme 12. Schematic representation of CO_2

The molecular properties of CO_2 lead to various coordination modes toward metal centers.[120,122,123,125] As shown in Figure 7, the side-on coordination mode **30** is formed when the C-O π-bond binds to a metal center; mode **31** requires electron-rich metal centers to generate the metal-carbon bond; mode **32** (end-on bonding) concerns the donation of a lone pair of an oxygen atom to a Lewis acidic metal center; mode **33** is found in dinuclear metal complexes, in which the CO_2 molecule acts as a bridging ligand. Until today, the coordination of CO_2 to iron complexes only exhibits side-on and bridging bonding modes. In fact, there is no structural

description of the end-on coordination modes (**31** and **32**) neither for iron nor for other transition metals.[123]

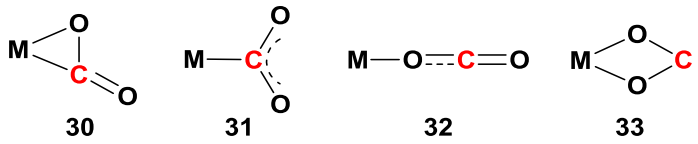

Figure 7. Coordination modes **30**-**33** of CO_2 with metal centers

1.3.1.1.1 Side-on coordination mode of CO_2 to iron

Three decades ago, several iron(0) complexes featuring phosphine ligands were shown to bind CO_2 in a side-on coordination mode (Figure 8). [119,126,127] The presence of donor phosphine ligands increased the electron density at the iron center, favoring the generation of these complexes. Two iron-CO_2 compounds bearing phosphine ligands (**34** and **35**) were computationally studied and their optimized geometry displays the CO_2 side-on coordination mode. The X-ray structure of compound **36** indeed indicated the presence of side-on coordinated CO_2 to the iron center bearing donor phosphine ligands. The O-C-O angles of 137.3° (**34**), 140.5° (**35**) and 124° (**36**) are strong evidence for the side-on coordination of CO_2 (Calculated data for **34** and **35**, X-ray data for **36**).

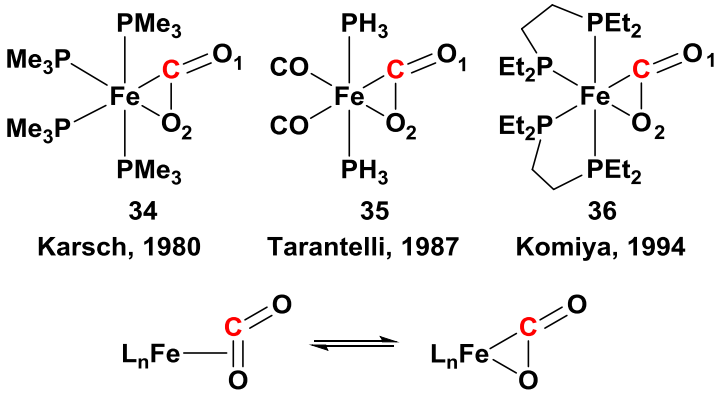

Figure 8. Side-on coordination mode of CO_2 to iron centers

1.3.1.1.2 Bridging coordination mode of CO_2 to iron

In the 1990's, Gibson et al. and Komiya et al. studied heterobimetallic complexes featuring CO_2 bridges.[128–130] CO_2 coordinated to one iron center via the carbon atom and further bonded to another metal (Re and Sn) through one or two oxygen atoms. X-ray structure analyses showed that CO_2 displayed two bridging modes, μ^2-η^2 (**37**) and μ^2-η^3 (**38** and **39**) (Figure 9). Complex **37** was synthesized by adding $Re(CO_4)(L)(BF_4)$ (L = CO or phosphine) to a metallocarboxylate

$[(Cp)Fe(CO)(PR_3)CO_2]^-(K)^+$; **37** afforded complex **38** after heating at 60 °C. The combination of $SnClR_3$ with $Fe(CO_2)(depe)_2$ (R = Me or Ph, depe = $Et_2PCH_2CH_2PEt_2$) led to the formation of **39**.

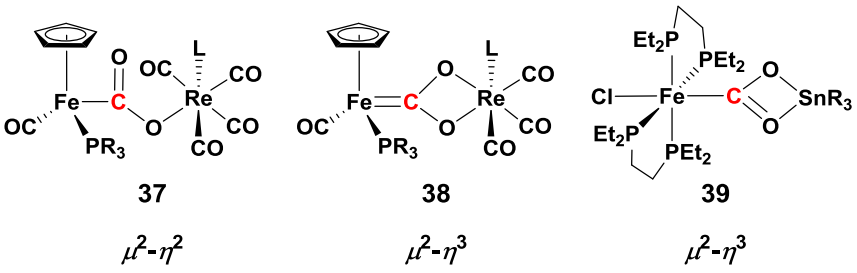

37 **38** **39**

μ^2-η^2 μ^2-η^3 μ^2-η^3

Figure 9. Heterobimetallic CO_2-bridge complexes **37**-**39** with μ^2-η^2 and μ^2-η^3 modes

Systematic investigation on these bridged CO_2 complexes revealed the vast majority displays a regular pattern of coordination of CO_2 as either μ^2-η^2 or μ^2-η^3 modes.[131] The coordination modes of CO_2 indeed depend on the substituents on the metallocarboxylates.

1.3.1.2 Insertion reactions of CO_2 to Fe-E bonds (E = H or C)

The insertion of CO_2 in M-E bonds (E = H or C) forming the corresponding metal carboxylates is of importance for the utilization of CO_2 to generate more valuable chemical compounds. The insertion of CO_2 into M-E (E = H or C) bonds is believed to play a key role in catalytic CO_2 transformations.[113,125,132–134] This reaction takes place via either direct insertion mechanisms (mediate M---OCO moiety) or direct S_E2 attack at the E atom (mediate M---E---CO_2 moiety), leading to the insertion compound M-O(O)C-E.[135–140]

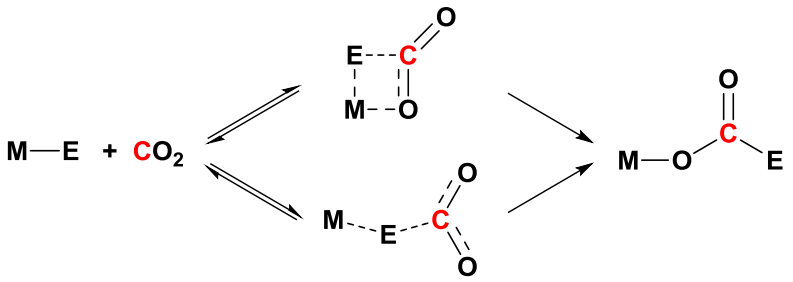

Scheme 13. Insertion of CO_2 into M-E bonds via two possible pathways

1.3.1.2.1 Insertion of CO_2 to Fe-H bonds

This type of insertion reaction has been investigated by Field and co-workers (Scheme 14).[141] The iron complex *cis*-$Fe(H)_2(dmpe)_2$ (**40**) features two diphosphine (dmpe = dimethylphosphinoethane) and two hydride ligands. The mono- and di-inserted products **41** and **42** were obtained by manipulating the CO_2 pressure from 1 to 5 atm.. Remarkably, the second

insertion step was reversible as complex **41** could be obtained from **42** by removing the excess of CO_2 under vacuum.

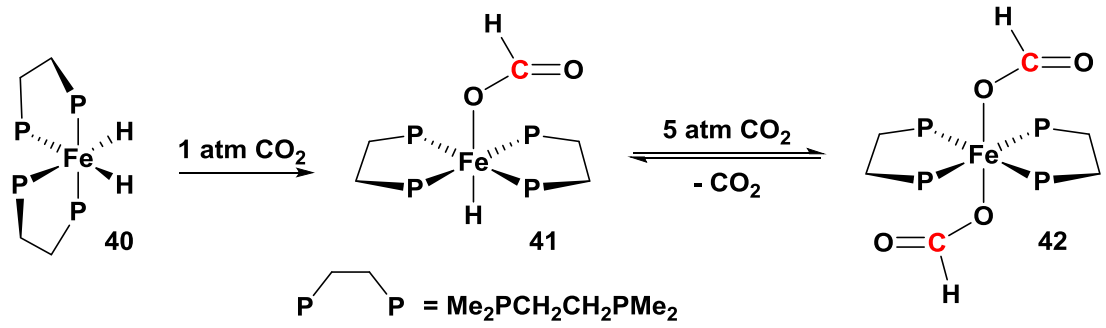

Scheme 14. Mono and double insertion of CO_2 into Fe-H bonds

Complex **41** was characterized by ^{1}H NMR with a high field signal at δ = -33.96 ppm for the hydride and a low field signal at δ = 7.78 ppm for the formyl proton, by a $^{13}C\{^{1}H\}$ NMR resonance at δ = 168.1 ppm for the formate moiety and by a single $^{31}P\{^{1}H\}$ NMR resonance at δ = 79.1 ppm. These data indicate a *trans* geometry for **41** as opposed to the *cis* geometry for complex **40**, which was characterized by ^{1}H NMR with a high field signal at δ = -13.95 ppm for the two hydrides and by $^{31}P\{^{1}H\}$ NMR at δ = 67.2 and 76.9 ppm. For *trans*-$Fe(OCHO)_2(dmpe)_2$ (**42**) the formyl groups gave one resonance in ^{1}H NMR at δ = 6.46 ppm, and in $^{13}C\{H\}$ NMR at δ = 170.5 ppm, respectively, whereas one signal was observed in the $^{31}P\{^{1}H\}$ NMR spectrum at δ = 69.6 ppm. Both the $^{13}C\{^{1}H\}$ NMR and IR data ($\upsilon_{Fe\text{-}H}$ = 1805 cm^{-1}, $\upsilon_{asym}(CO_2)$ = 1602 cm^{-1} and $\upsilon_{sym}(CO_2)$ 1328 cm^{-1} for **41**; $\upsilon_{asym}(CO_2)$ = 1607 cm^{-1}, $\upsilon_{sym}(CO_2)$ = 1322 cm^{-1} for **42**) are consistent with the coordination of η^1-O formate group(s) in **41** and **42**.

1.3.1.2.2 Insertion of CO_2 to Fe-C bonds

More recently, Field and co-workers reported the insertion of CO_2 into Fe-C bonds. Carboxylate complexes are formed with the generation of new C-C bonds (Scheme 15).[142] CO_2 insertion into the Fe-C bonds of the *cis*/*trans* mixture of complex $FeMe_2(dmpe)_2$ **43** led to results similar to those observed when starting from *cis*-$Fe(H)_2(dmpe)_2$**40**. The first equivalent of CO_2 insertion took place at ambient temperature under 1 atmosphere of CO_2, to afford complex **44** as a mixture of *cis*- and *trans*- isomers. By rising CO_2 pressure to 6 atm. and temperature up to 60 °C, a double insertion occurred and complex *trans*-$Fe(OCOCH_3)_2(dmpe)_2$ **45** was obtained. Rearrangement of the acetate ligand has also been observed with the formation of the iron complexes $[Fe(\eta^2\text{-}O_2CCH_3)(P2)_2]^+[OCOCH_3]^-$ **46** from either **44** or **45** in polar solvents (e.g.: DMF).

In the case of complex Fe $Me_2(depe)_2$ (**43**, depe = diethylphosphinoethane), only the mono-inserted complex **44** (depe) was obtained, which was explained by the slightly larger steric hindrance of the depe ligands. The rearrangement of the acetate ligand affording complex **46** (depe) was observed by using higher pressures of CO_2. The detailed mechanism for the formation of such salt **46** (both dmpe and depe ligands containing complexes) remains unclear and would need further investigation.

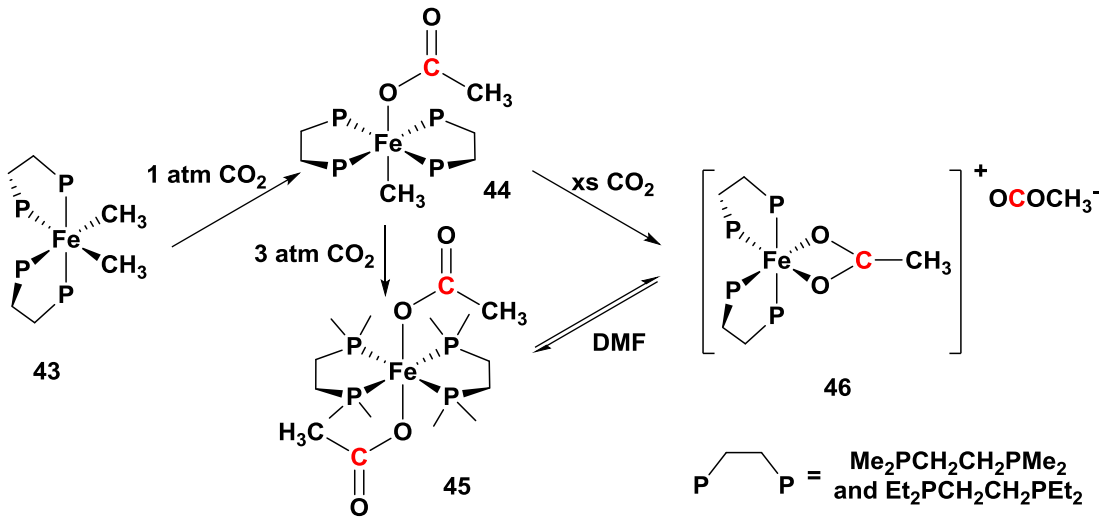

Scheme 15. CO_2 inserted into Fe-C bonds affording complexes **43**-**46** (*cis*-and *trans*- isomers for **43** (PP = dmpe and depe), **44** (PP = dmpe) were omitted for clarity)

1.3.1.3 CO_2 disproportionation

The disproportionation of CO_2, generating CO_3^{2-} and CO, could be an important step for further transformation. In 2007, a homobimetallic complex **48** was prepared from the reaction of complex **47** and CO_2. A C=O bond was formally cleaved yielding a double μ-CO/μ-O iron core complex **48** (Scheme 16). In the same system, the coupling of two molecules of CO_2 also occurred leading to another dinuclear complex [LFe(μ-η^2:η^2-oxalato)FeL] (**49**) as a minor product. Both **48** and **49** were structurally identified by X-ray diffraction. But in the crude mixtures of **48** and **49**, an additional complex [(LFe(CO)]$_2$(μ-η^2:η^2-oxalato) (**50**) was also present.[143] A detailed investigation on this Fe(I)-mediated CO_2 reductive cleavage and coupling process indicated that the formation of **48** and **49** was subject to the control of solvents and ancillary ligands. In THF, complex **49** was favored and ($PhBP^{CH_2Cy}_3$)Fe(I) was the only intermediated species. While in methylcyclohexane (MeCy), complex **48** was generated exclusively via several intermediate ($PhBP^{R}_3$)Fe(I) species (R = Ph, ^{i}Pr, *m*ter; *m*ter = 3,5-*meta*-terphenyl).[144]

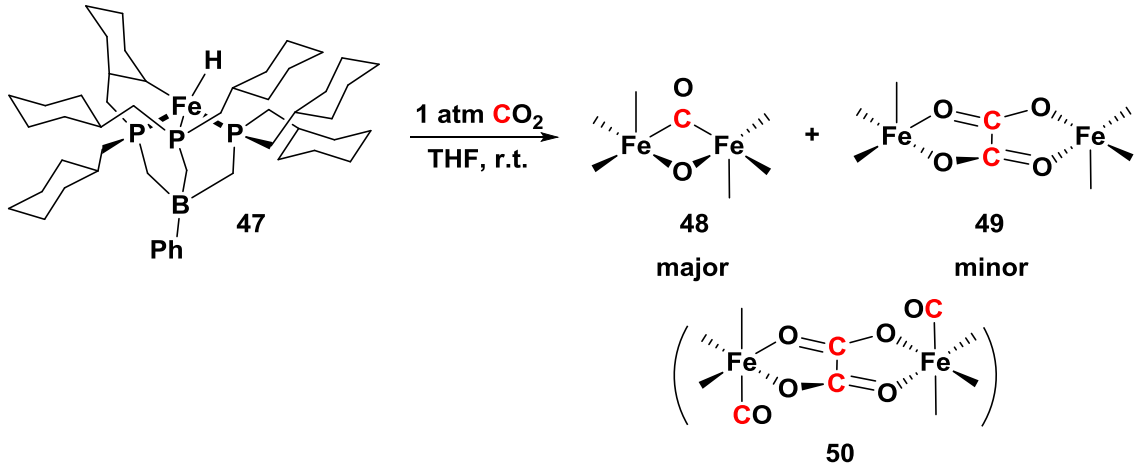

Scheme 16. Homobimetallic complexes **48**-**50** reported by Peters and coworkers

Holland and coworkers further studied CO_2 disproportionation processes with diiron (I) complexes **51**.[145,146,147] When 2 equivalents of CO_2 were added to **51**, CO_2 disproportionated formally into CO and carbonate, leading to a four-coordinated dicarbonyl iron complex **52** and the carbonate complex **53** (Scheme 17). Interestingly, complex **53** exhibited two different bridging modes: μ-η^1:η^2 (**53a**) and μ-η^2:η^2 (**53b**). The variable temperature ^{1}H NMR spectra (+70 to -70 °C) showed no decoalescence for complex **53** (**a** and **b**), indicating a rapid exchange between the two binding modes, and the two equivalent ligands (diketiminate) revealed a rapid rotation of the iron atom around the Fe-O bond of the carbonate.

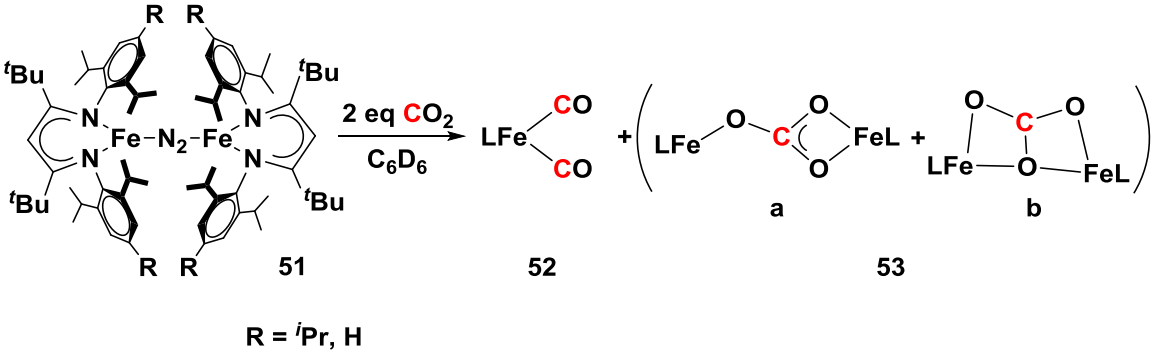

Scheme 17. Disproportionation of CO_2 with diiron(I) complex **51**

The proposed mechanism suggested reductive cleavage of CO_2 to afford CO and O^{2-} in a similar fashion as in Peters' example (Scheme 18).[143, 144] The proposed oxodiiron complexes (Fe-O-Fe) could not be detected during the reaction, but were independently synthesized.[147]

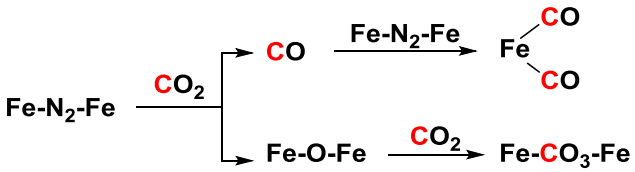

Scheme 18. Proposed mechanism for CO_2disproportionation

When investigating the insertion of CO_2 into Fe-C bonds (section 1.3.1.2.2), Field and co-workers observed CO_2 disproportionation.[142] CO_2 reacted with adventitious water generated in the reaction mixture, leading to carbonic acid. Complex Fe(dmpe)$_2$(η^2-O_2CO) **54** was thus observed from the reaction of **43** with carbonic acid, and possibly releasing CH_4 gas (Scheme 19).

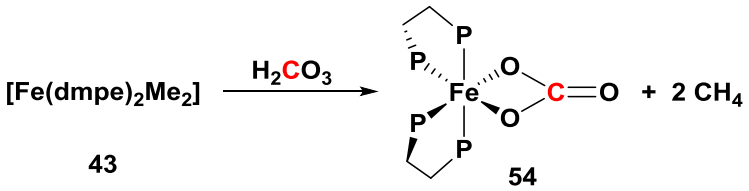

Scheme 19. Disproportionation observed with complex **43**

Disproportionation of CO_2 was also observed from iron hydride complexes **40**. After CO_2 insertion described earlier affording complex **41**, the bicarbonate salt [Fe(H)(CO)(dmpe)$_2$][HCO_3] **58** crystallized in approx. 20 % yield after a few days in the sealed NMR tube under CO_2.[148] The proposed mechanism involved an intermediate **55** resulting from formal CO_2 insertion into the Fe-O bond of **41** and intra-molecular rearrangement with breaking/binding of one Fe-P bond and a final decarbonylation step to produce the carbonyl complex with a bicarbonate counterion (Scheme 20). This mechanism was proposed in accordance with Karsch's study on the formation of [Fe(CO_3)(CO)(PMe_3)$_3$], [Fe(CO)$_2$(PMe_3)$_3$] and [Fe(CO)(PMe_3)$_4$] compounds,[149] and data on the structurally characterized [IrCl(C_2O_4)(PMe_3)$_3$] compound.[150]

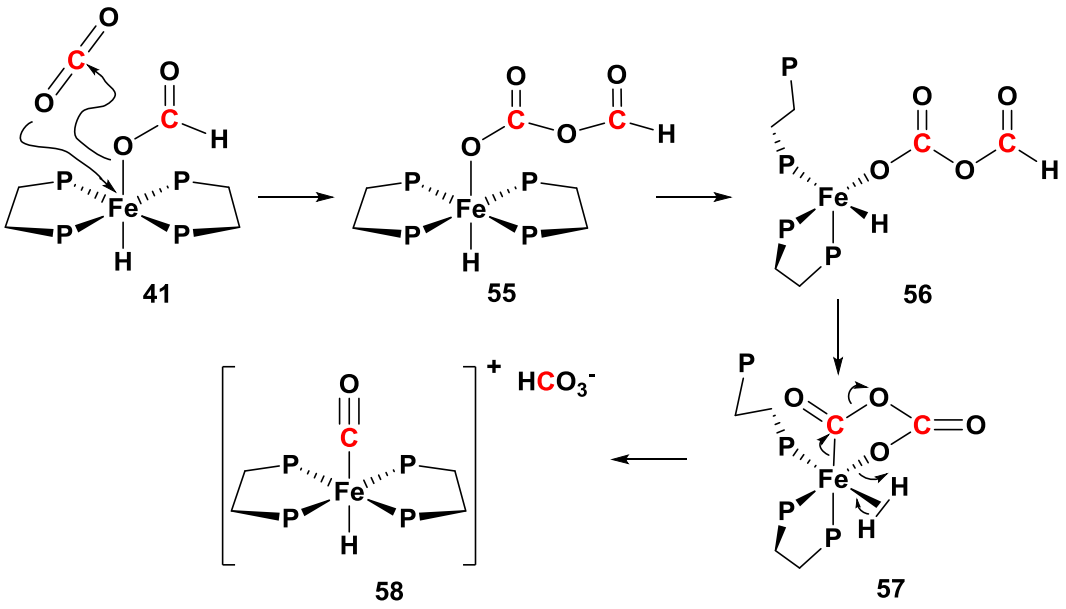

Scheme 20. Proposed mechanism for CO_2 disproportionation with **41**

1.3.1.4 Functionalization of CO_2 at iron: C-N and C-C bond formation

In 2002, the formation of a C-N bond, the carbon coming from CO_2, was reported by Field and coworkers.[151] As shown in Scheme 21, the structurally characterized heterocyclic complex **61** was obtained after sequential reactions of $Fe(H)_2(dmpe)_2$ (**40**) with EtNCS (isothiocyanate) and CO_2.

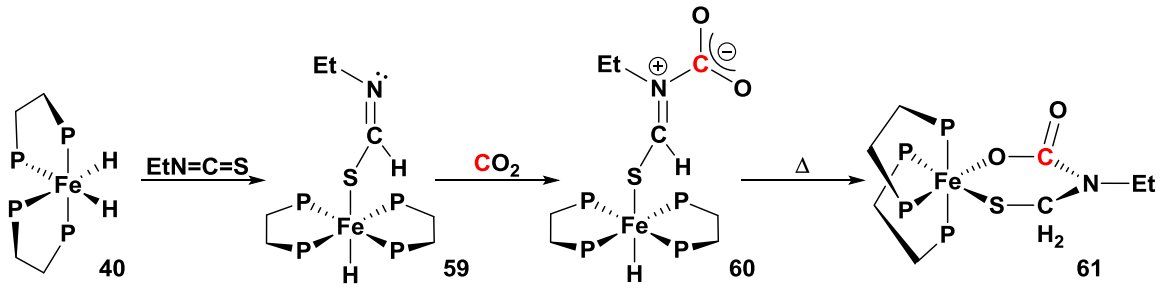

Scheme 21. Functionalization of CO_2 upon coordination to complex **40** and reaction with EtNCS

Hoberg and coworkers reported that CO_2 can react with an iron complex featuring a η^4-diene ligand (Scheme 22).[152, 153] At -80 °C the allylcarboxylate complex **63** was characterized. Upon warming, an equilibrium between complexes **63** and **64** took place. Complex **64** was characterized as a ferracyclobutenoate complex. Acid hydrolysis of **63** in methanol at -30°C yielded mainly methyl esters. When using the bis(ethylene) complex Fe(η^2-ethene)$_2$(PEt_3)$_2$ instead of complex **62**, C-C coupling between ethylene and CO_2 only took place in the presence

of additional phosphine ligands (PMe_3, DCPE (P,P'-ethylenebis(dicyclohexylphosphane)) or DMPE (P,P'-ethylenebis(dimethylphosphane)). The generated ferracyclopropionate or oxaferracyclobutanone could further react with CO_2.[154]

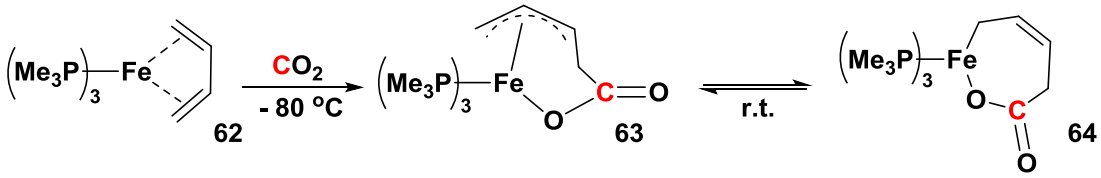

Scheme 22. C-C coupling reaction of CO_2 and [Fe(η^4-butadiene)(PMe_3)$_3$] **62**

In fact, the corresponding esters or dicarboxylic acids could be obtained after acid hydrolysis of the Fe-CO_2 adducts. These reactions represent a utilization of CO_2 as C_1 source mediated by iron in order to generate more complex organic molecules.

1.3.2 Iron-catalyzed transformation of CO_2

The transformation of CO_2 to more complex compounds is a challenge due to its inert and non-reactive properties. Thus the strategies to achieve this goal are either choosing the oxidized low energy synthetic targets, or using higher energy substances for example small-membered rings, H_2 and unsaturated compounds as reactants in order to drive the reactions. And in any cases, active catalysts are strictly required.[112,116]

1.3.2.1 Synthesis of cyclic carbonates and polycarbonates from CO_2

Cyclic- and poly- carbonates are one of the few commercial products synthesized from CO_2, and the synthetic strategy from CO_2 starts from the 1960's.[155,156] Metal catalysts have been developed for this process.[157] In 1986, iron-based complexes also begin to draw attention.[158] Kisch and coworkers firstly reported the combination of $FeCl_3$ with alkylammonium iodide ($(^nBu)_4NI$) as catalysts for the synthesis of cyclic carbonate from 2-methyloxirane. They obtained a yield of 31 % at room temperature in the presence of 1 atmosphere of CO_2. Until 2015, iron pre-catalysts are restricted to those bearing macrocyclic or chelating ligands, and are utilized in the catalytic cycloaddition, and symmetric or asymmetric copolymerization reactions of CO_2 with epoxides (Scheme 23).

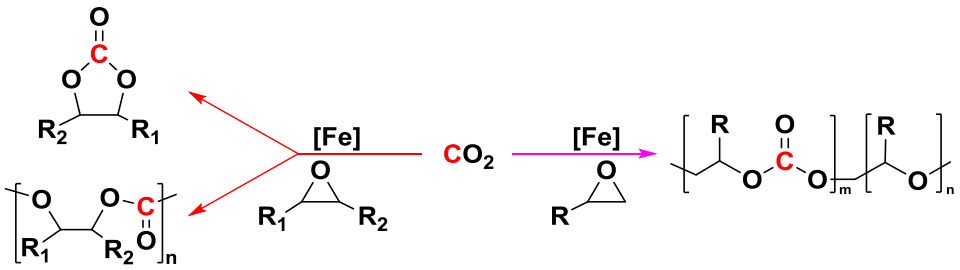

Scheme 23. Cycloaddition and symmetric or asymmetric copolymerization of CO_2 with epoxides catalyzed by iron complexes

A general mechanism is proposed for the iron catalyzed production of both cyclic carbonates and polycarbonates (Scheme 24). The first step concerns the coordination of the epoxide to the metal center. An anion promotes epoxide ring-opening, followed by the insertion of CO_2 to give intermediate **a**. This intermediate undergoes either a ring-closure reaction leading to the formation of the cyclic carbonate (pathway **I**), or further insertion of epoxide and CO_2 to generate the corresponding copolymers (pathway **II**).

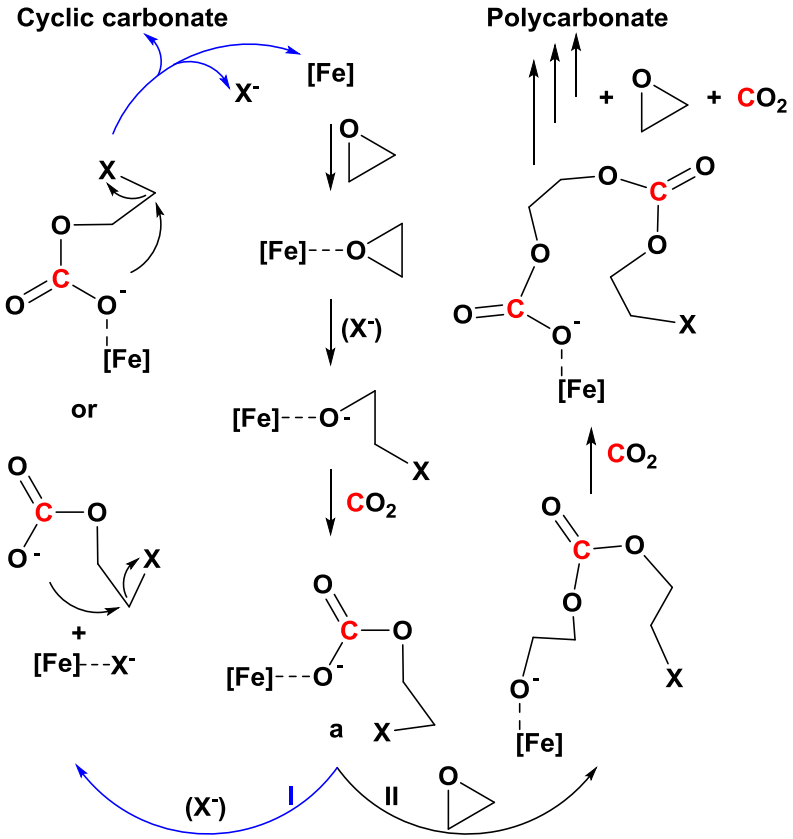

Scheme 24. General catalytic mechanism for the synthesis of cyclic or polymeric carbonates

1.3.2.1.1 Iron catalysts bearing macrocyclic ligands

A series of iron complexes bearing macrocyclic ligands were used as catalysts for the copolymerization reactions, while nucleophiles played a role as co-catalysts. The first examples of this series were reported in 2011 for the generation of cyclic carbonates and symmetric polycarbonates,[159] and in 2013 for the generation of asymmetric polycarbonates (Scheme 23).[160]

The di-iron complex **65** exhibited good activity and productivity in the copolymerization of CO_2 and cyclohexene oxide under mild conditions (Figure 10). The corresponding polycarbonate was obtained in high yield with a turnover number of 2570 and 30 % conversion of the epoxide. By adding bis(triphenylphosphino)iminium chloride ([PPN]Cl) as co-catalyst, the selective formation of *cis*-cyclohexene carbonate was performed with an improved conversion of epoxide of 98 %. The combination of the di-iron catalyst **65** and co-catalyst [PPN]Cl was also active in the synthesis of propylene carbonate and styrene carbonate in rather high yield under only 1 atmosphere of CO_2. The iron-corrole complexes **66** and **67** were used to catalyze the coupling of CO_2 with epoxides in the presence of [PPN]Cl, resulting in asymmetric copolymerization of not only CO_2/ propyloxide (CO_2/PO) with a yield of 65 %, but also CO_2/glycidylphenylether (CO_2/GPE) with a GPE conversion higher than 99 % for the first time.

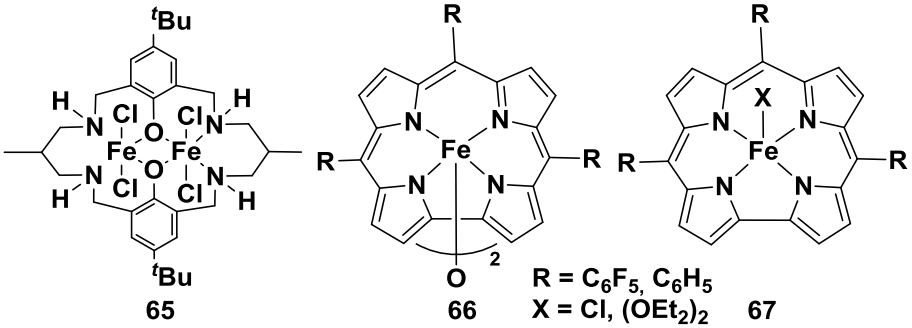

Figure 10. Iron complexes bearing macrocyclic ligands as catalysts for the copolymerization of CO_2 and epoxides

1.3.2.1.2 Iron catalysts bearing tetradentate chelating ligands

The use of tetradentate ligands aimed at improving the activity of the catalytic system: lower catalyst loading, larger range of epoxides, better selectivity of the organic carbonates (*cis*- or *trans*- cyclic carbonates, symmetric or asymmetric copolymer carbonates), milder reaction conditions and full understanding of the catalytic process.

Three well-defined tetraamine-iron complexes (Figure 11, **68** and **69**) showed high catalytic activity in the synthesis of cyclic propylene carbonates.[161] Notably, the catalytic system was

active without any activator. However, the addition of co-catalyst such as tetrabutylammonium (TBAB) could significantly improve the catalyst reactivity. More specifically, the use of a co-catalyst allowed to increase the conversion of propylene oxide from 80 % to 100 % with 1 mol% of iron complex and co-catalyst under 15 atmosphere of CO_2. The system was further improved with the use of 0.1 mol% of iron complexes (**70** and **71**) and co-catalysts under notable lower CO_2 pressure (< 5 atm.), which led to nearly 100 % yield and turnover numbers of 1000.[162] The use of catalysts **72** and **73** bearing O, N, N, O-chelating ligands allowed the copolymerization of CO_2 and propyl oxide without any co-catalyst, with nearly 100 % yield of the corresponding carbonate.[163,164]

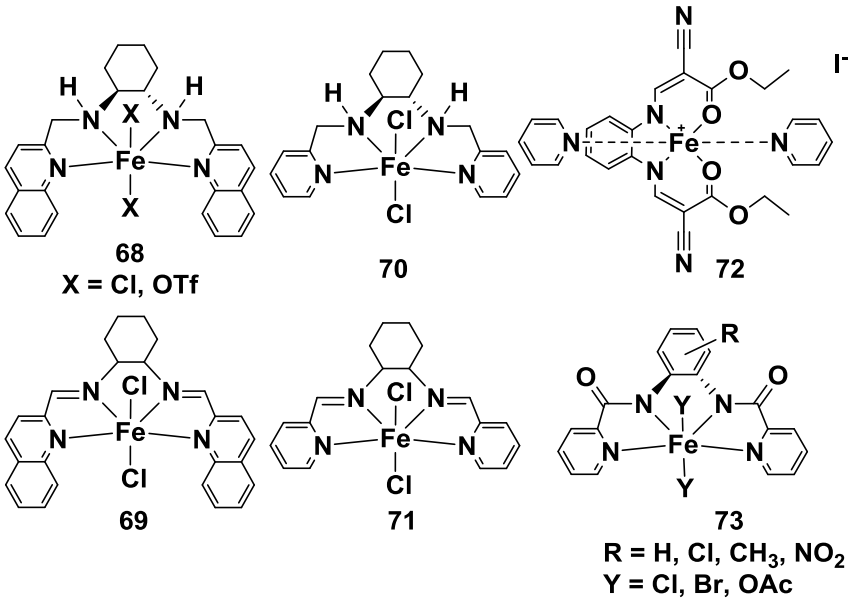

Figure 11. Iron catalysts bearing tetradentate ligands

Kleij and coworkers described several well-defined iron complexes bearing tetradentate ligands (Figure 12). Depending on the substituent in the *ortho*-position of the phenolate moiety, monomeric and dimeric structures were obtained.[165,166] Both types of iron complexes (**74**-**76**) exhibited good activity for the cycloaddition of CO_2 to a range of epoxides and especially terminal epoxide. The activity of monomeric iron complexes **74** was significantly higher than that of dimeric iron complexes **75** and **76**. However, the presence of a co-catalyst, Bu_4NX (X = Cl, Br or I), was necessary to improve the conversion of epoxides and the yield of products. The selectivity to either cyclic versus polycarbonates was investigated later on, and the results showed that the selectivity can be well controlled by modification of the catalysts and the co-catalysts loading. In addition, supercritical CO_2 was shown to enhance product yields.[167]

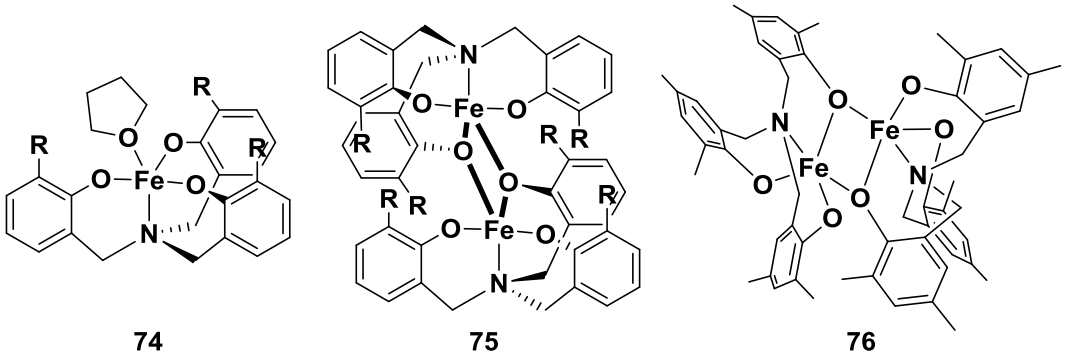

Figure 12.Monomeric (**74**) and dimeric complexes (**75** and **76**)

1.3.2.1.3 Iron complexes bearing other chelating ligands

Iron complexes $[FeCl(ON)_2]$ **77** (Figure 13) containing bidentate ligands and the di-iron thioether-triphenolate complex $[Fe(OSOSO)_2]_2$ **78** were used as catalysts in the cycloaddition process of CO_2 and epoxides. While the pre-catalyst **77** exhibited the highest activity with styrene oxide compared to the related Cr or Co complexes,[168] the air-stable catalyst **78** exhibited the highest turnover frequency (633 h^{-1}) for the solvent-free cycloaddition of CO_2 to propylene oxide under mild conditions.[169]

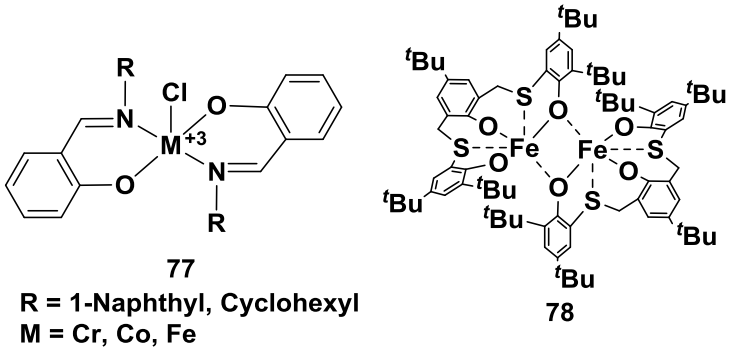

Figure 13. Pre-catalysts **77** and **78** for the cycloaddition reactions of CO_2 and epoxides

1.3.2.2 Hydrogenation of CO_2 to generate formic acid and its derivatives

The reduction of CO_2 with dihydrogen is an ideal reaction in term of atom economy, and hydrogenation reactions are catalyzed by iron complexes leading to formic acid and derivatives. The direct hydrogenation gives rise to formic acid, while the addition of alcohol affords carboxylic acid (Scheme 25).

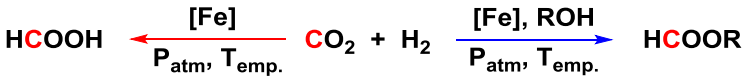

Scheme 25. Reductive hydrogenation of CO_2 with H_2 catalyzed by iron catalysts leading to formic acid and carboxylic acids

In 1975, complex $[Fe(H)_2(dppe)_2]$ (dppe = 1,2-bis(diphenylphosphino)ethane) was used as pre-catalyst for the catalytic hydrogenation of CO_2. In the presence of trimethylamine (Me_3N) and ethanol, ethyl formate was generated with a turnover number of 2 at 140 °C under 25 atm. of H_2 and 25 atm. of CO_2.[170] Three years later, a series of anionic iron carbonyl hydrides were chosen as pre-catalysts for a similar catalytic system under elevated temperatures and pressures.[171] The best result obtained was a turnover number of 5.8 when using $[N(P(C_6H_5)_3)_2][HFe_3(CO)_{11}]$ as catalyst.

The field of iron complexes catalyzing CO_2 hydrogenation to generate formic acid and its derivatives was quiet for more than twenty years until the next example came out in 2003.[172] A new screening method, which was a high-pressure combinatorial catalyst screening with a dye-based assay (bromothymol blue, DBU), was introduced to hydrogenate CO_2 into formic acid with in situ generated iron catalysts under elevated temperatures and pressures. The combination of $FeCl_3$ with 1,2-bis(dicyclohexylphosphino)ethane (dcpe)) created an active catalyst for the process with good reproducibility, with a turnover number of 113 at 50 °C under 200 atm. total pressure.

The combination of the iron precursor $Fe(BF_4)_2{\cdot}6H_2O$ and the tetradentate ligand tris(2-(diphenylphosphino)phenyl)phosphine (PP_3), gave an active iron catalyst ($[FeH(PP_3)]BF_4$ (**79**, X = H**)**, Figure 14) that could be used for the reductive hydrogenation of both carbon dioxide and bicarbonates to give formates and alkyl formates.[173] Sodium formate was produced with a yield of 88 % and a high turnover number of 610 under 60 atm. of H_2, and methyl formate with a yield of 56 % and a turnover number of 585 (30 atm. of CO_2 and 60 atm. of H_2). Later on, complex $[FeF(PP_3)]BF_4$ **79** (X = F) was proved to be the most active and productive iron catalyst so far for the hydrogenation of bicarbonates and CO_2 to formates and formamides.[174] Furthermore, such complex, air- and temperature- stable, gave similar catalytic activities compared to the in situ generated catalysts. More specifically, when 0.01 mol% $[FeF(PP_3)]BF_4$) was used for the hydrogenation of sodium bicarbonate under 60 atm. H_2 at 100 °C, a yield of 77 % and an excellent turnover number of 7546 could be obtained.

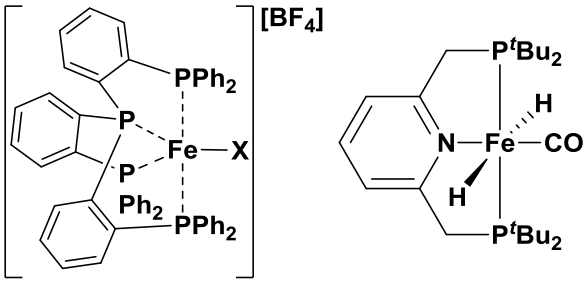

79 X = H, F 26

Figure 14. Well-defined iron catalysts **79** and **26** for reductive hydrogenation of CO_2

The iron dihydride complex *trans*-[Fe(H)$_2$(CO)(^{t}Bu-PNP)]) (**26**), bearing a PNP pincer ligand, afforded high efficiency for the hydrogenation of CO_2 and sodium bicarbonate under remarkably low pressure.[105] The observed activity was comparable to that of some known precious metal catalysts.[175, 176, 177, 178] For the hydrogenation of sodium bicarbonate, a yield of 32 % and turnover number of 320 were observed at 80 °C under 8.3 atm. of H_2. By elevating the concentration of sodium hydroxide, the highest activity of the catalyst was observed for the hydrogenation of CO_2 gas at remarkably low pressures (initial pressures: CO_2, 3.3; H_2, 6.7 atm., respectively), with a turnover number of 788 and a turnover frequency of 156 h^{-1}. Independent stoichiometric reaction of *trans*-[Fe(H)$_2$(CO)(^{t}Bu-PNP)] **26** with CO_2 as well as in situ NMR analysis were performed in order to understand the mechanism of the process. Yang also reported a theoretical study by DFT calculations using the similar catalyst (*trans*-[Fe(H)$_2$(CO)(^{i}Pr-PNP)]).[179] The proposed mechanism was similar to the mechanism of carbonyl reduction depicted in Scheme 11 (section 1.2.2.2.3), in which the dearomatization/aromatization of the pyridine ring played a key role.

As shown in Scheme 26, a general catalytic mechanism for the formation of formic acid from iron catalyzed CO_2 hydrogenation processes was suggested. The first step of the process was to generate Fe-H bonds, subsequent insertion of CO_2 to the Fe-H bond resulted in an unstable carboxylic intermediate. Formic acid was released by adding hydrogen source (H_2 or H_2O) to the carboxylic intermediate and regenerating the initial Fe-H bond.

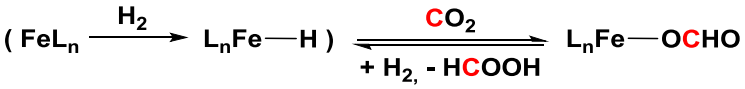

Scheme 26. General mechanism for the iron catalyzed hydrogenation of CO_2

Yang, Zhou and coworkers investigated a phosphine-free, air- and moisture-tolerant iron catalyst system for the hydrogenation of CO_2 and sodium bicarbonate.[97] The so-called "Knölker's iron complexes" **80** afforded a turnover number of 447 in sodium bicarbonate hydrogenation reaction under 30 atm. of H_2. Notably, the related iron catalyst **19** was also capable of hydrogenating bicarbonate under low hydrogen pressures (1-5 atm.) with corresponding turnover numbers of 47 to 163. The PNP pincer ligand containing iron catalyst (*trans*-[Fe(H)$_2$(CO)(^{t}Bu-PNP)], **26**) exhibited similar activity for the same process under low hydrogen pressure (6.2 atm., with a turnover number of 267).[105] A proposed mechanism based on the previous work[95,180] was proposed as depicted in Scheme 27. The hydride complex **21** was formed after hydroxide addition and CO_2 release from complex **19**. Protonation generated complex **22** followed by CO_2 insertion to form the corresponding formate complex **81**. Formic acid was liberated to form complex **82**, which regenerated the Knölker's iron complex **22** after oxidative addition of H_2. Remarkably, a cooperative non-innocent behavior arose in the cyclic reaction.

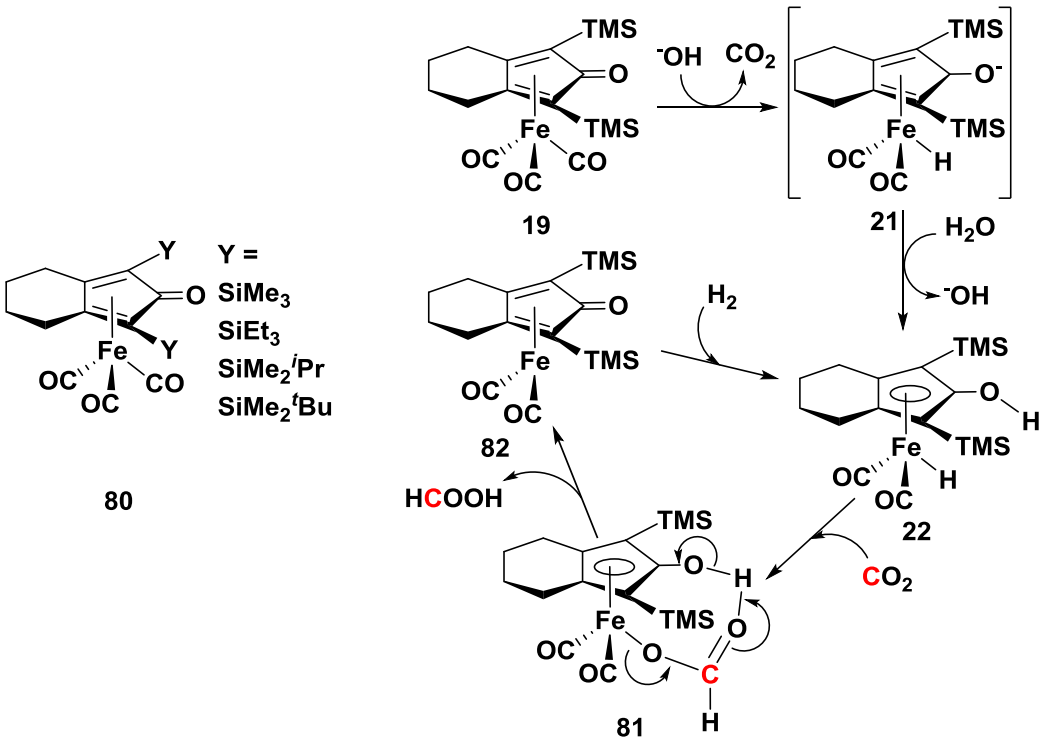

Scheme 27. The "Knölker's iron complexes" **80** and proposed mechanism for the hydrogenation of CO_2 by the related complex **19**

1.3.2.3 Reductive functionalization of CO_2 to produce C-C or C-N bonds containing organic compounds

As mentioned in section 1.3.1.4, stoichiometric C-C coupling of CO_2 and olefins were investigated with Fe(0) complexes. After multiple workup, yields of the corresponding esters or dicarboxylic acids were found as high as 60 %.[152,153,154] This iron catalyzed hydrocarboxylation process, which led to C-C bond containing organic compounds, was improved in 2012 (Scheme 28).[181] A range of sterically and electronically differentiated aryl alkenes were hydrocarboxylated efficiently using only 1 mol% $FeCl_2$, bis(imino)pyridine (**L**, 1 mol%), CO_2 (1 atm.) and a hydride source (EtMgBr, 1.2 eq.). This system exhibited high activity at room temperature, and excellent yields with near-perfect regioselectivity.

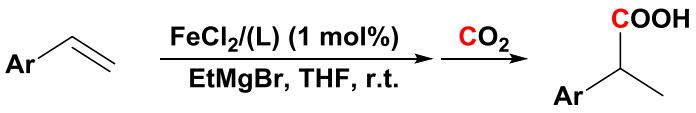

Scheme 28. Iron catalyzed hydrocarboxylation of aryl alkenes with CO_2

A plausible mechanism was suggested thanks to a battery of independent experiments (Scheme 29). Alkylation of the iron pre-catalyst (**$FeCl_2$L**) followed by coordination of styrene generated the organoferrate complex **84**, which reversibly underwent β-hydride elimination to generate the low-valent Fe-H complex **85**. This active complex led to the organoferrate complex **86** through reversible hydrometalation of styrene, which produced the initial organoferrate complex **83** and released the hydromagnesiated product **87** via a transmetalation reaction.

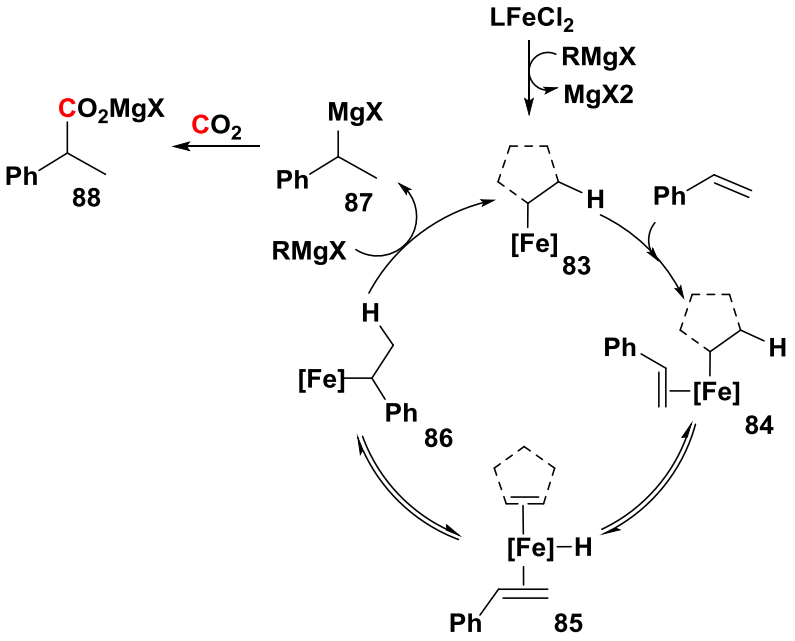

Scheme 29. Plausible mechanism for the iron catalyzed hydrocarboxylation

Kim, Shim and coworkers reported the synthesis of carbamates catalyzed by iron complexes in 1990.[182] Complex [(η^2-BPPF)Fe(CO)$_3$] (BPPF = 1'1-bis(diphenylphosphino)ferrocene) **89** was used to catalyze the reaction of CO_2 and secondary amines with alcohols (Scheme 30). The investigation revealed a reduced yield order depending on the utilization of secondary amines, and poorer yield was observed when using propargyl alcohol instead of acetylenic alcohol.

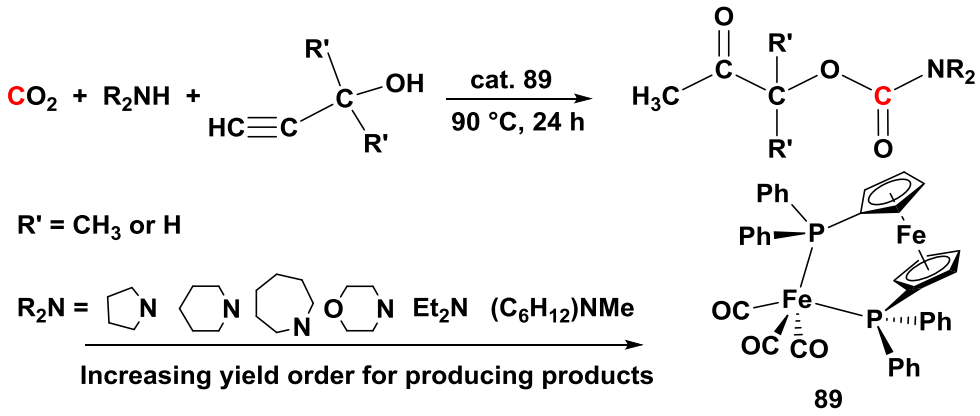

Scheme 30. Iron catalyzed synthesis of carbamates from CO_2 and secondary amines with alcohols

Reductive functionalization of CO_2 to generate C-N bond containing organic compounds was successfully achieved by using complex [FeX(PP_3)]BF_4 **79** (X = H or F) as pre-catalyst (Scheme 31). The catalytic reaction occurred at 100 °C in methanol. The reductive hydrogenation of CO_2 with

dimethylamine led to dimethylformamide (DMF) in a 75 % yield with a turnover number of 727 with catalyst **79** (X = H) under 30 atm. of CO_2 and 60 atm. of H_2. When using pre-catalyst **79** (X = F) the reaction produced DMF in 74 % yield and formic acid in 7.7 % under 30 atm. of CO_2 and 70 atm. of H_2, which corresponded to a turnover number higher than 5100.

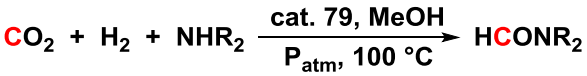

Scheme 31. Hydrogenation of CO_2 to formamides catalyzed by **79**

Using hydrosilanes as reductant, the reaction of CO_2 with amine was proved not only to afford formamides but also methylamines.[183] The transformation reaction was conducted in the presence of amines under only 1 atm. of CO_2 pressure at room temperature with 5 mol% of $Fe(acac)_2$ and tris[2-(diphenylphosphino)-ethyl]phosphine (PP_3) (Scheme 32) The activity of the catalytic system also depended on the nature of the hydrosilanes. For example, utilization of Et_3SiH, 1,1,4,4-tetramethyldisiloxane (TMDS) and PMHS led to no formylation while $PhSiH_3$ resulted in more than 95 % methylphenylformamide formation. Increasing the temperature to 100 °C led to methylamide with a 95 % yield after 22 hours.

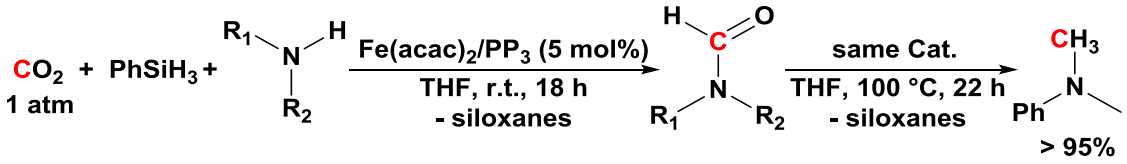

Scheme 32. Iron catalyzed reductive hydrosilylation of CO_2

1.3.3 Summary

Along these lines, iron complexes utilized in CO_2 transformation provided many interesting results, such as activation of CO_2 upon coordination, catalytic activation of CO_2 to generate carbonates and carbamates, reductive functionalization of CO_2 to formic acid or derived products, and to formamines or methylamines.

Although different types of highly active iron pre-catalysts have been reported including iron complexes bearing macrocyclic and chelating ligands (**65**-**80**, **89**) and even in situ generated iron compounds, there is still no clear guidance on choosing the most suitable iron complex as pre-catalyst. However, iron species such as the iron hydride complexes (**24**-**26**, **40**, **47** and **79** (X = H)) or in situ generated iron-hydride moieties (**18** and **22**) which supply Fe-H bonds for CO_2 insertion reactions, are of importance for further functionalization of this attractive C1 source.

Until now, the more valuable organic compounds formed from iron catalyzed reductive functionalization of CO_2 are very limited, with only C-N bond containing compounds been studied. An active and efficient iron based catalytic system for reductive functionalization of CO_2 is highly expected, and generation of larger scope of more valuable organic compounds from CO_2 will be the following goal.

Chapter 2

Chapter 2

Synthesis and characterization of a new family of iron complexes

2 Introduction

As mentioned in section 1.2, the Milstein PNL pincer type complexes featuring a picolyl fragment that can dearomatize/aromatize upon deprotonation/protonation at the benzylic position exhibit very impressive catalytic properties (Scheme 2 in section 1.2.1 and Figure 5 and Scheme 11 in section 1.2.2.2.3). In contrast, the coordination chemistry of another ligand featuring picolyl moieties, bis(2-picolyl)phenylphosphine (NPN), has been much less studied .[184–189] The presence of three donating atoms (two nitrogen and one phosphorus) as well as the methylene linker in the ligand allow it to adopt many different coordination modes, and the methylene linker has been found to be deprotonated upon coordination to lithium or tin (Figure 15).[185] However, the NPN ligand has never been shown to be engaged in a dearomatization/aromatization process when coordinated to a transition metal (or main group metal) center, despite the presence of two picolyl moieties by comparison to the series of PNL ligands.

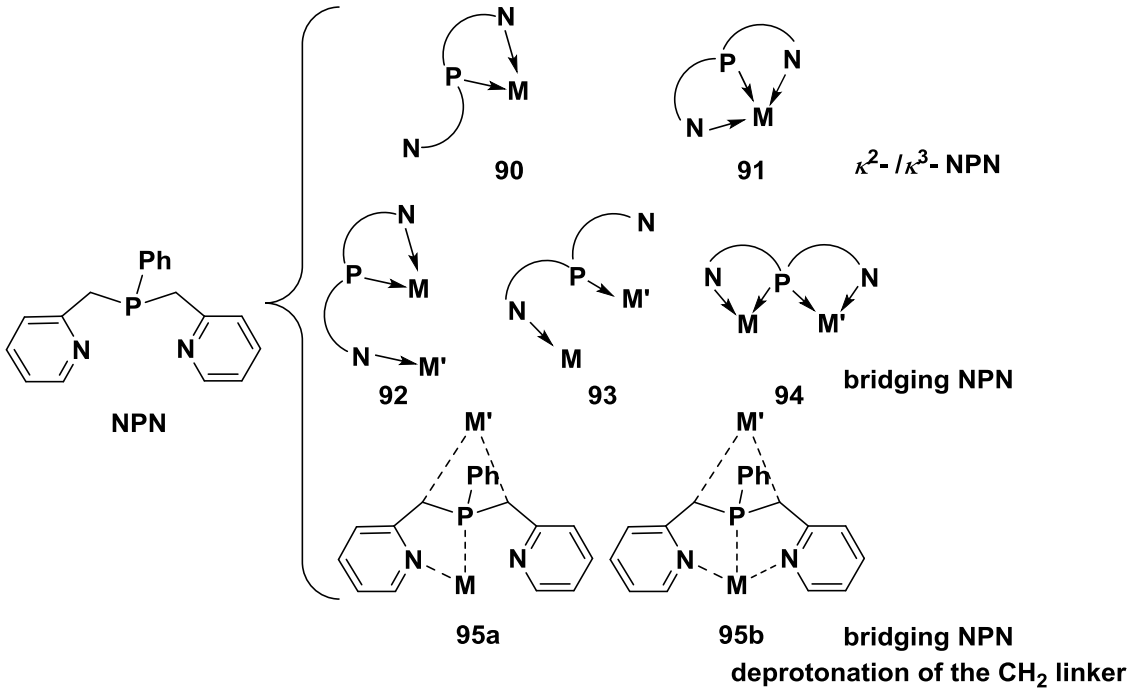

Figure 15. Reported different coordination modes of the NPN ligand

Due to the interesting properties of iron complexes bearing cooperative non-innocent ligands, we have selected the NPN (bis(2-picolyl)phenylphosphine) pincer ligand **96** (Figure 16) to prepare a new family of iron complexes. In this chapter, we describe the synthesis and characterization of a series of complexes illustrating the cooperative non-innocent behavior of

96. Three bonding modes of the ligand are described in section 2.2: bidentate $\kappa^{N,P}$-fashion **97**, bridging μ-$\kappa^{N,P}$:κ^{N}-fashion **98**, and tridentate $\kappa^{N,P,N}$-fashion **99**. Several ruthenium-based complexes and another bonding mode κ^{P}-NPN **100** are also reported in section 2.4.

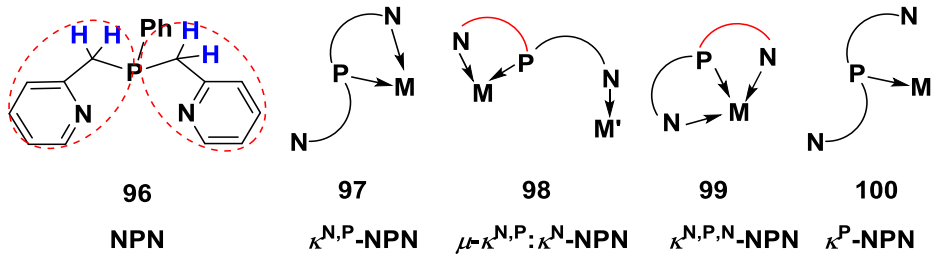

Figure 16. The cooperative non-innocent ligand NPN and its four coordination modes

The related NP ((2-picolyl)diphenylphosphine) ligand **101** has been reported to afford a bidentate PN-coordination with dearomatized pyridine ring to lithium, zinc or iron metal centers (**102**, Figure 16).[190,191] In our case, the coordination ability of the NP ligand to ruthenium and the two resulting bonding modes will be discussed in section 2.4.

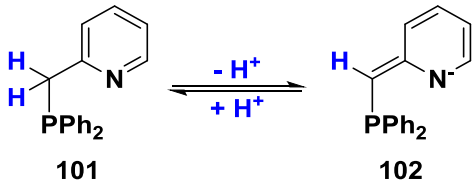

Figure 16. Bidentate ligand NP **101**

2.1 Synthesis of the iron precursor and of the ligands

2.1.1 Synthesis of the iron precursor ([Fe(N(TMS)$_2$)$_2$])

The highly reactive iron precursor [Fe(N(TMS)$_2$)$_2$] **103** was synthesized with a modified procedure from literature,[192,193] diethyl ether (Et_2O) being used as a solvent instead of THF (Scheme 33). The iron precursor FeX_2 (X = Cl or Br) in suspension in Et_2O was added to two equivalents of lithium bis(trimethylsilyl)amide in Et_2O at room temperature and stirred overnight. After workup, a green compound was obtained in 81 % yield. This green compound exists in two forms depending on temperature. At –40 °C, it is characterized as a dimer with trigonal planar iron centers and bridging amido groups by X-ray diffraction[193]. The dimeric form is maintained at -40 °C in solution. At room temperature, it is a liquid with a two-coordinate iron center possessing S_4 symmetry as indicated by NMR analyses.[192] For clarity, only the monomeric form of the iron precursor will be used during the discussion. ^{1}H NMR was characteristic of a

paramagnetic compound **103**, with a broad peak at δ = 59.42 ($w_{½}$ = 1.2 kHz) assigned to the protons of the methyl groups.

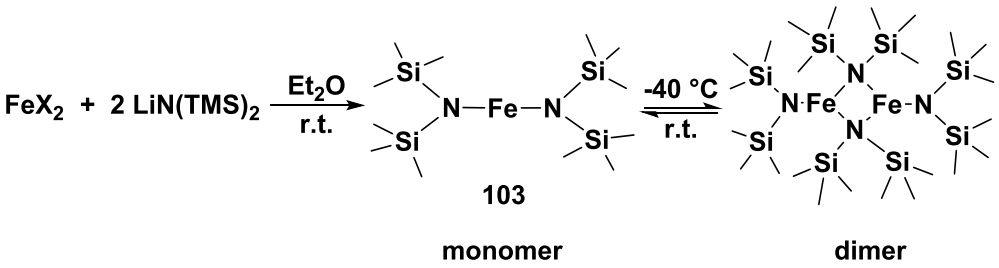

Scheme 33. Synthesis of iron precursor $[Fe(N(TMS)_2)_2]_2$ **103**

2.1.2 Synthesis of the ligands (NPN and NP)

The tri- and bi-dentate ligands were synthesized according to the literature methods, and pure compounds were obtained after work up with yields of 46 % and 36 %, respectively (Scheme 34).[184,194] Both ligands were characterized by multinuclear, ^{1}H, ^{31}P, ^{13}C NMR as well as infrared spectroscopy.

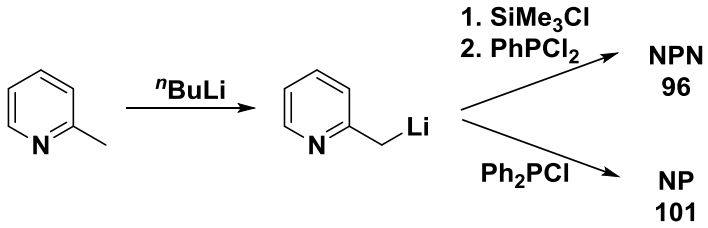

Scheme 34. Synthesis of ligands NPN **96** and NP **101** ligands

The ^{31}P NMR spectra of the tri- and bi-dentate ligands revealed single resonances at δ = -13.9 for NPN and δ = -10.6 for NP. The PCH_2 moieties in NPN were characterized by ^{13}C NMR with a resonance at δ = 37.7 ($^{1}J_{C\text{-}P}$ = 18.4 Hz), and similar doublet signal for PCH_2 was observed at δ = 39.1 ($^{1}J_{C\text{-}P}$ = 16.5 Hz) for NP. Characteristic NMR signals of the PCH_2 protons in NPN belonged to an ABX spin system (A = B = H, X = P).[184,195] The ^{1}H and ^{1}H{^{31}P} experiments evidenced that the two protons of the PCH_2 moieties in NPN were chemically inequivalent with the existence of $^{1}J_{H\text{-}H}$ = 13.3 Hz, while the PCH_2 protons in NP exhibited a single signal at δ = 3.63.

	δ_{PCH2}	δ_{PCH2}	$^1J_{P-C}$	δ_{PCH2}	$^1J_{H-H}$
NPN	-13.9	37.7 (d)	18.4	3.42(dd)/3.35(d)	13.3
NP	-10.6	39.1 (d)	16.5	3.63(s)	---

Table 1. Selected NMR parameters for NPN **96** and NP **101** ligands

2.2 Synthesis and characterization of the iron complexes

2.2.1 Synthesis of the iron complexes

Owing to the high reactivity of the iron precursor $[Fe(N(TMS)_2)_2]$ **103**, the coordination of NPN **96** to iron was conducted with special attention to temperature and time settings. This allowed isolating a series of complexes **104-106** displaying three different NPN coordination modes that will be described in detail in the next sections. After mixing NPN with the iron precursor at -78 °C, the pentane solution was warmed to -30 °C and stirred at this temperature for 90 min. A yellow precipitate was then observed and the complex $[Fe(N(TMS)_2)_2(\kappa^{N,P}\text{-NPN})]$ **104** could be isolated after filtration in 28 % yield. Monocrystals suitable for X-ray diffraction analysis were grown by mixing the precursor with NPN at -30 °C in a pentane/toluene solution. Complex **104** was not stable (neither in solution nor in the solid state) at room temperature, leading to the formation of the dinuclear green complex $[Fe(N(TMS)_2)(\mu\text{-}\kappa^{N,P}\text{:}\kappa^{N}\text{-NPN})]_2$ **105**, which was isolated in good yield of 81 % by the addition of NPN to the same precursor after prolonged stirring time (at -30 °C for 3 h and at room temperature for 45 min). Similarly to complex **104**, monocrystals of **105** for X-ray determination were grown in a pentane/toluene solution system by concentrating the mixture at room temperature. Solutions of **105** were unstable at room temperature giving rise to complex **106** and unexpected compounds with black particles among them. Complex $[Fe(\kappa^{N,P,N}\text{-NPN})_2]$ **106** could also be directly isolated as a brown powder in a 55 % yield from the reaction of two equivalents of NPN with precursor **103** after 36 h at room temperature. Unlike complexes **104** and **105**, crystals of **106** suitable for X-ray diffraction were obtained by mixing $[Fe(N(TMS)_2)_2]$ and NPN in Et_2O at -78 °C, and leaving the solution at room temperature within 2 days.

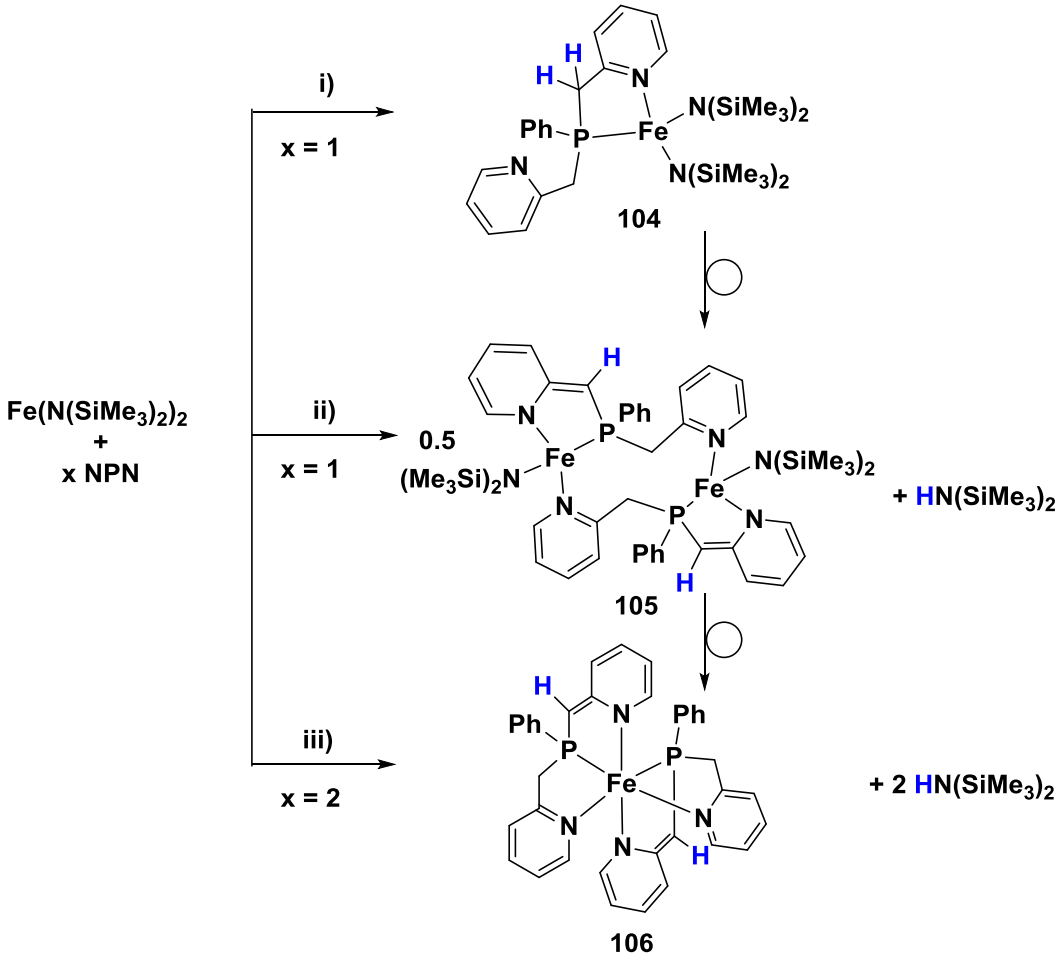

Scheme 35. Synthesis of complexes **104**-**106**. Conditions: (i) mixing at -78 °C and stirring at -30 °C for 90 min; (ii) mixing at -78 °C, stirring at -30 °C for 3 h and at r.t. for 45 min; (iii) mixing at -78 °C, stirring at -30 °C for 3 h, and then at r.t. for 36 h

The combination of several techniques: X-ray diffraction, NMR (in solution and in the solid state), powder X-ray diffraction, Evans method, Mössbauer, elemental analysis, high resolution mass spectrometry and infrared spectroscopy was carried out to clearly characterize this family of complexes, being either paramagnetic or diamagnetic.

2.2.2 X-ray diffraction of 104-106

Single crystals of **104** crystallized in the monoclinic space group *P* 1 $2_1/c$ 1 with Z = 4. Figure 17 depicts the coordination geometry of the iron(II) ion in a distorted tetrahedral geometry. The NPN ligand coordinates to the metal center in a bidentate $\kappa^{N,P}$-fashion, and one picolyl arm remains pendant. The two amido ligands remain on the iron center and complete the coordination sphere of the metal center. The Fe1-N1 and Fe1-P1 bond distances were 2.2236(12) Å and 2.5579(4) Å, and the N1-Fe1-P1 angle was 75.03(3) °. The two C-C bond distances from

related methylene moiety and pyridine ring were rather similar to each other (*d*C1-C2 = 1.500(2) Å and *d*C7-C8 = 1.498(2) Å), and comparable to the analogous distances in [$PdCl_2(\eta^2$-NPN)] (*d*C1-C2 = 1.490(5) Å and *d*C7-C8 = 1.499(5) Å).[187] The geometrical parameters are given in Table 2.

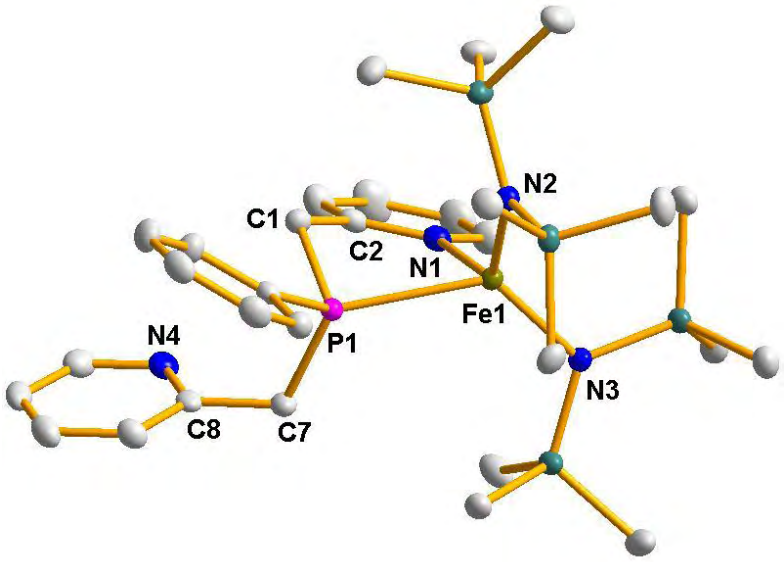

Figure 17. Molecular structure of complex [Fe(N(TMS)$_2$)$_2$($\kappa^{N,P}$-NPN)] **104**, ellipsoids are given at the 50 % probability level and hydrogen atoms are omitted for clarity

Complex **104**			
Fe(1)-N(1)	2.2236(12)	Fe(1)-N(2)	1.9663(11)
Fe(1)-N(3)	1.9799(11)	Fe(1)-P(1)	2.5579(4)
C(1)-C(2)	1.500(2)	C(7)-C(8)	1.498(2)
N(1)-Fe(1)-N(2)	122.52(5)	N(1)-Fe(1)-N(3)	99.66(5)
N(1)-Fe(1)-P(1)	75.03(3)	N(2)-Fe(1)-N(3)	124.28(5)
N(2)-Fe(1)-P(1)	100.73(3)	N(3)-Fe(1)-P(1)	125.98(4)
C(2)-C(1)-P(1)	109.04(10)	C(8)-C(7)-P(1)	116.36(10)

Table 2. Selected bond distances (Å) and angles (°) for **104**

Complex **105** crystallized in a monoclinic space group *P* $2_1/c$ with Z = 2. The X-Ray diffraction analysis on monocrystals of **105** revealed a dimeric structure with an inversion center. The iron centers exhibit a distorted tetrahedral geometry and the NPN ligands span the metal centers in a bidentate $\kappa^{N,P}$-mode for the first iron and N-monodentate κ^{N}-mode for the second iron. The coordination sphere is then completed by an amido ligand on each metal. The Fe-N distance of the dearomatized pyridine ring (*d*Fe1-N1 = 2.0654(15) Å) is shorter than the Fe-N distance of the

aromatic pyridine ring (*d*Fe1-N2 = 2.1548(15) Å). The lengthening of the later value could also arise from the absence of a chelate effect in **105** in comparison with complex **104**. The differences in Fe1-P1 bond distance (2.5579(4) Å in **104** and 2.4387(5) Å in **105**) and in N1-Fe1-P1 angle (75.03(3) ° in **104** and 82.49(4) ° in **105**) were caused by the absence of a chelate effect of the NPN ligand. Importantly, the methylene linker of the NP-bidentate moiety has been deprotonated. The anionic charge is thus formally delocalized over a C5=C6 double bond and a dearomatized pyridine ring. As expected the C5=C6 bond distance of 1.389(3) Å is shorter than the C-C single bond (*d*C17-C18 = 1.502(2) Å) of the other picolyl moiety on the same ligand or of the related C-C bond in complex **104** (*d*C1-C2 = 1.500(2) Å). The X-ray structure of **105** is presented in Figure 18, and selected bond distances and angles are displayed in Table 3.

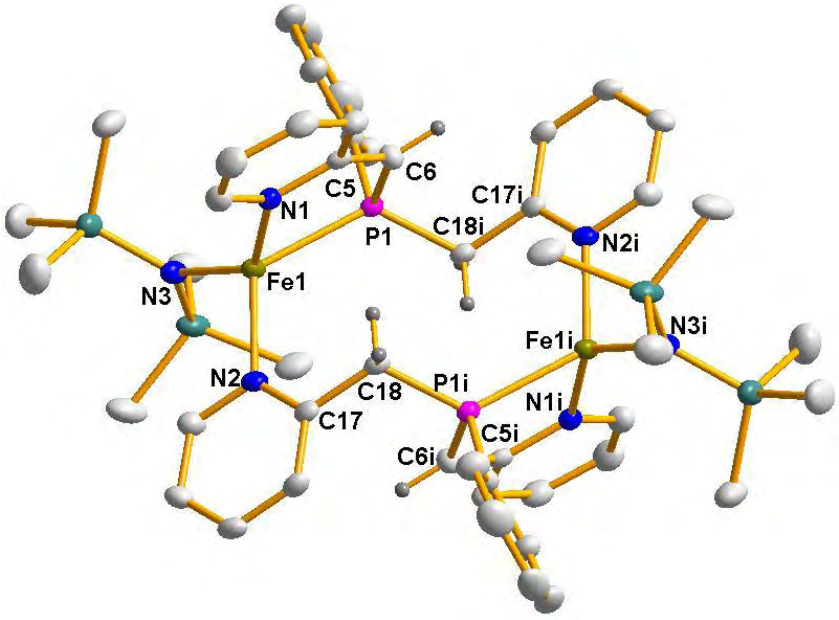

Figure 18. Molecular structure of complex [Fe(N(TMS)$_2$)(μ-$\kappa^{N,P}$:κ^{N}-NPN)]$_2$ **105** (full structure has been generated by applying the inversion center symmetry), ellipsoids are given at the 50 % probability level and hydrogen atoms are omitted for clarity except for the CH and CH$_2$ linkers between the phosphorus atom and the pyridine rings, symmetry operator for the generation equivalent position: -x+1, -y, -z (i)

Complex **105**			
Fe(1)-N(1)	2.0654(15)	Fe(1)-N(2)	2.1548(15)
Fe(1)-N(3)	1.9499(15)	Fe(1)-P(1)	2.4387(5)
C(5)-C(6)	1.389(3)	C(6)-P(1)	1.7524(19)
C(17)-C(18)	1.502(2)	C(18)-P(1)^{i}	1.8530(18)
N(1)-Fe(1)-N(2)	101.50(6)	N(1)-Fe(1)-N(3)	132.71(6)
N(1)-Fe(1)-P(1)	82.49(4)	N(2)-Fe(1)-N(3)	105.72(6)
N(2)-Fe(1)-P(1)	121.53(4)	N(3)-Fe(1)-P(1)	113.30(5)
C(5)-C(6)-P(1)	119.47(14)	C(17)-C(18)-P(1)^{i}	113.51(12)

Symmetry codes: ^{i} –x+1, -y, -z

Table 3. Selected bond distances (Å) and angles (°) for **105**

The X-Ray structure of **106** confirmed the coordination of two NPN ligands to one iron centre in a tridentate $\kappa^{N,P,N}$-coordination mode with dearomatization of one of the pyridine unit on each NPN ligand. Complex **106** crystallized in the monoclinic space group *P* $2_1/c$ with Z = 4. The coordination geometry of the iron center is in good approximation an octahedron with four nitrogen atoms and two phosphorus atoms from two equivalent NPN ligands. The axial positions are occupied by the two nitrogen atoms of the dearomatized rings with bond distances of *d*Fe1-N2 = 2.011(2) Å and *d*Fe-N3 = 2.013(2) Å, and with a bond angle of N2-Fe1-N3 = 177.51(10) °, respectively. The equatorial plane is occupied by the two phosphorus atoms in *cis* position and the two nitrogen atoms of the pyridine rings *trans* to the phosphorus atoms. The mean deviation from the plane is 0.0407 Å and the sum of the angles at Fe1 is 360.0 °. The Fe-N bond distances of the aromatic pyridine rings (*d*Fe1-N1 = 2.046(2) Å and *d*Fe1-N4 = 2.058(2) Å) are slightly longer than the Fe-N distances of the dearomatized pyridine rings. The C=C double bonds (*d*C7–C8 = 1.396(4) Å and *d*C19–C20 = 1.399(4) Å) are shorter than the related C-C single bonds (*d*(C1–C2) = 1.499(4) Å and *d*C25–C26 = 1.491 Å). In complex [Fe(κ^3-NPN)$_2$][Cl$_3$FeOFeCl$_3$],[184] in which two NPN ligands also coordinated to the iron center via a κ^3-fashion but without dearomatization of the pyridine rings, the corresponding C-C single bonds distances (1.506(8) Å and 1.506(8) Å) are very close to the ones in complex **106**. Figure 19 depicts the X-ray structure of complex **106**, Table 4 summarizes important bond lengths and angles.

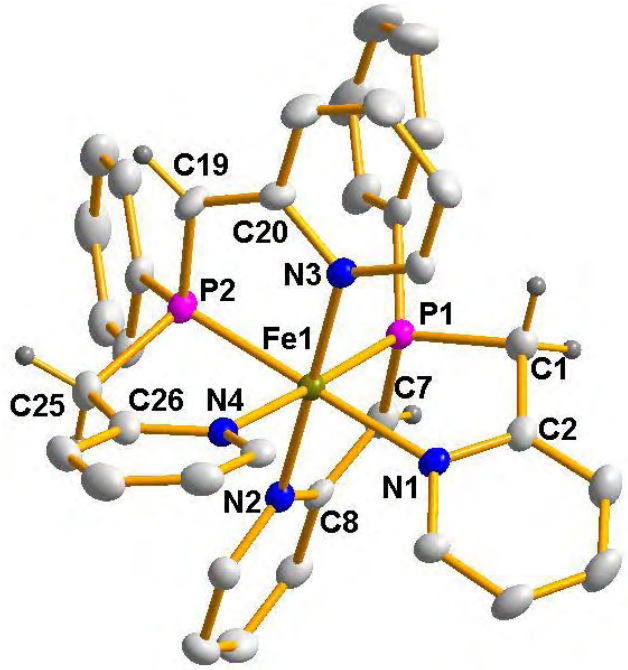

Figure 19. Molecular structure of complex [Fe($\kappa^{N,P,N}$-NPN)$_2$] **106**, ellipsoids are given at the 50 % probability level and hydrogen atoms are omitted for clarity except for the CH and CH_2 linkers between the phosphorus atom and the pyridine rings

Complex **106**			
Fe(1)-P(1)	2.1564(9)	P(2)-Fe(1)	2.1547(9)
N(1)-Fe(1)	2.046(2)	N(2)-Fe(1)	2.011(2)
N(3)-Fe(1)	2.013(2)	N(4)-Fe(1)	2.058(2)
C(1)-C(2)	1.499(4)	C(7)-C(8)	1.396(4)
C(19)-C(20)	1.399(4)	C(25)-C(26)	1.491(4)
P(2)-Fe(1)-P(1)	96.80(3)	N(1)-Fe(1)-P(1)	82.28(7)
N(2)-Fe(1)-P(1)	84.75(7)	N(3)-Fe(1)-P(1)	93.34(8)
N(4)-Fe(1)-P(1)	177.73(8)	N(1)-Fe(1)-P(2)	179.07(8)
N(2)-Fe(1)-P(2)	93.50(7)	N(3)-Fe(1)-P(2)	85.12(8)
N(4)-Fe(1)-P(2)	81.13(7)	N(2)-Fe(1)-N(1)	86.27(10)
N(3)-Fe(1)-N(1)	95.07(10)	N(1)-Fe(1)-N(4)	99.79(10)
N(2)-Fe(1)-N(3)	177.51(10)	N(2)-Fe(1)-N(4)	96.30(10)
N(3)-Fe(1)-N(4)	85.56(10)		

Table 4. Selected bond distances (Å) and angles (°) for **106**

2.2.3 NMR characterization of 104 -106

The solution ^{1}H NMR spectra of complexes **104** and **105** revealed broad paramagnetic signals spanning from +130 to -30 and +175 to -30 ppm, respectively. No signals were observed by ^{13}C or ^{31}P NMR for both complexes in reason of the iron paramagnetic centers. Additional NMR characterization for compounds **104** and **105** were conducted in the solid state. The solid state MAS ^{1}H NMR spectra of **104** and **105** did not provide any useful information for characterization. The solid state MAS ^{31}P NMR signals were also difficult to observe, the phosphorus atoms being in close proximity to the iron centers: for both complexes, the detected signals were very broad, δ = 39 ($w_{1/2}$ = 13.7 KHz) and 41 ($w_{1/2}$ = 13.0 KHz), for **104** and **105**, respectively (Figure 20). In addition, due to the sensitivity of both compounds, decompositions were observed during the analyses and intense MAS ^{31}P NMR signals for free NPN **96** (δ = -12.2 ($w_{1/2}$ = 1.0 KHz)) and complex **106** (δ = 86.5 ($w_{1/2}$ = 1.8 KHz)) were observed; partially masking the signal of compounds **104** and **105**. The time dependence MAS ^{31}P NMR experiments were controlled with compound **105**, and signal for free NPN **96** decreased while the signal for **106** increased obviously within 5 hours (Figure 21). More interestingly, the MAS ^{13}C NMR spectra exhibited specific NMR signatures for **104** and **105**, with signals spanning from *ca.* +600 to –100 ppm.

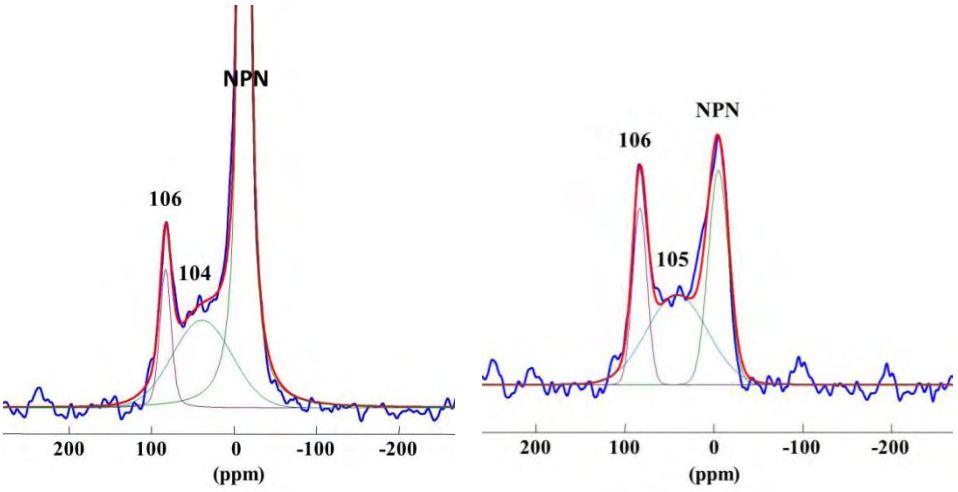

Figure 20. MAS ^{31}P NMR spectra of complex **104** (left) and **105** (right) in the solid state

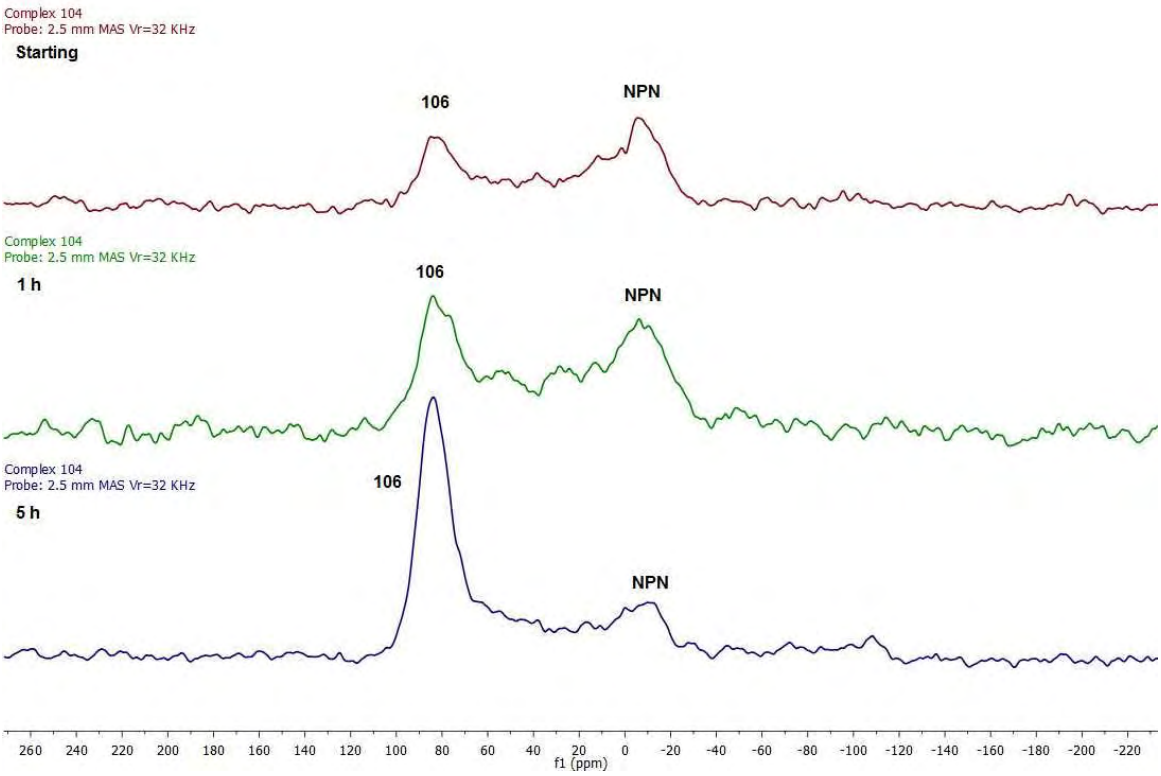

Figure 21. Time dependence of MAS ^{31}P NMR spectra (161.8 MHz, 298 K) of **105** in the solid state

Solution state NMR analyses indicated that complex **106** is a diamagnetic compound in agreement with a low spin iron(II) complex. NMR data allowed to characterize the NPN ligands around the iron center, and particularly to evidence the deprotonation of one benzylic moiety on each NPN ligand. The ^{31}P NMR spectrum showed one resonance at δ = 87.0 ppm (in toluene-D_8, δ = 86.0 ppm in C_6D_6) indicating two equivalent NPN ligands in solution. The ^{1}H NMR spectrum showed three signals in the aliphatic region between 3 and 4.5 ppm. The signals at δ = 4.06 and δ = 3.14 correspond to the inequivalent protons of the methylene linkers (PCH_2 moieties) resonating as an AB pattern upon ^{31}P decoupling ($^{2}J_{H\text{-}H}$ = 15.5 Hz) whereas the third signal at δ = 3.50 appears as a singlet and was assigned to the PCH moieties (Figure 19). ^{13}C NMR chemical shifts supported the formulation of the protonated/deprotonated methylene arms: the resonance at δ = 44.4 for the PCH_2 moiety and at δ = 58.7 for the PCH (deprotonated methylene arm) moiety, respectively. MAS ^{31}P NMR allowed the solid state characterization of this nucleus.

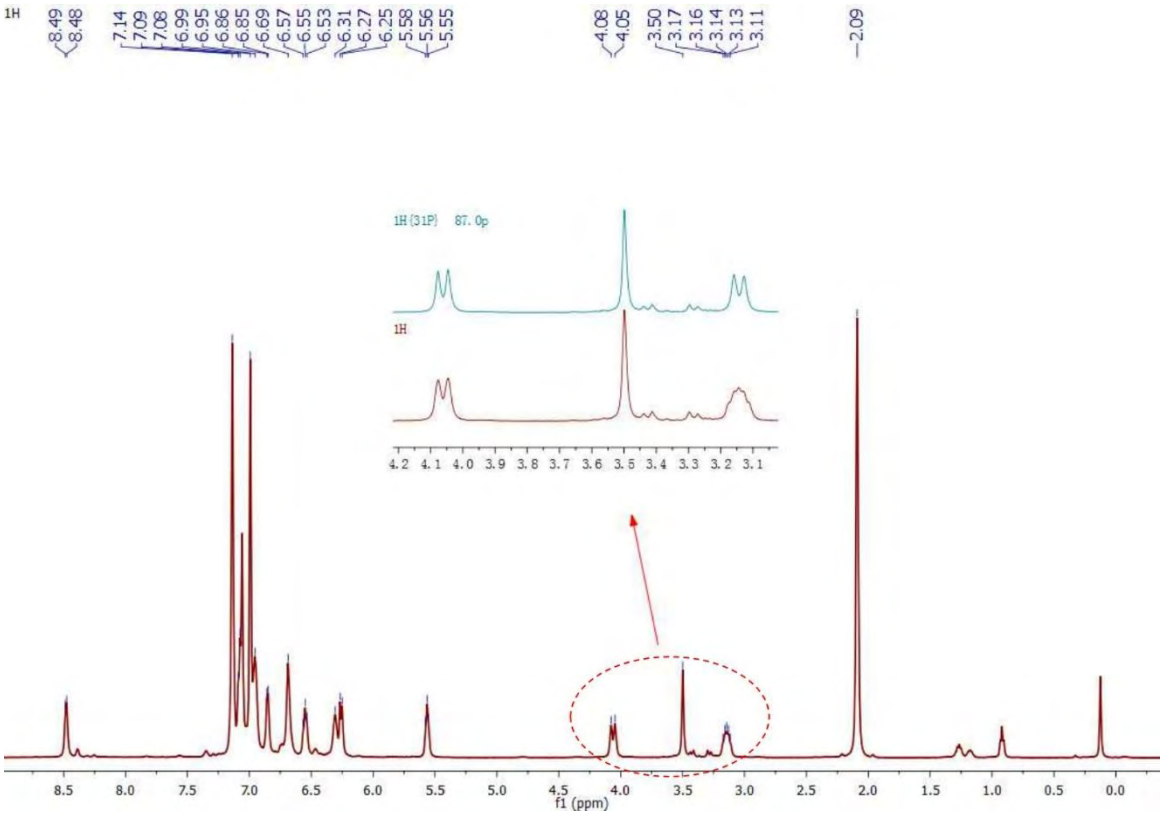

Figure 22. ^{1}H NMR spectrum of complex **106** in solution (500.3 MHz, Tol-D_8, 240 K)

2.2.4 Mössbauer data for the paramagnetic complexes 104 and 105

^{57}Fe Mössbauer measurements for **104** and **105** were performed at different temperatures. For complex **104**, the spectrum consisted of a doublet with an isomer shift of δ = 0.7676(18) mm·s^{-1} and a quadrupole splitting of ΔE_q = 0.9572(35) mm·s^{-1} ($W_{1/2}$ = 0.29(12) mm s^{-1}) for a high spin iron(II) at 80 K. Rising the temperature to 260 K, the spectrum featured a doublet with δ = 0.680(12) mm·s^{-1} and ΔE_q = 0.910(23) mm·s^{-1} ($W_{1/2}$ = 0.27(11) mm s^{-1}), indicating a high spin iron(II) as well, comparable to the data obtained at 80 K. Due to the instability of this complex, higher temperature Mössbauer measurements could not be recorded.

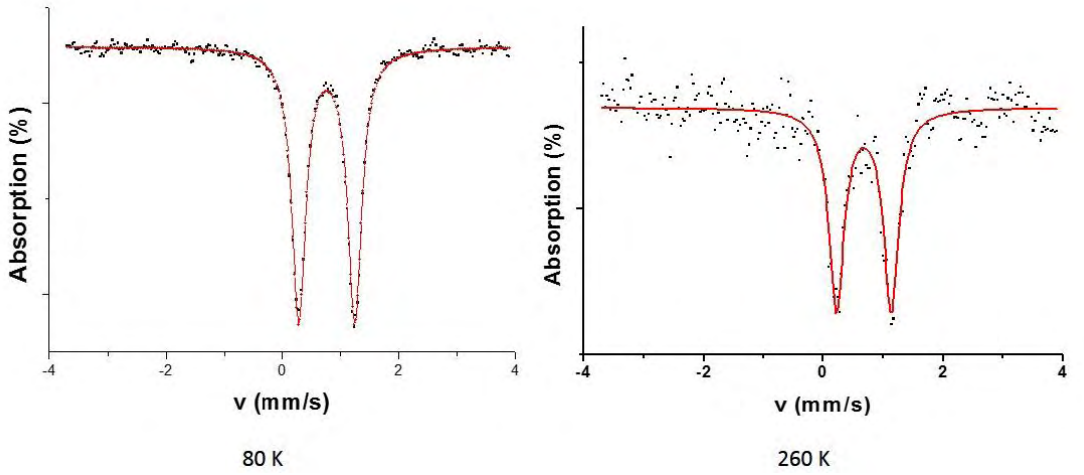

Figure 23. Mössbauer spectra of complex **104** at 80 K and 260 K

In the case of complex **105**, the spectrum exhibited a symmetric quadrupole doublet with an isomer shift of δ = 0.7164(12) mm·s^{-1} and a quadrupole splitting of ΔE_q = 2.1553(23) mm·s^{-1} ($W_{1/2}$ = 0.72(20) mm s^{-1}) for a high spin iron(II) at 80 K. The room temperature (293 K) spectrum displayed a superposition of two doublets featuring a high spin iron(II) (δ = 0.600(16) mm·s^{-1} and ΔE_q = 2.078(32) mm·s^{-1} ($W_{1/2}$ = 0.43(49) mm s^{-1})) and a low spin iron(II) (δ = 0.357(44) mm·s^{-1} and ΔE_q = 1.069(93) mm·s^{-1} ($W_{1/2}$ = 0.25(23) mm s^{-1}) with relative fraction of 49 % and 51 %, respectively. This observation clearly revealed the existence of an intermediate phase at 293 K with almost equal amounts of high spin and low spin iron(II) species. No higher temperature Mössbauer experiments were conducted because complex **105** is too sensitive at higher temperature as well as in air (Mössbauer measurements at higher temperatures are performed under air).

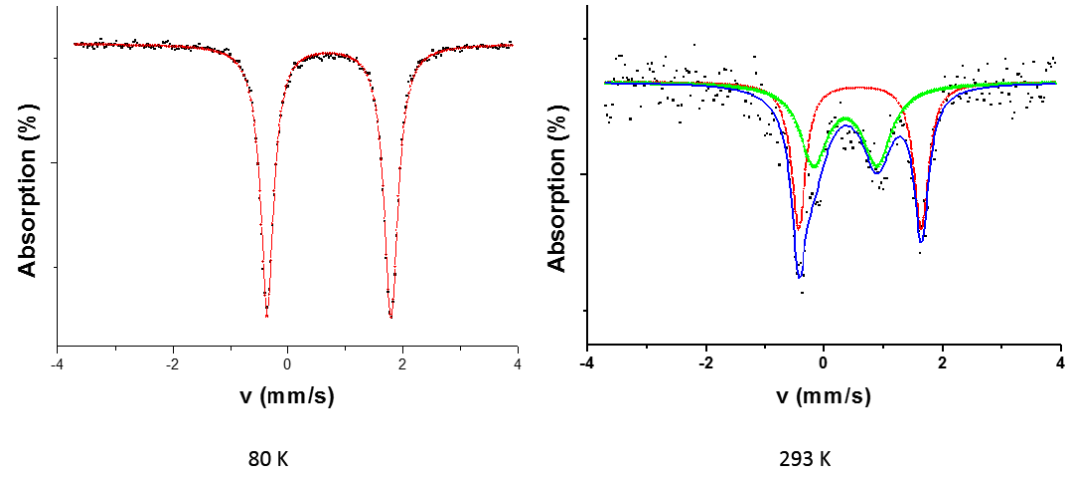

Figure 24. Mössbauer spectra of complexes **104** at 80 K and 293 K

2.2.5 Evans method and EPR measurements of 105

Evans measurements is a NMR method that allows to determine the magnetic susceptibility of a compound in solution.[196,197] The paramagnetic complex **105** was dissolved in C_6D_6 solution containing tetramethylsilane as an inert reference substance in a NMR tube. A capillary, containing the same concentration of tetramethylsilane in C_6D_6, was placed into the prepared NMR tube. By ^{1}H NMR, two resonances (at δ = 0.00 and -0.03, Figure25) for the methyl protons of tetramethylsilane in the two solutions were obtained due to the different volume susceptibilities.

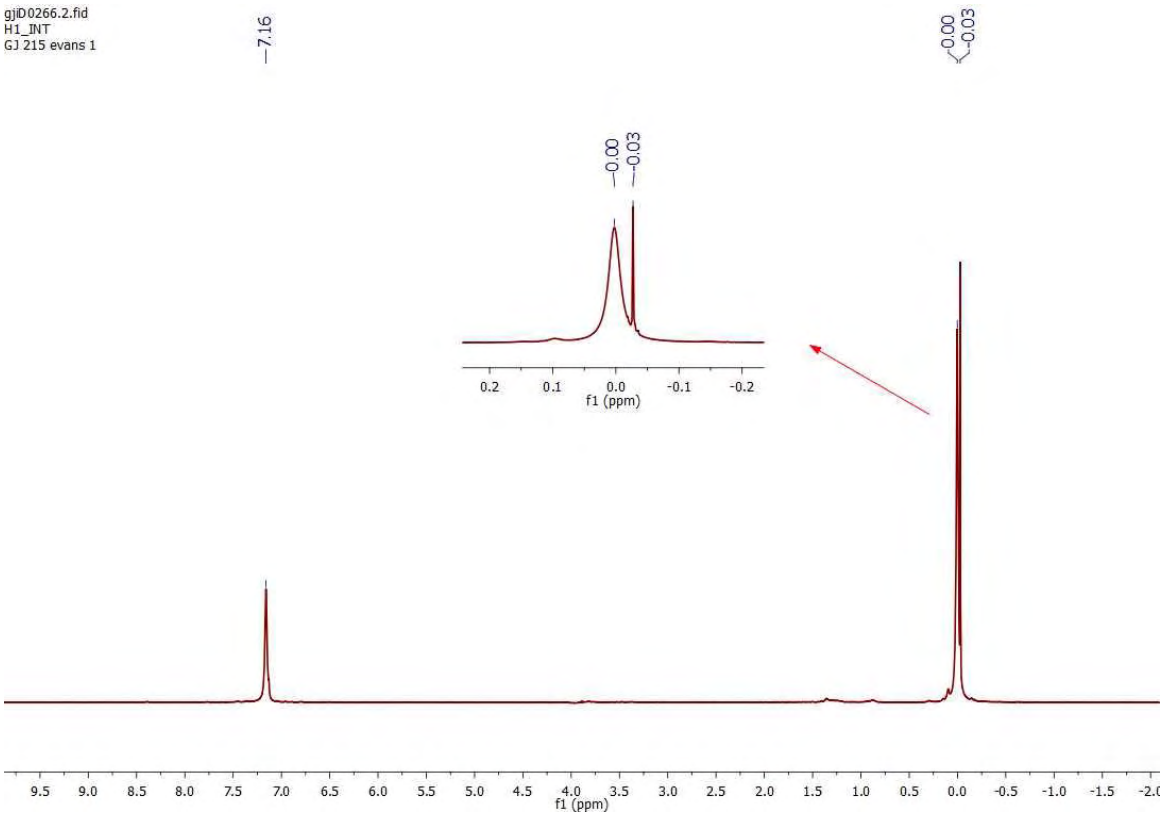

Figure 25. ^{1}H NMR of complex **105** in 1 % tetramethylsilane C_6D_6 solution with a capillary containing atetramethylsilane C_6D_6 solution, 5.1 mM, 400.1 MHz, 298 K

The mass susceptibility (X_g) was then calculated according to equation 1 in Scheme 36. By multiplying the molar mass (M) of the complex one obtains the molar susceptibility (X_M eq 2), which yielded the paramagnetic susceptibility (X_{para}) after correction of diamagnetic susceptibility (X_{dia}, eq 3 and 4). The effective magnetic moment (μ_{eff}) was the then calculated according to equation 5. Where X_g stands for mass susceptibility of the solute ($cm^3 \cdot g^{-1}$), Δf stands for the observed frequency shift of reference resonance (Hz), F is the frequency at which the proton resonances are being taken (Hz), and m equals to the mass of substance per cm^3 of

solution. For complex **105**, the calculated effective magnetic moment was 2.17 μ_B, which was lower than the spin-only value of a dimeric Fe(II) (μ_{SO} = 6.9 μ_B). This difference might be the result of antiferromagnetic couplings between the two iron ions.

$$X_g = -\frac{3\Delta f}{4\pi Fm} \quad (1)$$

$$X_M = X_g M \quad (2)$$

$$X_{para} = X_M + |X_{dia}| \quad (3)$$

$$X_{dia} = 0.5\ M*10^{-6}\ cm^3\ g^{-1} \quad (4)$$

$$\mu_{eff} = 2.828\sqrt{X_{para}\ T} \quad (5)$$

Scheme 36. Step by step calculating the effective magnetic moment (using tetramethylsilane as reference)

Electron paramagnetic resonance (EPR) spectroscopy is a technique for studying substances (particularly metal complexes) with unpaired electrons. EPR measurements have been conducted for complex **105** in the solid state and in solution (THF or toluene) at 4 K. However, it was impossible to extract any useful information from the observed spectra.

2.2.6 Powder X-ray measurement

As shown in Figure 26, the powder X-ray experimental data of complex **105** fitted with the simulated data from its single crystal at the beginning of the measurement but then completely differed. This observation might result from rapid decomposition under the measurement conditions. (Powder X-ray measurement was performed with a closed capillary under air.)

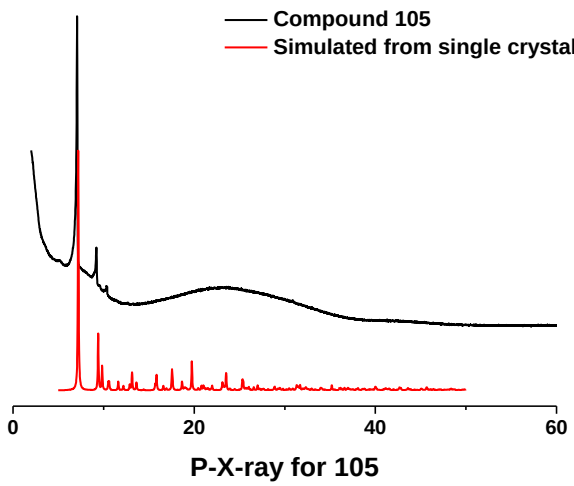

Figure 26. Powder X-ray diffraction spectrum of complex **105**

2.3 Reactivity of complex 105

Upon coordination to the iron precursor, deprotonation of the NPN ligand was observed leading to the dearomatization of a pyridine ring and the formation of a dinuclear compound **105**. It is noteworthy that dinuclear iron species are key species in hydrogenase processe,[198,199] as very active molecular catalysts for hydrogen production and uptake.[200] To exploit the reactivity of complex **105** featuring an activated ligand is thus of interest.

2.3.1 Reactivity of 105 toward CO_2

When subjecting complex **105** at room temperature to a pressure of CO_2, a red precipitate **107** was formed immediately regardless the pressure of CO_2 (1 to 3 atm.) and the solvent (Et_2O, THF or C_6D_6). It was not necessary to control the reaction temperature rigorously (unlike the synthesis of compound **104**-**106**) due to the rapid generation of **107** and its stability at room temperature. Compound **107** was found insoluble in organic solvents and no solution state NMR analysis could be conducted.

When performing the reaction in C_6D_6, ^{31}P NMR control of the filtrate showed two doublet signals at δ = 94.5 and 78.7. ^{1}H NMR gave a diamagnetic signal but no ^{13}C-H coupling resonance was observed when using $^{13}CO_2$ for the reaction, which indicated that the CO_2 adduct compound **107** was the red precipitate formed during the reaction. Solid state NMR , Mössbauer, elemental analysis and infrared spectroscopy analyses were thus conducted to analyze this compound.

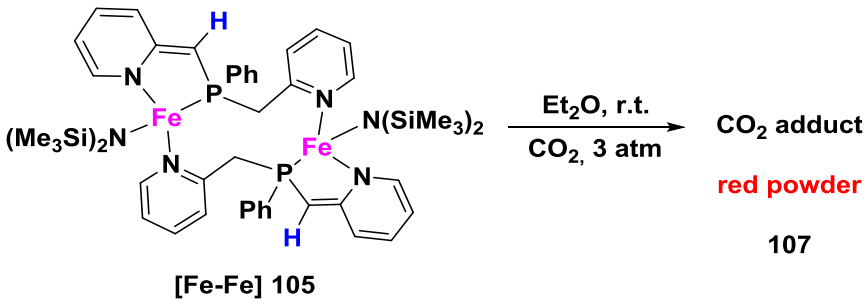

Scheme 37. Preparation of CO_2 adduct **107**

2.3.1.1 NMR characterization of 107 in the solid state

The MAS ^{31}P NMR spectrum revealed a broad signal at δ = 82.4 ($w_{1/2}$ = 6.9 KHz) for compound **107**, which was close to the signal corresponding to compound **106** (sandwich-like (NPN)Fe(NPN) structure, δ = 86.5 ($w_{1/2}$ = 1.8 KHz)). It might signify that the coordination environment of the iron centers could be similar to **106** and not to **105**. In addition, **107** was very stable under such solid state NMR measurement conditions (a high temperature effect can always happen due to high spinning conditions), no free ligand or other compounds were observed even upon prolonged measurement times. Compound **107** was also sensitive as colour changed in 3 minutes upon air exposure. No useful information was gained from the MAS ^{1}H and ^{13}C NMR measurements.

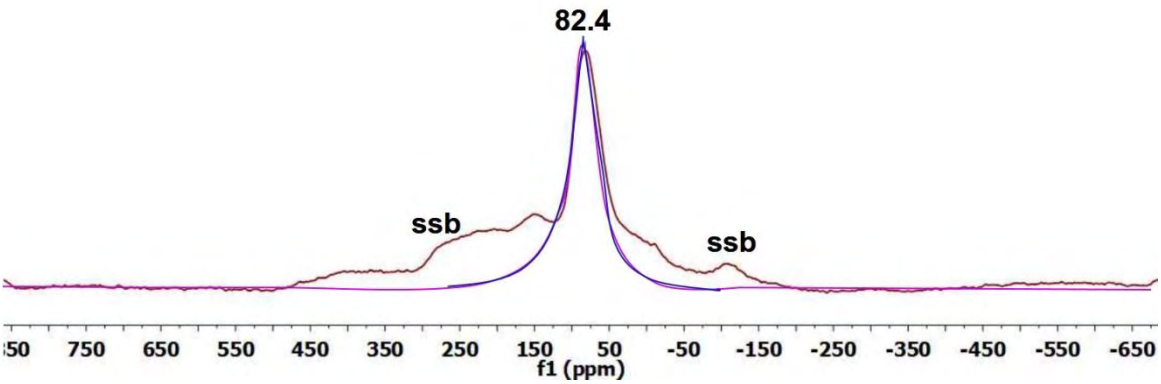

Figure 27. MAS ^{31}P NMR spectrum of compound **107** in the solid state

2.3.1.2 Mössbauer measurement of 107

^{57}Fe Mössbauer measurements of **107** were performed at three different temperatures. At 80 K, the spectrum showed a superposition of two doublets featuring low spin and high spin iron(II) with relative fractions of 49 % and 51 % (isomer shifts and quadrupoles of δ = 0.3410(51) and

ΔE_q = 0.646(10) mm·s^{-1} ($W_{1/2}$ = 0.25(9) mm s^{-1}), and δ = 1.121(12) and ΔE_q = 2.465(24) mm·s^{-1} ($W_{1/2}$ = 0.55(21) mm s^{-1})), respectively. At 260 K, the spectrum showed only one doublet with δ = 0.286(15) mm·s^{-1} and ΔE_q = 0.766(25) mm·s^{-1} ($W_{1/2}$ = 0.29(11) mm s^{-1}) featuring low spin iron(II). Rising the temperature to 293 K, similar doublet was observed with δ = 0.290(22) mm·s^{-1} and ΔE_q = 0.741(36) mm·s^{-1} ($W_{1/2}$ = 0.27(23) mm s^{-1}) which pointed to low spin iron(II). This observation revealed the existence of an intermediate phase of both high and low spin iron(II) species in almost equal amounts, and thus a structure of HS ↔ (HS/LS)/2 ↔ LS type.[201–203]

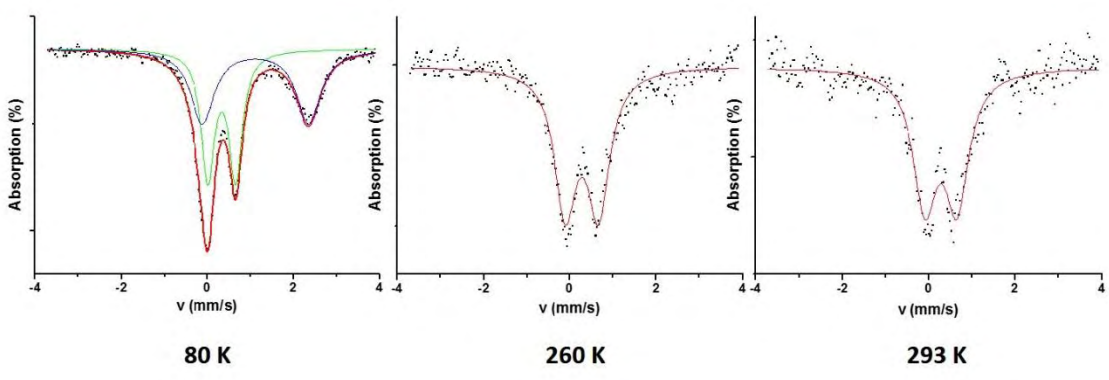

Figure 28. ^{57}Fe Mössbauer spectra of **107** at 80, 260 and 293 K

2.3.1.3 Infrared characterization of 107

It is interesting to compare our data with the compounds resulting from the reaction of CO_2 with the Milstein PNL pincer type complexes.[99,41,40,105–107,100,30,108,109] Several species are listed in Figure 29.[22,26,108,109,204–206] CO as a ligand was also considered due to the known disproportionation of CO_2 upon coordination to metal complexes (chapter 1, section 1.3.1.3).

Complex **108** was synthesized from the CO_2 insertion into a Fe-H bond of complex **26**. Complex **110** was obtained by the nucleophilic addition of the anionic carbon of an activated pincer arm to the central carbon of CO_2. An oxygen atom can then interact with the Ru center in **110**. Complex **109** was reported to account for the possible CO_2 disproportionation. The infrared spectroscopic data of the CO_2 (CO) moieties are shown in Table 5.

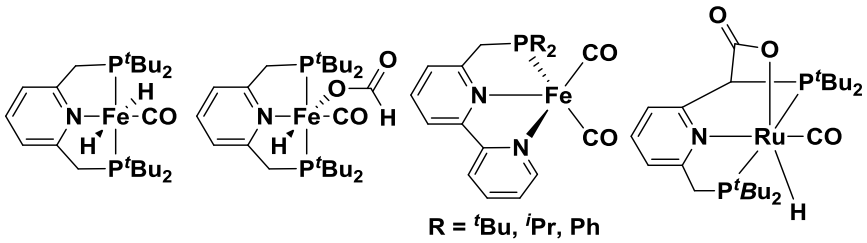

26 **108** **109** **110**

Figure 29. Several compounds resulting from CO_2 addition to M-PNL compounds

	26	**108**	**109**	**110**
ν_{CO} (cm^{-1})	1865	1885	R = ^{t}Bu, 1838, 1895	1912
			R = ^{i}Pr, 1847, 1907	
			R = Ph, 1857, 1917	
ν_{OCO} (cm^{-1})		1612 ν_{asym}		1628
		1319 ν_{sym}		

Table 5. Selected infrared spectroscopic data

The experimental infrared spectrum of **107** features a strong band at ν = 2195 cm^{-1} (ν = 2141 cm^{-1} when using $^{13}CO_2$ for the reaction), which clearly indicates the presence of the carbon atom of CO_2 in the formed product. In addition, this is a very high frequency value for C-O bond stretching even compared to the stretching of free CO (ν = 2143 cm^{-1}). However, this data does not match with any of the reported frequencies in Table 5. In addition, other iron-CO_2 adducts generated from CO_2 disproportionation reactions did not display similar bands (for example: **48**: ν_{CO} = 1730 cm^{-1}; **49**: ν_{CO} = 1647 cm^{-1}; **50**: ν_{CO} = 1644 cm^{-1}; **52**: ν_{CO} = 1994 cm^{-1}; **53**(**a**): ν_{CO} = 1654 cm^{-1}). But another stretching band was found in compound **107** at ν = 1654 cm^{-1}, featuring a oxalato or carbonate group which probably generated after the reaction by comparing to compounds **49**, **50** and **53**(**a**).

The insertion of CO_2 into metal-amido bonds (M-N(TMS)$_2$) is a known reaction.[207–210] In the case of complex [(dtbpe)Rh(μ-NCO)]$_2$ **111** (dtbpe = 1,2-bis(di-tert-butylphosphino)ethane),[210] a band at ν = 2154 cm^{-1} was observed for NCO stretching. As for complex [(κ^4-Tptm)ZnNCO] ([Tptm]H = tris(2-pyridylthio)methane) **112**,[209] the NCO group featured stretching at ν_{asym} = 2223, ν_{sym} = 1339 for N^{12}CO, and ν_{asym} = 2153, ν_{sym} = 1325 cm^{-1} for N^{13}CO. In complex (Al-Mg--NCO) **113**,[211] the frequency of NCO was at ν = 2202 cm^{-1}, which was also close to that observed for **107**. These information strongly suggest that our compound **107** contains one, or even more, NCO groups.

At this stage, further investigation on the nature of compound **107** is necessary to propose a reasonable structure.

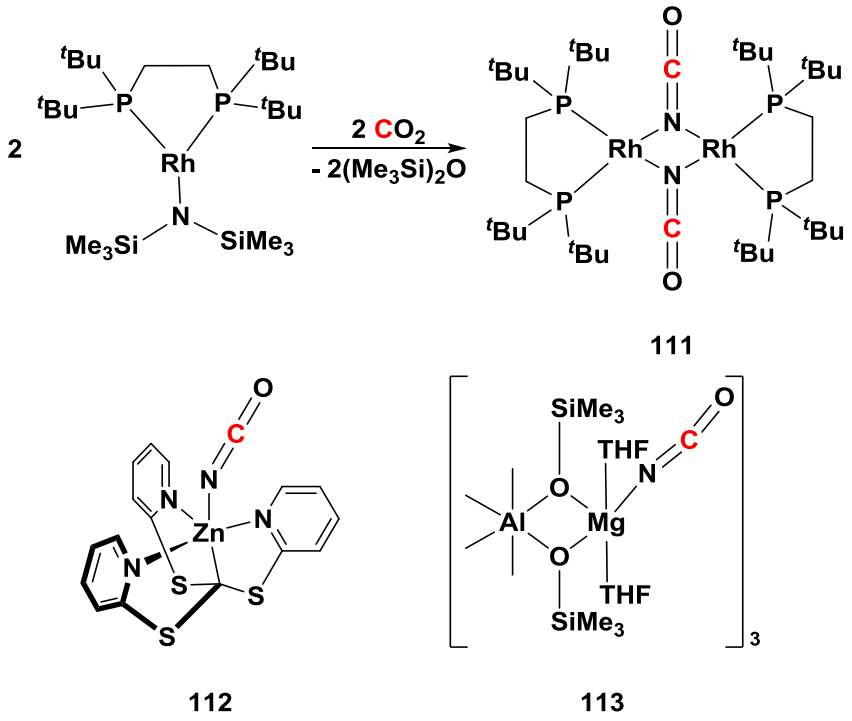

Figure 30. Complexes **111**-**113** bearing NCO ligands (a general scheme is shown for the synthesis of complex **111**)

In addition, by comparing to the IR spectrum of free NPN, the characteristic signals of NPN could be found in the compound **107** (Figure 31).

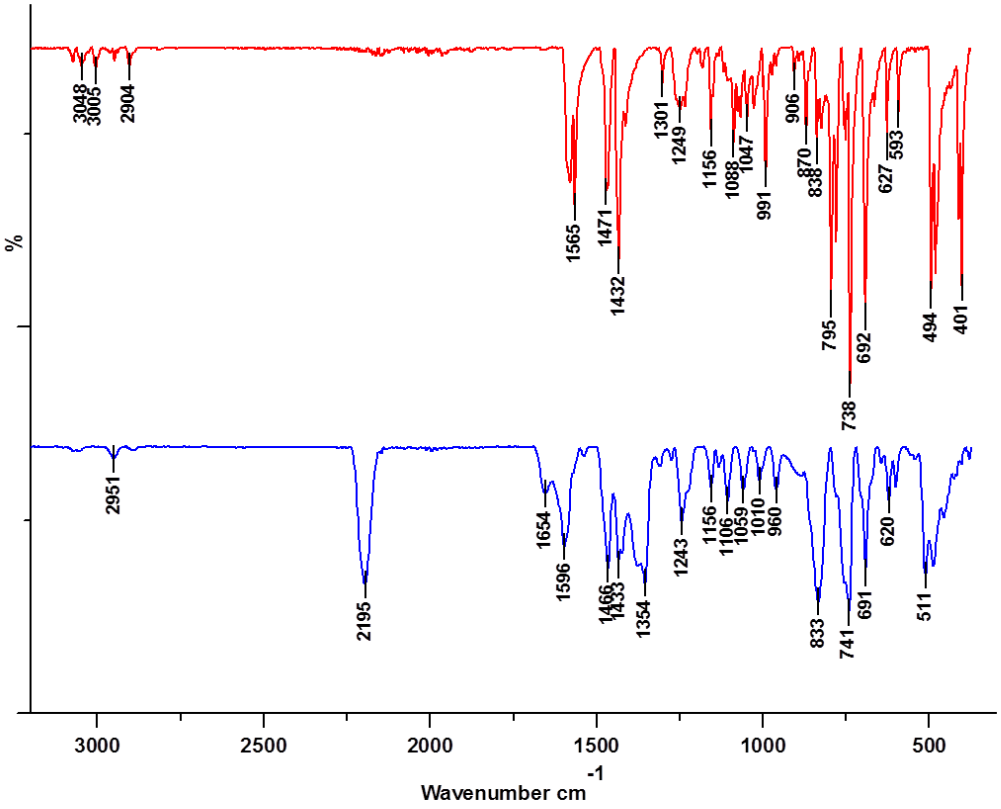

Figure 31. Infrared spectra of NPN (top) and **107** ($^{12}CO_2$ adduct, bottom)

2.3.1.4 Proposed structure of compound 107

Along these lines, one can tentatively assign for compound **107** a polymeric or oligomeric structure owing to its insolubility; NPN ligands, mono- or bridging- NCO groups and oxalato or carbonate groups should be present. However, further study on **107** is needed to find out its structure by optimizing the crystallization conditions and determining other properties. It would also be interesting to conduct some reactivity studies.

2.3.2 Reactivity of 105 toward other substrates

The Fe-H moiety plays an important role for the reactivity of the iron complexes (see chapter 1), and it is of interest to synthesize an iron complex containing a hydride and to use it for catalytic applications. There are many routes to synthesize iron-hydride complexes, such as substitution of halides, and oxidative addition of H_2 or H-E to the starting iron complexes.[212] In this section, different substrates such as KC_8, HCl, H_2, hydrazide, hydrosilanes, hydrodithiol and hydroboranes have been tested. Potassium graphite is a very reactive reducing agent, and has been utilized for

dehydrogenation or reduction of iron complexes successfully.[213–217] However, the reactions with KC_8 and HCl only led to decomposition products, and no reaction occurred with either dihydrogen or triphenylsilane (Ph_3SiH) or phenylhydrazine ($PhHNNH_2$)) was used.

Initial testing of the reactivity of **105** toward dithiol substrates was carried out with 1,2-ethanedithiol ($HSCH_2CH_2SH$) in Et_2O at -30 °C: a rapid decomposition took place just after the addition of 1,2-ethanedithiol to **105** leading to unknown iron species and free ligand. Using 1,2-benzenedithiol (HSC_6H_4SH) instead of 1,2-ethanedithiol can slow down the reaction and the in situ mixture could be controlled by NMR. By stirring the mixture of 1,2-benzenedithiol and **105** for 30 minutes at -30 °C and for 30 minutes at room temperature, a purple precipitate was obtained after workup. ^{31}P NMR characterization of the solid showed two resonances at δ = 75.4 and 67.3. ^{1}H NMR revealed two hydride signals at δ = -31.53 and -36.03, both peaks were broad due to the paramagnetic impurities in the solid. (Figure 32 and 33) However, it was impossible to isolate the precipitate because it was rather unstable: the purple solid can decompose to black iron species in solution within several minutes.

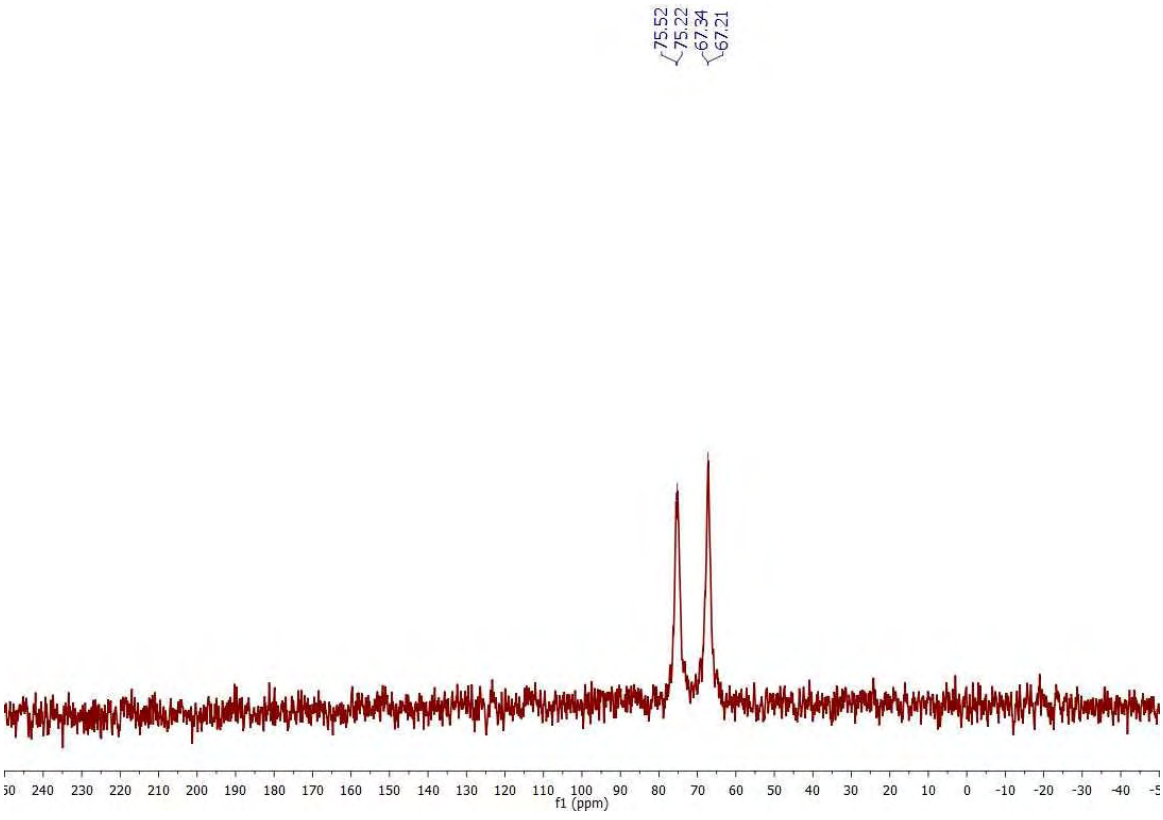

Figure 32. ^{31}P NMR spectrum of the purple solid generated from the reaction of **105** and 1,2-benzenedithiol (HSC_6H_4SH) (162.0 MHz, 298 K, Toluene-D_8)

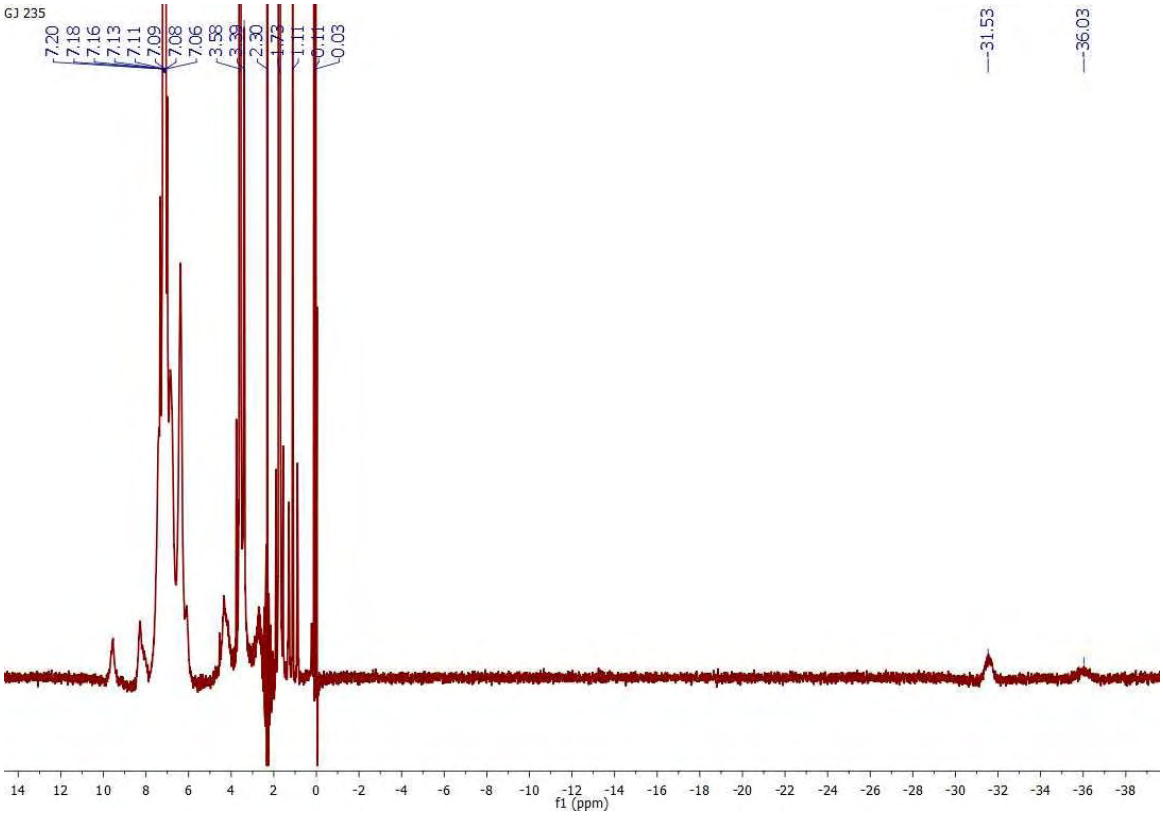

Figure 33. ^{1}H NMR spectrum of the purple solid generated from the reaction of **105** and 1,2-benzenedithiol (HSC_6H_4SH) (400.1 MHz, 298 K, THF-D_8)

By adding hydroborane reagents to a metal-amido moiety, it could be possible to generate a hydride ligand on the metal center. A related reactivity has indeed been observed on a copper complex bearing an alkoxy ligand. The addition of HBpin led to a metathesis-type reaction to generate a Cu-H bond and a pinB-OR compound.[218] Initial testing of the hydroboration of **105** was conducted with pinacolborane (HBpin) for this metathesis type reaction at room temperature. The addition of two equivalents or an excess of borane yielded new paramagnetic resonances: many peaks were observed by ^{1}H NMR just after the combination of the reagents, while a very high field signal at δ = -90.65 was obtained together with typical ^{1}H NMR signals at lower field assigned for a paramagnetic compound. The characterization by ^{11}B{^{1}H} NMR at δ = 25.8 for the generated B-N bond containing compound (pinB-N(TMS)$_2$) indicated that the expected reaction might have occurred. However, no crystals could be grown from the mixture and formation of complex **106** was slowly observed. The use of various solvents (e.g.: pentane or THF), temperature, pressure of dihydrogen led to the same result. While using catecholborane (HBcat) for the reaction, only decomposition of **105** to **106** could be observed.

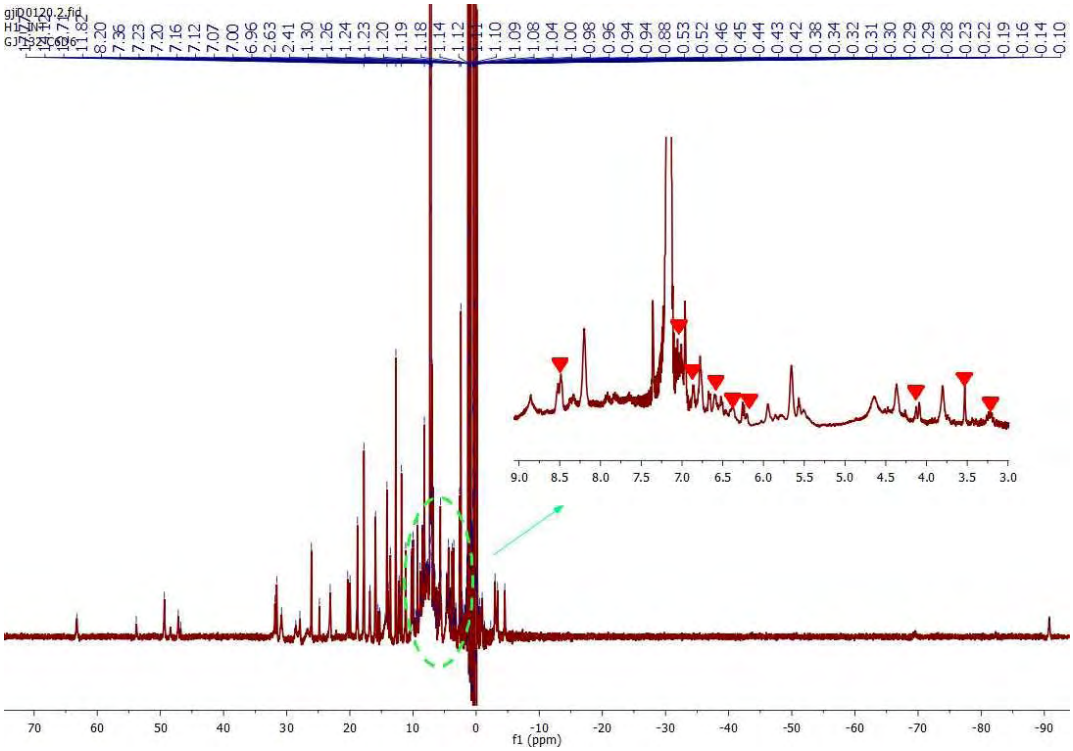

Figure 34. ^{1}H NMR spectrum of the reaction mixture at 30 min (marked signals stand for **106**)

2.3.3 Catalytic hydroboration of CO_2 with complex 105

The hydroboration of CO_2 using complex **105** as catalyst was then tested. 20 mol% catalyst loading in C_6D_6, under 0.6 atmosphere of $^{13}CO_2$, led to the observation of compounds **114**-**117** (Scheme 38). The reaction mixture was kept at ambient temperature and the catalytic system was followed by $^{13}C\{^{1}H\}$ NMR (Figure 35). Compounds **114** (δ = 85.5) and **115** (δ_{CH2} = 82.9 and δ_{CHO} = 158.6) were observed after 3 hours, and compounds **116** (δ = 158.6) and **117** (δ = 52.3) were also observed after 14 days at room temperature. In addition, the compounds **114**-**117** have been confirmed to release or to be a very reactive C1 source of formaldehyde (CH_2O), and compound **115** featuring two reduced CO_2 units was only previously observed with ruthenium polyhydride complexes.[219–221] However, the activity of this catalytic system was low with only 30 % of HBpin converted.

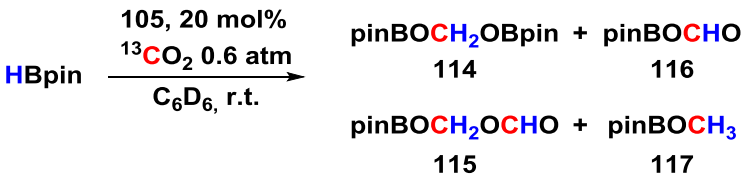

Scheme 38. Catalytic transformation of $^{13}CO_2$ with HBpin and compound **105**

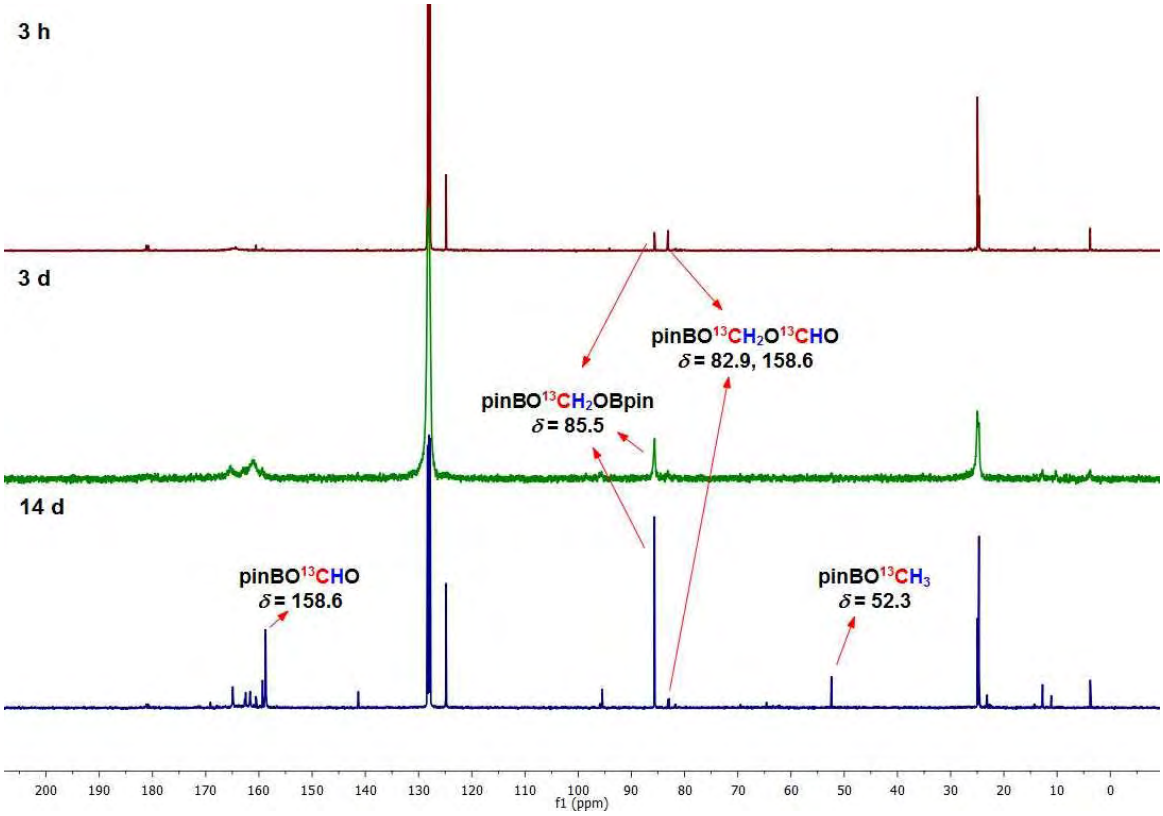

Figure 35. $^{13}C\{^{1}H\}$ NMR spectra of $^{13}CO_2$ transformation over time

2.4 Synthesis and characterization of ruthenium complexes bearing NPN and NP ligands

The compound Ru(COD)(COT) (**118**, COD = cyclooctadiene, COT = cyclooctatriene) was chosen as a ruthenium precursor for investigating NPN and NP ligand coordination. The synthesis and characterization of three new ruthenium complexes **119**-**121** are described in this section and their structural features are compared with the family of iron complexes **104**-**106**.

2.4.1 Synthesis and NMR characterization of the ruthenium complexes

Crystals of the ruthenium complex [Ru(κ^{P}-NPN)($\kappa^{N,P}$-NPN)(COD)] **119** suitable for X-ray diffraction analysis were grown from the mixture of Ru(COD)(COT) and NPN in Et_2O after one hour without stirring, and leaving the filtrate of the mixture at -37 °C for 48 hours. When performing the reaction in a pentane/toluene solution, crystals of the homoleptic complex [Ru($\kappa^{N,P,N}$-NPN)$_2$] **120** suitable for X-ray diffraction were obtained after 10 days at -37 °C. Neither **119** nor **120** were isolated in larger scale due to their instability in solution.

Complex [Ru(κ^{P}-NP)($\kappa^{N,P}$-NP)(COD)] **121** was isolated as a red powder in a 56 % yield after stirring Ru(COD)(COT) and the NP ligand for 16 hours in Et_2O solution at room temperature. This

compound was stable upon storing in the glove box at ambient temperature for months. Crystals of **121** were grown from an Et_2O solution of Ru(COD)(COT) and NP at -37 °C.

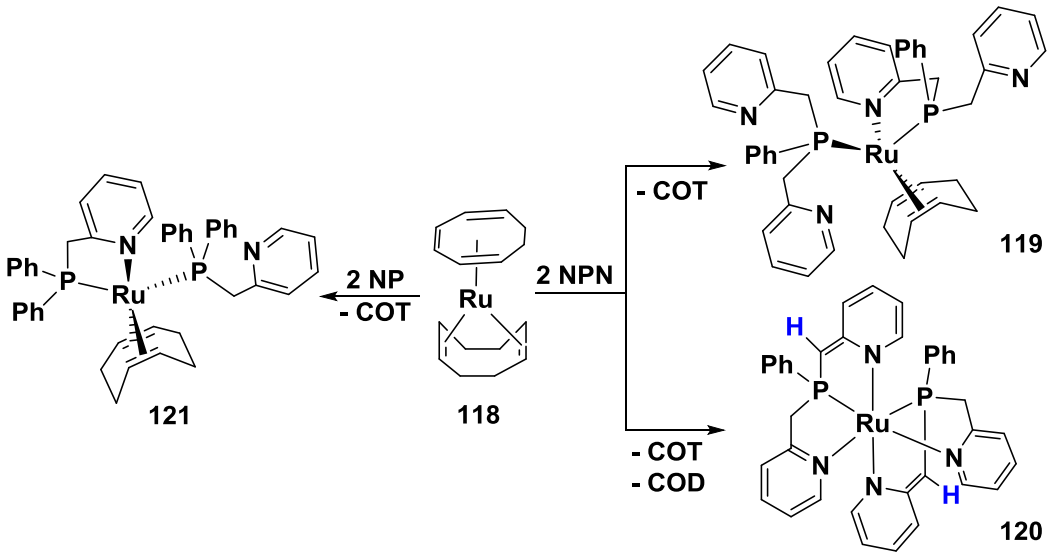

Scheme 39. Synthesis of complexes **119**-**121**. Et_2O was the solvent for the synthesis at room temperature

NMR characterization of the crystals of complex **119** turned to be impossible due to its decomposition in solution. Several $^{31}P\{^1H\}$ NMR signals were always obtained. As shown in Figure 36, three doublet signals at δ = 35.6, 35.0 and 32.6 decreased rapidly (within 1h), and two singlet resonances at δ = 53.7 and 44.6 increased meanwhile. It was notable that the latter two signals corresponded to hydride resonances at δ = -6.94 and -7.76, respectively, as determined by multinuclear selective decoupling experiments. Further work is needed to properly characterize complex **119** by NMR, by conducting low temperature experiments. The same problem was also observed for complex **120**.

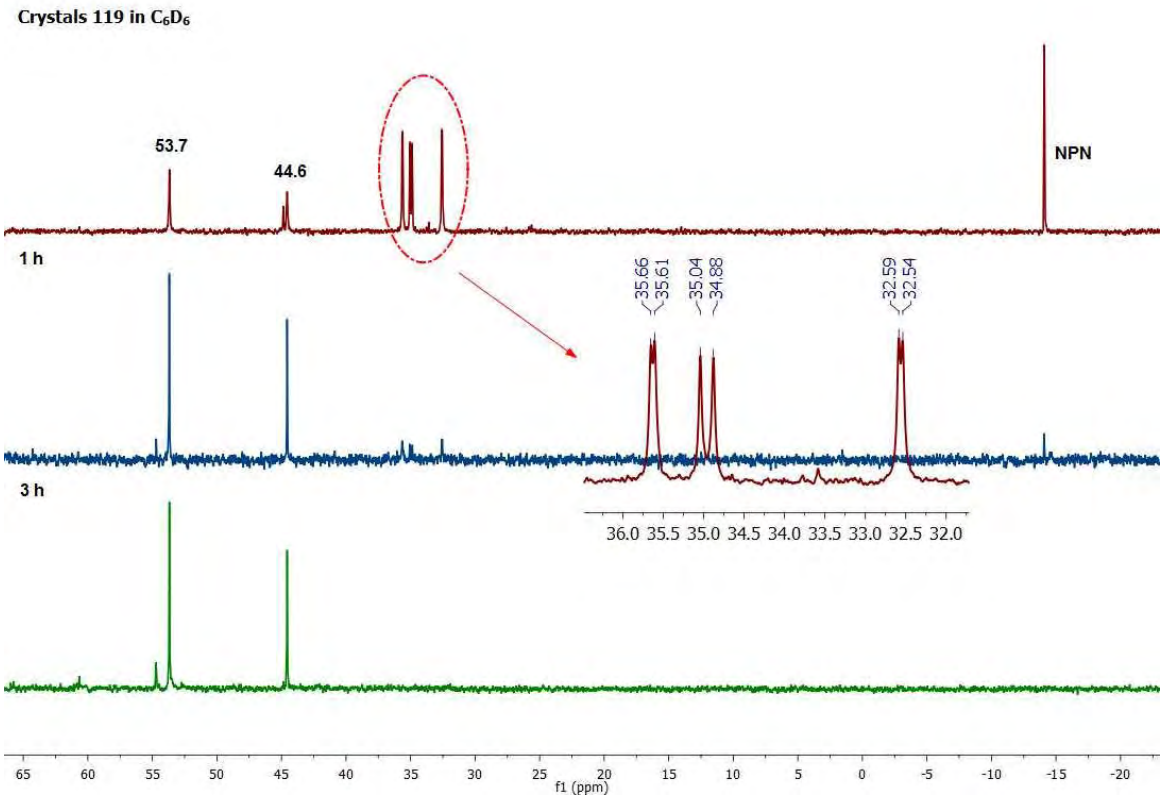

Figure 36. Evolution of complex **119** detected by $^{31}P\{^{1}H\}$ NMR

In the case of complex **121**, the $^{31}P\{^{1}H\}$ NMR spectrum showed two doublet signals at δ = 55.6 and 39.3 ($^{2}J_{P\text{-}P}$ = 20.5 Hz), corresponding to the two inequivalent phosphorus atoms in cis position as indicated by the small $^{2}J_{P\text{-}P}$ value and as corroborated by the X-ray structure. A typical ^{1}H NMR spectrum indicated that **121** was a diamagnetic compound. Interestingly, an ABX (A = B = H, X = P) spin system was observed in the aliphatic region between 1.5 and 4.0 ppm. The signals at δ = 3.36 and δ = 1.58 ppm corresponded to the inequivalent protons of the methylene linker (PCH_2 in $\kappa^{N,P}$-NP ligand) resonating as an AB pattern upon ^{31}P decoupling ($^{2}J_{H\text{-}H}$ = 17.5 Hz), and the corresponding ^{13}C resonance was found at δ = 43.6 ppm (d, $^{1}J_{C\text{-}P}$ = 15.9 Hz) by $^{13}C\{^{1}H$ NMR}. While for the PCH_2 moiety in κ^{P}-NP ligand, a resonance at δ = 4.18 ppm (ps quartet) for the two protons and at δ = 40.1 ppm for the carbon was observed by ^{1}H and $^{13}C\{^{1}H$ NMR}, respectively.

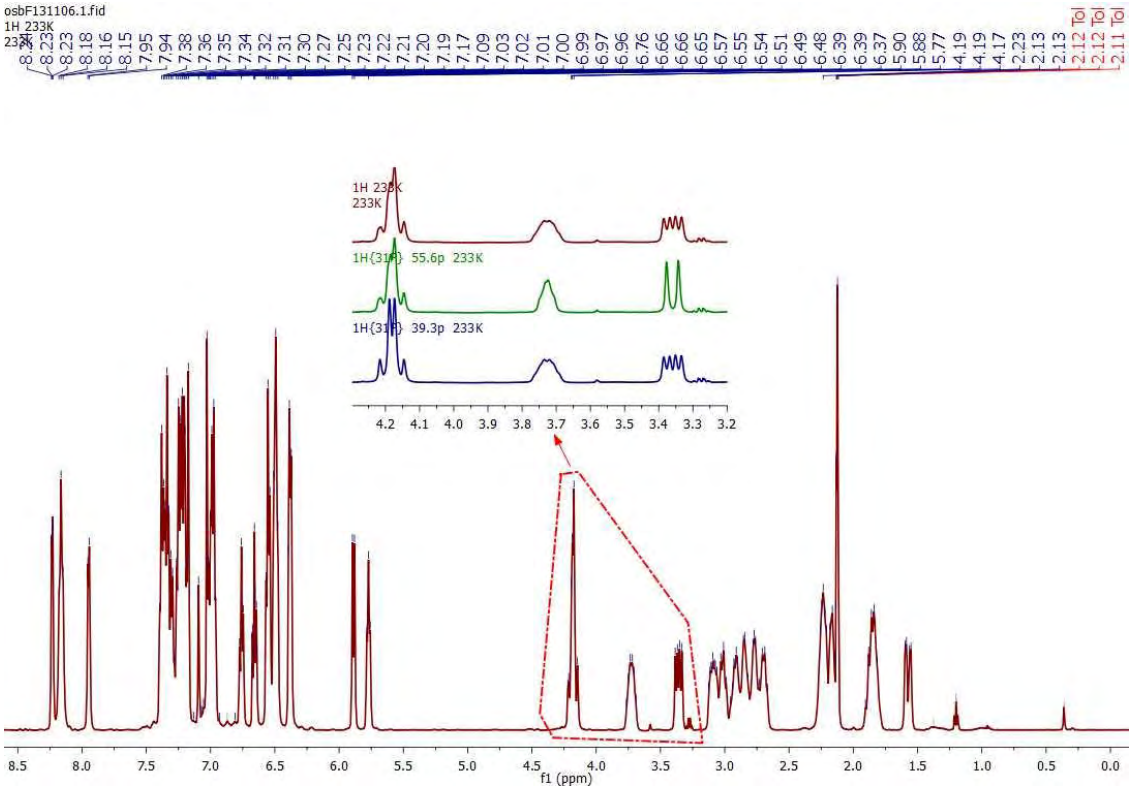

Figure 37. ^{1}H NMR spectrum of complex **121**

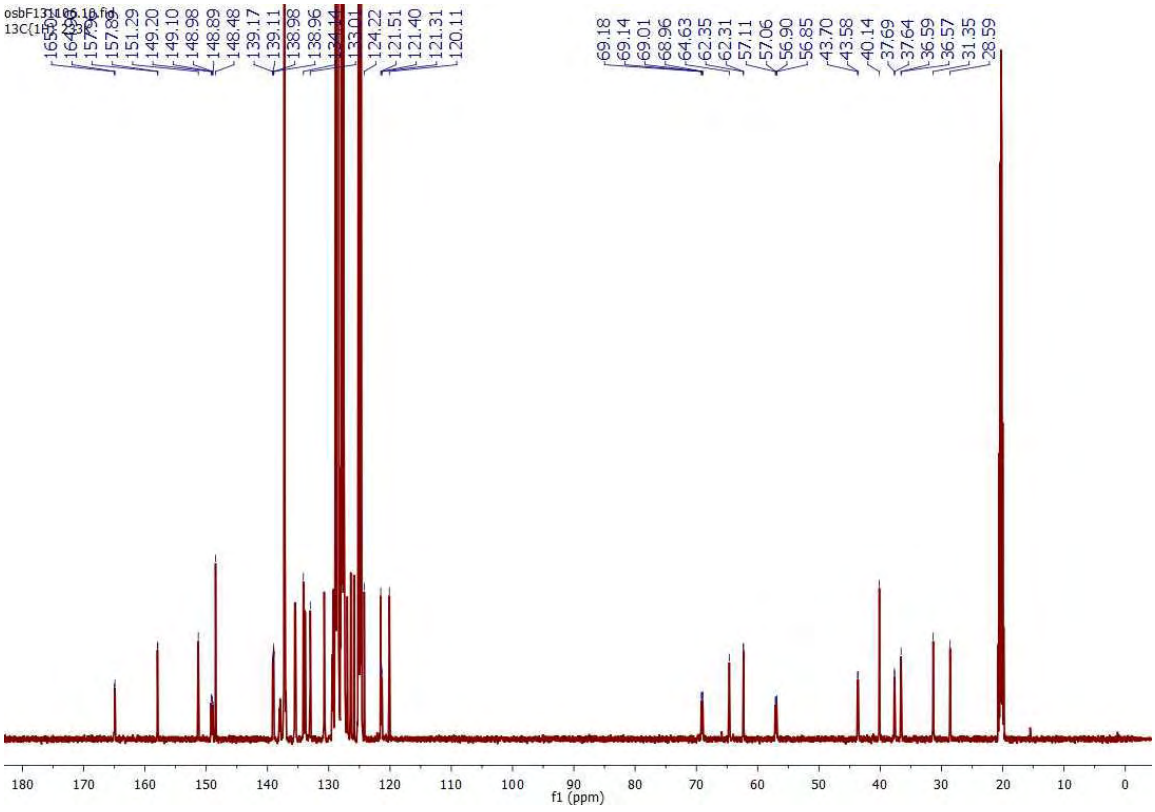

Figure 38. ^{13}C{^{1}H} NMR spectrum of complex **121**

2.4.2 X-ray diffraction of complexes 119 -121

The crystallographic analysis revealed that **119** crystallized in the triclinic space group *P*-1 with Z = 2. The ruthenium center is in a distorted square pyramidal geometry, and the oxidation state of the 18 e^- metal center is 0. The two NPN ligands coordinated to the ruthenium center in monodentate κ^P- and bidentate $\kappa^{N,P}$-modes, respectively. Cyclooctadiene (COD) remained coordinated to the metal while the starting cyclooctatriene (COT) was not any more present. The Ru1-P2 bond distance (2.3443(4) Å) belonging to the monodentate κ^P-NPN ligand was longer than that of Ru1-P1 (2.3210(4) Å) for the bidentate $\kappa^{N,P}$-NPN ligand, because P2 is roughly trans to the vacant site of the metal center and the constraint effect of the five membered ring (Ru1-P1-C14-C13-N1). The four C-C bond distances between the methylene moieties and the pyridine rings were quite closed to each other (*d*C13-C14 = 1.498(2) Å, *d*C15-C16 = 1.511(2) Å, *d*C27-C28 = 1.501(2) Å, *d*C33-C34 = 1.499(2) Å) and similar to those in complex [Fe(N(TMS)$_2$)$_2$($\kappa^{N,P}$-NPN)] **104** (*d*C1-C2 = 1.500(2) Å and *d*C1-C8 = 1.498(2) Å). The X-ray structure of **119** is depicted in Figure 39 and the selected bond distances and angles are given in Table 6.

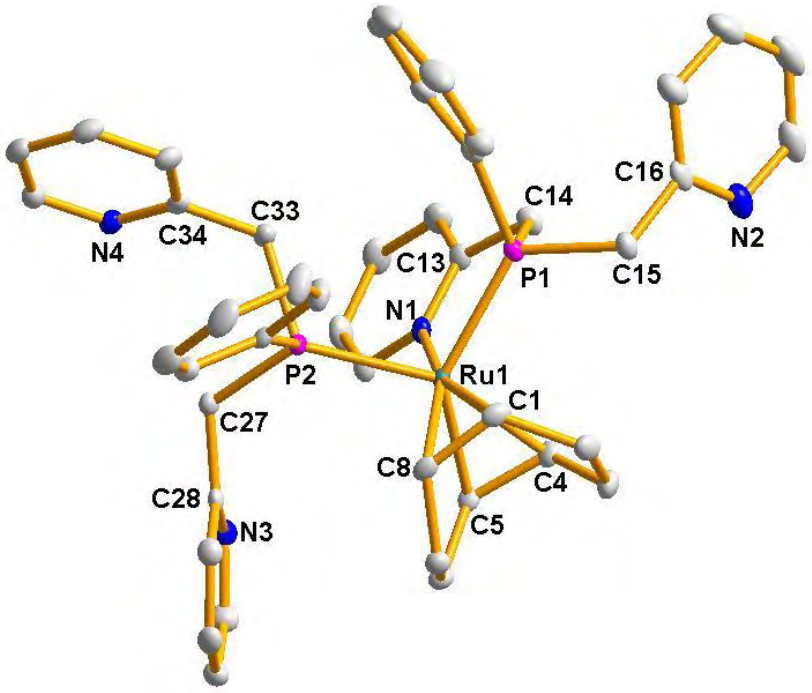

Figure 39. Molecular structure of complex [Ru(κ^P-NPN)($\kappa^{N,P}$-NPN)(COD)] **119**, ellipsoids are given at the 50 % probability level and hydrogen atom are omitted for clarity

Complex **119**			
Ru(1)-P(1)	2.3210(4)	Ru(1)-P(2)	2.3443(4)
Ru(1)-N(1)	2.1395(12)	Ru(1)-C(1)	2.1926(15)
Ru(1)-C(4)	2.1445(14)	Ru(1)-C(5)	2.1427(14)
Ru(1-C(8))	2.1983(14)	C(13)-C(14	1.498(2)
C(15)-C(16)	1.511(2)	C(27)-C(28)	1.501(2)
C(33)-C(34)	1.499(2)	N(1)-Ru(1)-P(1)	81.82(3)
N(1)-Ru(1)-P(2)	86.64(3)	P(1)-Ru(1)-P(2)	104.391(13)
C(13)-C(14)-P(1)	111.57(10)	C(16)-C(15)-P(1)	116.20(11)
C(28)-C(27)-P(2)	117.92(10)	C(34)-C(33)-P(2)	117.25(10)

Table 6. Selected bond distances (Å) and angles (°) for **119**

The X-ray structure of **120** is quite similar to that of **106**, the two NPN ligands coordinating to the metal center via a tridentate $\kappa^{N,P,N}$-fashion with dearomatization of one of the pyridine ring on each ligand. Single crystals of **120** crystallized in the monoclinic space group *P* 1 2_1/c with Z = 4, and the coordination geometry of Ru1 is also a distorted octahedron. Notably, the oxidation state of the 18 e^- ruthenium center is +2, as a result of deprotonation of the two NPN ligands upon coordination. The axial positions are occupied by one phosphorus atom and one nitrogen atom of the aromatic pyridine ring with the bond angle of P1-Ru1-N4 = 177.55(4) °. In the equatorial plane, the two nitrogen atoms of the dearomatized rings, as well as the phosphorus atom and the nitrogen atom of the non-dearomatized pyridine ring, are in trans positions to each other, respectively. The mean deviation from the plane was 0.0008 Å and the sum of the angles at Ru1 was 359.98 °.The Ru-P bond distances (*d*Ru1-P1 = 2.2126(5) Å and *d*Ru1-P2 = 2.2108(5) Å) were shorter than those of **119**, probably due to the more compact geometry of **120**. When the nitrogen atoms were from aromatic pyridine rings, the Ru-N bond distances (*d*Ru1-N3 = 2.2009(15) Å and *d*Ru1-N4 = 2.1847(15) Å) were longer than those of nitrogen atoms from dearomatizated pyridine rings (*d*Ru1-N1 = 2.1174(16) Å and *d*Ru1-N2 = 2.1086(16) Å). Similarly, the C=C double bond lengths (*d*C11-C12 = 1.405(3) Å and *d*C31-C32 = 1.403(3)) were shorter than those of related C-C single bond (*d*C17-C18 = 1.500(2) Å and *d*C23-C24 = 1.502(3) Å). Figure 40 depicts the X-ray structure of complex **120**, Table 7 summarizes selected bond distances and angles.

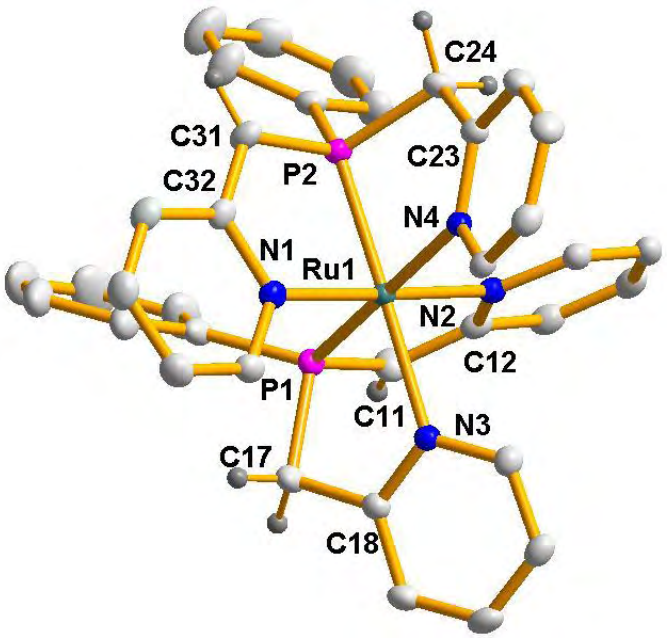

Figure 40. Molecular structure of complex [Ru($\kappa^{N,P,N}$-NPN)$_2$] **120**, ellipsoids are given at the 50 % probability level and hydrogen atom are omitted for clarity except for the CH and CH_2 linkers between the phosphorus atom and the pyridine rings

Complex **120**			
Ru(1)-P(1)	2.2126(5)	Ru(1)-P(2)	2.2108(5)
Ru(1)-N(1)	2.1174(16)	Ru(1)-N(2)	2.1086(16)
Ru(1)-N(3)	2.2009(15)	Ru(1)-N(4)	2.1847(15)
C(11)-C(12)	1.405(3)	C(17)-C(18)	1.500(3)
C(31)-C(32)	1.403(3)	C(23)-C(24)	1.502(3)
N(2)-Ru(1)-N(1)	177.94(6)	N(1)-Ru(1)-N(4)	85.18(6)
N(2)-Ru(1)-N(4)	95.46(6)	N(1)-Ru(1)-N(3)	97.06(6)
N(2)-Ru(1)-N(3)	84.73(6)	N(2)-Ru(1)-P(2)	95.74(4)
N(4)-Ru(1)-N(3)	101.36(6)	N(4)-Ru(1)-P(2)	79.57(4
N(1)-Ru(1)-P(2)	82.45(4)	N(2)-Ru(1)-P(1)	82.48(4)
N(3)-Ru(1)-P(2)	178.92(4)	N(4)-Ru(1)-P(1)	177.55(4)
N(1)-Ru(1)-P(1)	96.83(4)	N(3)-Ru(1)-P(1)	79.81(4)
P(2)-Ru(1)-P(1)	99.276(18)	C(12)-C(11)-P(1)	114.79(15)
C(18)-C(17)-P(1)	107.11(13)	C(23)-C(24)-P(2)	106.71(13)
C(32)-C(31)-P(2)	114.47(14)		

Table 7. Selected bond distances (Å) and angles (°) for **120**

Single crystals of **121** crystallized in the monoclinic space group *C* 1 2_1/c with Z = 4. The NP ligands are coordinated to the ruthenium center via monodentate κ^P- and bidentate $\kappa^{N,P}$-modes. Similar to **119**, COD remained coordinated to the metal center while the cyclooctatriene (COT) was liberated. The oxidation state of the 18 e- ruthenium center is still 0. The Ru-P bond lengths are 2.3827(12) Å and 2.2527(12) Å, thus quite different in agreement with the two different coordination modes of the NP ligands (phosphorus in $\kappa^{N,P}$-NP and κ^P-NP ligands, respectively). The C-C single bond distances of the methylene linkers and the pyridine rings are similar as none of the ligands were deprotonated upon coordination (*d*C13-C14 = 1.495(7) Å and *d*C32-C33 = 1.507(6) Å). The X-ray structure of **121** is shown in Figure 41 and selected bond distances and angles are listed in Table 8.

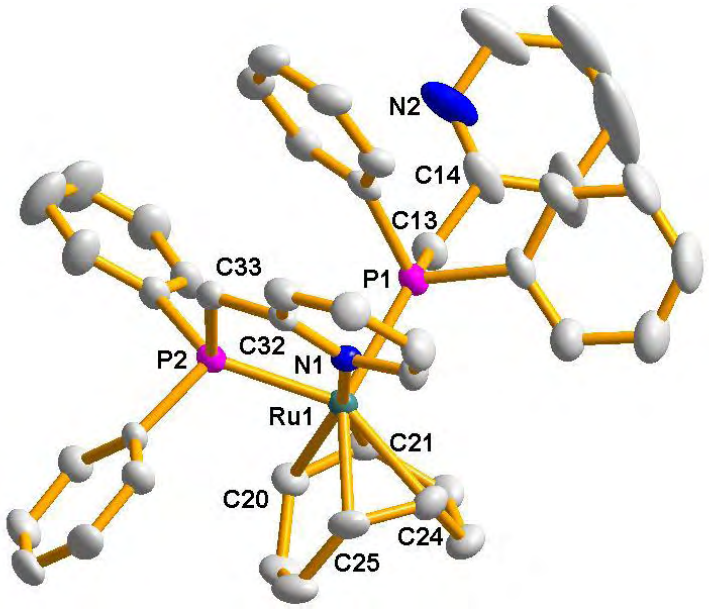

Figure 41. Molecular structure of complex [Ru(κ^P-NP)($\kappa^{N,P}$-NP)(COD)] **121**, ellipsoids are given at the 50 % probability level and hydrogen atom are omitted for clarity

Complex **121**			
Ru(1)-N(1)	2.158(4)	Ru(1)-P(1)	2.3827(12)
Ru(1)-P(2)	2.2527(12)	Ru(1)-C(20)	2.202(5)
Ru(1)-C(21)	2.168(5)	Ru(1)-C(24)	2.178(5)
Ru(1)-C(25)	2.146(4)	C(13)-C(14)	1.495(7)
C(32)-C(33)	1.507(6)	N(1)-Ru(1)-P(2)	80.99(10)
N(1)-Ru(1)-P(1)	85.63(10)	P(2)-Ru(1)-P(1)	101.54(4)

Table 8. Selected bond distances (Å) and angles (°) for **121**

2.5 Conclusion

The bis(2-picolyl)phenylphosphine compound has demonstrated that it acts as a versatile NPN ligand toward the reactive precursor [Fe{N(SiMe$_3$)$_2$}$_2$], affording access to several different coordination modes. Thanks to a fine control of the experimental temperature and time conditions, complexes **104**-**106** could be isolated. These paramagnetic and diamagnetic compounds have been characterized by X-ray diffraction analyses and NMR spectroscopy both in solution and in the solid state. The paramagnetic complex **105** was also characterized by Mössbauer measurements, Evans method, EPR as well as powder X-ray diffraction.

Upon coordination, deprotonation of NPN was observed giving rise to the dearomatization of a pyridine ring in complex **105** and **106**. This is the first time that such a behavior is reported for this ligand. Such a behavior is one key parameter for the strategy of "non-innocent" (outer-sphere) utilization in catalysis. In addition its flexibility allows the formation of an original dimer, complex **105**. The exploitation of the reactivity of this type of dimeric structure featuring an activated ligand has been tested with different substrates and we gained some interesting results. The possibility of using such a complex as catalyst for small molecule activation, such as catalytic transformation of CO_2 with pinacolborane, has also been explored. Further investigations toward circumventing the stability issues encountered in this study are highly expected.

With the precursor [Ru(COD)(COT)], the coordination chemistry of NPN and of the related compound (2-picolyl)diphenylphosphine (NP) was also studied for comparison with the iron chemistry. Several complexes **119**-**121** have been obtained and characterized by X-ray diffraction. The properties of the NPN ligand containing ruthenium complexes **119** and **120** were similar with those of the iron complexes **104**-**106**: instability, difficulties in NMR characterization, and even the crystallographic structures (**120** and **106**). In addition, the crystallographic structures of complexes **119** and **121** are almost the same: COD is remaining as a ligand on the ruthenium(0) center and two other phosphine ligands are coordinated to the metal centers via κ^P and $\kappa^{N,P}$ fashions, with the only difference of the functional groups on the ligands (NPN in **119** and NP in **121**, respectively). It should be noted that complex **121,** containing the NP ligand, is rather stable by comparison to all the NPN type complexes.

Chapter 3

Chapter 3

Iron-catalyzed reductive functionalization of CO_2

3 Introduction

With respect to global warming, climate changes and the desire of carbon-based societies, the utilization of carbon dioxide, which is a renewable, cost-efficient, and rather non-toxic source of carbon when compared to other C1 sources, has been developed in various fields of chemistry despite its intrinsic high thermodynamic stability.[133,157,222,140,223–225] In chapter 1, the activation of CO_2 upon coordination to iron-based compounds, and iron-catalyzed functionalization processes leading to carbonates, carbamates, formic acid or derived products, formamines and methylamines have been described.

In this chapter, a general bibliography overview of functionalization, reduction and reductive functionalization of CO_2 is summarized in sections 3.1 and 3.2. My work concerning the selective reduction of CO_2 into a versatile C1 source catalyzed by iron-hydride complexes is presented in section 3.3; the expanded scope of value-added compounds from CO_2, including not only C-N but also C-O, C-S and C-C bonds formation, is reported in section 3.4.

3.1 Functionalization and reduction of CO_2

Nowadays, the synthesis of organic compounds featuring a C^{IV} center(s) by CO_2 functionalization has been developed rapidly.[226] In the most advanced processes of transformation of CO_2, the O-C-O unit is maintained as in carbonate or salicylic acid (C^{III}) syntheses, and / or at least one of the C=O bonds from CO_2 is retained, for example in urea derivatives.[227–229,112]

However, to fully use CO_2 as a C1 building block, the full range of carbon oxidation states needs to be accessible. Homogeneous catalyzed CO_2 reduction with concomitant oxygen abstraction was investigated with dihydrogen,[230,231] silanes[232] and boranes[233,234] as reducing agents. As a consequence, the complete list of C1 compounds: carbon monoxide, formic acid, formaldehyde, methanol and methane were obtained. This family of C1 compounds are of interest as energy carrier or chemical building blocks.[133,222,231,235–240]

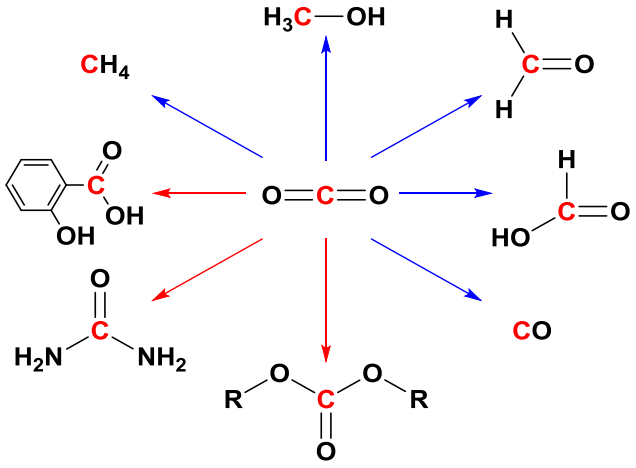

Scheme 40. Products from CO_2 functionalization and reduction reactions

It should be pointed out that the scope of chemicals from direct CO_2 functionalization and reduction is rather narrow by comparison to the current available petrochemicals. For example, ketones, esters and hydrocarbons, are not available from CO_2. To expand the scope of produced chemicals, reductive functionalization of CO_2 appears as a key strategy.

3.2 Reductive functionalization of CO_2

The use of dihydrogen as a reductant gave rise to methanol,[241–244] whereas the addition of amines, imines or olefins to the hydrogenation process afforded formamides,[245] formamidines,[246] methylamines[247–251] and aliphatic alcohols,[252,253] thus generating new C-N and C-C bonds. These processes are conducted with Ru catalysts for the most efficient systems at temperatures greater than 135 °C and H_2/CO_2 pressures greater than 40 atm. The only examples using iron catalysts to generate formamides are also performed under similar conditions (100 °C and H_2/CO_2 pressures greater than 90 atm., chapter 1, section 1.3).[173,174] While CO_2 hydrogenation appears as the ideal reaction in term of atom economy, a sustainable source of "carbon free" dihydrogen, milder reaction conditions and less expensive catalysts remain to be found.

In the case of hydrosilanes and hydroboranes as reductants, significantly milder operating conditions are allowed: ambient temperature and one atm of CO_2. This feature might be explained by weaker and slightly polarized Si-H and B-H bonds compared to the strong non-polar H-H bond (bond dissociation energy: 92, 99 and 104 kcal·mol^{-1} in SiH_4, BH_3 and H_2, respectively). In addition, the bond energies are 110, 125, and 109 kcal·mol^{-1} for Si-O, B-O and H-O bonds, respectively. So it is potentially more favorable to break the Si-H or B-H bonds and to generat

the corresponding Si-O or B-O bonds. By adding amines to CO_2 hydrosilylation[254–261,183] or hydroboration[262,219,220,218,263,264] processes, the corresponding formamides, formamidines, formimine and methylamines can be obtained. Remarkably, the hydrosilylation system can also be activated by iron-based catalysts leading to formamides at room temperature and methylamines at 100 °C, although the silane reagent is only limited to $PhSiH_3$.[183]

Key mechanistic insights were gained and up to 4 consecutive hydrofunctionalization reactions have been described yielding formoxy **122**, acetal **123** and / or formaldehyde, methoxy **124**, and ultimately methane, the latter being only obtained in the case of hydrosilanes (Scheme 41).[232,233,263,265,266] The first observation of bis(boryl)acetal **123** and formaldehyde was described in our group with a ruthenium-catalyzed CO_2 hydroboration system with HBpin.[219,220,221] Later on, the bis(boryl)acetal **123** was also observed in base-catalyzed hydroboration of CO_2 with 9-BBN.[263,266] Very recently, the first X-ray characterization of a bis(boryl)acetal compound (BR_2 =(2,4,5-trimethylphenyl, 2-dimethylaminophenyl)borane) was reported.[267] The formation of formamides, formamidines and methylamines is explain via the functionalization of the formoxy compound **122** which corresponds to the first reduction step for CO_2.

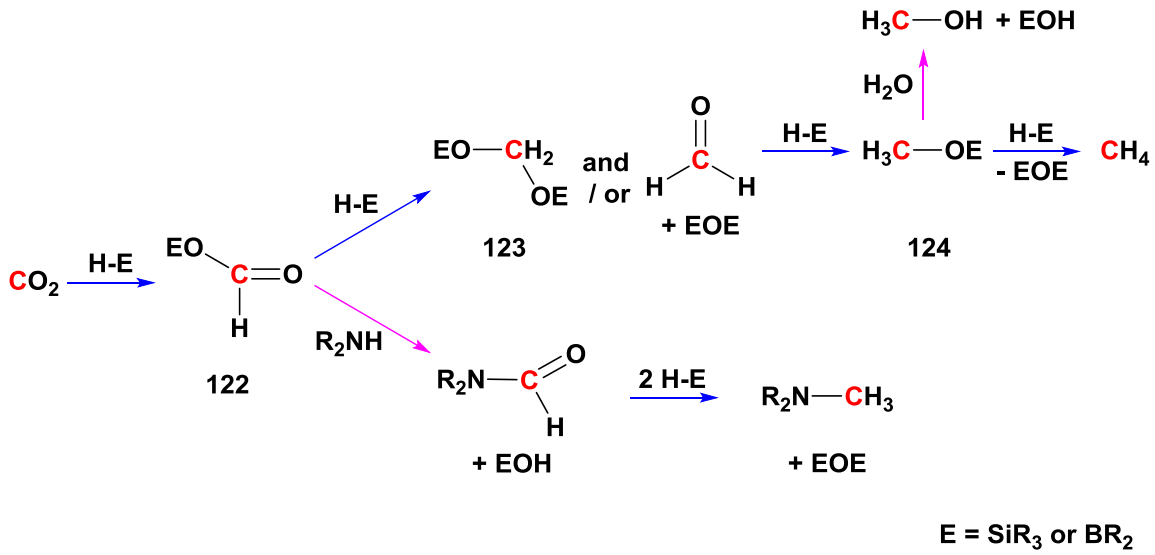

Scheme 41. General scheme for the reduction and reductive functionalization of CO_2

Until now, reductive functionalization of CO_2 only generated C-N bonds with the use of amines as trapping agents. In order to largely expand the scope of accessible compounds and functions, the strategy is to target the second stage of reduced CO_2 and its subsequent functionalization. As it has been shown that trapping of formaldehyde allowed to form imine functions, the hypothesized proposal is that the bis(boryl)acetal would allow to stabilize the oxidation state 0 of the carbon atom more easily than formaldehyde but would afford similar versatile high

reactivity as formaldehyde as a methylene transfer reagent not only to form C-N but also C-O, C-C, C-S, C=N and C=C bonds in a one-pot two-steps process.

For reductive functionalization of CO_2, there are indeed very few systems using iron-based compounds as pre-catalysts.[173,174,183] Thus, to transpose the ruthenium expertise[219–221] to iron complexes featuring hydride ligands is of interest.

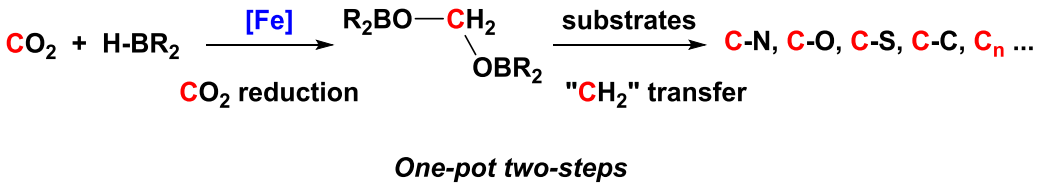

Scheme 42. An iron catalyzed one-pot two-steps process for reductive functionalization of CO_2 under mild conditions

3.3 Preparation of bis(boryl)acetal at iron-catalyzed system

3.3.1 Preparation of $Fe(H)_2(dxpe)_2$

The dihydride iron complex $[Fe(H)_2(dmpe)_2]$ **40** was chosen as catalyst for the hydroboration of CO_2, owning to its reactivity with CO_2 as described by Leslie Field et al. (see chapter 1).[141,148,268] In addition, our group used this complex for direct C-H borylation of arenes under irradiation.[269] The related dihydride iron complex $[Fe(H)_2(depe)_2]$ (depe = bis(diethylphosphino)ethane) **126** was also tested. Because a similar complex $[Fe(Me)_2(depe)_2]$ (**43**, pp = depe), has also been shown that can react with CO_2 (see chapter 1).[142] Both complexes were synthesized following a modified procedure from the literature.[268,270] Two equivalents of diphosphine ligands were added to the solution of $FeCl_2$ (in toluene for dmpe and in THF for depe) at room temperature and stirred for 12 hours. After workup, green solids (for both phosphine ligands) corresponding to the dichlorobis(diphosphine) complexes **125** were obtained in good yield (> 88 % for both phosphine ligands). The addition of two equivalent of super hydride $LiHBEt_3$ (Lithium triethylborohydride) at room temperature afforded the iron complexes **40** and **126**, respectively. ^1H NMR spectra of complexes **40** and **126** revealed high field signals at δ = -14.51 and -14.77 ppm for the hydrides, respectively and ^{31}P NMR spectra showed two resonances for each complex at δ = 76.7 and 66.8 ppm (t, $^2J_{P\text{-}P}$ = 27 Hz), and at δ = 102.4 and 88.4 ppm (br), respectively standing for the *cis*-coordinated diphosphine. (Complex $[Fe(H)_2(dmpe)_2]$ **126** was prepared by Dr. C. Gunnar Werncke.)

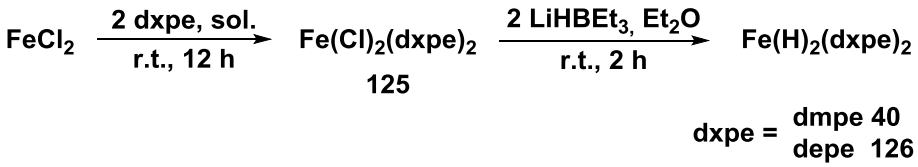

Scheme 43. Synthesis of iron complexes $[Fe(H)_2(dmpe)_2]$ **40** and $[Fe(H)_2(depe)_2]$ **126**

3.3.2 Variation of the hydroboranes - Choice of the oxygen scavenger

Catalytic hydroboration of CO_2 was carried out with 5 mol% of complex **40** with three different hydroboranes: catecholborane (HBcat), pinacolborane (HBpin) and 9-borabicyclo[3.3.1]nonane (9-BBN). The reactions were conducted at room temperature under 1 atmosphere of CO_2 in a NMR tube and except for $BR_2OCH_2OBR_2$ (bis(boryl)acetal), BR_2OCH_3 (methoxyborane) and BR_2OBR_2 (bis(boryl)ether), no other compound in significant amount was observed by NMR during the hydroboration processes (Scheme 44). The yields of bis(boryl)acetal versus methoxyborane were determined by ^1H NMR integrations (9,10-dihydroanthracene was used as internal standard, Table 9). With HBcat, CO_2 was fully converted to the related methoxyborane within 3 hours. With HBpin, while the formation of the bis(boryl)acetal was observed during the reaction, a ratio of 30 % : 18 % was observed at full conversion level (5 h). In contrast, the reaction with 9-BBN led to 36 % : 3 % ratio after 1 hour. After 3 hour, the bis(boryl)acetal raised to 56 % and decreased to 46 % when all the 9-BBN has been converted (5 h).

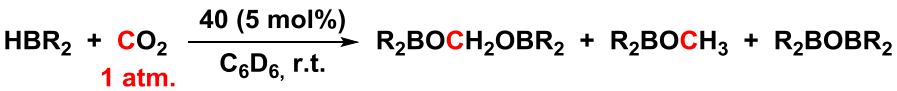

Scheme 44. Iron complex **40** catalyzed CO_2 hydroboration reaction; three compounds bis(boryl)acetal, methoyborane and oxodiboron were observed by NMR

HBR_2	Time (h)	$R_2BOCH_2OBR_2$ (%)	R_2BOCH_3 (%)
HBcat	1	0	41
	3	0	59
HBpin	1	4	6
	3	21	10
	5	30	18
9-BBN	1	36	3
	3	56	15
	5	46	27

Table 9. CO_2 hydroboration: relative ratios of the corresponding bis(boryl)acetal and methoxyborane

Phosphines (PR_3, R = ^{t}Bu, Ph, 4-MeC_6H_4 and 3,5-$Me_2C_6H_3$) have already been shown to reductively catalyze CO_2 with 9-BBN giving rise to a mixture of formatoborane, bis(boryl)acetal and methoxyborane under mild conditions (5 atm. of CO_2 and at room temperature). The highest yield of bis(boryl)acetal generation in this metal-free catalytic system was 41 % when all 9-BBN was consumed.[266] In this context, blank experiments with only the phosphine ligand (dmpe) as catalyst precursor were also conducted with the three hydroboranes under the standard reaction conditions (1 atm. of CO_2, at room temperature and 10 mol% of catalyst loading). The relative ratios between the bis(boryl)acetal and the methoxyborane were estimated by ^{1}H NMR and shown in Table 10. It should be pointed out that all the hydroboranes (HBcat, HBpin and 9-BBN) can potentially react with dmpe; a lot of white precipitate was observed just after mixing HBcat and dmpe, whereas HBpin and 9-BBN gave colorless solutions after mixing. The reaction of hydroboranes with dmpe was not considered in the conversion fraction. With HBcat and HBpin, no CO_2 conversion was observed even after 24 hours. In the case of 9-BBN, NMR monitoring showed in addition to the 9-BBN resonances, new signals at δ = -6.3 ppm by $^{31}P\{^1H\}$ NMR, and at δ = -16.0 ppm by $^{11}B\{^1H\}$ NMR that could correspond to the phosphine adduct as well as signals for bis(boryl)acetal and methoxyborane. After 1 hour only 7 % conversion of 9-BBN was observed and after 24 hours, 36 % of 9-BBN was converted for a ratio of bis(boryl)acetal and methoxyborane of 0.7 : 1.

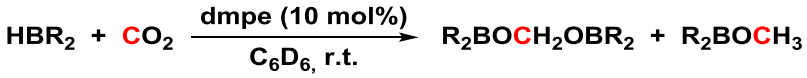

Scheme 45. Blank experiments in the same conditions with only dmpe as catalyst precursor

HBR_2	Time (h)	Conv. of HBR_2 (%)	$R_2BOCH_2OBR_2$	R_2BOCH_3
HBcat	1	0	0	0
	24	0	0	0
HBpin	1	0	0	0
	24	0	0	0
9-BBN	1	7	1	0
	24	36	0.7	1

Table 10. Dmpe as catalyst precursor with the three hydroboranes

In this context, 9-BBN was chosen for the selective synthesis of the bis(boryl)acetal.

3.3.3 Optimization of the conditions for the selective generation of bis(boryl)acetal 127

The experimental conditions for a selective synthesis of the bis(boryl)acetal **127** were first studied in NMR tubes. Pre-catalyst **40** and 9-BBN were placed in 0.5 mL of a solvent, degassed and placed under a CO_2 pressure. The tube was then introduced in the NMR machine at the requested temperature for regular NMR controls.

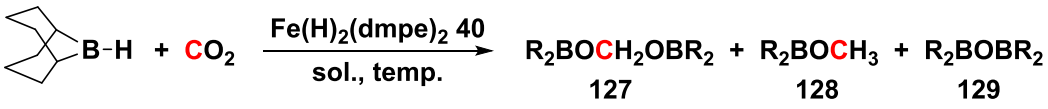

Scheme 46. Optimization of the conditions for selective synthesis of compound **127**

As depicted in Table 11, the relative ratio of **127** : **128** and the corresponding time were given for the highest quantity of bis(boryl)acetal compound **127** formed. The standard reaction was performed with 5 mol% of catalyst loading, 1 atmosphere of CO_2 and at 25 °C in C_6D_6 (entry 1), and a ratio of 5.6 : 1 was observed after 170 minutes of the reaction for 95 % conversion of 9-BBN. Lowering the temperature both decreased the reaction rate and the selectivity in **127** (entry 7). In contrast, rising the temperature afforded rapid conversion of 9-BBN (> 99 % within 47, 20 and 10 minutes, at 45, 50 and 60 °C, respectively. entries 8-10) and higher ratios of **127**

(up to 13.4 : 1, entry 10). Changing the solvent to THF favored the formation of the bis(boryl)acetal **127** in terms of rate and selectivity (entries 11-14). It is important to note that no hydroboration reaction occurred in the absence of catalyst, even upon heating the mixture of the reactants up to 50 °C for two weeks (entry 17).

#	mol %	$P(CO_2)$	T °C	Time (min.)	Conv. of 9-BBN (%)	relative ratio **127** : **128**	Solvent
1	5	1	25	170	95	5.6 : 1	C_6D_6
2[a]	5	1	25	225	93	1.9 : 1	C_6D_6
3	10	1	25	145	98	3.4 : 1	C_6D_6
4	10	3	25	165	89	0.6 : 1	C_6D_6
5	1	1	25	180	95	2.4 : 1	C_6D_6
6	5	3	25	135	93	1.1 : 1	C_6D_6
7	5	3	10	455	64	0.6 : 1	C_6D_6
8	5	1	45	47	> 99	8.8 : 1	C_6D_6
9	5	1	50	20	> 99	12.6 : 1	C_6D_6
10	5	1	60	10	> 99	13.4 : 1	C_6D_6
11	5	1	25	30	> 99	18.2 : 1	THF-D_8
12	1	1	25	47	> 99	19.9 : 1	THF-D_8
13	1	3	25	47	> 99	11.2 : 1	THF-D_8
14	0.1	1	25	53	> 99	12.3 : 1	THF-D_8
15	5	1	25	150	> 99	2.1 : 1	Tol-D_8
16[b]	2	1	60	47	4[c]	3.5:1	THF-D_8
17[d]	---	3	---	2 weeks	0	0	THF-D_8

[a]: 0.26 mmol of 9-BBN and related 5 mol% catalyst; [b]: dmpe as catalyst; [c]: the reaction of 9-BBN with dmpe did not count into the conversion of 9BBN; [d]: without any catalyst, up to 50 °C for two weeks.

Table 11. Optimization of the conditions of the CO_2 reduction with 9-BBN and blank experiments

Based on these experimental data, the optimized general method for the generation of compound **127** was achieved with 1 mol% of catalyst loading, after 47 minutes at room temperature in THF. Using 9,10-dihydroanthracene or paramethylanisole as internal standards, a yield of 85 % in **127** by ^1H NMR integration and full conversion of 9-BBN by $^{11}B\{^1H\}$ NMR were determined, which corresponds to a turnover number of 85, while the turnover number is defined as the number of moles of **127** formed per mole of iron catalyst. Experimental data

revealed that the two internal standards were inert against the reductive process since adding them at the beginning or at the end of the reaction had no influence on the results.

The catalytic performance of the depe complex $[Fe(H)_2(depe)_2]$ **126** was also tested (Table 12). Using a similar procedure, initial testing with 1 mol% catalyst loading gave a very good 94 % yield of **127** corresponding to a turnover number of 94 (entry 1). Increasing the temperature afforded faster reactions: 15 minutes at 40 °C and 3 minutes at 60 °C for similar yields. Interestingly, the catalyst loading could be decreased to 0.1 mol% for an 89 % yield, with the corresponding turnover number of 890 (entry 4).

#	mol %	T °C	Time (min.)	Conv. of 9-BBN (%)	yield **127** %: **128** %
1	1	25	47	> 99	94 : 6
2	1	40	15	> 99	86 : 3
3	1	60	3	> 99	87 : 3
4	0.1	25	47	> 99	89 : 6

Table 12. Catalytic performance of complex $[Fe(H)_2(depe)_2]$ **126** (in THF solvent and under 1 atm. of CO_2)

3.3.4 Evolution of the bis(boryl)acetal compound 127

In the reported base catalyzed CO_2 hydroboration system, the bis(boryl)acetal was formed transiently and then fully reduced to methoxyborane within 7 hours.[263] By comparison, in our iron-catalyzed system, compound **127** was not further reduced to **128**, at least in a significant amount. After 47 min., the yield of **127** and **128** are 85 % and 8 %, respectively. After 15 hours, more than 50 % of **127** and only 11 % of **128** were observed (Figure 42). The yield in **128** does not increase by a large factor. The decrease in **127** might be explained by rearrangement leading to uncharacterized products (B-attached products) exhibiting methylene signals in the ^1H NMR spectra (Figure 43).

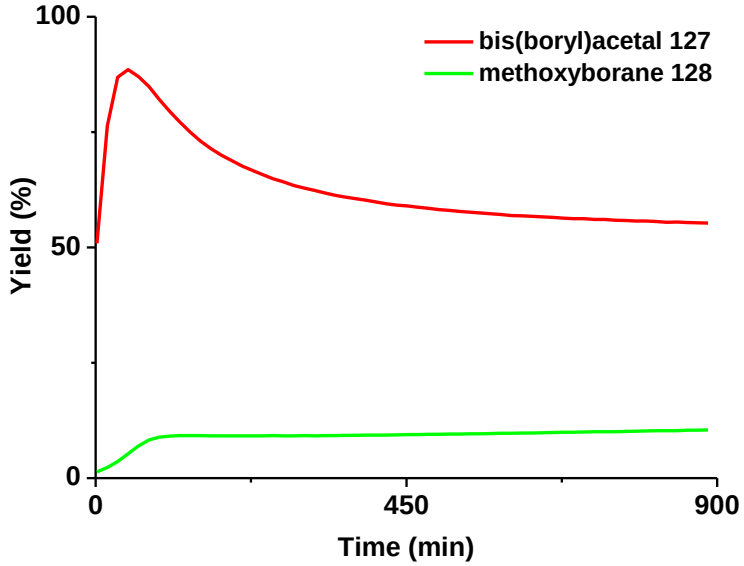

Figure 42. Evolution of the catalytic mixture **127** and **128**.

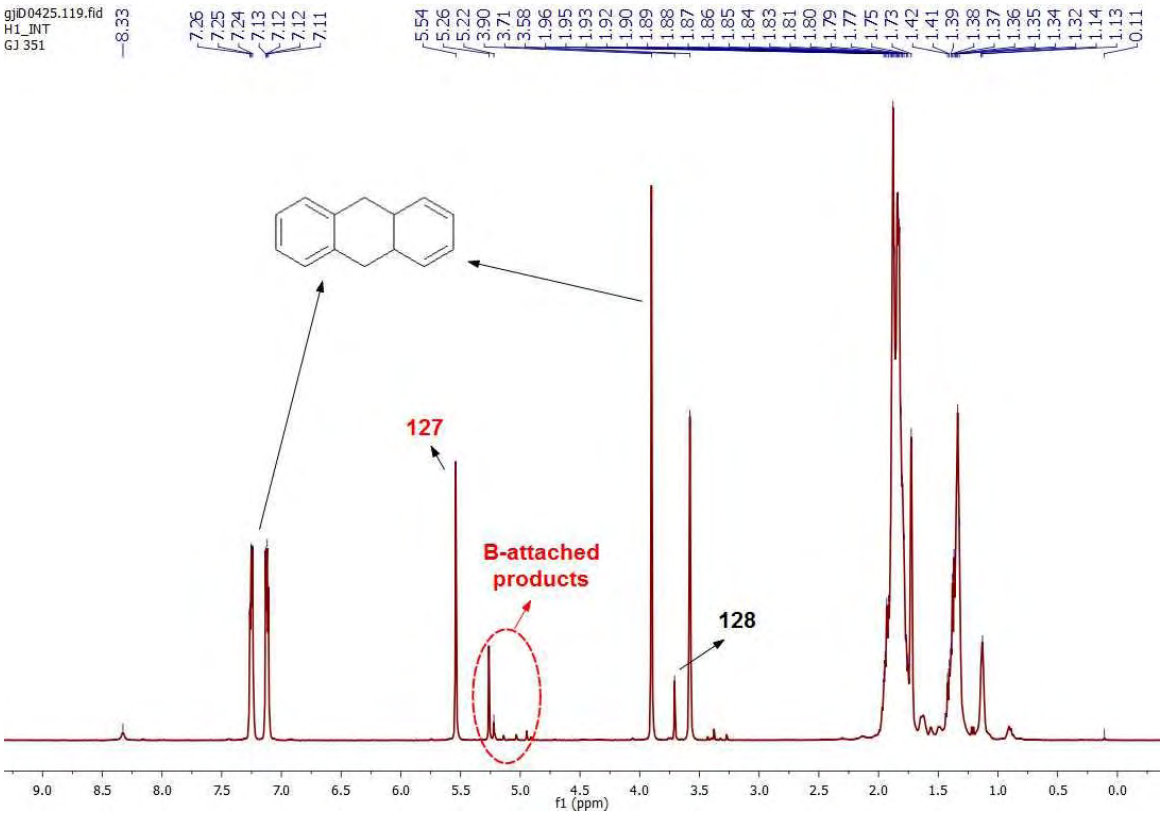

Figure 43. ^{1}H NMR spectrum of the iron-catalyzed CO_2 hydroboration system (after 15 h)

Interestingly, some crystals were obtained from the reaction mixture kept eight weeks at room temperature. X-ray diffraction analysis of these crystals revealed the compound

[((C8H14)(HOOC)B(OCH2)PMe2)2C2H4] **130** (Figure 44), presumably generated from the reaction of free dmpe with the bis(boryl)acetal derivative. Each phosphorus are indeed linked to a formaldehyde moiety, linked to a formoxyborane moiety. This is reminiscent of the results presented by Stephan et al.,[266] [(R3PCH2O)(HCOO)B(C8H14)] (R = tBu or 1,4-MeC6H4), with comparable B-O bond distances (in the range of 1.4932(18) to 1.5693(18) Å).

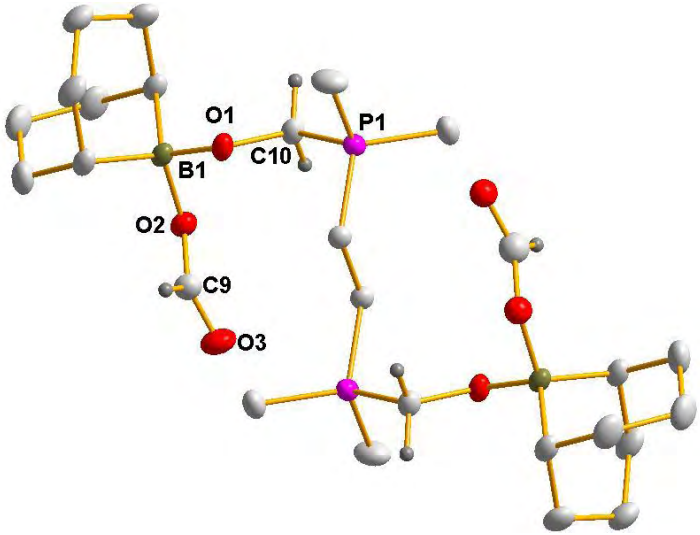

Figure 44. Molecular structure [((C8H14)(HOOC)B(OCH2)PMe2)2C2H4] **130** (full structure has been generated by applying the inversion center symmetry), ellipsoids are given at the 50 % probability level and hydrogen atoms are omitted for clarity except for the ones on carbon atoms from CO2.

3.3.5 Scale-up synthesis of compound 127

Ten-fold scale up syntheses of compound **127** were also investigated. Unfortunately, the ratio in compound **127** was not comparable when applying the optimized NMR tube procedure to experiments in Fisher-Porter bottles. Changing the pressure of CO_2 (static or dynamic pressures) had little impact on the results. An average yield of 35 % was always obtained for the generation of **127**, while the related average yield of 60 % for all "CH_2" moieties (acetal and B-attached products featuring methylene units) was calculated by ^{1}H NMR integration. Despite many attempts, it was impossible to identify the reasons for such a difference. However, at 60 °C, full conversion of 9-BBN was observed after only 10 minutes, and a yield of 69 % in compound **127** and a yield of 87 % in all "CH_2" moieties were obtained by ^{1}H NMR integration (Figure 45).

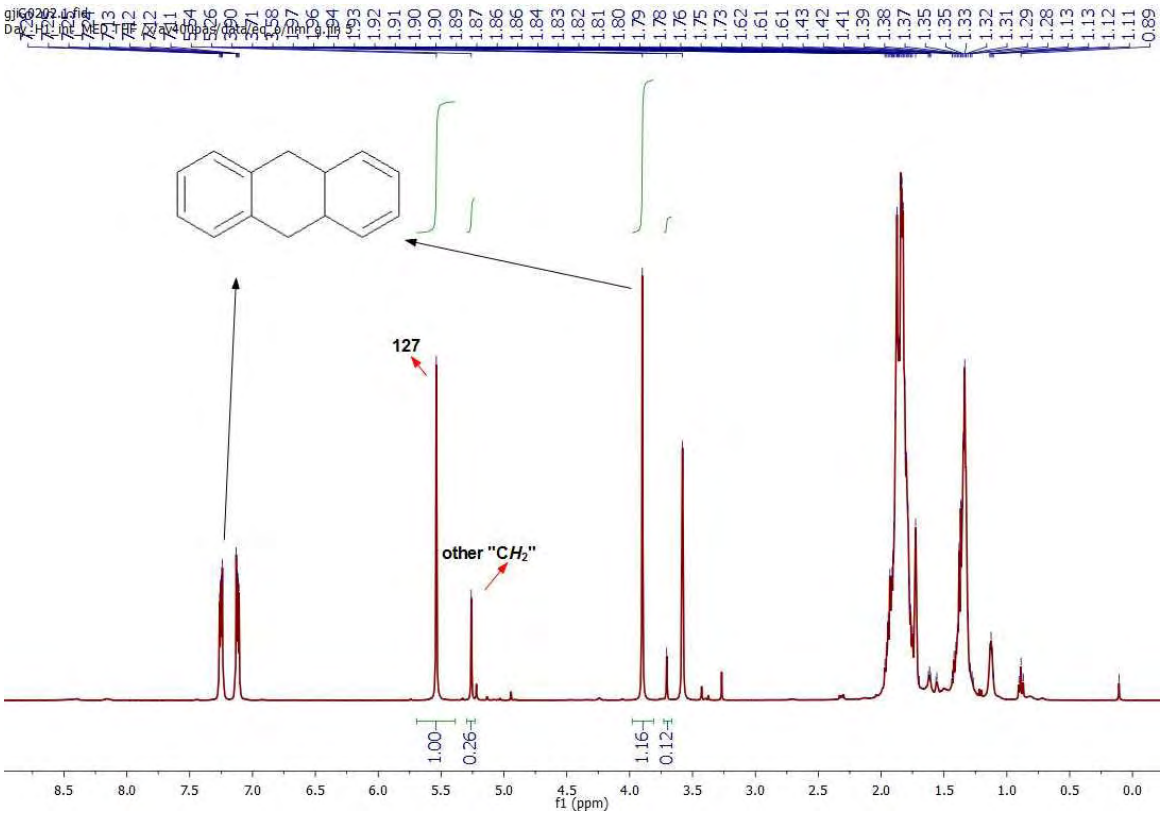

Figure 45. ^{1}H NMR spectrum of the scale up catalytic reaction at 60 °C after 10 min (400.2 MHz, 298 K, THF-D_8)

3.3.6 Conclusion

In conclusion, the (dihydrido)iron complex [Fe(H)$_2$(dmpe)$_2$] **40** is an efficient catalyst for the reduction of CO_2 into either bis(boryl)acetal or methoxyborane depending on the hydroborane used as reductant. The bis(boryl)acetal compound has been synthesized in a very good yield of 85 % at room temperature under only 1 atm. of CO_2. In the case of catalyst [Fe(H)$_2$(depe)$_2$] **126**, the yield reaches 96 %. Additional experiments will be needed to really evaluate the potential of catalyst **126** whose properties are quite similar to **40.**

3.4 Reductive functionalization of CO_2

The standard CO_2 reduction was carried out with 1 mol% of catalyst (complex **40**) loading, using 9-BBN as reagent in THF solution under an atmosphere of CO_2 at room temperature for 47 minutes. For scale up reactions, the standard reduction was performed at 60 °C for 10 minutes. An average yield of 85 % for bis(boryl)acetal **127** was set as total carbon source input for the functionalization reactions.

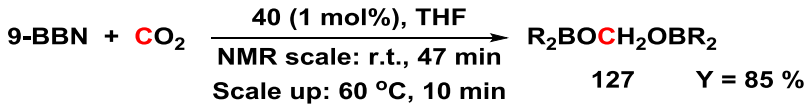

Scheme 47. Standard iron-catalyzed selective reduction of CO_2 into bis(boryl)acetal **127**

3.4.1 Ability of 127 as a methylene source

Formaldehyde is one of the simplest organic compounds. It is a very reactive C1 source that can provide the methylene moiety for the synthesis of more complex and value-added compounds. It is also known that formaldehyde is stabilized in alcohol solutions as hemiacetals (R_3C-OCH_2O-H)[271,272] and the formation of hemiacetal from formaldehyde and methanol has been mechanistically studied.[273] Interestingly, the bis(boryl)acetal compound pinB-OCH_2O-Bpin has been identified to have a reactivity similar to formaldehyde.[220] Thus, the in situ generated compound **127** is postulated to be a reactive methylene source for further applications.

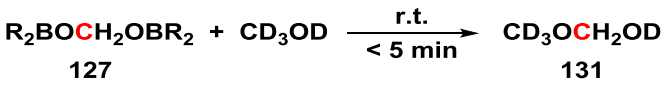

Scheme 48. Initial testing of **127** as a methylene source

The ability of compound **127** to transfer the methylene moiety was first tested with the addition of 0.4 equivalent of deuterated methanol compared to 9-BBN. NMR analyses indicated the formation of the corresponding hemiacetal **131** (^{1}H NMR at δ = 4.54 ($^1J_{C\text{-}H}$ = 160 Hz) and $^{13}C\{^1H\}$ at δ = 91.0) in 89 % (and 72 %) NMR yield based on the trapping agent (and 9-BBN) respectively, within 5 minutes. The 10-fold scale up test was performed by adding excess of methanol after the standard CO_2 reduction, and a yield of 86 % based on 9-BBN for the generation of compound **131** was observed by ^{1}H NMR integration with an internal standard. Even if the two systems cannot be compared directly, it is interesting to note that in the case of the previously reported ruthenium system, compound **131** was obtained in 37 % yield based on HBpin from the CO_2 hydroboration with 1 mol% of ruthenium catalysts.[220]

The versatile reactivity of compound **127** was then investigated in some representative reactions of formaldehyde. Unless otherwise stated, yields are based on the trapping agent to account for the efficiency of the trapping reactions.

Both $^{13}CO_2$ and $^{12}CO_2$ were used to confirm by multinuclear NMR and HRMS that the methylene carbon atom in the produced compounds resulted from the reduction of CO_2. Beneficial from

detailed experiments performed in NMR tubes, scale-up functionalized products were also isolated in good yields.

3.4.2 Generation of C=N and C-N bonds

3.4.2.1 Reaction with primary amines to afford imines (C=N bond)

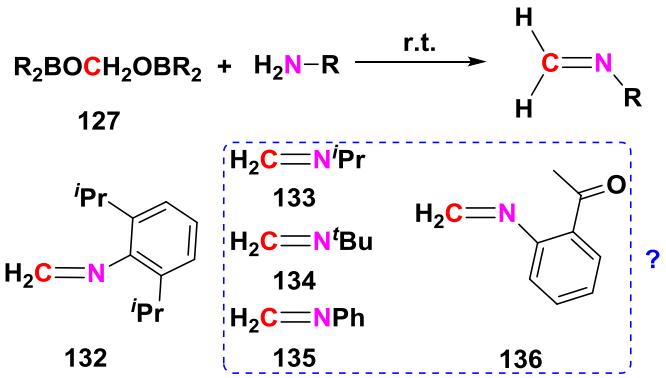

Scheme 49. In situ generation of imines (C=N bond)

In situ generated compound **127** was reacted at room temperature with diisopropylaniline to afford the corresponding imine compound **132** (Scheme 49), within 20 minutes, in a 83 % (and 66 %) NMR yield based on the trapping agent (and 9-BBN) respectively. The reaction was performed with $^{13}CO_2$ and both ^{1}H (δ = 7.73 ($^{1}J_{C\text{-}H}$ = 150.9 Hz) and 7.30 ($^{1}J_{C\text{-}H}$ = 132.0 Hz) ppm, $^{13}CH_2$) and $^{13}C\{^{1}H\}$ (δ = 156.5 ppm, $^{13}CH_2$) NMR characterization indicated the generation of **132**.

Other amines like 2-propanamine, *tert*-butylamine, benzenamine and 2-(methylcarbonyl)benzenamine were also tested to get the corresponding imines (**133**-**136**), but no direct evidence for the generation of the imines either by NMR or by HRMS was obtained. The reason for that is probably due to the high reactivity of the amino group toward acetals, leading to uncontrolled reactions.[274]

3.4.2.2 Reaction with secondary amines to form acyclic aminals (C-N bonds)

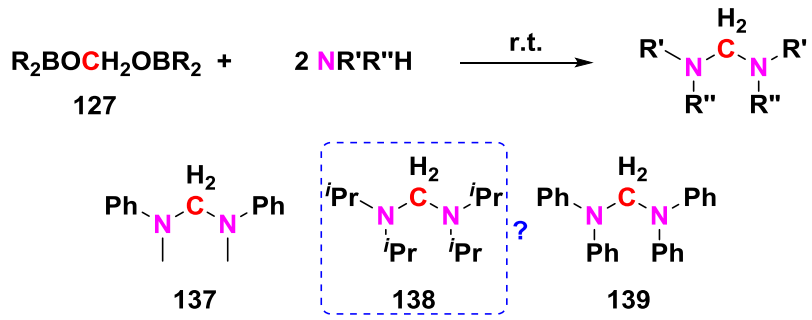

Scheme 50. In situ generation of acyclic aminals (C-N bonds)

The addition of N-methylbenzenamine to **127** at room temperature afforded the acyclic aminal **137** in 92 % yield within 1 hour. Compound **137** was characterized by ^{1}H NMR with a doublet signal at δ = 4.77 ppm ($^{1}J_{C\text{-}H}$ = 146.3 Hz) for the two protons and by $^{13}C\{^{1}H\}$ NMR with a resonance at δ = 71.0 ppm for the carbon atom of the $^{13}CH_2$ linker. The independent synthesis of compound **137** was also conducted by reacting a formaldehyde solution with N-methylbenzenamine. After 16 hours at room temperature, **137** was obtained after workup in 72 % yield. In this context, the bis(boryl)acetal **127** seems to be a more reactive surrogate of formaldehyde in terms of reaction rate and yield.

When adding bis(diisopropyl)amine to the in situ generated **127**, although the NMR characterization revealed a resonance at δ = 4.93 ppm with $^{1}J_{C\text{-}H}$ = 155.7 Hz in ^{1}H NMR and at δ = 77.0 ppm in $^{13}C\{^{1}H\}$ NMR, thus in the range of a methylene moiety, the HRMS analysis did not afford the correct data for compound **138**. In the case of the reaction between bis(phenyl)amine and **127**, compound **139** was formed in one hour with a very good yield of 91 %. In situ characterization for the methylene linker gave one resonance in ^{1}H NMR at δ = 5.63 ppm ($^{1}J_{C\text{-}H}$ = 158.0 Hz), and in $^{13}C\{^{1}H\}$ NMR at δ = 79.3 ppm.

These observations might be due to the different influence of the substituents on the nitrogen atom, the stronger electron-donating groups (^{i}Pr) on bis(diisopropyl)amine probably led to other by-products and were unproductive in the formation of the corresponding aminal.

3.4.2.3 Reaction with diamines to form cyclic aminals (C-N bonds)

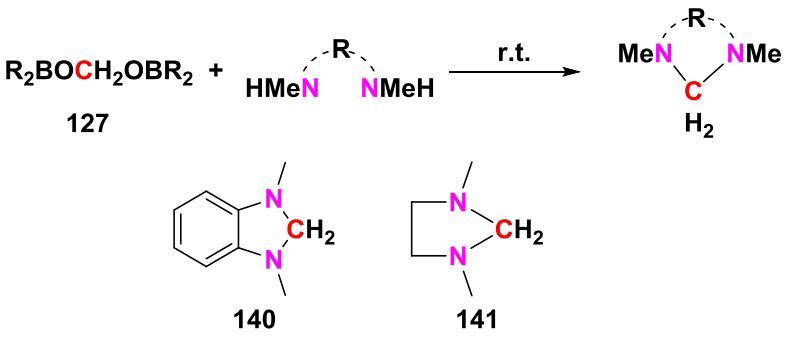

Scheme 51. In situ generation of cyclic aminals (C-N bonds)

The cyclic aminals are notably used as organic hydride donors or strong one-electron reducing agents, and as N-heterocyclic precursors.[275–277] The addition of N,N-dimethyl-1,2-benzenediamine to **127** at room temperature afforded the cyclic aminal **140** within 3 hours with a 77 % yield. ^{1}H NMR spectrum showed the resonance for the two protons on the methylene linker: a doublet at δ = 4.24 ppm with $^{1}J_{C\text{-}H}$ = 148.0 Hz when $^{13}CO_2$ was used and the $^{13}C\{^{1}H\}$ NMR spectrum showed a resonance at δ = 81.3 ppm.

For the reaction of **127** and N,N-dimethyl-1,2-ethanediamine, compound **141** was generated at room temperature after 2 hours in 69 % yield. In situ characterization by ^{1}H NMR revealed a resonance at δ = 3.21 ppm ($^{1}J_{C\text{-}H}$ = 144.0 Hz) for the protons of the $^{13}CH_2$, at δ = 2.68 ppm ($^{3}J_{C\text{-}H}$ = 3.4 Hz) for the CH_2 moieties of the linker and at δ = 2.29 ppm ($^{3}J_{C\text{-}H}$ = 5.6 Hz) for the methyl groups. The signal observed in $^{13}C\{^{1}H\}$ NMR at δ = 81.1 ppm was assigned to the $^{13}CH_2$ linker. In addition a signal at δ = 160.8 ppm was detected in the reaction mixture and pointed out to the formation of a carboxylato group, which could be an intermediate or a by-product of the reductive functionalization reaction. Moreover, some crystals ([(OCO)N(Me)(C_2H_4)N(Me)(C_8H_{14})] **142**) were obtained when keeping the mixture at room temperature for 6 days. X-ray diffraction showed that the CO_2 group was indeed existing. The diamine is bonded to BBN on one side and to the carbon of the carboxylato group on the other side. The carboxylato function also bonded to BBN gave rise to the formation of a seven membered ring (Figure 46).

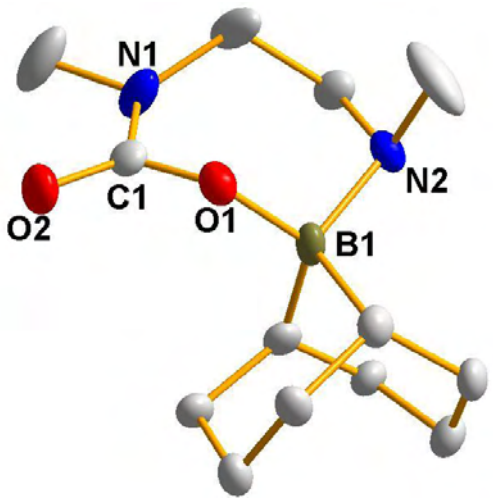

Figure 46. Molecular structure of crystals **142** obtained after the reaction between **127** and N,N-dimethyl-1,2-ethanediamine, ellipsoids are given at the 50 % probability level and hydrogen atoms are omitted for clarity

3.4.3 Generation of C-O and N-C-O bonds

3.4.3.1 Reaction with diol to form acetal (C-O bonds)

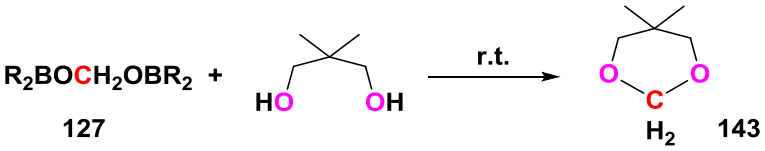

Scheme 52. In situ In situ generation of other acetal (C-O bonds)

The addition of 1,3-dihydroxy-2,2-dimethylpropane to in situ generated compound **127** gave rise to a new compound tentatively assigned as acetal **143** in a 77 % estimated yield based on NMR data: ^{1}H resonance for the $^{13}CH_2$ moiety: at δ = 4.62 ppm ($^{1}J_{C\text{-}H}$ = 159.5 Hz)) and $^{13}C\{^{1}H\}$ resonance at δ = 90.8 ppm.

3.4.3.2 Reaction with aminoalcohols to form hemiaminals (N-C-O bond)

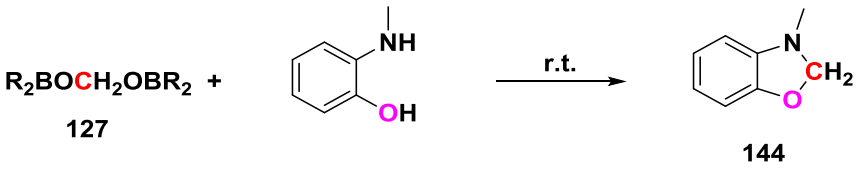

Scheme 53. In situ generation of cyclic hemiaminals (O-C-N bonds)

Similar to the synthesis of cyclic / acyclic aminals, in situ generated compound **127** was reacted at room temperature with N,N-dimethyl-1,2-benzenediamine giving rise to the corresponding cyclic hemiaminal **144** in 67 % yield within 1 hour. The $^{13}CH_2$ linker gave one resonance in ^{1}H NMR at δ = 5.13 ppm ($^{1}J_{C\text{-}H}$ = 160.1 Hz), and in $^{13}C\{^{1}H\}$ NMR at δ = 91.8 ppm.

3.4.4 Generation and isolation of hexamethylenetetramine (cage compound)

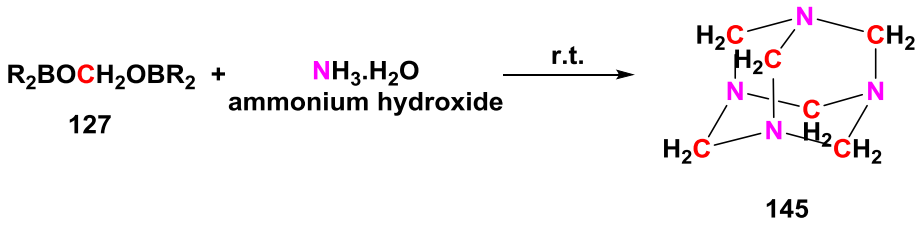

145

Scheme 54. In situ generation of cage compound **145**

Ammonia is an important building block, but its reactivity is usually difficult to control. However, the reaction of ammonia with formaldehyde is a known reversible condensation which affords the cage compound hexamethylenetetramine **145**, a versatile organic reagent.[278–280] In situ generated compound **127** exposed to an ammonia solution led to compound **145** after 16 hours at room temperature; a yield of 32 % based on ammonia was obtained when using one equivalent of ammonium hydroxide, and a yield of 84 % based on 9-BBN was obtained when adding an excess of ammonium hydroxide. This compound features six methylene moieties, all resulting from the bis(boryl)acetal compound, thus six carbon resulting from CO_2. Both ^{1}H and $^{13}C\{^{1}H\}$ NMR characterization indicated the generation of **145**, the resonances at δ = 4.61 ($^{1}J_{C\text{-}H}$ = 149.0 Hz) and δ = 76.0 for the protons and carbon atoms of the $^{13}CH_2$ moieties, respectively.

In a next stage, the isolation of compound **145** was achieved. On a 10-fold scale up synthesis, compound **127** was selectively generated at 60 °C within 10 minutes, and subsequently trapped to afford compound **145** after 36 hours in an isolated yield of 98 % based on ammonium hydroxide. Furthermore, a 100-fold scale up synthesis led to compound **145** (106.2 mg) in two days at room temperature with a 70 % isolated yield based on 9-BBN. Elemental analysis confirmed the purity of the isolated **145**.

3.4.5 Generation of dithiolmethylene (C-S bonds)

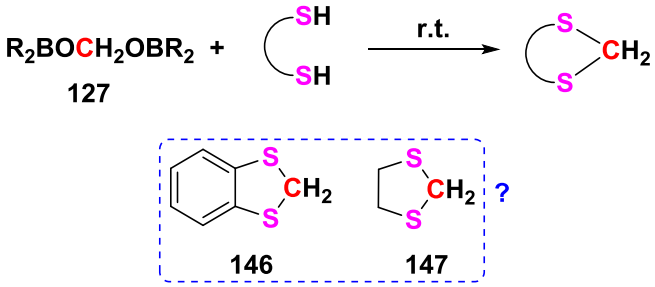

Scheme 55. In situ generation of dithiolmethylene (C-S bonds)

Preliminary experiments were performed on two dithiol substrates, 1,2-benzenedithiol and 1,2-ethanedithiol. After 5 hours, compound **127** was totally consumed for both reactions. NMR monitoring showed the $^{13}CH_2$ resonances at δ = 5.35 ppm ($^1J_{C\text{-}H}$ = 160.1) and 5.08 ppm ($^1J_{C\text{-}H}$ = 158.0 Hz) by ^{1}H NMR, and at δ = 70.3 ppm and at δ = 68.8 ppm by $^{13}C\{^1H\}$ NMR for the reactions of **127** with 1,2-benzenedithiol and 1,2-ethanedithiol in THF-D_8, respectively. HRMS measurement on the mixtures gave evidence for the existence of **146** but more detailed characterization will be needed to ascertain the formation of the dithiolmethylene and the formation of the postulated new C-S bonded products (**146** and **147**). It should be noted that NMR data of the S-*CH*$_2$-S resonances for compounds **146** (δ = 4.48 ppm by ^{1}H MMR (in $CDCl_3$)) and **147** (δ = 3.86 ppm by ^{1}H NMR, δ = 34.3 ppm by $^{13}C\{^1H\}$ NMR (in $CDCl_3$)) in literature[281–283] are quite different from those that we observed.

3.4.6 Generation of C-C bonds

3.4.6.1 Reaction with ylide to form an olefin (C=C bond)

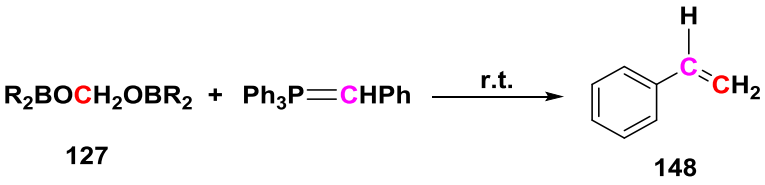

Scheme 56. In situ generation of compound **151** (C=C bond)

In order to generate a C=C double bond, a Wittig reaction was envisioned. It is a chemical reaction of an aldehyde or ketone with a triphenyl phosphonium yilde to give an alkene.[284–286] Thus compound **148** (styrene) was generated from the reaction of **127** and tripheny(phenylmethylene)-phosphorane in a good yield of 72 % after 5 hours at room temperature. The in situ generated compound **148** was characterized with a terminal methylene

moiety at δ = 5.75 and 5.18 ppm in ^{1}H NMR and at δ = 113.8 ppm in ^{13}C{^{1}H} NMR as well as by high resolution mass spectrometry.

3.4.6.2 Generation of C-C-N bonds via Mannich reation

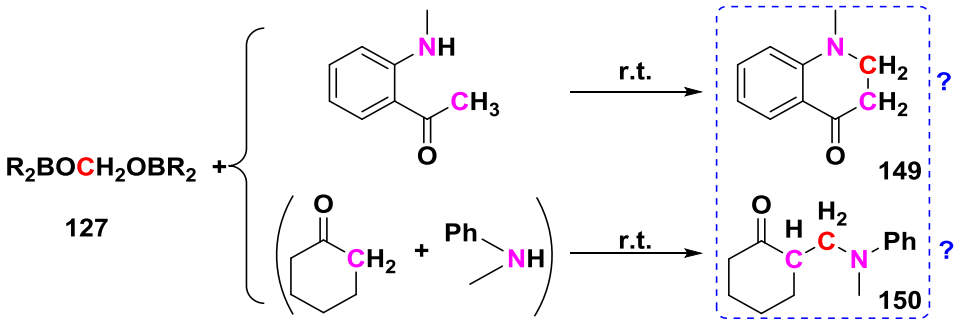

Scheme 57. In situ generation of other hemiacetals (C-C-O bond)

A major goal was also to generate a C-C bond in those conditions. Mannich reaction is an important reaction in organic synthesis that is able to generate a C-C bond between formaldehyde and an activated nucleophilic carbon[287,288]. It is an amino alkylation process introducing an aminomethyl group generally in the α-position to a carbonyl function.[289,290] Thus the substrates 1-acetyl-2-aminobenzene and the combined cyclohexanone and N-methylbenzenamine were tested with compound **127** to generate cyclic and acyclic hemiacetal compounds. Unfortunately, neither NMR nor HRMS characterization indicated the formation of **149** and **150**. In this context, further investigation on different substrates and reaction conditions is desired.

3.4.6.3 Generation and isolation of bis-(2,4-tert-butyl-phenol)methylene (C-C bonds)

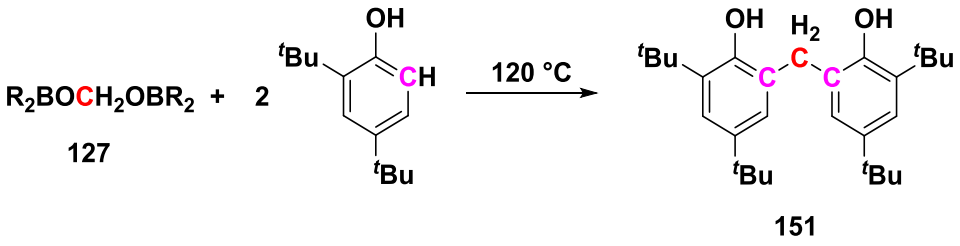

Scheme 58. In situ generation of compound **151** (C-C bonds)

In order to form C-C single bonds, phenols were considered as reagents. Formaldehyde is indeed used at the industrial scale in phenol resins, via condensation reaction generating C-C bonds. For a proof of concept, a protected phenol in the positions 2 and 4 with *tert*-butyl groups was chosen. Compound bis-(2,4-tert-butyl-phenol)methylene **151** was first generated from the

reaction of paraformaldehyde with the substituted phenol compound for comparison and NMR signature in THF. In the presence of a base (KOH), compound **151** was generated in an in-situ measured yield of 48 % at 120 °C after 16 hours.

When in situ generated compound **127** was used instead of paraformaldehyde, the reaction occurred with the production of **151** in a 23 % yield after 16 hours at 120 °C and in a 46 % yield after 36 hours at 120 °C. Longer reaction time (48 h) did not improve the yield. Notably, this reaction was performed without the need for base (KOH) addition. When 13 labelled CO_2 was used, the methylene moiety of **151** exhibited one resonance in ^{1}H NMR at δ = 3.88 ppm ($^{1}J_{C\text{-}H}$ = 126.1 Hz) and in $^{13}C\{^{1}H\}$ NMR at δ = 32.6 ppm.

The isolation of the functionalized compound **151** was performed with a 10-fold scale up synthesis. After 48 hours at 120 °C, an isolated yield of 37 % was obtained after workup. Elemental analysis certified the purity of the isolated compound **151**.

3.4.7 Conclusion

Selective reduction of CO_2 to the acetal level and subsequent functionalization in a one-pot two-steps procedure allows to transform CO_2 into methylene and to considerably enlarge the scope of accessible functions by generating not only new C-N, but also C-O, C-S and C-C bonds. In addition, scale up reactions allow to isolate the value-added compounds.

The important variations of ^{1}H and ^{13}C NMR chemical shifts (from $\delta(^{13}C)$ = 32.6 ppm and $\delta(^{1}H)$ = 3.88 ppm for compound **151** to $\delta(^{13}C)$ = 156.5 ppm and $\delta(^{1}H)$ = 7.73 ppm for compound **148**), indicating different types of methylene, highlight the versatile reactivity of the bis(boryl)acetal compound **127**.

In parallel of the present work, Cantat et al. reported their investigation on CO_2 reductive functionalization.[291] A metal-free system was used to generate aminals or by heating the mixture of aromatic amines and $PhSiH_3$ in CD_3CN at 80 °C under 1 atmosphere of CO_2 in NMR tube scale. Using a malonate compound instead of an amine, C-C bonds were also generated. By comparison, the advantage of their system is that it allowed to put all the reagents in one-pot one-step for the reductive functionalization of CO_2. However, the temperature is higher (80 °C), only NMR tube scale reactions were described, and the scope of value-added compounds are still narrow with C-N and one example of C-C bond formation.

Chapter 4

General conclusion

The main aim of this work was a detailed study of the use of iron in coordination chemistry and catalysis.

In the first part of this work, a family of iron complexes bearing a cooperative non-innocent ligand has been prepared thanks to careful experimental temperature and time controls. The pincer type ligand bis(picolyl)phosphine (NPN) gave access to different coordination modes starting from the reactive precursor [Fe{N(SiMe$_3$)$_2$}$_2$]. The resulting paramagnetic and diamagnetic iron complexes could be isolated and fully characterized by X-ray diffraction analyses and NMR spectroscopy both in solution and in the solid state. The dimeric complex [Fe(N(TMS)$_2$)(μ-$\kappa^{N,P}$:κ^{N}-NPN)]$_2$ **105** was also characterized by Mössbauer measurements, Evans method, EPR as well as powder X-ray diffraction.

For the first time, the non-innocent behavior of the NPN ligand was observed upon coordination. Deprotonation of NPN gave rise to the dearomatization of a pyridine ring in complex [Fe(N(TMS)$_2$)(μ-$\kappa^{N,P}$:κ^{N}-NPN)]$_2$ **105** and [Fe($\kappa^{N,P,N}$-NPN)$_2$] **106**. The reactivity of the original dimer complex **105** featuring an activated ligand has been tested with different substrates and some interesting results were gained. Preliminary tests show the possibility of using this complex as catalyst for small molecule activation, in particular for catalytic transformation of CO_2 with pinacolborane. Although the results showed low reactivity using this pre-catalyst, the observation of borane-attached compounds indicates the potential ability of **105** to be used for other catalytic applications. However, deeper investigation on this family of complexes is still needed. There are two main challenges for their use as pre-catalysts: in order to perform the catalytic reactions at ambient temperature one needs to solve the stability problems of these complexes and to properly monitor and characterize catalytic reactions involving paramagnetic species.

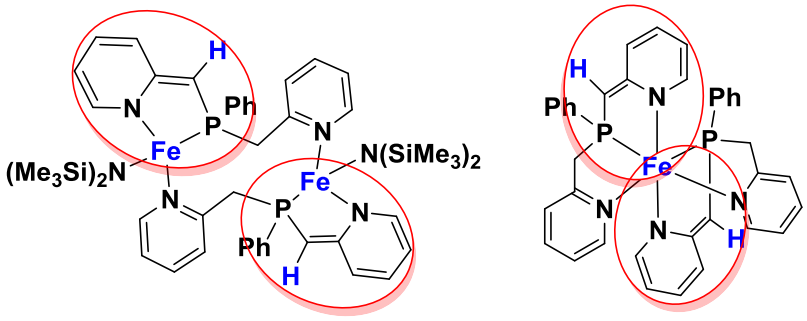

In the second part of this work, the first iron-catalyzed CO_2 reductive functionalization system, under mild conditions, was established successfully. In this system, hydroboranes were used as oxygen scavenger and hydrogen source for the selective reduction of CO_2 into a very reactive and versatile C1 source (bis(boryl)acetal). The process is catalyzed by iron-dihydride complexes [$Fe(H)_2$(diphosphine)$_2$] at ambient temperature. Through a one-pot two-steps procedure, CO_2 is transformed into a large scope of functions by generating not only new C-N, but also C-O, C-S and C-C bonds.

During the first step, CO_2 could be reduced into either bis(boryl)acetal or methoxyborane depending on the hydroborane used as a reductant. The nature of the solvent was also a key factor to influence the ratio between bis(boryl)acetal and methoxyborane. With an intensive study on the optimization of the experimental conditions, the bis(boryl)acetal compound **127** could be generated selectively using 9-borabicyclo(3.3.1)nonane (9-BBN) as the hydroborane, THF as solvent and 1 mol% of catalyst loading. Within 47 minutes, 85 % or 96 % yields were obtained when using catalysts [$Fe(H)_2(dmpe)_2$] **40** or [$Fe(H)_2(depe)_2$] **126**, respectively. In addition, a turnover number of 890 was achieved for bis(boryl)acetal generation with 0.1 mol% of catalyst loading. Scale-up synthesis conditions were also disclosed to afford a methylene compound in 87 % yield at 60 °C after only 10 minutes.

The unprecedented selective generation of bis(boryl)acetal and subsequent functionalization, allowed to transform CO_2 into methylene and for the first time, to expand the scope of value-added compounds synthesized from CO_2. The formation of two C-H bonds (reduction) and two C-E bonds (functionalization, E = N, O, S and C) resulted from complete deoxygenation of CO_2 via either 4 or 6 electrons transfer. Some of the interesting value-added compounds have been isolated in scale up reactions, indicating the potential and interest of such a system for further investigation and even industrial use.

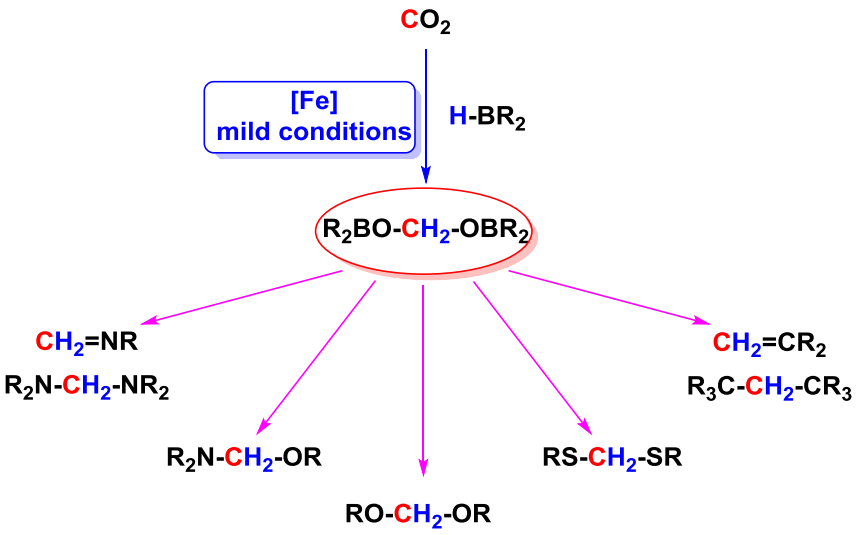

Detailed study on the mechanism of this process is still needed in order not only to improve the activity of the iron-based catalysts but also to further expand the product scope. A simpler procedure (one-pot one-step) to perform similar reactions under mild conditions is highly desirable, and replacement of the hydrogen source to silanes or H_2 is also a perspective in the near future.

The utilization of environmentally benign, inexpensive, selective and highly reactive catalysts is highly desired for industrial applications, and it will be interesting to monitor in the near future the improvements resulting from the use of iron based systems.

Chapter 5

Chapter 5

Experimental Section

General Methods

Manipulations were carried out following standard Schlenk line and glove box techniques (with O_2 and H_2O < 1 ppm), and Ar as the inert gas. Solvents were dried using an MBraun SPS column. Deuterated solvents were freeze-pump-thaw degassed and stored under Ar and over 4 Å molecular sieves. THF-d_8 was dried over sodium. Quick Pressure Valve NMR tubes were used for the reactions with CO_2.

Solution state NMR spectra were collected on several Bruker machines: a Bruker Avance 500 MHz, a Bruker Avance 400 MHz, a Bruker Avance 300 MHz and a Bruker 300 MHz DPX. NMR spectra on the Bruker Avance 500 MHz, including variable temperatures, were collected by C. Bijani and Y. Coppel. Solid-state NMR experiments were recorded on a Bruker Avance 400 spectrometer equipped with a 2.5 mm probe and operated by Y. Coppel. Samples were spun between 22 to 32 kHz with external temperatures at 280 K or 289 K. For ^{1}H MAS, ^{13}C MAS and ^{31}P MAS Hahn echo experiments were used with recycle delays of 1, 0.1 and 0.1 s, respectively.

All chemical shifts for ^{1}H and ^{13}C were relative to tetramethylsilane (TMS, δ = 0 ppm). ^{31}P chemical shifts were referenced to an external 85 % H_3PO_4 sample. Chemical shifts are given in ppm, coupling constants in Hz. ^{1}H and ^{13}C were referenced to internal residual protio solvent resonances.[292] The following abbreviations are used: br, broad; s, singlet; d, doublet; dd, doublet of doublets; t, triplet; pt, pseudo triplet; m, multiplet; ssb, spinning side bands.

Infrared spectroscopy was carried out using a Perkin Elmer 1725 Spectrometer and a Bruker Alpha P Spectrometer for ATR measurements. Microanalyses were performed by A. Moreau on a Perkin Elmer 2400 Series II Analyzer fitted with a catharometer. EPR data were recorded on an Elexys E500 Bruker spectrometer by L. Salmon, Mössbauer spectra were recorded on a Wissel System (transducer Wissel Ma260, controller Wissel Mr360, digital function generator Wissel Dfg1000) by J. F. Meunier. Isomer shifts are relative to the centroid of a spectrum of a metallic foil of α-iron at room temperature. Mass spectroscopy was carried out at the University (ICT) by E. Leroy, using a TSQ 7000 Thermo Electron mass spectrometer.

Unless otherwise indicated, all commercial available reagents were used as supplied and were purchased from Aldrich or AlfaAesar. 9-Borabicyclo[3.3.1]nonane (9-BBN) was bought as a dimer in the solid state.

Experimental Section Chapter 2

Synthesis of the iron precursor [FeN(SiMe$_3$)$_2$)$_2$] 103

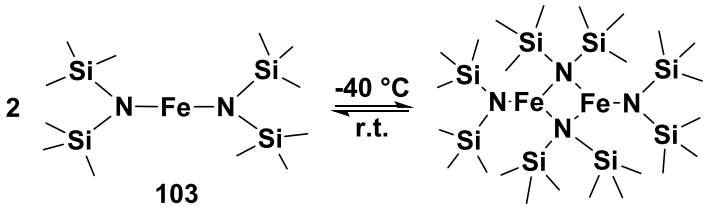

103

monomer dimer

$FeBr_2$ (5.39 g, 24.98 mmol) suspended in diethyl ether (50 mL) was added to $LiN(TMS)_2$ (8.35 g, 49.97 mmol) in diethyl ether (50 mL). The dark green suspension was then stirred overnight at room temperature to afford a brown-green solution. The solvent was removed under reduced pressure to leave a dark residue. The product was extracted with pentane (60 mL) giving rise to a dark green solution. The pentane was removed under reduced pressure and the resulting dark residue was purified by trap to trap distillation to yield a bright green solid below 243 K (bright green liquid at room temperature) in 81 % (7.6 g) yield. ^{1}H NMR (400.1 MHz, Toluene-D_8, 298 K,): δ = 59.42 (br), 0.60 (s). IR (ATR, cm^{-1}): *v* = 2949 (m), 2897 (w), 1429 (w), 1395 (w), 1244 (s), 990 (s), 970 (s), 917 (s), 815 (s), 787 (s), 751 (s), 665 (s), 634 (s), 610 (s).

Synthesis of Bis(2-picoly)phenylphosphine 96

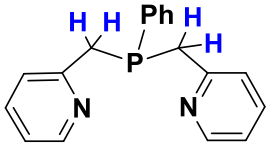

NPN 96

Dichlorophenylphosphine (2.7 mL, 3.559 g, 20.0 mmol) was added at -78 °C to a solution of 2-[(trimethylsilyl)methyl]pyridine (7.18 mL, 6.604 g, 40.0 mmol) in THF (50 mL) and diethyl ether (50 mL). Stirring was maintained overnight at room temperature. The solvent was then removed under reduced pressure to leave an orange oil. The product was extracted with hexane (at 50 °C, 75 mL) and the solvent removed under reduced pressure to yield a white solid, (2.630 g, 46 %). ^{1}H NMR (400.2 MHz, $CDCl_3$, 298 K): δ = 8.48 (m, 2H, H_{arom}), 7.53 – 7.42 (m, 4H, H_{arom}), 7.38 – 7.29 (m, 3H, H_{arom}), 7.09 – 6.98 (m, 4H, H_{arom}), 3.42 (dd, $^2J_{H\text{-}H}$ = 13.4, $^2J_{P\text{-}H}$ = 2 Hz, 2H, PC*H*$_2$), 3.35 (d, $^2J_{H\text{-}H}$= 13.4 Hz, 2H, PC*H*$_2$). ^{31}P{^{1}H} NMR (162.0 MHz, $CDCl_3$, 298 K): δ = -13.9. ^{13}C{^{1}H} NMR (100.6 MHz, $CDCl_3$, 298 K): δ = 158.2 (d, $^2J_{P\text{-}C}$ = 6 Hz), 149.2 (s), 136.8 (d, $^1J_{P\text{-}C}$ = 19 Hz), 136.0 (s), 132.6 (d, $^2J_{P\text{-}C}$ = 20 Hz), 128.3 (d, $^3J_{P\text{-}C}$ = 7 Hz), 123.6 (d, $^3J_{P\text{-}C}$ = 5 Hz), 120.8 (d, $^4J_{P\text{-}C}$ = 2 Hz), 37.7 (d, $^1J_{P\text{-}C}$ = 18 Hz). IR (ATR, cm^{-1}): *v* = 3102 (w), 3048 (w), 3005 (w), 2949 (w), 2904 (w), 1578 (s), 1565 (s), 1471 (s),

1432 (s), 1301 (m), 1249 (m), 1156 (m), 1088 (m), 991 (s), 838 (s), 795 (s), 780 (s), 738 (s), 692 (s), 627 (m), 592 (m), 494 (s), 481 (s), 411 (s), 402 (s).

Synthesis of 2-[(diphenylphophino)methyl]pyridine 101

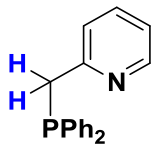

NP 101

A THF (24 mL) solution of 2-picolyllithium (0.594 g, 6.0 mmol) was added to a THF (5 mL) solution of Ph_2PCl (1.07 mL, 1.322 g, 6.0 mmol) at -78 °C. The solution was stirred for 1 h at -78 °C and 1 h at -40 °C and THF was removed under reduced pressure. A yellow solid was obtained. The latter was dissolved in EtOH and H_2O, and stored overnight at -30 °C giving a cream colored precipitate. The product was obtained after filtration and extraction with hexane at room temperature. After removing the solvent a white solid was obtained (0.602 g, 36.2 %). ^{1}H NMR (400.1 MHz, C_6D_6, 298 K): δ = 8.40 (m, 1H, H_{arom}), 7.53 – 7.43 (m, 4H, H_{arom}), 7.10 – 6.98 (m, 6H, H_{arom}), 6.91 (m, 1H, H_{arom}), 6.80 (dd, $^3J_{H\text{-}H}$ = 8 Hz, $^4J_{H\text{-}H}$ = 1 Hz, 1H, H_{arom}), 6.50 (dt, $^3J_{H\text{-}H}$ = 7 Hz, $^4J_{H\text{-}H}$ = 1 Hz, 1H, H_{arom}), 3.63 (s, 2H, PCH_2). $^{31}P\{^1H\}$ NMR (162.0 MHz, C_6D_6, 298 K): δ = -10.6. IR (ATR, cm^{-1}): ν = 3055 (w), 3011 (w), 2906 (w), 1962 (w), 1579 (m), 1566 (m), 1469 (s), 1432 (m), 1304 (w), 1253 (w), 1155 (m), 1081 (m), 1066 (m), 1049 (m), 1024 (m), 991 (m), 864 (m), 787 (s), 735 (strong), 693 (s), 627 (m), 591 (m), 504 (s), 488 (s), 472 (s), 425 (m), 405 (m).

Synthesis of complex [Fe(N(TMS)$_2$)$_2$($\kappa^{N,P}$-NPN)] 104

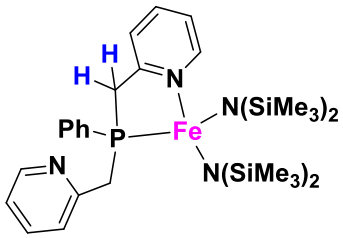

104

A pentane (8 mL) solution of [Fe(N(SiMe$_3$)$_2$)$_2$] (0.376 g, 1.0 mmol) was added to a pentane (6 mL) suspension of NPN (0.292 g, 1.0 mmol) at -78 °C under argon. After 90 min of stirring at -30 °C, a yellow precipitate of compound **104** was formed. The product was then isolated after filtration and washing with 6 mL of cold pentane (0.190 g, 28 %). Crystals suitable for X-ray diffraction were obtained by mixing a pentane solution of [Fe(N(SiMe$_3$)$_2$)$_2$] and a toluene solution of NPN at -78 °C, stirring for 90 min at -30 °C and letting crystallization occur at -37 °C. ^{1}H NMR (500.4 MHz,

Tol-d_8, 230 K): δ = 113.9 (br), 65.6 (s), 61.7 (s), 21.75 (br), 14.7 (br), 13.4 (br), 8.4 (br), 6.5 (br), 3.4 (s), 3.3 (s), 1.3 (br), 0.20 (s), -3.2 (br), -3.6 (br), -5.9 (s), -14.9 (br). Elementary pure samples could not be obtained due to the presence of small amount of free NPN and/or complex **105** in any prepared sample. IR (ATR, cm^{-1}): υ = 2944 (m), 2892 (w), 1596 (w), 1471 (w), 1435 (m), 1237 (s), 958 (s), 883 (m), 860 (m), 818 (s), 788 (m), 737 (m), 691 (s), 610 (m), 593 (m), 486 (s).

Synthesis of complex $[Fe(N(TMS)_2)(\mu\text{-}\kappa^{N,P}\text{:}\kappa^{N}\text{-NPN})]_2$ 105

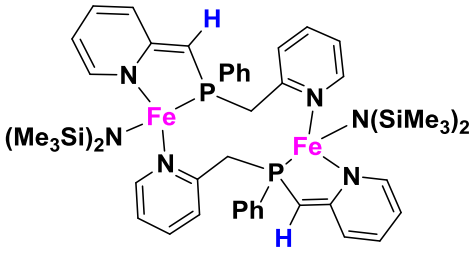

105

A solution of $[Fe(N(SiMe_3)_2)_2]$ (0.752 g, 2.0 mmol) in pentane (14 mL) was added to a suspension of NPN (0.584 g, 2.0 mmol) in pentane (8 mL) at -78 °C. After stirring for 3 h at -30 °C and 45 min at room temperature, **105** was isolated as a green precipitate, and washed with pentane (12 mL) to afford **105** as a dark green powder (0.820 g, 81 %). Alternatively, a pentane solution of $[Fe(N(SiMe_3)_2)_2]$ was added to NPN in a toluene solution at -78 °C, the solution was stirred at -30 °C for 3 hours and then 45 minutes at room temperature. Crystals suitable for X-ray diffraction were obtained by concentrating the mixture at room temperature. ^{1}H NMR (500.4 MHz, Tol-d_8, 301 K): δ = 169.3, 166.5, 146.0, 78.9, 61.8, 56.8, 52.7, 32.5, 22.5, 21.4, 10.7, 0.1, -2.4, -23.1, -28.3. Elemental Analysis: Calcd. for $C_{48}H_{68}N_6P_2Si_4Fe_2$: C, 56.80; H, 6.75; N, 8.28. Found: C, 56.54; H, 6.80; N, 7.60. Solid state MAS ^{31}P NMR (161.8 MHz, 289 K): δ = 41.0 ($w_{1/2}$ = 13.0 KHz). Solid state Mas ^{13}C NMR (100.5 MHz, 289 K): δ = 519.8, 344.4, 312.2, 298.6, 253.1, 240.9, 146.8, 33.0, 19.8. IR (ATR, cm^{-1}): ν = 2943 (m), 1614 (s), 1470 (s), 1443 (s), 1432 (s), 1368 (m), 1273 (m), 1240 (s), 988 (s), 975 (s), 901 (m), 867 (s), 815 (s), 774 (s), 749 (s), 738 (s), 725 (s), 694 (s), 665 (s), 610 (s), 496 (m), 482 (m), 413 (m).

Synthesis of complex [Fe(κ^{N,P,N}-NPN)$_2$] 106

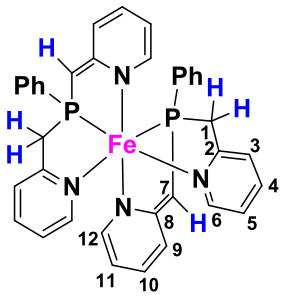

106

A pentane (4 mL) solution of [Fe(N(SiMe$_3$)$_2$)$_2$] (0.075 g, 0.199 mmol) was added to a pentane (2 mL) suspension of NPN (0.117 g, 0.40 mmol) at -78 °C. After stirring the solution for 3 h at -30 °C and 36 h at room temperature, **106** was isolated as a brown precipitate after filtration and washing with pentane (6 mL) (0.070 g, 55 %). Crystals suitable for X-ray diffraction were obtained by mixing [Fe(N(SiMe$_3$)$_2$)$_2$] and NPN in Et$_2$O at -78 °C, and leaving the solution at room temperature for two days. ^{1}H NMR (500.3 MHz, Tol-d$_8$, 240 K): δ = 8.48 (br, *H*6, 2H), 7.09 - 6.95 (*H*$_{phenyl}$, 10H), 6.85 (d, $^3J_{H\text{-}H}$ = 6 Hz, *H*12, 2H), 6.69 (br, *H*3 and *H*4, 4H), 6.55 (pt, $^3J_{H\text{-}H}$ = 7.5 Hz, *H*10, 2H), 6.31 (br, *H*5, 2H), 6.26 (d, $^3J_{H\text{-}H}$ = 8.7 Hz, *H*9, 2H), 5.56 (pt, $^3J_{H\text{-}H}$ = 6.2 Hz, *H*11, 2H), 4.06 (d, $^1J_{H\text{-}H}$ = 15.5 Hz, C*H*$_2$, 2H), 3.50 (s, C*H*, 2H), 3.14 (m, C*H*$_2$, 2H); ^{13}C{^{1}H} NMR (125.8 MHz, Tol-d$_8$, 240 K): δ = 175.3 (pt, $J_{C\text{-}P}$ = 12 Hz, *C*8), 167.1 (s, *C*2), 154.1 (s, *C*6), 149.1 (s, *C*12), 135.4 - 125.3 (*C*$_{phenyl}$), 133.5 (s, *C*4), 130.2 (s, *C*10), 123.6 (s, *C*3), 121.4 (s, *C*5), 112.9 (pt, $^3J_{C\text{-}P}$ = 9 Hz, *C*9), 104.1 (s, *C*11), 58.7 (pt, $J_{C\text{-}P}$ = 29 Hz, *C*7), 44.4 (pt, $J_{C\text{-}P}$ = 8 Hz, *C*1); ^{31}P{^{1}H} NMR (202.6 MHz, Tol-d$_8$, 240 K): δ = 87.0. Solid state MAS ^{31}P NMR (161.8 MHz, 280 K): δ = 86.5 ppm ($w_{1/2}$ = 1.8 KHz). HRMS (DCI-CH$_4$): Anal. Calcd. for $C_{36}H_{32}N_4P_2Fe$: 638.1452 g·mol^{-1}. Found: 638.1447 g·mol^{-1}. Elementary pure samples could not be obtained due to a rapid decomposition. IR (ATR, cm^{-1}): υ = 3047 (w), 3004 (w), 1591 (s), 1565 (m), 1462 (s), 1431 (s), 1358 (m), 1278 (m), 1267 (m), 1144 (m), 1103 (m), 992 (s), 888 (m), 827 (m), 796 (m), 736 (s), 723 (s), 692 (s), 603 (m), 490 (s).

Reaction of 105 with CO$_2$

A pressure of CO$_2$ (1 to 3 atm.) was introduced to a solution (Et$_2$O or THF, 5 mL) of **105** (81.2 mg, 0.080 mmol) at room temperature in a Fischer-Porter bottle. The mixture was stirred for 30 minutes, and a red precipitate was obtained after filtration and washing with Et$_2$O (6 mL). No solution state NMR was conducted due to its insolubility in all organic solvents. Solid state MAS ^{31}P NMR (161.8 MHz, 280 K): δ = 82.4 ppm ($w_{1/2}$ = 6.9 KHz). IR (ATR, cm^{-1}): υ = 3073 (w), 3057 (w), 2952 (w), 2892 (w), 2196 (s, υ_{NCO}) (2141, $\upsilon_{N^{13}CO}$), 1654 (m, υ_{CO}) (1559, υ^{13}_{CO}), 1597 (s), 1537 (w),

1466 (s), 1434 (s), 1354 (s), 1310 (s), 1275 (w), 1243 (w), 1155 (m), 1132 (m), 1105 (w), 1059 (m), 1010 (m), 960 (m), 833 (s), 741 (s), 691 (s), 621 (m), 600 (m), 511 (s), 487 (s), 455 (m).

Catalytic hydroboration of CO_2 with 105

Pinacolborane (HBpin) (76.9 mg, 0.60 mmol) was added to a C_6D_6 (0.5 mL) solution of **105** (30.5 mg, 0.030 mmol) at room temperature in a NMR tube. $^{13}CO_2$ (0.6 atm.) was then introduced to the mixture. The reaction mixture was kept at ambient temperature and the catalytic system was followed by NMR.

Crystallization of [Ru(κ^P-NPN)($\kappa^{N,P}$-NPN)(COD)] 119

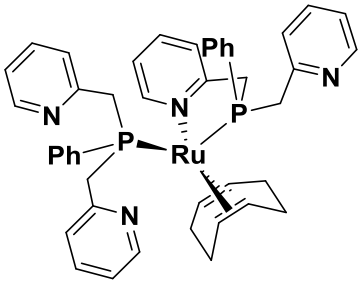

119

An Et_2O (2 mL) solution of NPN (29.2 mg, 0.10 mmol) was added to an Et_2O (2 mL) solution of Ru(COD)(COT) (15.7 mg, 0.050 mmol). The mixture was maintained at room temperature for one hour. The red solution obtained after filtration was stored at -37 °C. Crystals of **119** were obtained after 48 hours. NMR characterization of the crystals of complex **119** turned to be impossible due to its decomposition in solution.

Crystallization of [Ru($\kappa^{N,P,N}$-NPN)] 120

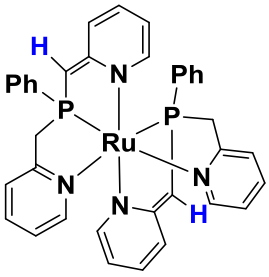

120

A toluene (1 mL) solution of NPN (116.8 mg, 0.40 mmol) was added to a pentane (6 mL) solution of Ru(COD)(COT) (62.8 mg, 0.20 mmol). The mixture was stirred at room temperature for 6 hours before filtration. The filtrate was then kept at -37 °C. Crystals of **120** were obtained after

10 days. NMR characterization of the crystals of complex **120** turned to be impossible due to its decomposition in solution.

Synthesis of [Ru(κ^{P}-NP)(κ^{N,P}-NP)(COD)] 121

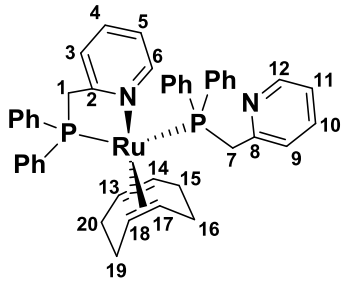

121

An Et_2O (2 mL) solution of Ru(COD)(COT) (0.126 g, 0.41 mmol) was added to an Et_2O (4 mL) solution of ligand NP (0.222 g, 0.80 mmol) at room temperature. The mixture was stirred at room temperature for 16 h. The compound was obtained after filtration, washing with cold pentane (2*5 mL) and drying under reduced pressure, with a yield of 56 % (0.170 g). Crystals suitable for X-ray diffraction were grown from an Et_2O solution at -37 °C. ^{1}H NMR (500.3 MHz, Toluene-D_8, 240 K): δ = 8.24 (br, 1H, *H*12), 8.16 – 6.55 (m, 20H, H_{phenyl}), 7.95 (d, $^{3}J_{H\text{-}H}$ = 5.4 Hz, 1H, *H*6), 6.66 (pt, $3J_{C\text{-}H}$ = 7.6 Hz, 1H, *H*10), 6.49 (pt, $^{3}J_{C\text{-}H}$ = 8.1 Hz, 1H, *H*4), 6.38 (br, 2H, *H*3 and *H*11), 5.89 (d, $^{3}J_{H\text{-}H}$ = 7.9 Hz, 1H, *H*9), 5.77 (t, $^{3}J_{H\text{-}H}$ = 6.3, 6.1 Hz, 1H, *H*5), 4.18 (pq, 2H, PCH_2 (κ^{P}-NP)), 3.73 (br, 1H, *H*17), 3.36 (q, $^{2}J_{P\text{-}H}$ = 8.8, $1J_{H\text{-}H}$ = 17.1 Hz, 1H, PCH_2 ($\kappa^{N,P}$-NP)), 3.09 (br, 1H, *H*18), 3.01 (br, 1H, *H*20), 2.91 (br, 1H, *H*19), 2.84 (br, 1H, *H*19), 2.77 (br, 1H, *H*14), 2.69 (br, 1H, *H*15), 2.25 (br, 1H, *H*20), 2.22 (br, 1H, *H*15), 2.17 (br, 1H, *H*13), 1.85 (br, 2H, *H*16), 1.58 (q, $^{2}J_{P\text{-}H}$ = 5.5, $^{1}J_{H\text{-}H}$ = 17.5 Hz, 1H, PCH_2 ($\kappa^{N,P}$-NP)). ^{31}P{^{1}H} NMR (202.6 MHz, Toluene-D_8, 240 K): δ = 55.6 (d, $^{2}J_{P\text{-}P}$ = 20.5 Hz), 39.3 (d, $^{2}J_{P\text{-}P}$ = 20.5 Hz). ^{13}C{^{1}H} NMR (125.8 MHz, Toluene-D_8, 240 K): δ = 165.0 (d, $^{2}J_{C\text{-}P}$ = 15.4 Hz, *C*2), 157.9 (d, $^{2}J_{C\text{-}P}$ = 9.3 Hz, *C*8), 151.3 (*C*6), 149.2 – 125.2 (C_{phenyl}), 148.5 (*C*12), 134.1 (*C*10), 133.0 (*C*4), 124.2 (*C*9), 121.5 (*C*3), 121.4 (d, $^{4}J_{C\text{-}P}$ = 107 Hz, *C*5), 120.1 (*C*11), 69.1 (dd, $^{2}J_{C\text{-}P}$ = 21.9, 5.5 Hz, *C*13), 64.6 (*C*17), 62.3 (d, $^{2}J_{C\text{-}P}$ = 4.7 Hz, *C*18), 57.0 (dd, $^{2}J_{C\text{-}P}$ = 26.8, 6.5 Hz, *C*14), 43.6 (d, $^{1}J_{C\text{-}P}$ = 15.9 Hz, P*C*H$_2$ ($\kappa^{N,P}$-NP)), 40.1 (P*C*H$_2$ (κ^{P}-NP)), 37.7 (d, $^{3}J_{C\text{-}P}$ = 7.1, *C*19), 36.6 (*C*15), 31.4 (*C*16), 28.6 (*C*20). Elemental Analysis: Calcd. for $C_{44}H_{44}N_2P_2Ru$: C, 69.19; H, 5.81; N, 3.67. Found: C, 68.70; H, 5.47, N, 3.52. IR (ATR, cm^{-1}): υ = 3043 (w), 3001 (w), 2934 (w), 2894 (w), 2843 (w), 2795 (w), 2781 (m), 1582 (m), 1566 (m), 1470 (m), 1429 (m), 1317 (m), 1230 (m), 1151 (m), 1093 (m), 1082 (m), 1067 (m), 1024 (m), 993 (w), 954 (w), 813 (s), 738 (s), 695 (s), 519 (s), 502 (s), 487 (s), 458 (s), 429 (s), 407 (s).

Experimental Section Chapter 3

Synthesis of $[Fe(H)_2(dmpe)_2]$ 40

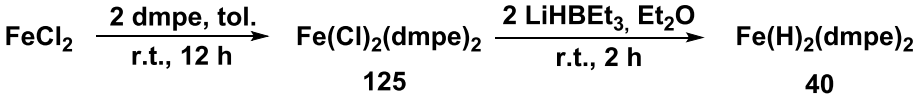

A toluene (4 mL) solution of dmpe (dmpe = 1,2-bis(dimethylphosphino)ethane, 0.60 g, 4.00 mmol) was added to a toluene (16 mL) suspension of $FeCl_2$ (0.256 g, 2.03 mmol), and stirred at room temperature for 12 h to get a green solution. After filtration and concentration under reduced pressure, the resulting solution was stored at -37 °C. Green crystals of $FeCl_2(dmpe)_2$ were collected after 2 d in 89 % yield. $FeCl_2(dmpe)_2$ (0.639 g, 1.50 mmol) was dissolved in Et_2O (20 mL), and a THF solution of $LiHBEt_3$ (3.2 mL, 1.0 M) was added dropwise to the Et_2O solution. The mixture was stirred at room temperature for 2 h and the solvents were removed under reduced pressure, leaving an orange colour precipitate. A yellow solid of $Fe(H)_2(dmpe)_2$ was obtained after sublimation (40 – 60 °C, 60 mTorr) (0.46 g, 72 %). ^{1}H NMR (400.2 MHz, THF-D_8, 298 K): δ = 1.57 (br, 10H, PC*H*$_2$/PC*H*$_3$), 1.32 (br, 4H, PC*H*$_2$), 1.19 (br, 12H, PC*H*$_3$), 1.07 (br, 6H, PC*H*$_3$), -14.35 (m, 2H, Fe-*H*). ^{31}P{^{1}H} NMR (162.0 MHz, THF-D_8, 298 K): δ = 76.9 (t, $^3J_{P\text{-}P}$ = 27 Hz), 67.2 (t, $^3J_{P\text{-}P}$ = 27 Hz).

Variation of the hydroboranes

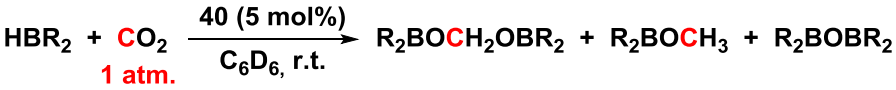

In a NMR tube, a C_6D_6 (0.5 mL) solution of $Fe(H)_2(dmpe)_2$ (2.3 mg, 0.0065 mmol) and HBR_2 (0.13 mmol, HBcat: 15.6 mg; HBpin: 16.7 mg; 9-BBN: 15.9 mg) was degassed and placed under 1 atm. of CO_2. The tube was then placed at 25 °C and the yields in bis(boryl)acetal and methoxyborane were estimated by ^{1}H NMR integration with an internal standard (9,10-dihydroanthracene).

Blank experiments with only dmpe as catalyst precursor

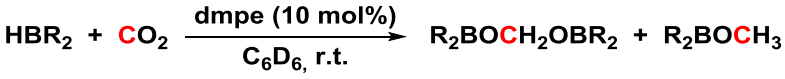

In a NMR tube, a C_6D_6 (0.5 ml) solution of dmpe (2.0 mg, 0.0133 mmol) and HBR_2 (0.13 mmol) was degassed and placed under 1 atm of CO_2. The tube was then placed at 25 °C and the relative ratio between the bis(boryl)acetal and the methoxyborane was estimated by ^{1}H NMR. All the hydroboranes (HBcat, HBpin and 9-BBN) formed corresponding adducts with dmpe. While a

white precipitate was observed after mixing HBcat and dmpe, HBpin and 9-BBN gave colorless solutions after mixing.

Optimization of the conditions for the generation of compound 127

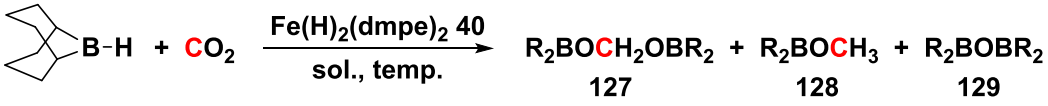

In a NMR tube, $Fe(H)_2(dmpe)_2$ and 9-BBN were placed in 0.5 mL of the solvent, degassed and placed under a CO_2 pressure. The tube was then introduced in the NMR machine at the requested temperature for regular NMR controls.

Optimized general method for the generation of 127

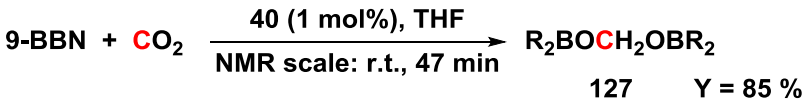

In a NMR tube, a THF-D_8 (0.5 mL) solution of $Fe(H)_2(dmpe)_2$ (0.47 mg, 0.00131 mmol, 1 mol %) and 9-BBN (15.9 mg, 0.130 mmol,) was degassed and placed under 1 atm (static) of CO_2. After 47 min, ^1H NMR integration with an internal standard (methoxytoluene or 9,10-dihydroanthracene) indicated the formation of **127** in 85 % yield.

General method for the in-situ trapping of 127

Following the general method for the generation of **127** in 85 % yield, the NMR tube was vented in the glove box and the trapping agent was added in the NMR tube. The yield of the resulting compound was calculated by ^1H NMR integration (RD = 30 s) using 9,10-dihydroanthracene or methyoxytoluene as internal standards. Several experiments have shown that the internal standard can be placed in the tube prior to the addition of CO_2 or after the generation of the bis(boryl)acetal compound for the same outcome. Both $^{13}CO_2$ and $^{12}CO_2$ were used to confirm by multinuclear NMR and HRMS that the methylene carbon atom in the produced compounds resulted from the reduction of CO_2. ^1H, $^{13}C\{^1H\}$, HSQC, HMBC and COSY NMR experiments were used to fully characterize the compounds formed.

Reaction of 127 with CD_3OD: generation and characterization of compound 131

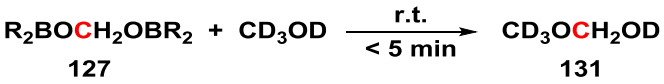

After the generation of **127**, the NMR tube was vented in the glove box and CD_3OD (0.052 mmol, 1.9 mg) was added to the mixture. Just after the addition, the ^1H NMR spectrum indicated the complete disappearance of compound **127** and the appearance of $CD_3O^{13}CH_2OD$ **131** in 89 % yield based on CD_3OD and 72 % yield based on 9-BBN. ^1H NMR (400.1 MHz, THF-D_8, 298 K): δ = 4.54 (d, 2H, $^1J_{C\text{-}H}$ = 160 Hz, $^{13}CH_2$); $^{13}C\{^1H\}$ NMR (100.6 MHz, THF-D_8, 298 K): δ = 91.0 (s, $^{13}CH_2$).

10-fold scale up synthesis of compound 131

In a Fisher-Porter bottle, a THF-D_8 (5 mL) solution of $Fe(H)_2(dmpe)_2$ (4.7 mg, 0.0131 mmol, 1 mol %) and 9-BBN (159.0 mg, 1.302 mmol) was placed under 1 atm. of CO_2. After stirring 10 min at 60 °C, an excess of CD_3OD was added to the Fisher-Porter. The yield calculated by ^1H NMR integration with an internal standard indicated the formation of CD_3CH_2OD in 86 % yield based on 9-BBN.

Reaction of 127 with 2,6-bis(diisopropyl)phenylamine: generation and characterization of compound 132

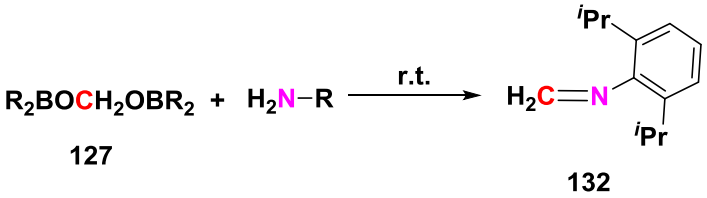

After the generation of **127**, the NMR tube was vented in the glove box and 2,6-bis(diisopropyl)-phenylamine (9.2 mg, 0.0519 mmol) was added. The NMR analyses showed the complete conversion of the bis-borylacetal compound and the formation of the corresponding methylene aniline **132** within 20 min in 83 % yield based on amine and 66 % based on 9-BBN. ^1H NMR (400.1 MHz, THF-D_8, 298 K): δ = 7.73 (dd, 1H, $^1J_{C\text{-}H}$ = 150.9 Hz, $^2J_{H\text{-}H}$= 18.4 Hz, $^{13}CH_2$), 7.30 (dd, 1H, $^1J_{C\text{-}H}$= 132.0 Hz, $^2J_{H\text{-}H}$= 18.4 Hz, $^{13}CH_2$); $^{13}C\{^1H\}$ NMR (100.6 MHz, THF-D_8, 298 K): δ = 156.5 (s, $^{13}CH_2$).

Independent synthesis and isolation of N,N'-Dimethyl-N,N'-diphenyl-methanediamine 137

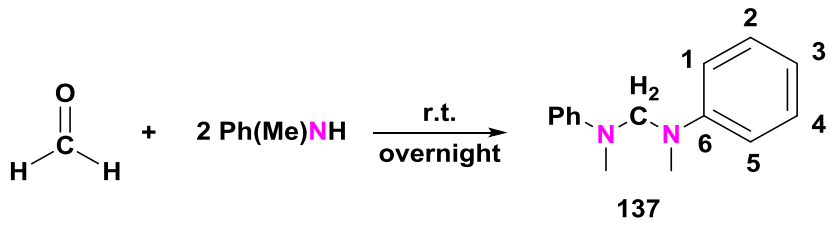

A formaldehyde solution (4.0 mL, 0.05 mmol, 37 % wt aqueous solution) was added to N-methylaniline (10.7 g, 0.1 mmol) and the mixture was stirred overnight at room temperature. After extraction with diethyl ether (2 x 25 mL), the combined organic phases were dried with Na_2SO_4. The solvents were removed under reduced pressure and the crude compound was purified by fractional distillation (b.p. 138 – 142 °C / 0.2 Torr) to afford the expected product **137** as a colorless oil (8.14 g, 72 %). ^{1}H NMR (400.1 MHz, THF-D_8, 298 K): δ = 7.15 (dd, $^3J_{H\text{-}H}$ = 8.9 Hz, $^3J_{H\text{-}H}$ = 7.3 Hz, 4H, H(2 and 4)), 6.83 (d, $^3J_{H\text{-}H}$ = 7.9 Hz, 4H, H(1 and 5)), 6.67 (tt, 2H, $^3J_{H\text{-}H}$ = 7.3 Hz, $^4J_{H\text{-}H}$ = 1.0 Hz, H(3)), 4.78 (s, 2H, CH_2), 2.85 (s, 6H, CH_3); ^{13}C{^{1}H} NMR (125.8 MHz, THF-D_8, 298 K): δ = 150.6 (C6), 129.8 (C2 and 4), 118.5 (C3), 114.7 (C1 and 5), 71.0 (*C*H_2), 36.7 (*C*H_3).

Reaction of 127 with N-methylaniline: generation and characterization of 137

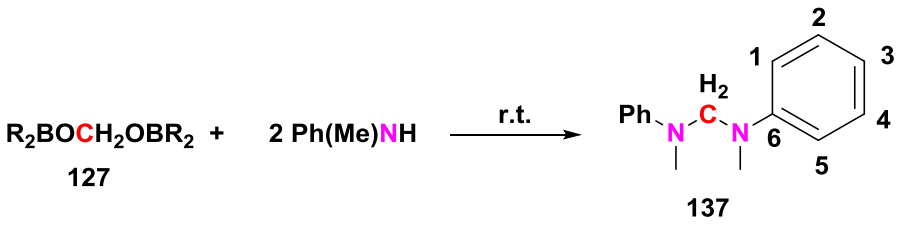

After the generation of **127**, the NMR tube was vented in the glove box and N-methylaniline (11.2 mg, 0.1046 mmol) was added. The NMR analyses showed the complete conversion of the bis(boryl)acetal and the formation of the corresponding aminal **137** within 1 h in 92 % yield. The reactions have been carried out with $^{13}CO_2$ and $^{12}CO_2$ to afford **137**(^{13}C) and **137**(^{12}C), respectively. **137**(^{13}C): ^{1}H NMR (400.2 MHz, THF-D_8, 298 K): δ = 4.77 (d, $^1J_{C\text{-}H}$ = 146.3 Hz, 2H, ^{13}CH_2); ^{13}C{^{1}H} NMR (100.6 MHz, THF-D_8, 298 K): δ = 71.0 (^{13}CH_2); HRMS (DCI-CH_4): m/z (Cl^+:$^{13}CC_{14}H_{18}N_2$): calculated: 226.1470, found: 226.1462. **137**(^{12}C): ^{1}H NMR (500.3 MHz, THF-D_8, 250 K): δ = 7.16 (dd, 4H, $^3J_{H\text{-}H}$=8.7, $^3J_{H\text{-}H}$=7.1 Hz, H2 and 4), 6.85 (d, 4H, $^3J_{H\text{-}H}$ = 8.1 Hz, H(1 and 5)), 6.68 (t, 2H, $^3J_{H\text{-}H}$ = 7.3 Hz, H3), 4.84 (s, 2H, CH_2), 2.83 (s, 6H, CH_3); ^{13}C{^{1}H} NMR (125.8 MHz, THF-D_8, 250 K): δ = 129.9 (C2 and 4), 118.2 (C3), 114.3 (C1 and 5), 70.5 (*C*H_2), 36.6 (*C*H_3); HRMS (DCI-CH_4): m/z (Cl^+: $C_{15}H_{18}N_2$): calculated: 227.1548, found: 227.1560.

Reaction of 127 with bis(phenyl)amine: generation and characterization of 139

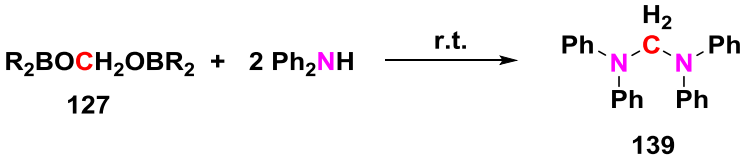

127 139

After the generation of **127**, the NMR tube was vented in the glove box and bis(phenyl)amine (17.6 mg, 0.1041 mmol) was added. The NMR analyses showed the complete conversion of the bis(boryl)acetal and the formation of the corresponding aminal **139** within 1 h in 91 % yield. The reactions have been carried out with $^{13}CO_2$ and $^{12}CO_2$ to afford **139**(^{13}C) and **139**(^{12}C), respectively. **139**(^{13}C): ^{1}H NMR (400.2 MHz, THF-D_8, 298 K): δ = 5.63 (d, $^{1}J_{C\text{-}H}$= 157.9 Hz, 2H, $^{13}CH_2$); $^{13}C\{^{1}H\}$ NMR (100.6 MHz, THF-D_8, 298 K): δ = 79.3 ($^{13}CH_2$); HRMS (DCI-CH_4): m/z (Cl^+:$^{13}CC_{24}H_{22}N_2$): calculated: 351.1817, found: 351.1816. HRMS (DCI-CH_4): m/z (Cl^+: $C_{25}H_{22}N_2$): calculated: 350.1783, found: 350.1793.

Reaction of 127 with N,N'-dimethyl-1,2-benzenediamine: generation and characterization of 140

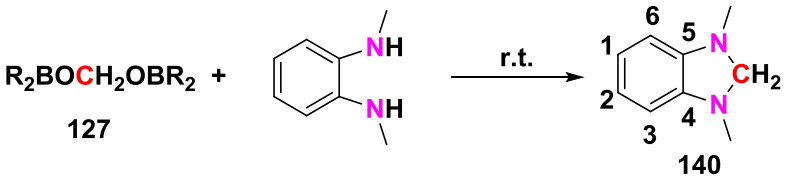

127 140

After the generation of **127**, the NMR tube was vented in the glove box and *N,N'*-dimethyl-1,2-benzenediamine (7.1 mg, 0.0522 mmol) was added. The NMR analyses showed the complete conversion of the bis(boryl)acetal compound and the formation of the corresponding aminal **127** within 3 h in 77 % yield. The reactions have been carried out with $^{13}CO_2$ and $^{12}CO_2$ to afford **140**(^{13}C) and **140**(^{12}C), respectively. **140**(^{13}C): ^{1}H NMR (400.1 MHz, THF-D_8, 298 K): δ = 4.24 (d, $^{1}J_{C\text{-}H}$= 148.0 Hz, $^{13}CH_2$), 2.66 (d, $^{3}J_{13C\text{-}H}$= 5 Hz, NCH_3): $^{13}C\{^{1}H\}$ NMR (100.6 MHz, THF-D_8, 298 K): δ = 81.3 ($^{13}CH_2$); HRMS (DCI-CH_4): m/z (Cl^+:$^{13}CC_8H_{12}N_2$): calculated: 149.1034, found: 149.1024. **140**(^{12}C): ^{1}H NMR (400.1 MHz, THF-D_8, 298 K): δ = 6.52 (dd, $^{3}J_{H\text{-}H}$= 5.5 Hz, $^{4}J_{H\text{-}H}$= 3.2Hz, 2H, H(1, 2)), 6.32 (dd, $^{3}J_{H\text{-}H}$= 5.4 Hz, $^{4}J_{H\text{-}H}$= 3.2Hz, 2H, H(3, 6)), 4.24 (s, 2H, CH_2), 2.66 (s, 6H, CH_3); $^{13}C\{^{1}H\}$ NMR (100.6 MHz, THF-D_8, 298 K): δ = 144.6 (C4 and 5), 119.7 (C1 and 2), 106.7 (C3 and 6), 81.3 (CH_2), 34.4 (CH_3); HRMS (DCI-CH_4): m/z (Cl^+: $C_9H_{12}N_2$): calculated: 147.0922, found: 147.0931.

Reaction of 127 with N,N-dimethyl-1,2-ethanediamine: generation and characterization of 141

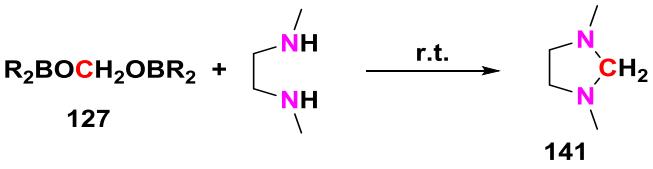

After the generation of **127**, the NMR tube was vented in the glove box and N,N-dimethyl-1,2-ethanediamine (4.6 mg, 0.0522 mmol) was added. The NMR analyses showed the complete conversion of the bis(boryl)acetal compound and the formation of the corresponding aminal **141** within 2 h in 69 % yield. ^{1}H NMR (400.1 MHz, THF-D_8, 298 K): δ = 3.21 (d, $^{1}J_{C\text{-}H}$ =144.0 Hz, 2H, $^{13}CH_2$), 2.68 ($^{3}J_{C\text{-}H}$ = 3.4 Hz, 4H, CH_2), 2.29 ($^{3}J_{C\text{-}H}$ = 5.6 Hz, 6H, CH_3). ^{13}C{^{1}H} NMR (100.6 MHz, THF-D_8, 298 K): δ = 81.1 ($^{13}CH_2$).

Reaction of 127 with 1,3-dihydroxy-2,2-dimethylpropane: generation and characterization of 143

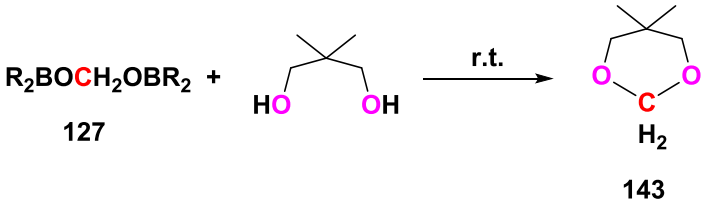

After the generation of **127**, the NMR tube was vented in the glove box and 1,3-dihydroxy-2,2-dimethylpropane (5.5 mg, 0.0528 mmol) was added. The NMR analyses showed the complete conversion of the bis(boryl)acetal compound and the formation of the corresponding compound **143** within 10 min in 77 % yield. ^{1}H NMR (400.1 MHz, THF-D_8, 298 K): δ = 4.62 (d, $^{1}J_{C\text{-}H}$ =159.5 Hz, $^{13}CH_2$). ^{13}C{^{1}H} NMR (100.6 MHz, THF-D_8, 298 K): δ = 90.8 ($^{13}CH_2$).

Reaction of 127 with 2-methylamino-phenol: generation and characterization of 144

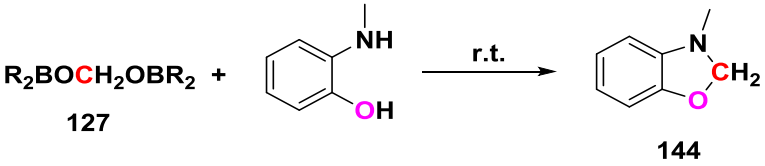

After the generation of **127**, the NMR tube was vented in the glove box and 2-(methylamino)-phenol (6.4 mg, 0.0520 mmol) was added. The NMR analyses showed complete conversion of **127** and formation of 2,3-dihydro-3-methyl-benzoxazole **144** within 1 h in 67 % yield. The reactions have been carried out with $^{13}CO_2$ and $^{12}CO_2$ to afford **144**(^{13}C) and **144**(^{12}C), respectively. **144**(^{13}C): ^{1}H NMR (400.1 MHz, THF-D_8, 298 K): δ = 5.13 (d, $^{1}J_{C\text{-}H}$= 160.1 Hz, 2H, $^{13}CH_2$);

$^{13}C\{^{1}H\}$ NMR (100.6 MHz, THF-D_8, 298 K): δ = 91.8 ($^{13}CH_2$); HRMS (DCI-CH_4): m/z (Cl^+:$^{13}CC_7H_9NO$): calculated: 136.0718, found: 136.0711. **144**(^{12}C): ^{1}H NMR (500.3 MHz, THF-D_8, 298 K): δ = 6.69 (m, 1H, H_{arom}), 6.57 (m, 2H, H_{arom}), 6.51 (d, $^{3}J_{C\text{-}H}$ = 7.5 Hz, 1H, H_{arom}), 5.13 (s, 2H, CH_2), 2.70 (s, 3H, CH_3); $^{13}C\{^{1}H\}$ NMR (125.8 MHz, THF-D_8, 298 K): δ = 152.5 (C_{quat}), 142.1 (C_{quat}), 122.1 (C_{arom}), 120.1 (C_{arom}), 108.6 (C_{arom}), 108.4 (C_{arom}), 91.8 (CH_2), 34.3 (CH_3); HRMS (DCI-CH_4): m/z (Cl^+: C_8H_9NO): calculated: 135.0684, found: 135.0686.

Independent synthesis and characterization of hexamethylenetetramine 145

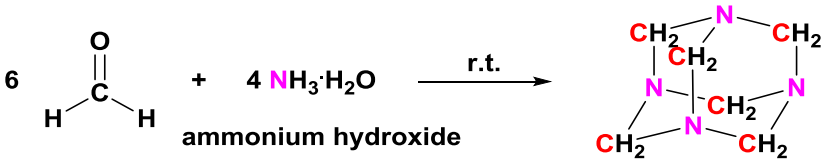

145

An ammonium hydroxide solution (16.4 mL, 0.28 mol, 32 % wt aqueous solution) was added slowly to a stirred formaldehyde solution (10.0 mL, 0.12 mol, 37 % wt aqueous solution). The solution was concentrated and a white precipitate formed. The precipitate was dried under reduced pressure to afford compound **145** (2.78 g, 97 % based on formaldehyde). The solubility of compound **145** is good in water and moderate in THF. ^{1}H NMR (400.2 MHz, D_2O, 298 K): δ = 4.67 (s, CH_2); ^{1}H NMR (400.2 MHz, THF-D_8, 298 K): δ = 4.60 (s, CH_2); ^{13}C NMR (100.6 MHz, D_2O, 298 K): δ = 71.8 (s, CH_2); $^{13}C\{^{1}H\}$ NMR (100.6 MHz, THF-D_8, 298 K): δ = 76.1 (s, CH_2).

Reaction of 127 with ammonium hydroxide: isolation and characterization of 145

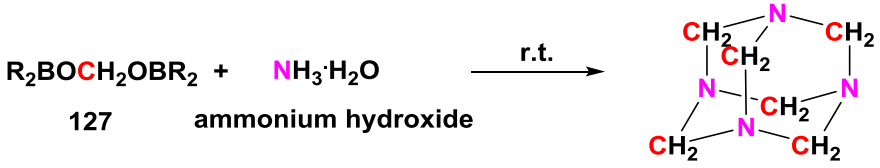

145

After the generation of **127**, one equivalent of ammonium hydroxide (2.0 mL, 0.035 mmol) was added to the NMR tube. ^{1}H NMR analysis showed the complete conversion of **127** and compound **145** was obtained after 16 h at r.t. in 32 % yield based on ammonia. The addition of 5-fold excess of ammonium hydroxide (10.0 mL, 0.175 mmol) instead of 1 equivalent, gave rise to a 84 % yield based on 9-BBN. The reactions have been carried out with $^{13}CO_2$ and $^{12}CO_2$ to afford **145**(^{13}C) and **145**(^{12}C), respectively. **145**(^{13}C): ^{1}H NMR (400.1 MHz, THF-D_8, 298 K): δ = 4.61 (d, $^{1}J_{C\text{-}H}$ = 149.0 Hz, 12H, $^{13}CH_2$); $^{13}C\{^{1}H\}$ NMR (100.6 MHz, THF-D_8, 298 K): δ = 76.0 (s, $^{13}CH_2$). **145**(^{12}C): ^{1}H NMR (400.2 MHz, THF-D_8, 298 K): δ = 4.61 (s, CH_2); ^{1}H NMR (400.2 MHz, D_2O, 298 K):

δ = 4.69 (s, CH_2); $^{13}C\{^1H\}$ NMR (100.6 MHz, THF-D_8, 298 K): δ = 76.1 (s, CH_2); elemental analysis: Calculated. for $C_6H_{12}N_4$: C, 51.41; H, 8.63; N, 39.97. Found: C, 51.15; H, 8.60; N, 39.90.

Scale up syntheses:

10-fold scale up: A THF solution (5 mL) of $Fe(H)_2(dmpe)_2$ (4.7 mg, 0.0131 mmol) and 9-BBN (159.0 mg, 1.302 mmol) was prepared in a Fisher-Porter and placed under 1 atm of CO_2. The solution was stirred at 60 °C for 10 min. Ammonium hydroxide (20.4 mL, 0.35 mmol) was then added at room temperature and the resulting solution was stirred at room temperature for 36 h. The solvents were removed under reduced pressure and compound **145** was isolated by silica-gel chromatography in 98 % yield (11.9 mg) based on ammonium hydroxide. When performing the same reaction with an excess of ammonium hydroxide (0.2 mL, 3.5 mmol), a 85 % isolated yield of compound **145** based on 9-BBN was obtained.

100-fold scale up: A THF solution (50 mL) of $Fe(H)_2(dmpe)_2$ (47.0 mg, 0.131 mmol) and 9-BBN (1.59 g, 13.02 mmol,) was prepared in a Fisher-Porter and placed under 1 atm (static) of CO_2. The Fisher-Porter was placed in a 60 °C oil bath immediately and stirred 10 min at this temperature. After removing the oil bath, excess ammonium hydroxide was added to the Fisher-Porter and the mixture was stirred at room temperature for 2 days. The solvents were removed under reduced pressure, and the compound **145** was obtained by silica-gel chromatography in 70 % yield (106.2 mg) based on 9-BBN.

Synthesis of triphenyl(phenylmethylene)-phosphorane (Ph_3PCHPh)

$$Ph_3PCH_2PhBr \xrightarrow[\text{-78 °C to r.t.}]{^n\text{BuLi, THF}} Ph_3P{=}CHPh$$

^{n}BuLi (1.9 mL, 1.6 M in hexane) was added to a THF (8 mL) solution of triphenyl-(phenylmethyl)-phosphonium bromide (1.296 g, 3.00 mmol) at -78 °C. The mixture was stirred at -78 °C for 2 h and 20 min at room temperature. The THF was removed under reduced pressure, and Et_2O (5 mL) was added to the precipitate. After 5 min of stirring, Et_2O was removed and the resulting solid was extracted with toluene (3*4 mL). A yellow powder was obtained after dryness (0.803 g, 76%). ^1H (400.1MHz, C_6D_6, 298 K): δ = 7.8 – 6.77 (20H, H_{aryl}), 2.96 (d, $^2J_{P\text{-}H}$ = 19 Hz, 1H, C*H*). $^{31}P\{^1H\}$ (162.0 MHz, C_6D_6, 298 K): δ = 7.9.

Reaction of 127 with triphenyl(phenylmethylene)-phosphorane: generation and characterization of 148

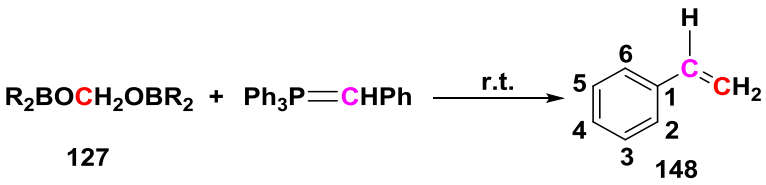

After the generation of **127**, the NMR tube was vented in the glove box and triphenyl(phenylmethylene)-phosphorane (18.3 mg, 0.0520 mmol) was added. After 5 h at room temperature, the ^{1}H NMR analysis showed the complete disappearance of **127** and the formation of compound **148** in 72 % yield. The reactions have been carried out with $^{13}CO_2$ and $^{12}CO_2$ to afford **148**(^{13}C) and **148**(^{12}C), respectively. **148**(^{13}C): ^{13}C{^{1}H} NMR (100.6 MHz, THF-D_8, 298 K): δ = 113.8 ($^{13}CH_2$); HRMS (DCI-CH_4): m/z (Cl^+:$^{13}CC_7H_8$ + H^+): calculated: 106.0738, found: 106.0734. **148**(^{12}C): ^{1}H NMR (500.3 MHz, THF-D_8, 298 K): δ = 7.40 (d, $^{3}J_{H\text{-}H}$ = 8.8 Hz, 2H, H (2 and 6)), 7.27 (t, $^{3}J_{H\text{-}H}$ = 7.4 Hz, 2H, H (3 and 5)), 7.20 (t, $^{3}J_{H\text{-}H}$ = 7.4 Hz, 1H, H (4)), 6.71 (dd, $^{3}J_{H\text{-}H}$ = 18 Hz, $^{3}J_{H\text{-}H}$ = 11 Hz, 1H, C*H*), 5.75 (d, $^{3}J_{H\text{-}H}$ = 18 Hz, 1H, CH_2), 5.18 (d, $^{3}J_{H\text{-}H}$ = 11 Hz, 1H, CH_2); HRMS (DCI-CH_4): m/z (Cl^+:C_8H_8 + H^+): calculated: 105.0704, found: 105.0676.

Independent synthesis and characterization of 151

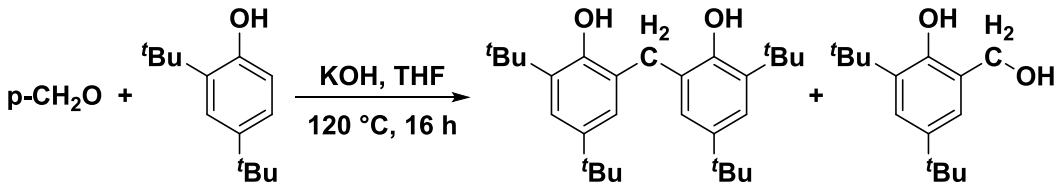

151

2,4-tert-butylphenol (0.206 g, 1.00 mmol) and KOH (0.056 g, 1.00 mmol) were added to a THF solution of paraformaldehyde (0.03 g, 1.00 mmol). The mixture was stirred at 120 °C for 16 h. THF was removed under reduced pressure, leaving an off-white residue. The residue was dissolved in Et_2O and neutralized with acidified water. The Et_2O solution was collected and dried with Na_2SO_4. After evaporation under reduced pressure, a mixture of bis-(2,4-tert-butyl-phenol)methylene (**151**)[3] (48 %), 2,4-di-tert-butyl-6-(hydroxymethyl)phenol (24 %), and the reagent 2,4-tert-butylphenol (28 %) was obtained. When performing the same reaction in the absence of KOH, only traces of compound **151** (5 %) and 2,4-di-tert-butyl-6-(hydroxymethyl)phenol (6 %) could be observed by ^{1}H NMR after 16 h, with unreacted 2,4-tert-butylphenol (89 %). **151**: ^{1}H NMR (400.2 MHz, THF-D_8, 298 K): δ = 7.38 (s, 2H, O*H*), 7.14 (d, $^{4}J_{H\text{-}H}$ = 2.5 Hz, 2H, CH_{aryl}), 6.92 (d, $^{4}J_{H\text{-}H}$ = 2.5 Hz, 2H, CH_{aryl}), 3.88 (s, 2H, CH_2), 1.41 (s, 18H, CH_3), 1.21 (s,

18H, CH_3). **2,4-di-tert-butyl-6-(hydroxymethyl)phenol**: ^{1}H NMR (400.2 MHz, THF-D_8, 298 K): δ = 8.51 (s, 1H, CO*H*), 7.18 (d, $^4J_{H\text{-}H}$ = 2.4 Hz, 1H, CH_{aryl}), 6.87 (d, $^4J_{H\text{-}H}$ = 2.5 Hz, 1H, CH_{aryl}), 5.22 (t, $^3J_{H\text{-}H}$ = 5.4 Hz, 1H, CH_2OH), 4.72 (d, $^3J_{H\text{-}H}$ = 5.6 Hz, 2H, CH_2), 1.40 (s, 9H, CH_3), 1.26 (s, 9H, CH_3). **2,4-tert-butylphenol**: ^{1}H NMR (400.2 MHz, THF-D_8, 298 K): δ = 7.92 (s, 1H, CO*H*), 7.22 (d, 1H, $^4J_{H\text{-}H}$ = 2.4 Hz, 1H, CH_{aryl}), 6.97 (dd, 1H, $^4J_{H\text{-}H}$ = 2.5 Hz, $^3J_{H\text{-}H}$ = 8.3 Hz, 1H, CH_{aryl}), 6.56 (d, 1H, $^4J_{H\text{-}H}$ = 2.5 Hz, 1H, CH_{aryl}), 1.38 (s, 9H, CH_3), 1.26 (s, 9H, CH_3).

Reaction of 127 with 2,4-tert-butylphenol: isolation and characterization of 151

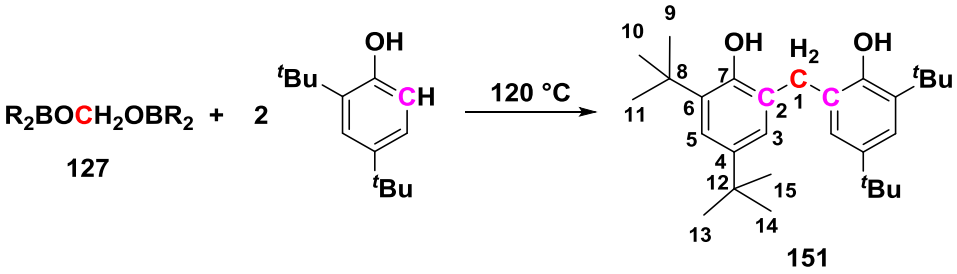

After the generation of **127**, the NMR tube was vented in the glove box and 2,4-tert-butylphenol (21.4 mg, 0.1038 mmol) was added to the mixture and the NMR tube was kept at 120 °C in a sand bath. ^{1}H NMR analyses showed the generation of **151** in 23 and 46 % yield after 16 and 36 h, respectively. Longer reaction time (48 h) did not improve the yield. The reactions have been carried out with $^{13}CO_2$ and $^{12}CO_2$ to afford **151**(^{13}C) and **151**(^{12}C), respectively. When adding KOH to compare with the independent experiment, no conversion into compound **151** was observed. **151**(^{13}C): ^{1}H NMR (400.2 MHz, THF-D_8, 298 K): δ = 3.88 (d, $^1J_{C\text{-}H}$ = 126.1 Hz, 2H, $^{13}CH_2$); $^{13}C\{^1H\}$ NMR (100.6 MHz, THF-D_8, 298 K): δ = 32.6 ($^{13}CH_2$); HRMS (DCI-CH_4): m/z (Cl^+:$^{13}CC_{28}H_{24}O_2$ + H^+): calculated: 425.3375, found: 425.3370. **151**(^{12}C): ^{1}H NMR (500.3 MHz, THF-D_8, 301 K): δ = 7.39 (s, 2H, O*H*), 7.14 (d, $^4J_{H\text{-}H}$ = 2.3 Hz, 2H, CH_{aryl}), 6.92 (d, $^4J_{H\text{-}H}$ = 2.3 Hz, 2H, CH_{aryl}), 3.88 (s, 2H, CH_2), 1.41 (s, 9H, CH_3), 1.21 (s, 9H, CH_3); $^{13}C\{^1H\}$ NMR (125.8 MHz, THF-D_8, 301 K): δ = 151.7 (C2), 142.9 (C4), 137.3 (C6), 128.3 (C7), 125.8 (C3), 122.4 (C5), 35.9 (C12), 35.0 (C8), 32.6 (C1), 32.2 (C9, 10 and 11), 30.6 (C13, 14 and 15); elemental analysis: calculated for $C_{29}H_{44}O_2$: C, 82.02; H, 10.44. Found: C, 81.65; H, 10.64; HRMS (DCI-CH_4): m/z (Cl^+:$C_{29}H_{24}O_2$): calculated: 424.3341, found: 424.3340.

10-fold scale up synthesis: A THF solution (5 mL) of $Fe(H)_2(dmpe)_2$ (4.7 mg, 0.0131 mmol,) and 9-BBN (159.0 mg, 1.302 mmol) was prepared in a Fisher-Porter and 1 atm of CO_2 was introduced. The solution was stirred at 60°C for 10 min. 2,4-tert-butylphenol (0.214 g, 1.038 mmol,) was then added and the mixture was stirred at 120 °C for 48 h. The solvent was removed under reduced pressure and compound **151** was isolated by silica-gel chromatography (Eluent: Hexane : Et_2O = 97 : 3) in 37 % yield (81.2 mg) based on phenol.

Appendices

Appendix 1

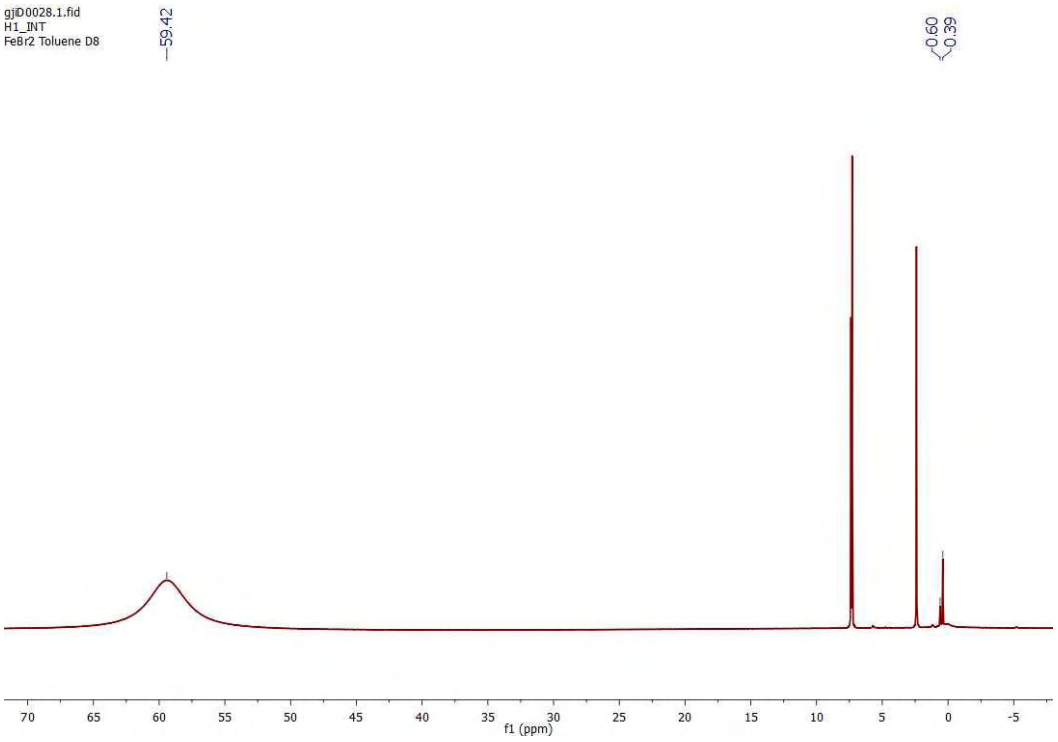

Figure 47. ^{1}H NMR of iron precursor **103** (400.1 MHz, 298 K, Toluene-D_8)

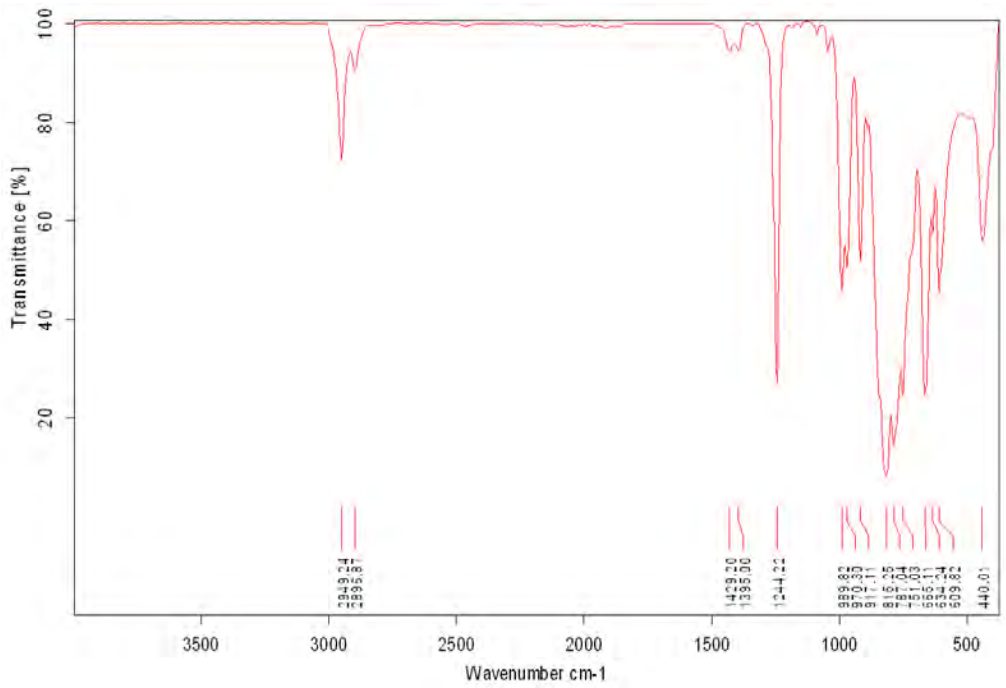

Figure 48. Infared spectroscopy of iron precursor **103**

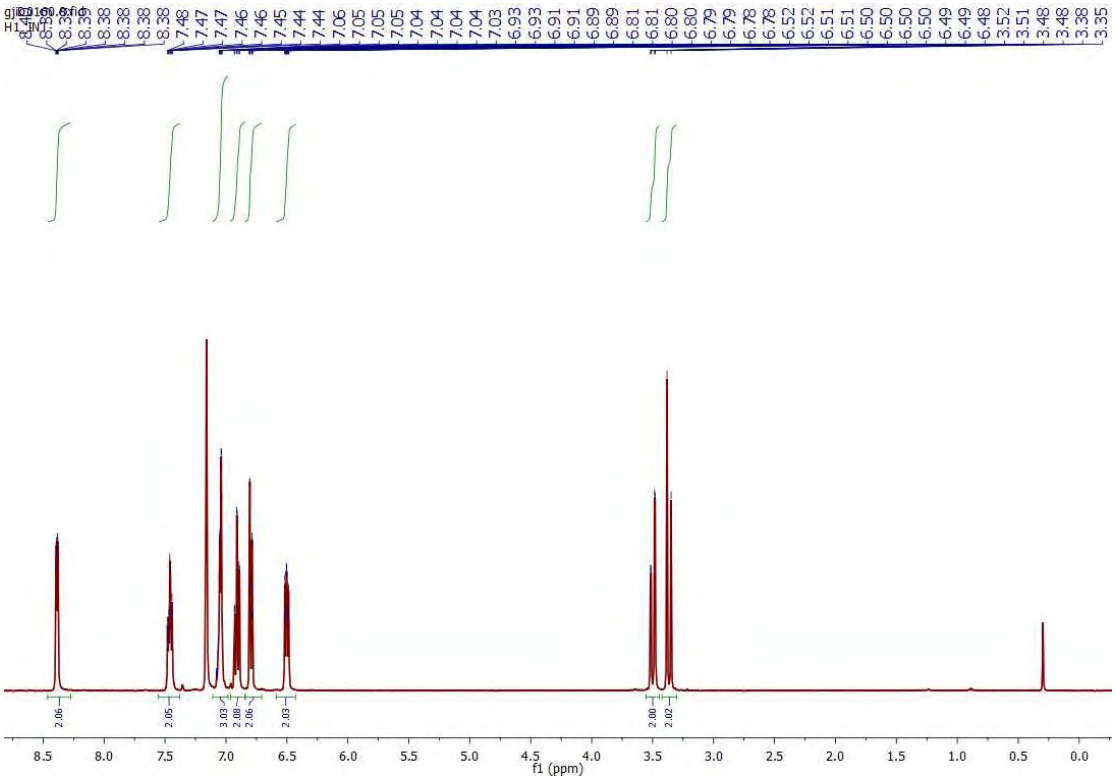

Figure 49. ^{1}H NMR of bis(2-picoly)phenylphosphine **96** (400.1 MHz, 298 K, C_6D_6)

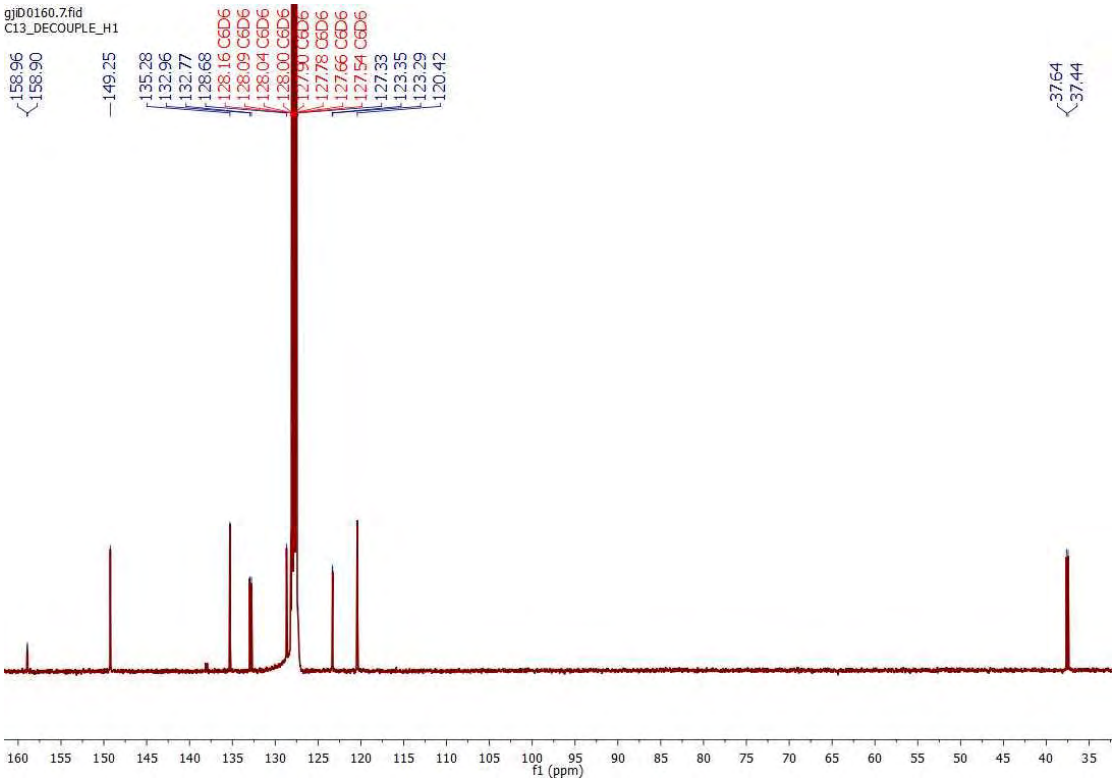

Figure 50. $^{13}C\{^{1}H\}$ NMR spectrum of bis(2-picoly)phenylphosphine **96** (100.6 MHz, 298 K, C_6D_6)

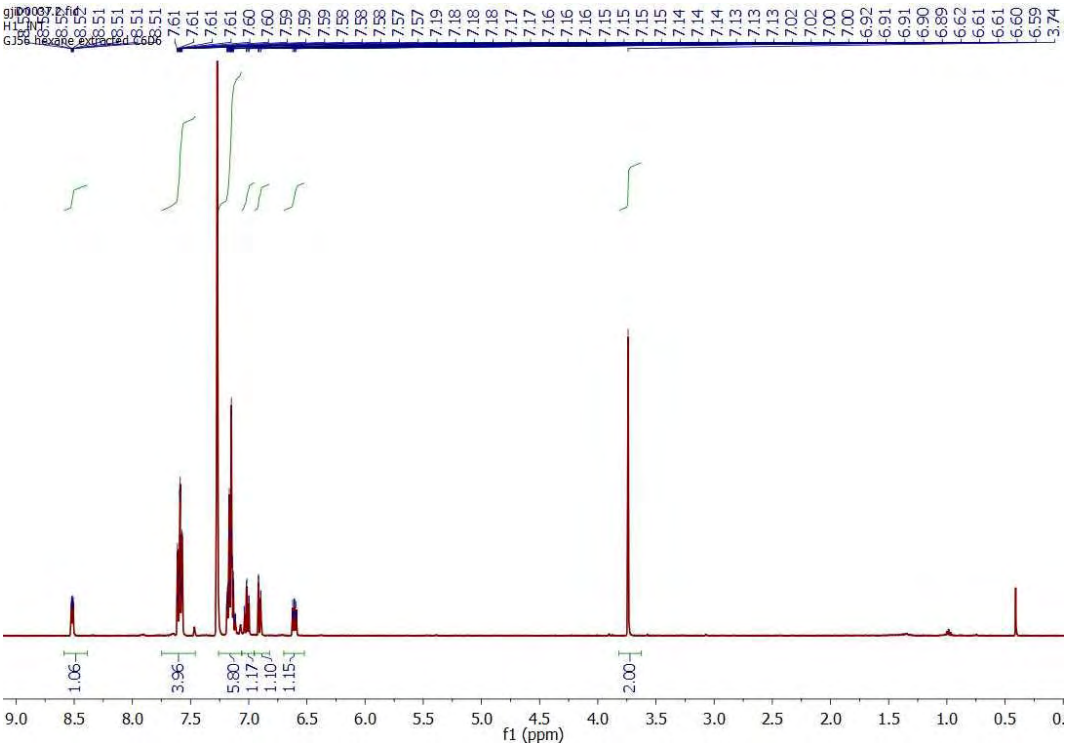

Figure 51. ^{1}H NMR spectrum of 2-[(diphenylphophino)methyl]pyridine **101** (400.1 MHz, C_6D_6, 298 K)

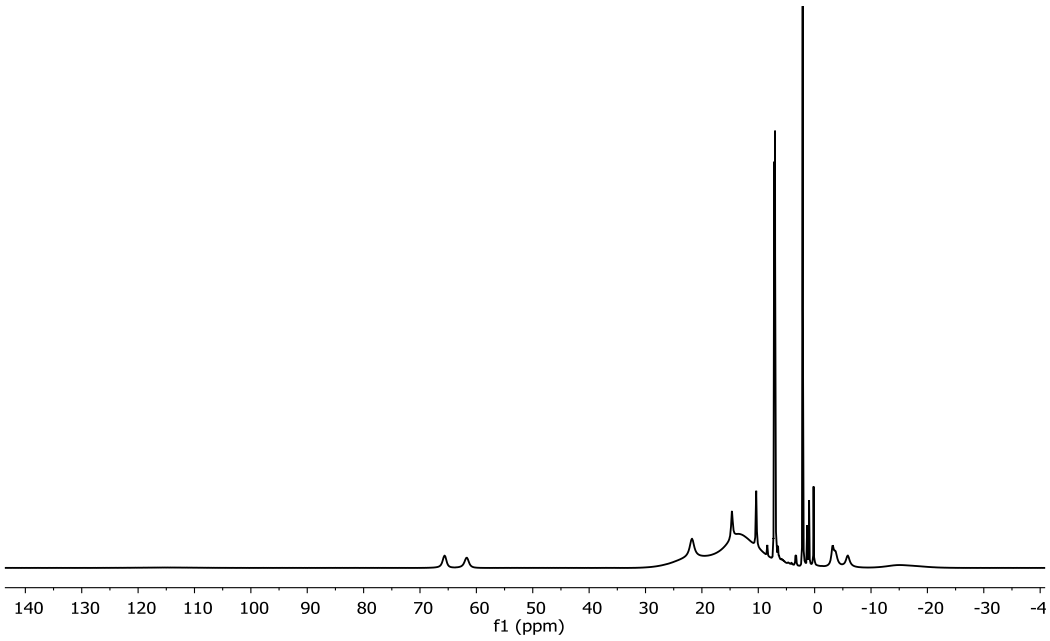

Figure 52. ^{1}H NMR spectrum of complex **104** (500.4 MHz, 230 K, Toluene-d_8)

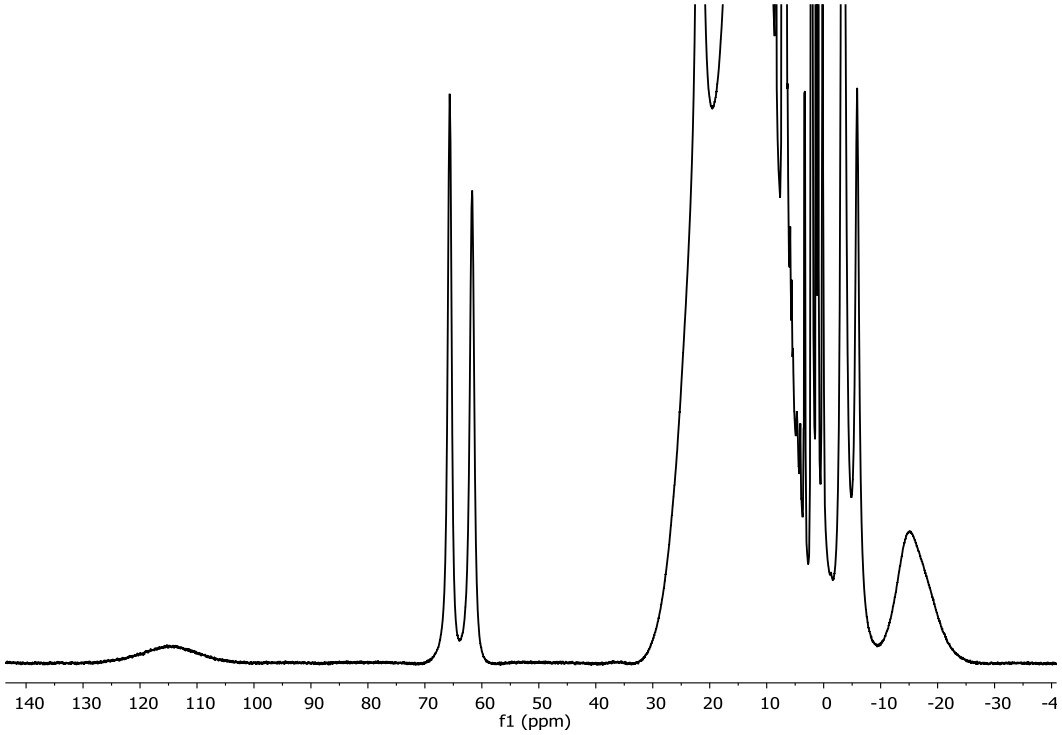

Figure 53. ^{1}H NMR spectrum of complex **104** (increased intensity)

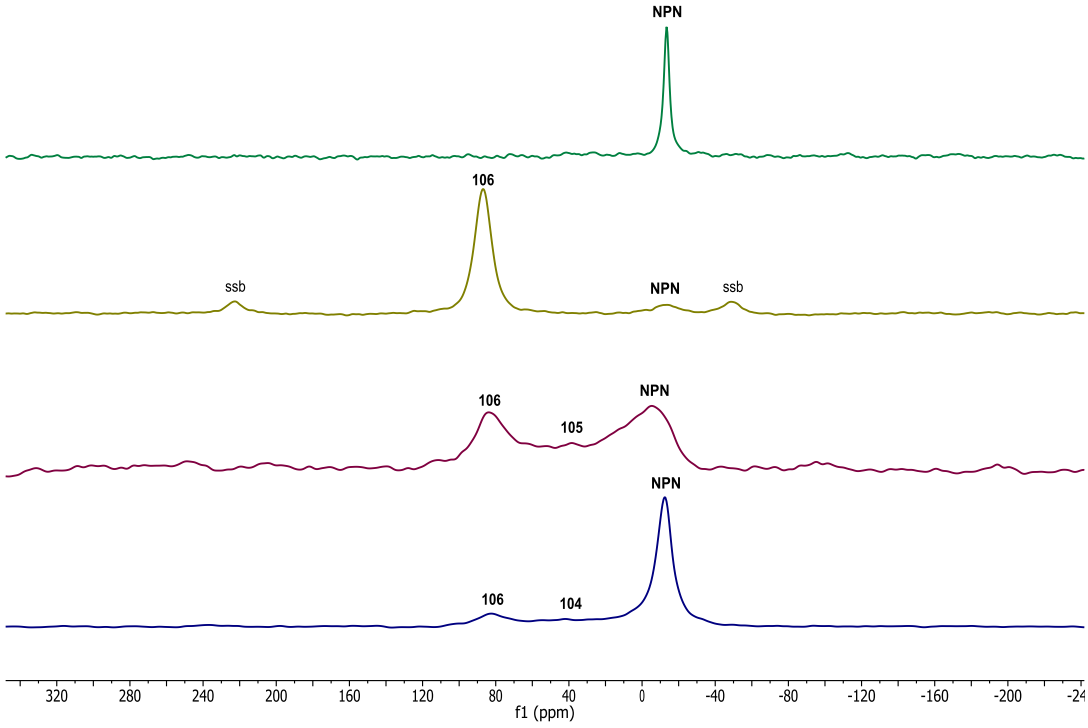

Figure 54. MAS ^{31}P NMR spectra (161.8 MHz) of NPN **96** (280 K), compounds **106** (280 K), **105** (289 K), and **104** (289 K) (from top to bottom) in the solid state

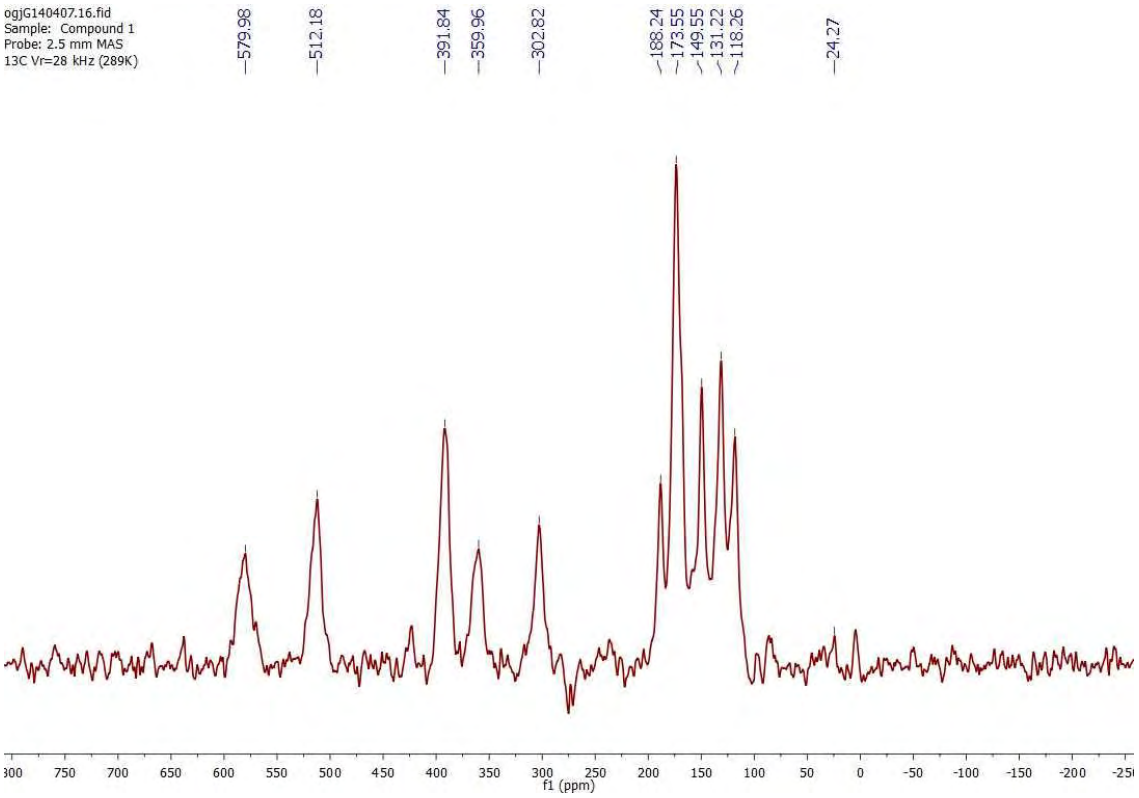

Figure 55. MAS ^{13}C NMR spectrum (100.5 MHz, 280 K) of **104** in the solid state

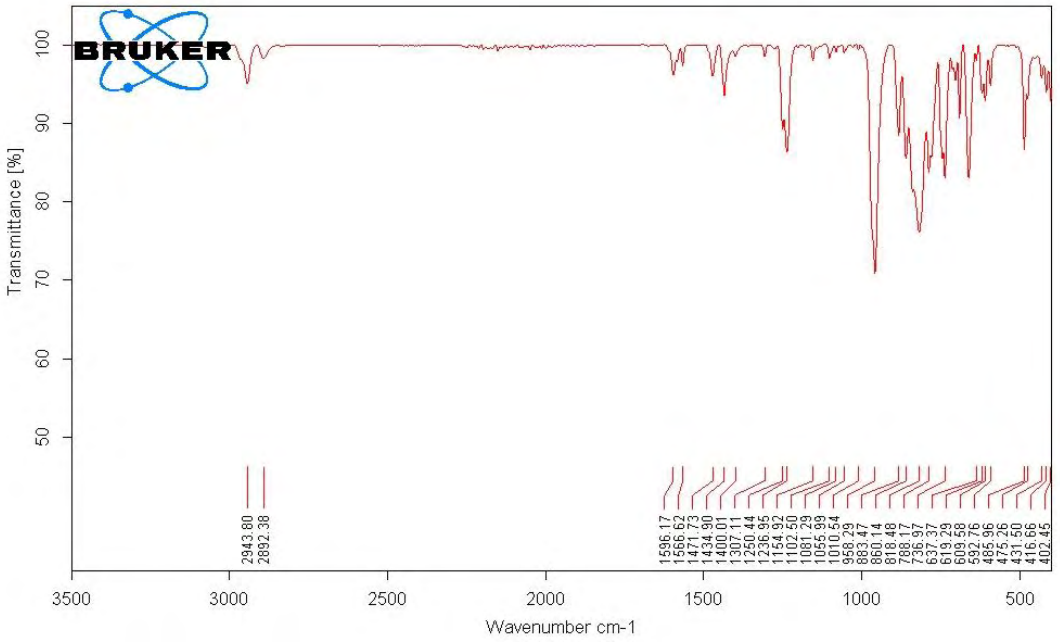

Figure 56. ATR IR spectrum of **104**

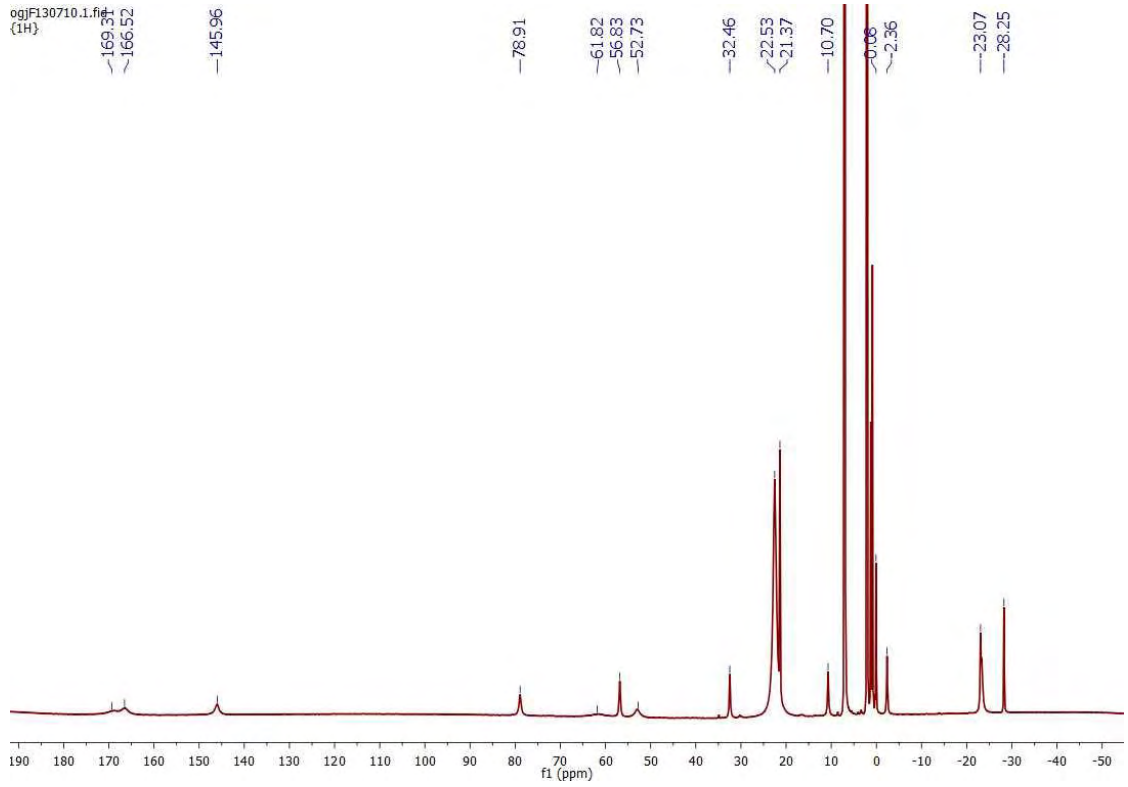

Figure 57. ^{1}H NMR spectrum of complex **105** (500.4 MHz, 301 K, Toluene-D8)

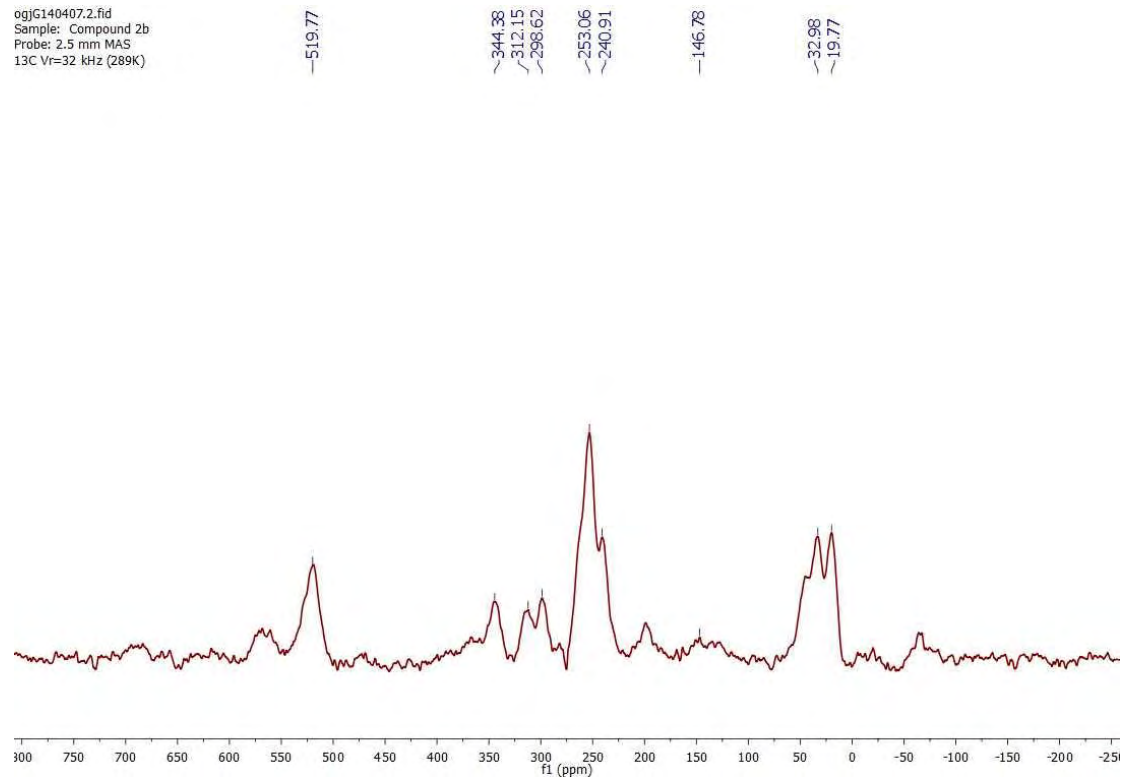

Figure 58. MAS ^{13}C NMR spectrum for **105** in the solid state (100.5 MHz, 289 K)

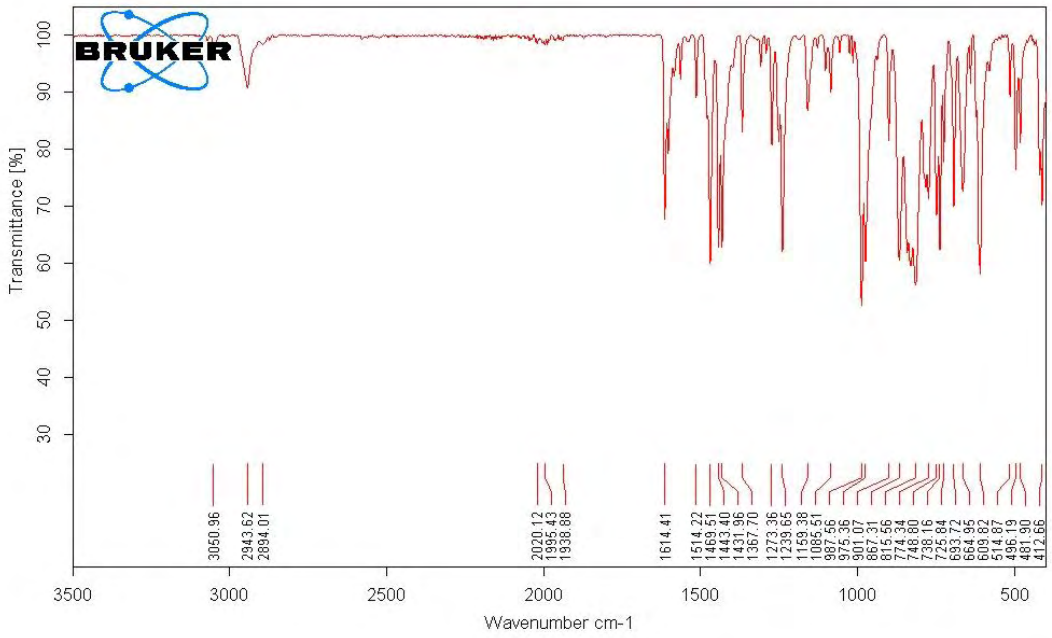

Figure 59. ATR IR spectrum of **105**

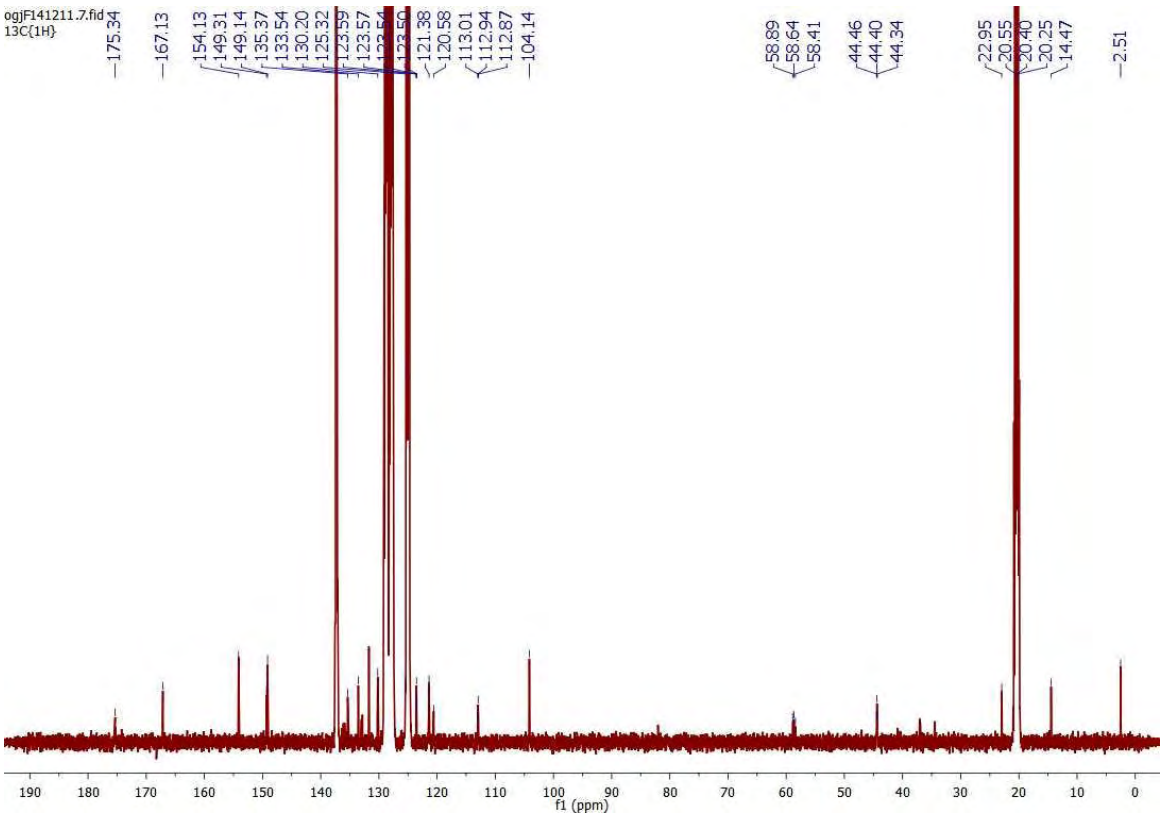

Figure 60. $^{13}C\{^{1}H\}$ NMR spectrum of complex **106** (125.8 MHz, Toluene-D_8, 240 K)

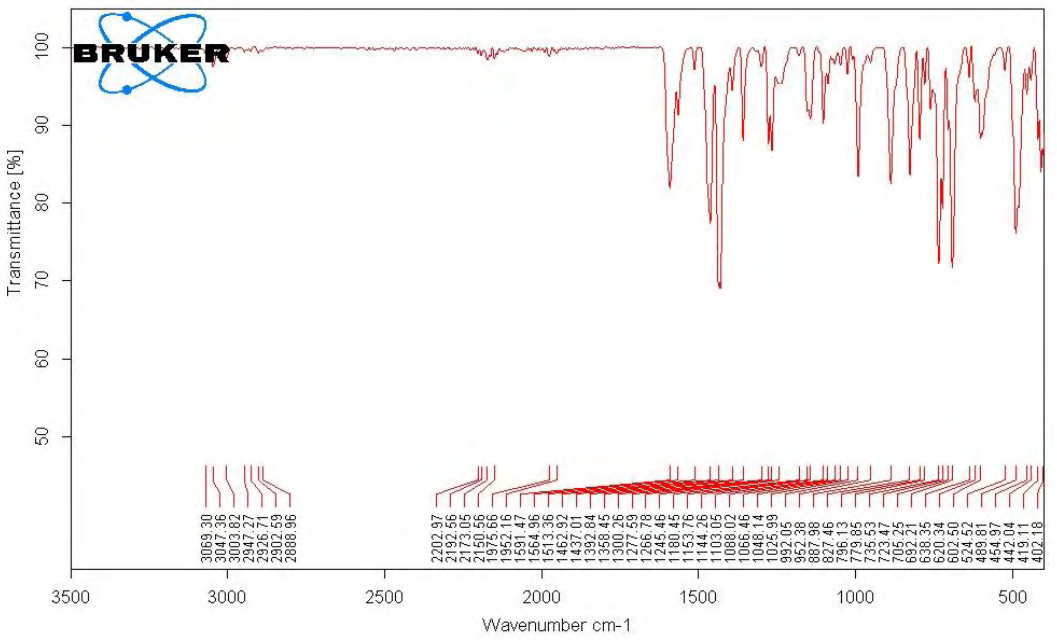

Figure 61. ATR IR spectrum of **106**

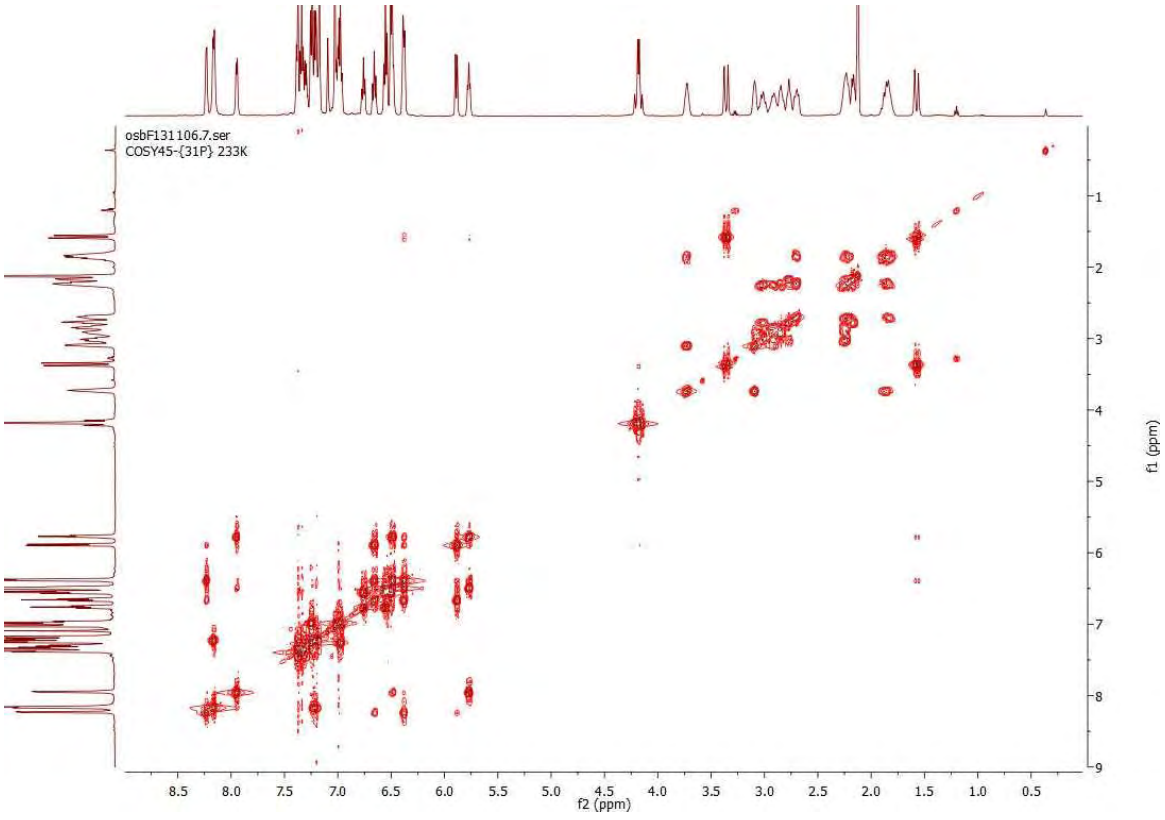

Figure 62. COSY NMR spectrum of complex **121**

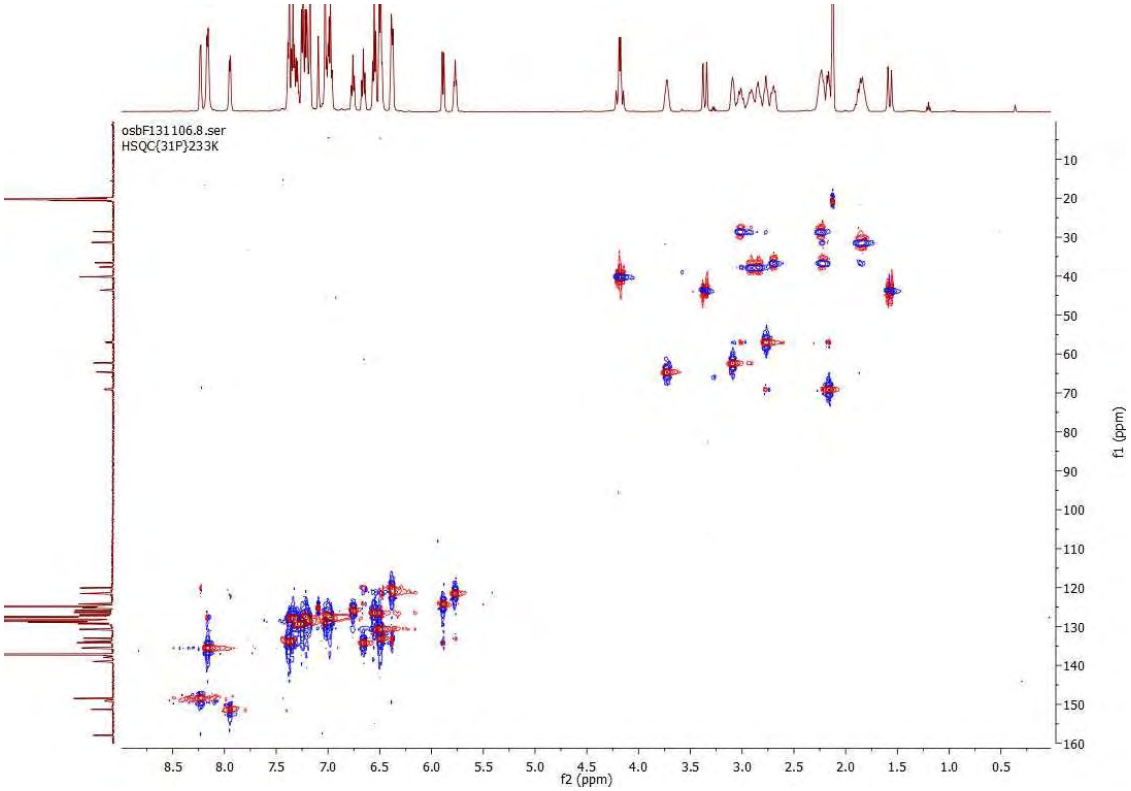

Figure 63. HSQC NMR spectrum of complex **121**

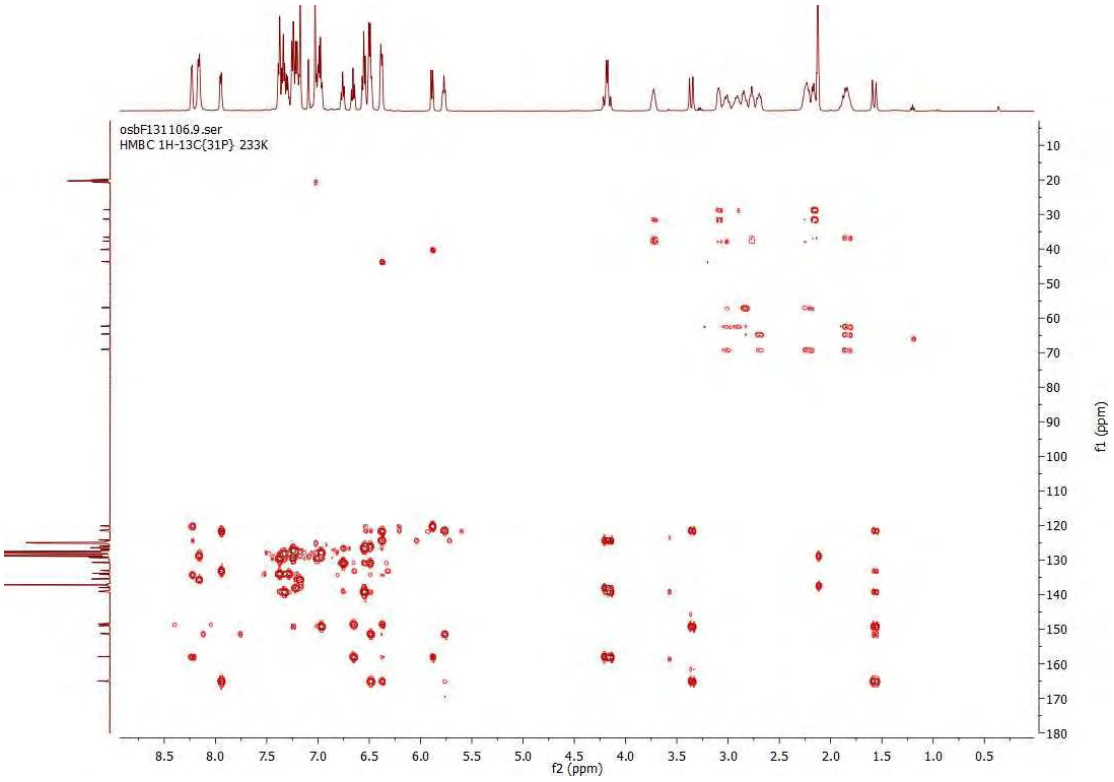

Figure 64. HMBC NMR spectrum of complex **121**

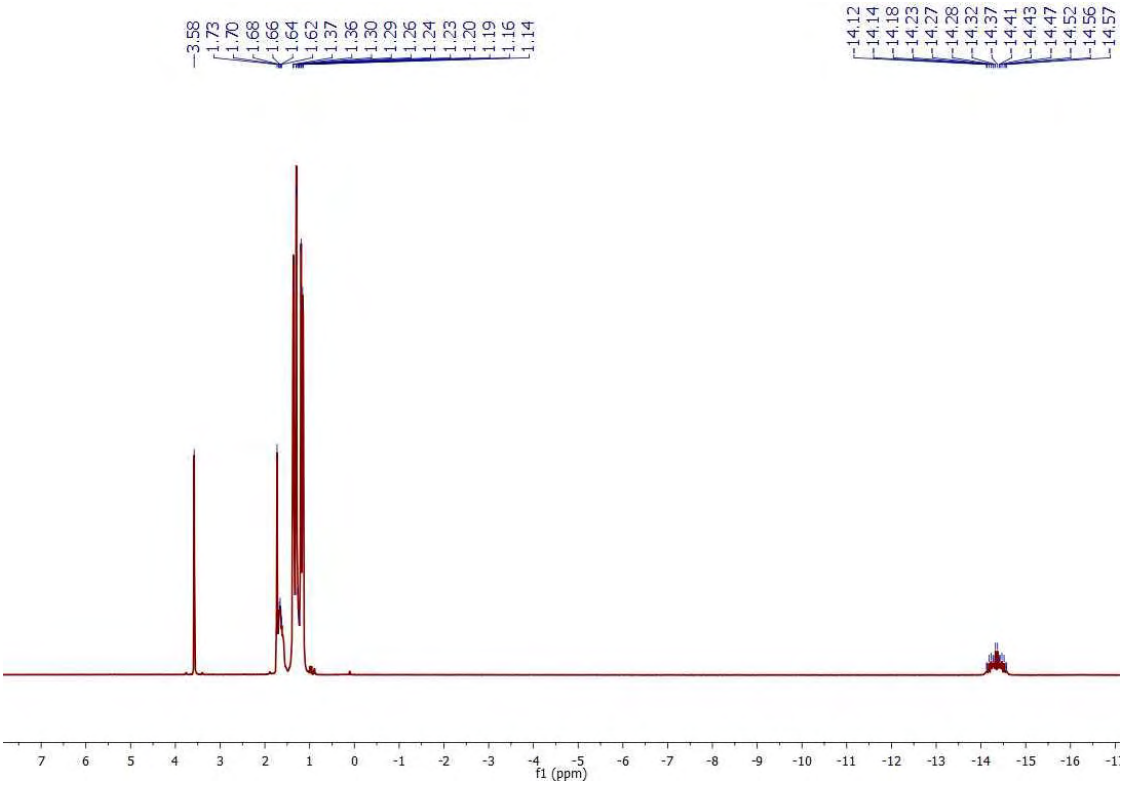

Figure 65. ^{1}H NMR spectrum of $Fe(H)_2(dmpe)_2$ **40** (400.2 MHz, THF-D_8, 298 K)

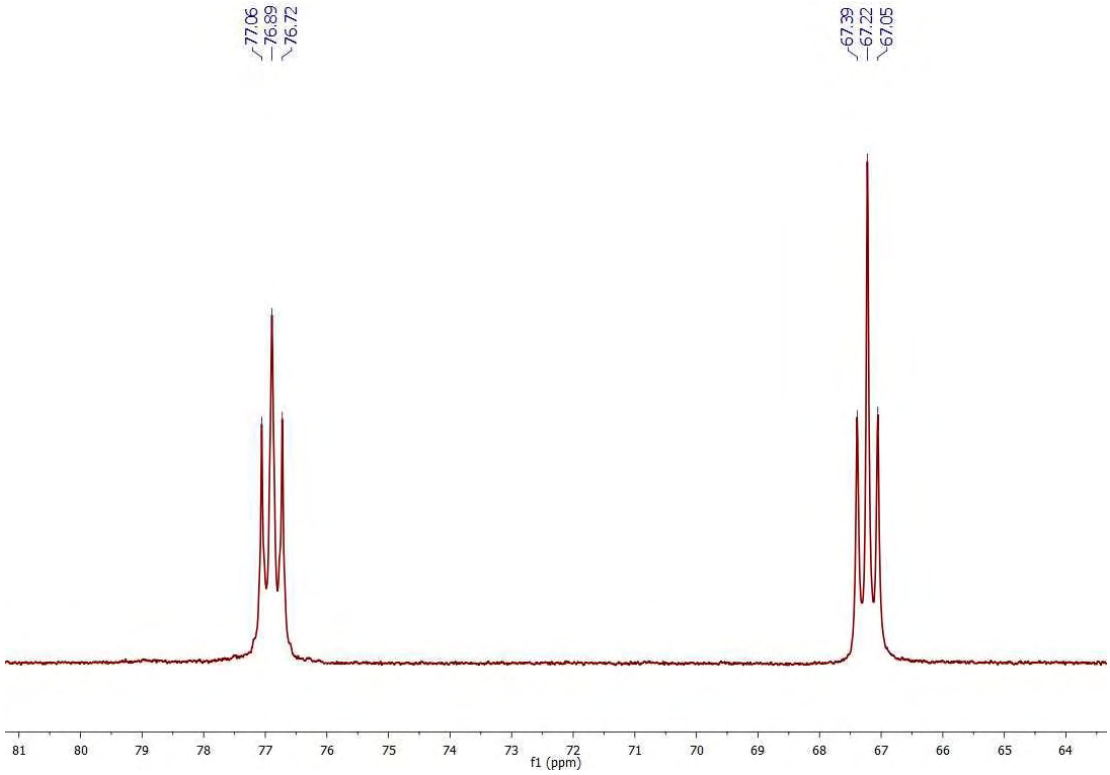

Figure 66. ^{31}P NMR spectrum of $Fe(H)_2(dmpe)_2$ **40** (162.0MHz, THF-D_8, 298 K)

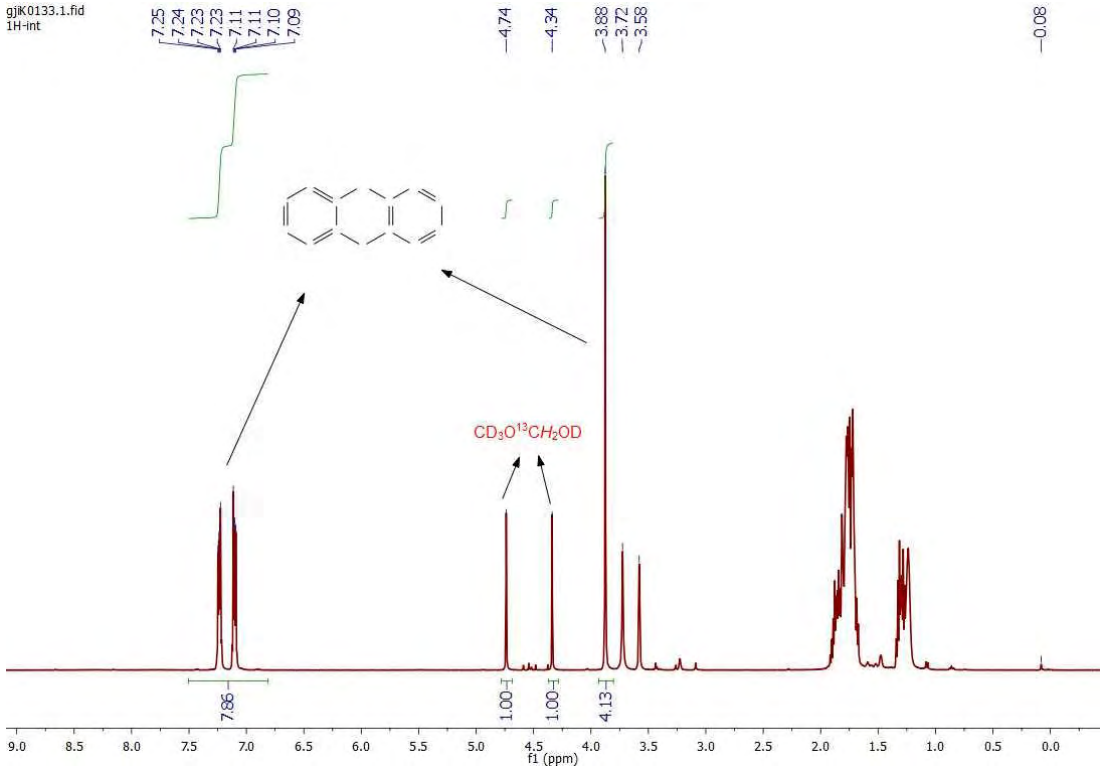

Figure 67. ^{1}H NMR spectrum for in situ characterization of compound **131**

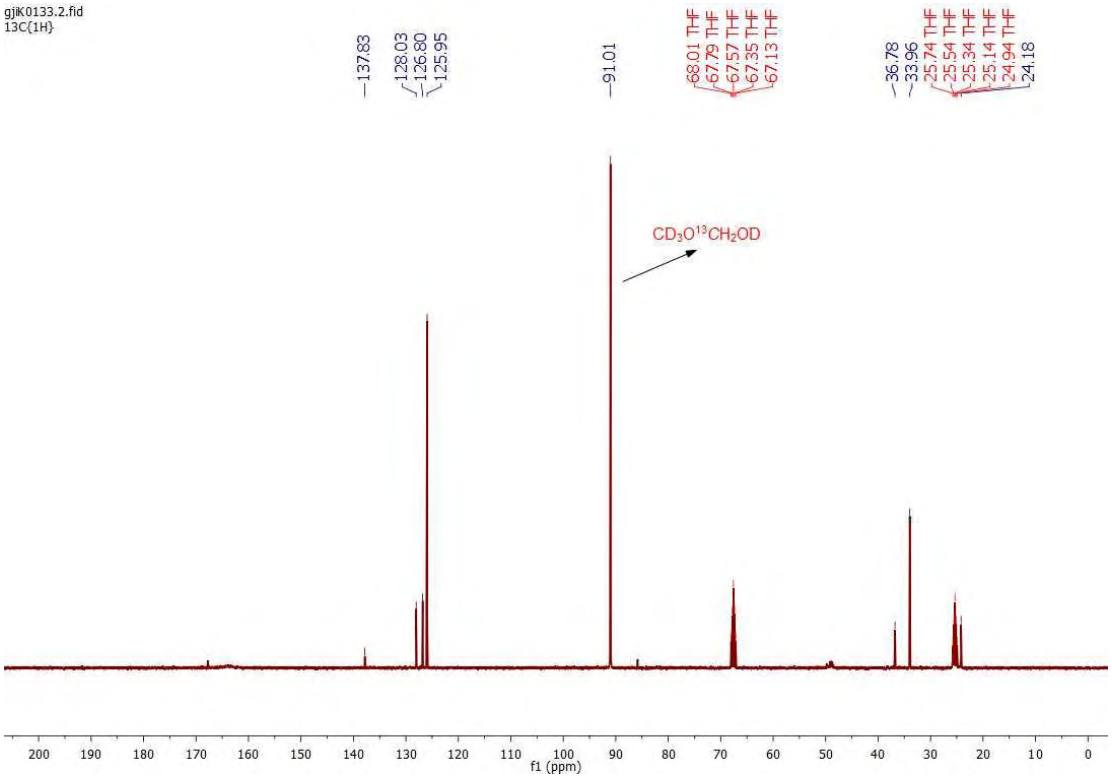

Figure 68. ^{13}C{^{1}H} NMR spectrum for in situ characterization of compound **131**

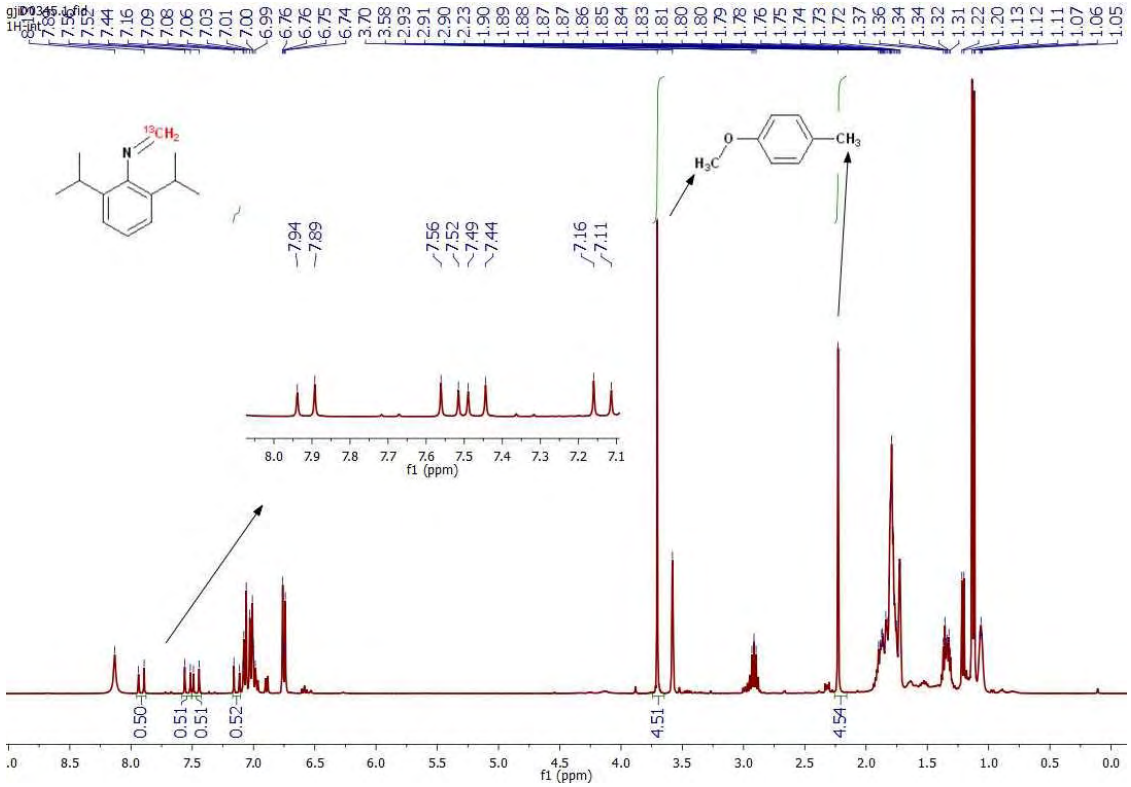

Figure 69. ^{1}H NMR spectrum for in situ characterization of compound **132**

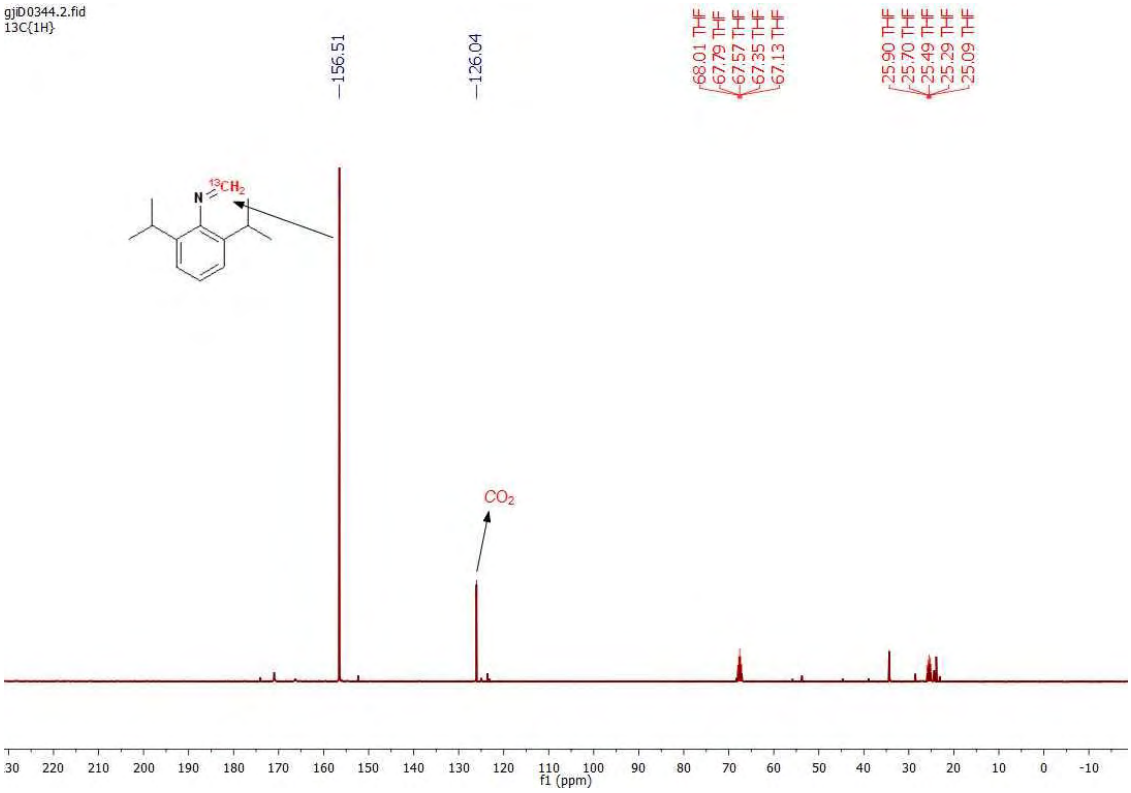

Figure 70. ^{13}C{^{1}H} NMR spectrum for in situ characterization of compound **132**

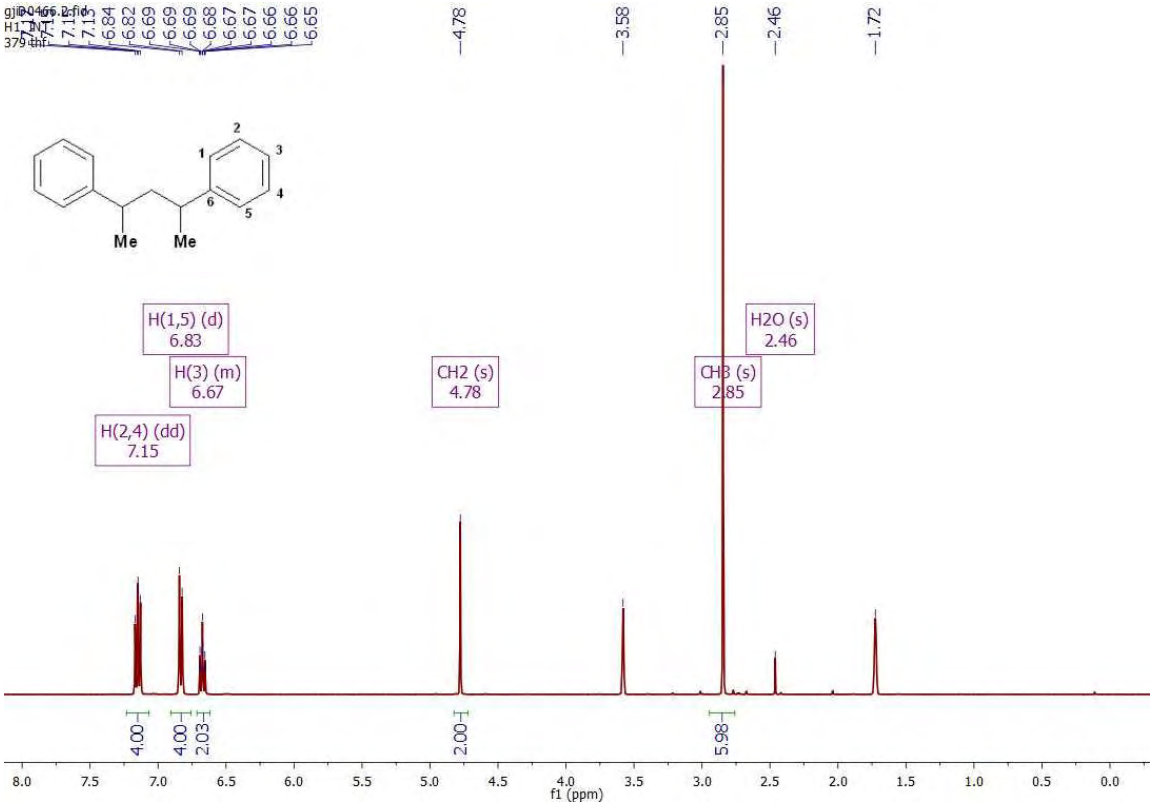

Figure 71. ^{1}H NMR spectrum of compound **137**

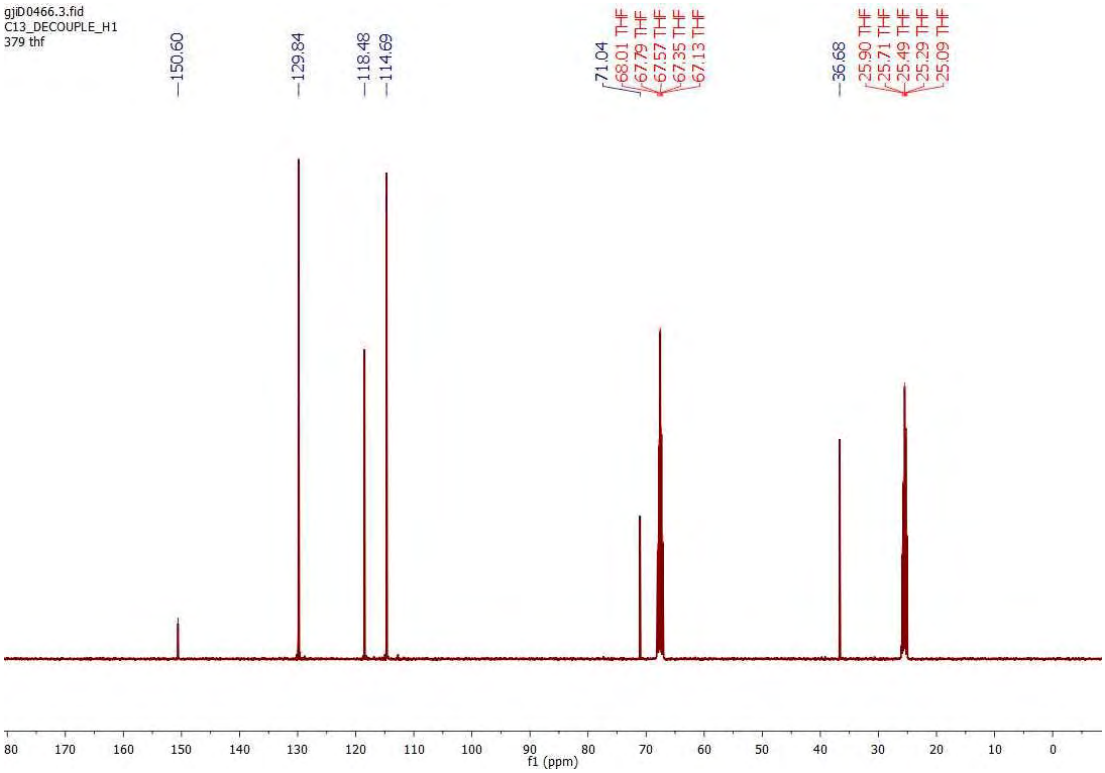

Figure 72. ^{13}C{^{1}H} NMR spectrum of compound **137**

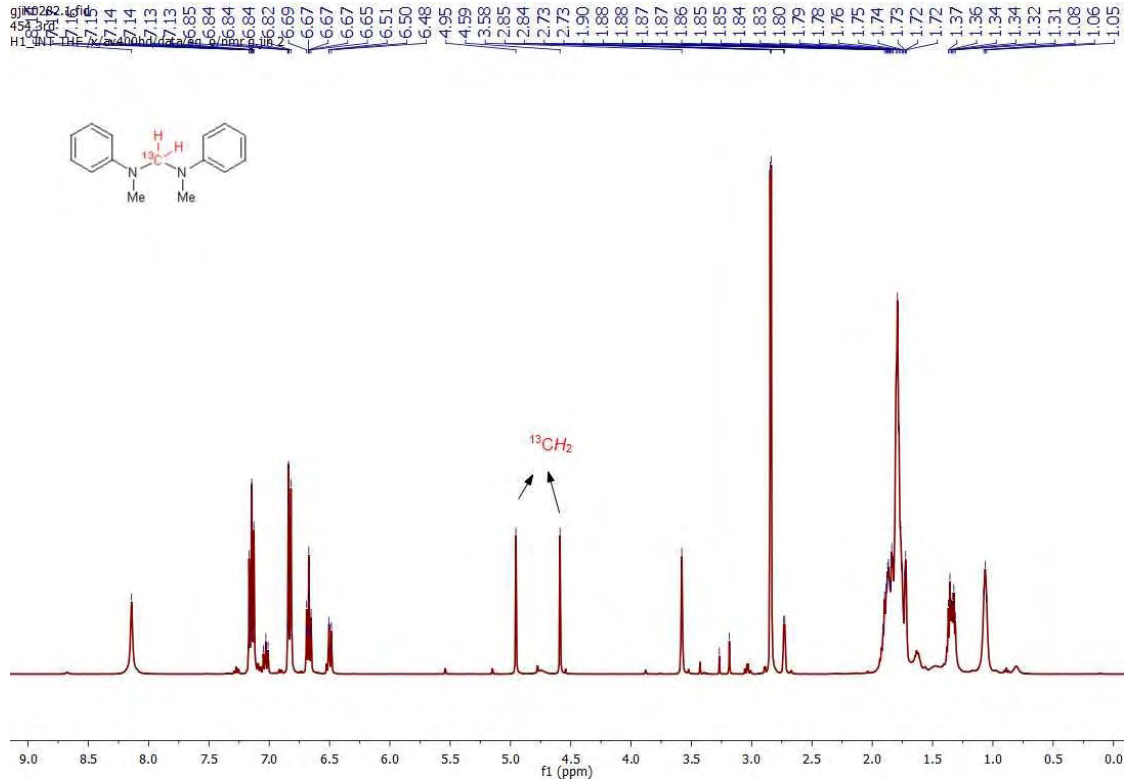

Figure 73. ^{1}H NMR spectrum for in situ characterization of compound **137**(^{13}C)

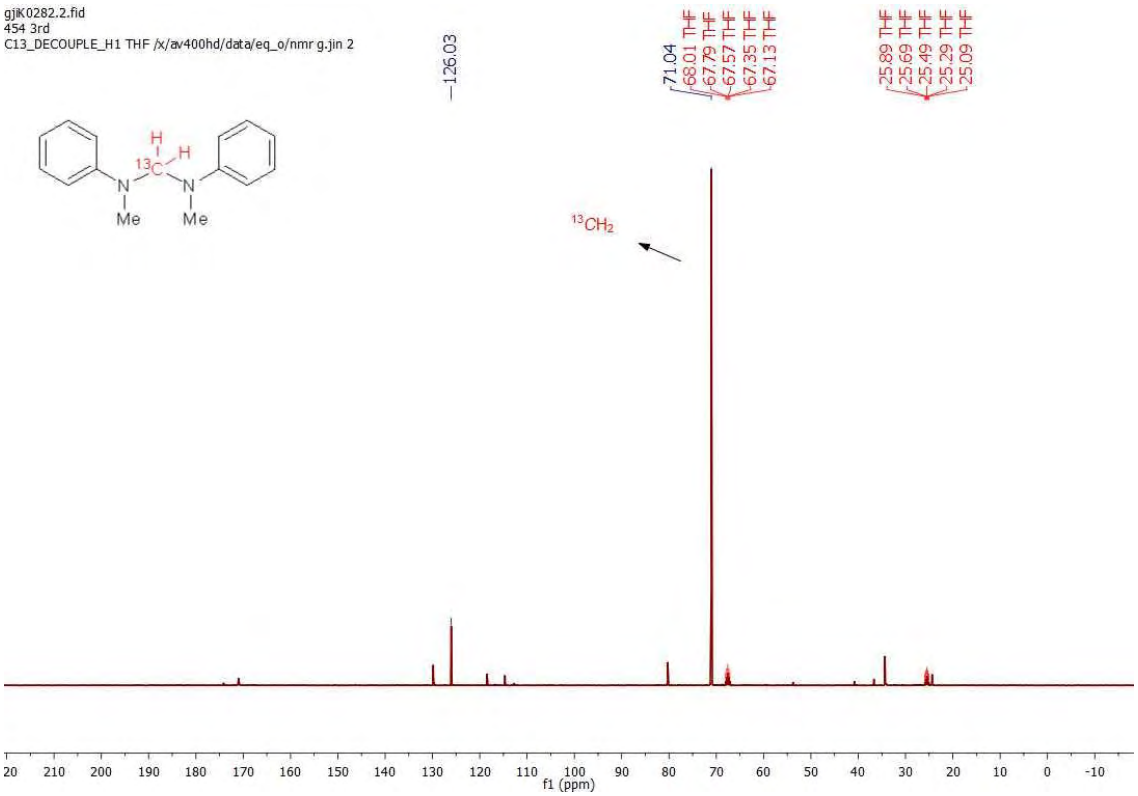

Figure 74. ^{13}C{^{1}H} NMR spectrum for in situ characterization of compound **137**(^{13}C)

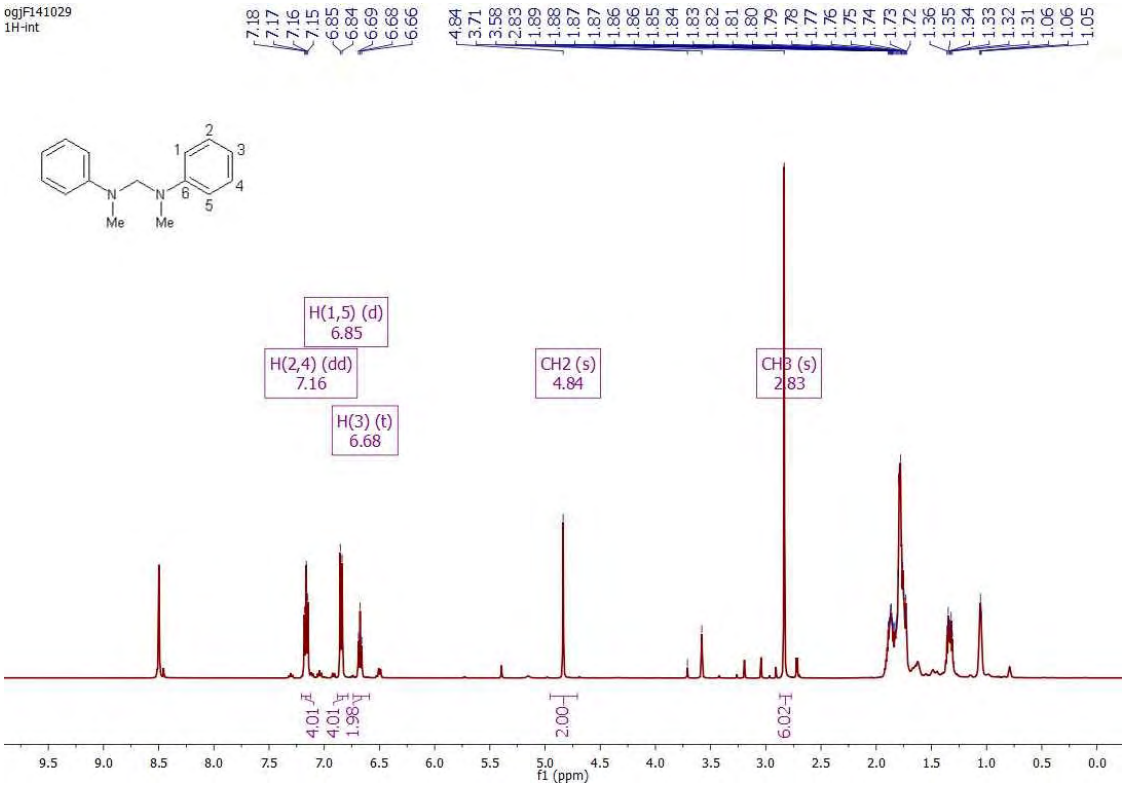

Figure 75. ^{1}H NMR spectrum for in situ characterization of compound **137**(^{12}C)

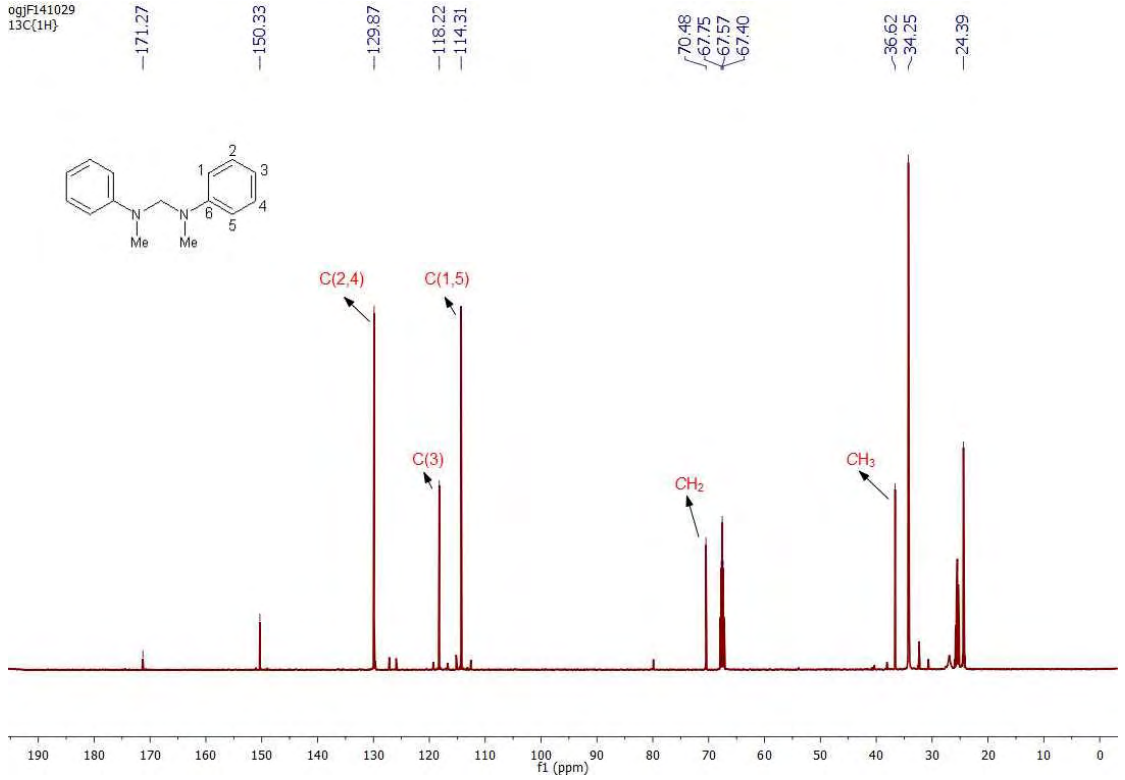

Figure 76. ^{13}C{^{1}H} NMR spectrum for in situ characterization of compound **137**(^{12}C)

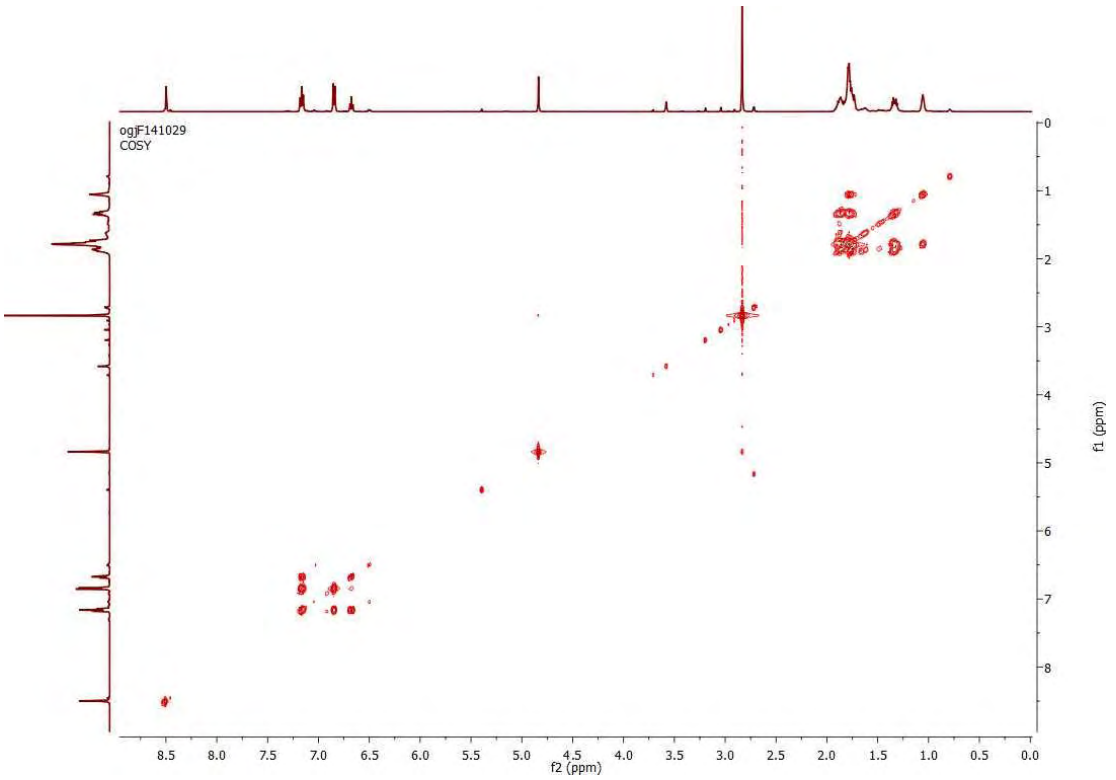

Figure 77. COSY analysis for in-situ characterization of compound **137**(^{12}C)

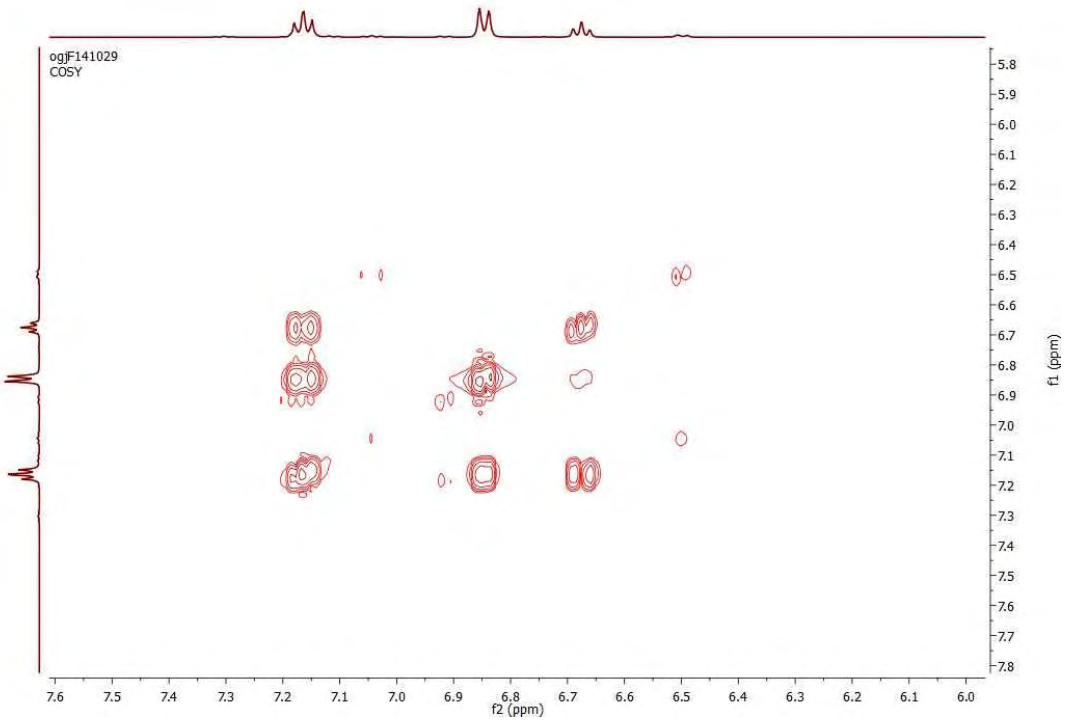

Figure 78. COSY analysis for in-situ characterization of compound **137**(^{12}C) (aromatic region)

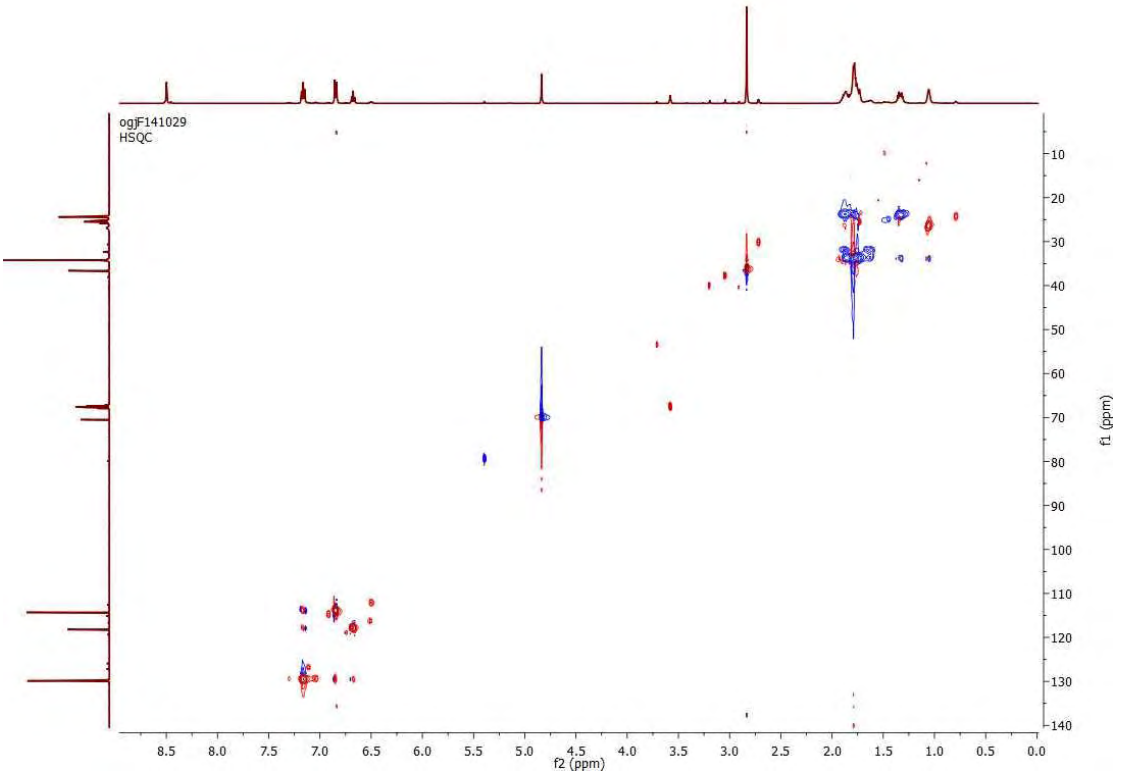

Figure 79. HSQC analysis for in-situ characterization of compound **137**(^{12}C)

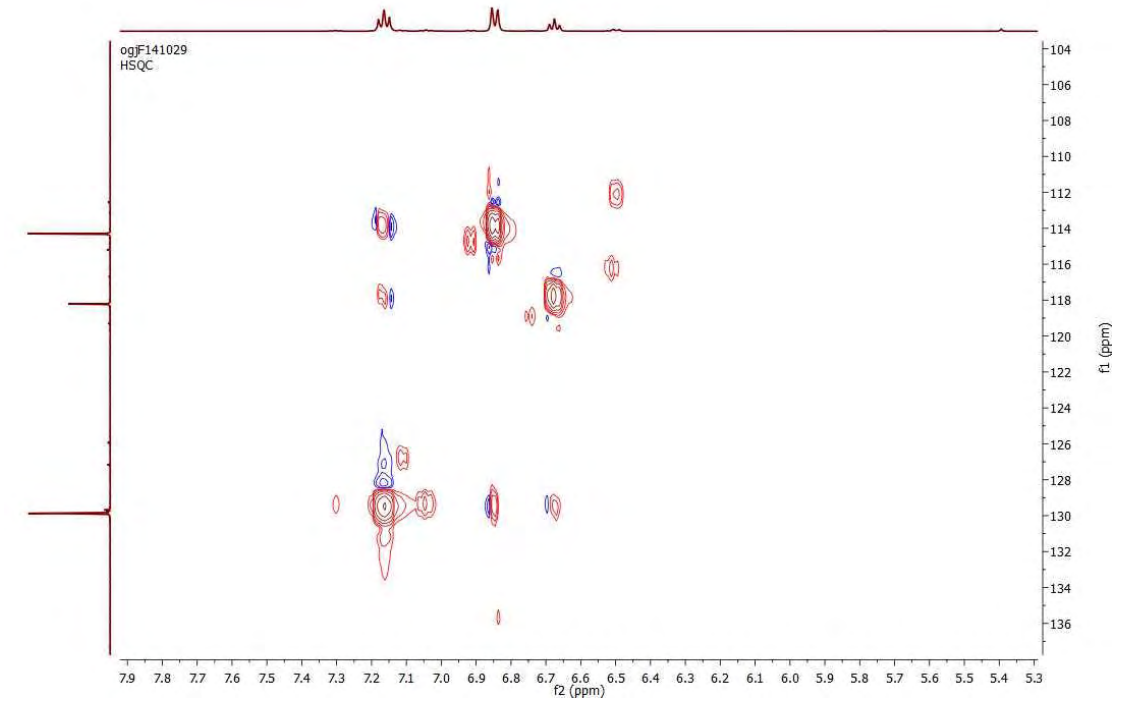

Figure 80. HSQC analysis for in-situ characterization of compound **137**(^{12}C) (aromatic region)

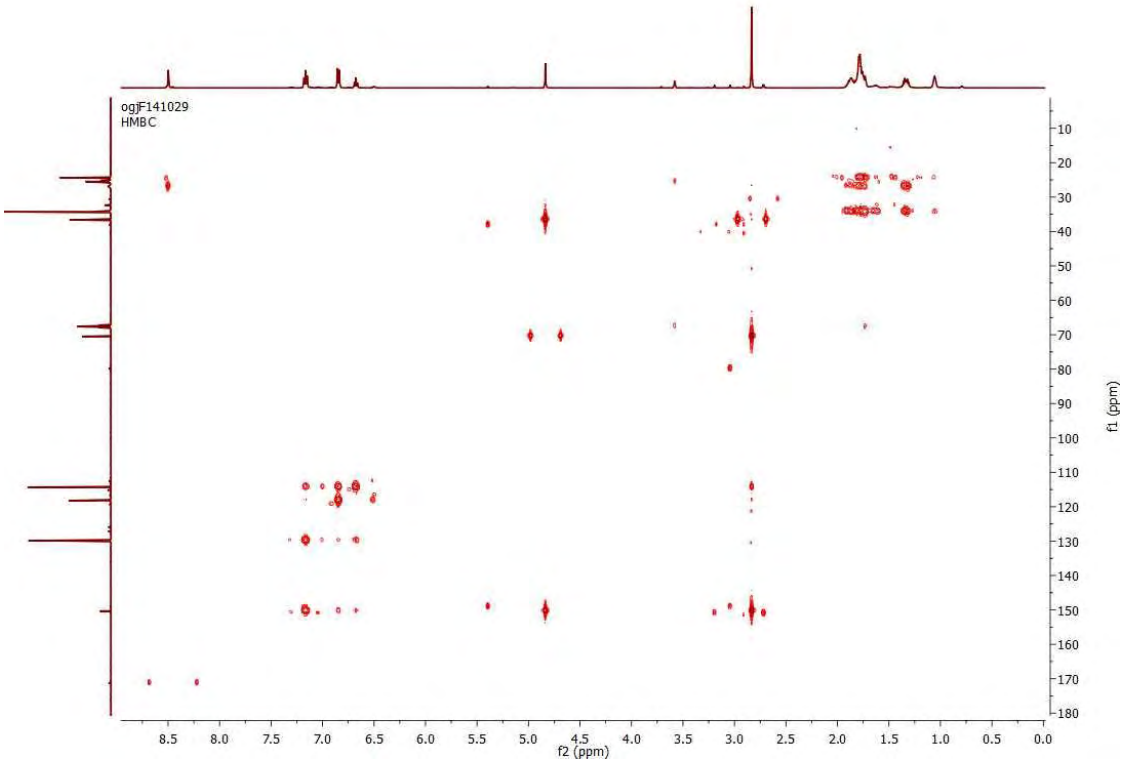

Figure 81. HMBC analysis for in-situ characterization of compound **137**(^{12}C)

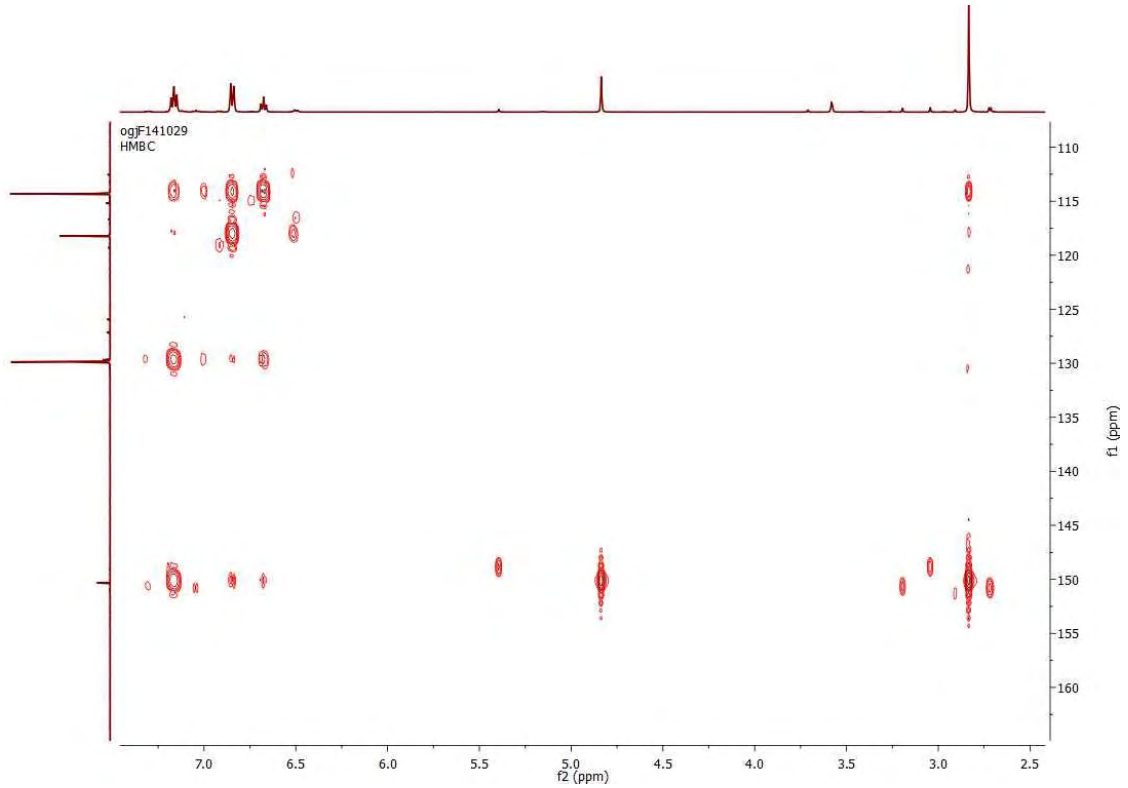

Figure 82. HMBC analysis for in-situ characterization of compound **137**(^{12}C)

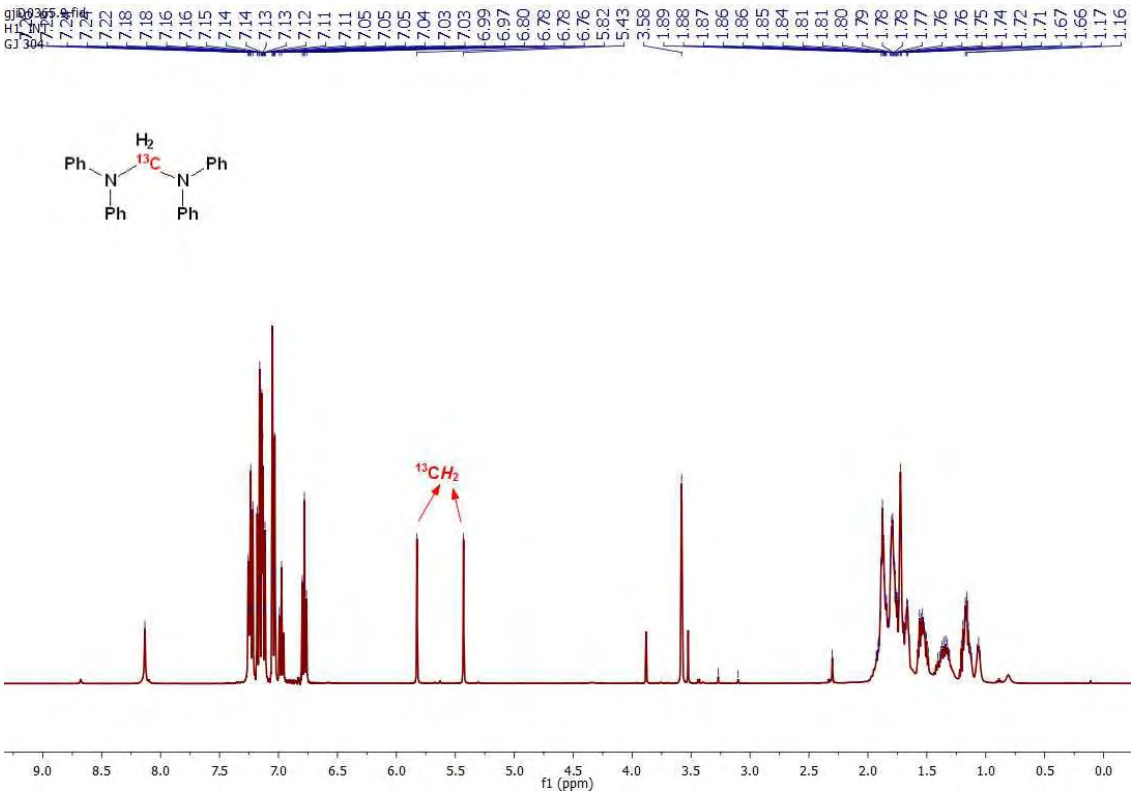

Figure 83. ^{1}H NMR spectrum for in situ characterization of compound **139**(^{13}C)

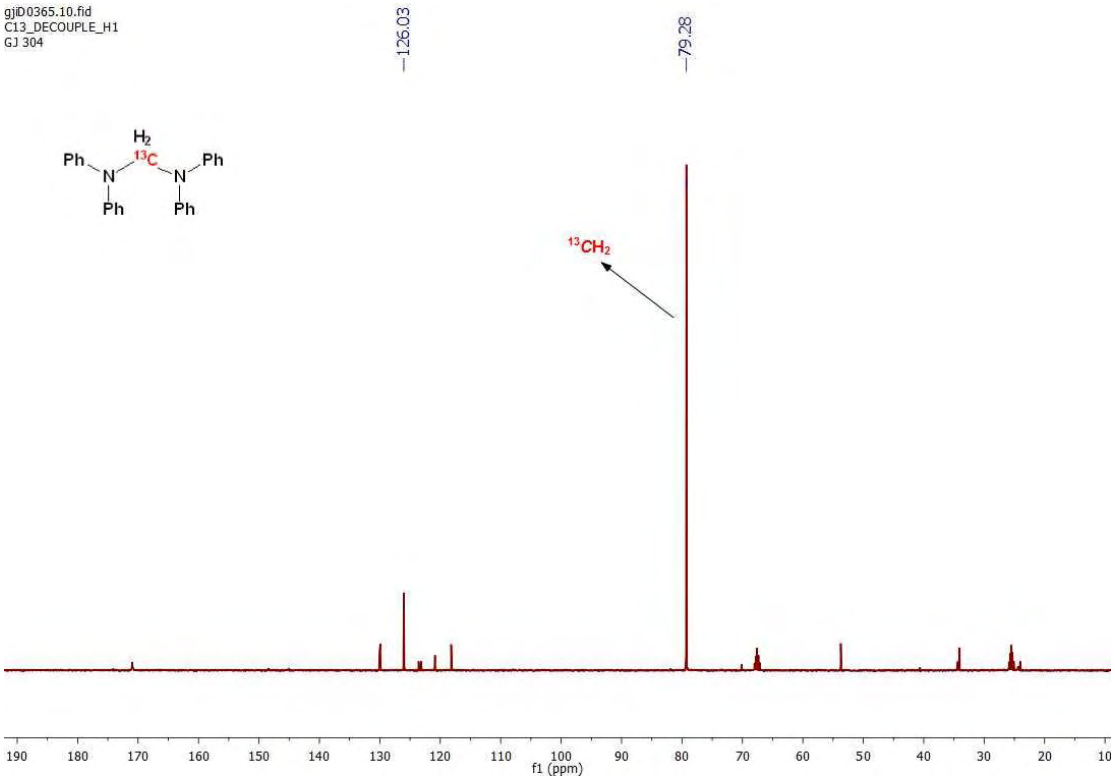

Figure 84. ^{13}C{^{1}H} NMR spectrum for in situ characterization of compound **139**(^{13}C)

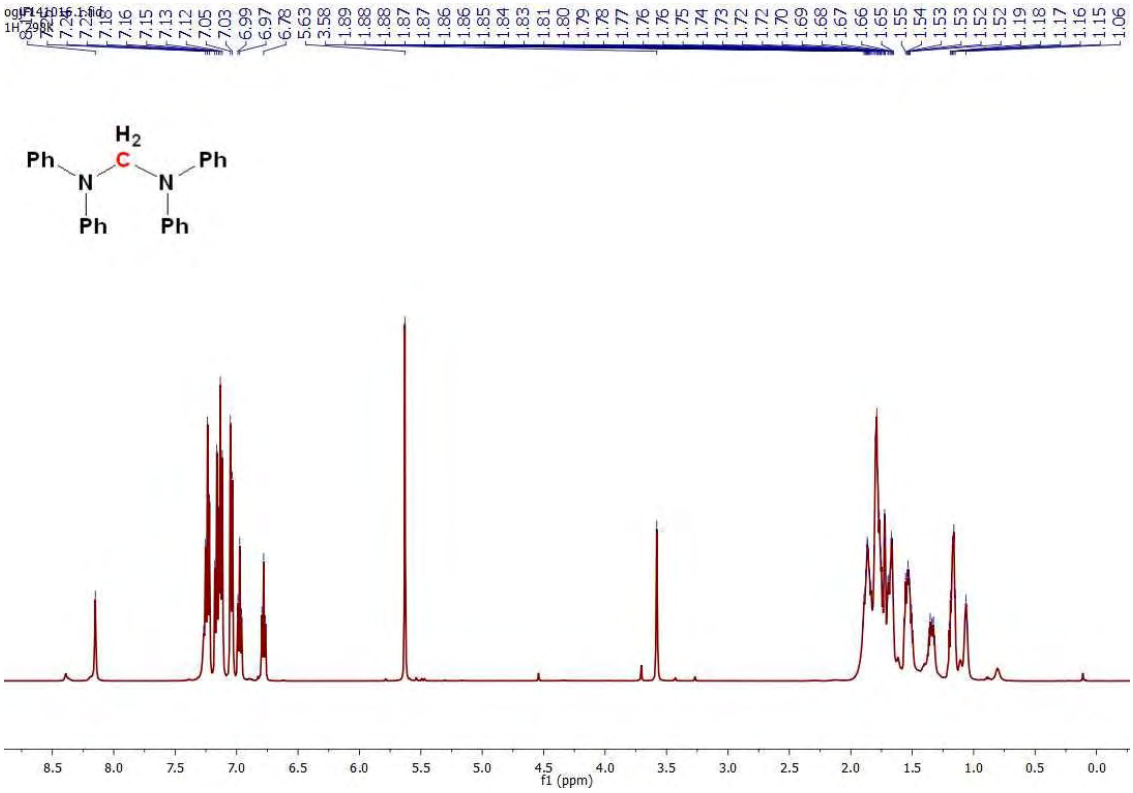

Figure 85. ^{1}H NMR spectrum for in situ characterization of compound **139**(^{12}C)

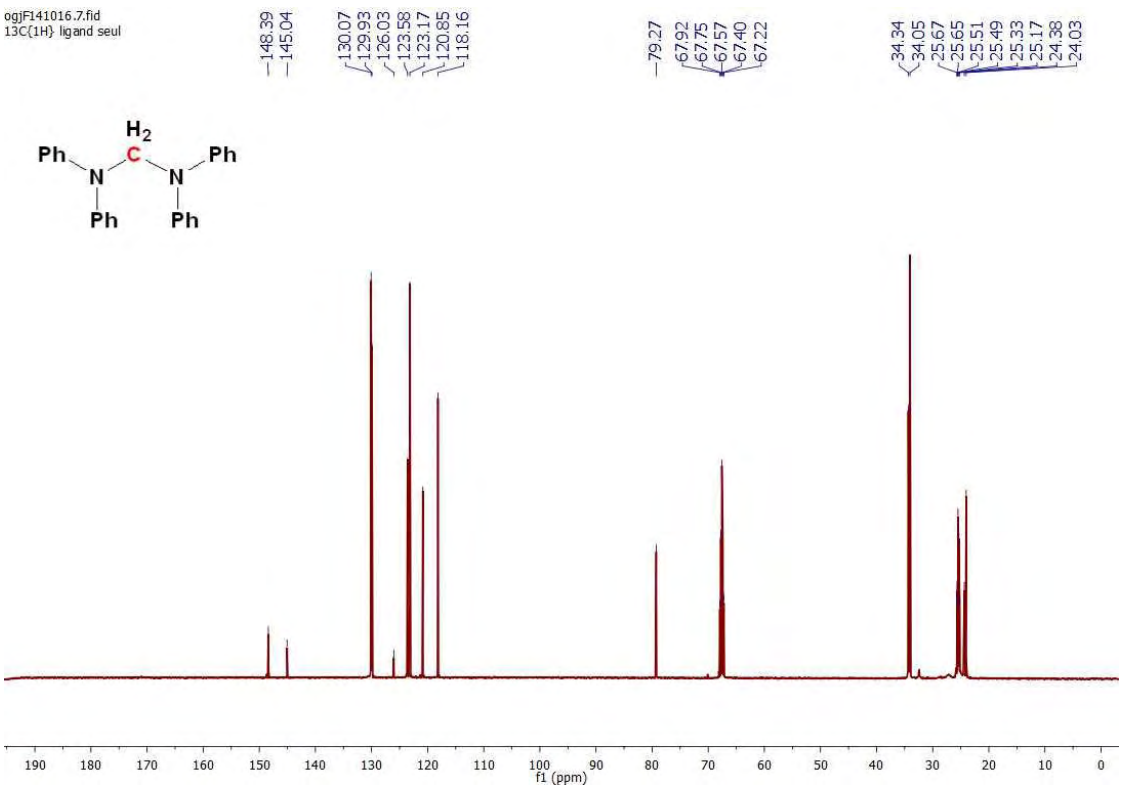

Figure 86. ^{13}C{^{1}H} NMR spectrum for in situ characterization of compound **139**(^{12}C)

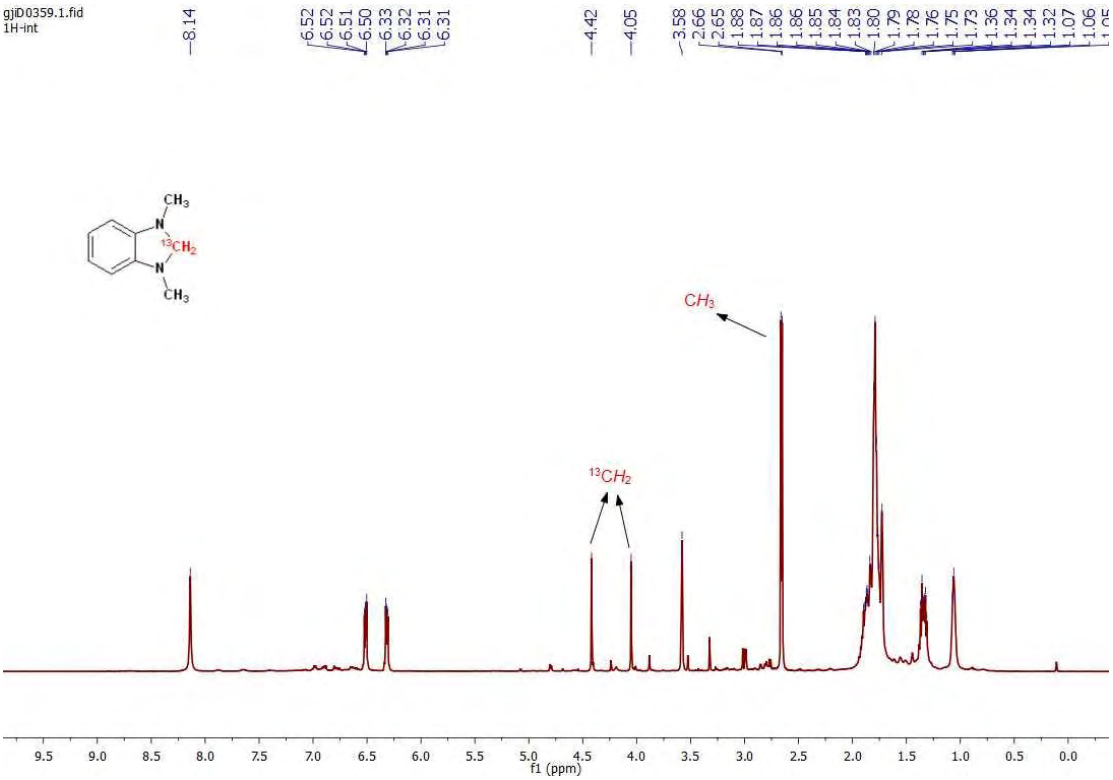

Figure 87. ^{1}H NMR spectrum for in situ characterization of compound **140**(^{13}C)

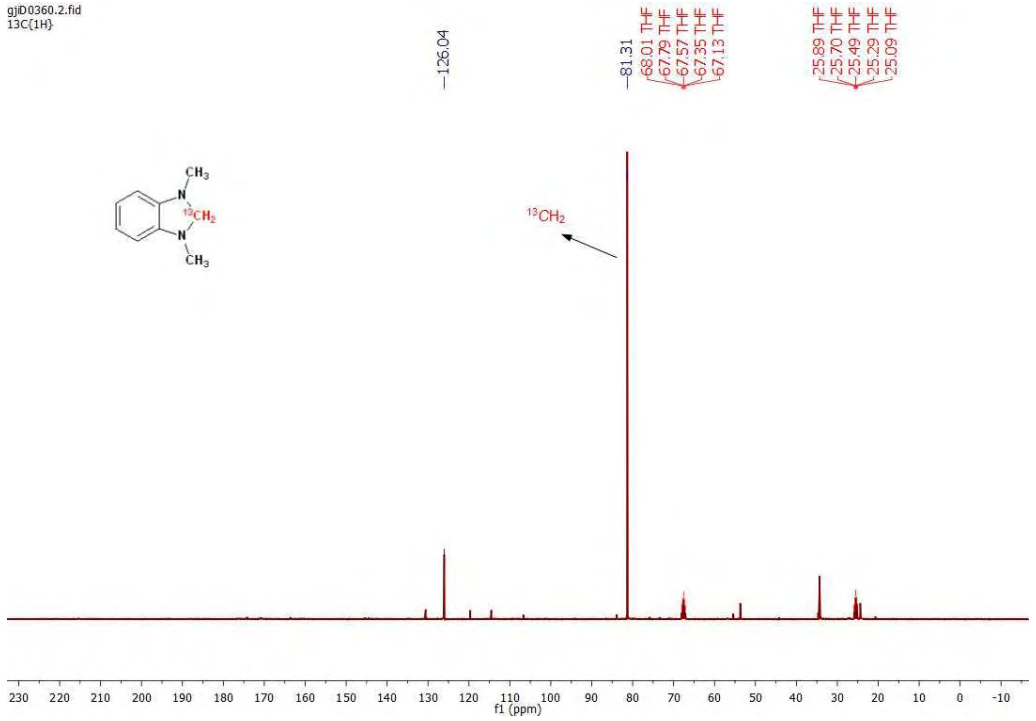

Figure 88. ^{13}C{^{1}H} NMR spectrum for in situ characterization of compound **140**(^{13}C)

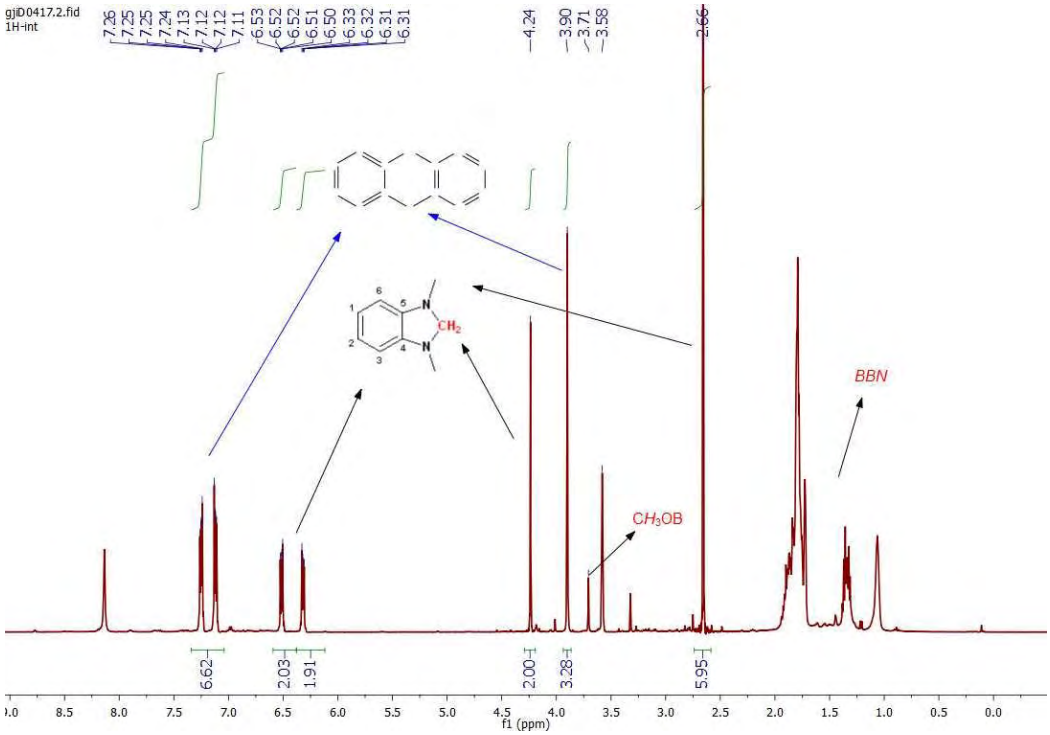

Figure 89. ^{1}H NMR spectrum for in situ characterization of compound **140**(^{12}C)

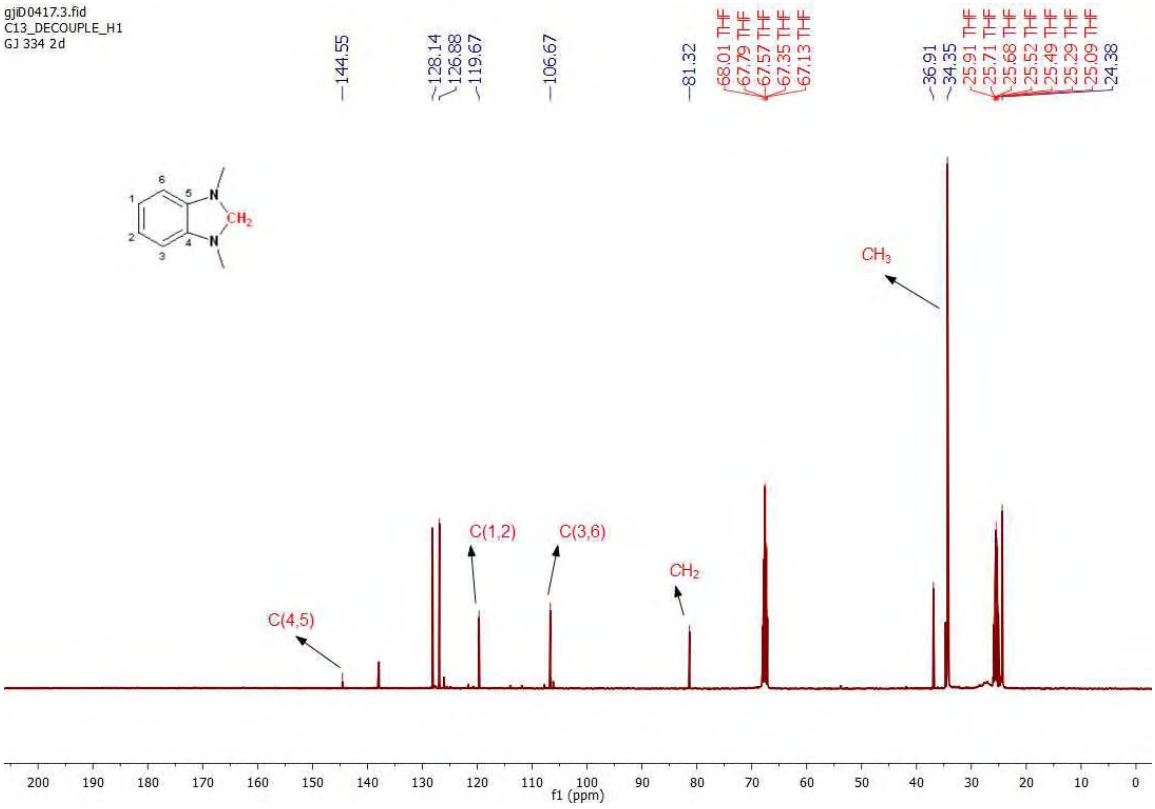

Figure 90. ^{13}C{^{1}H} NMR spectrum for in situ characterization of compound **140**(^{12}C)

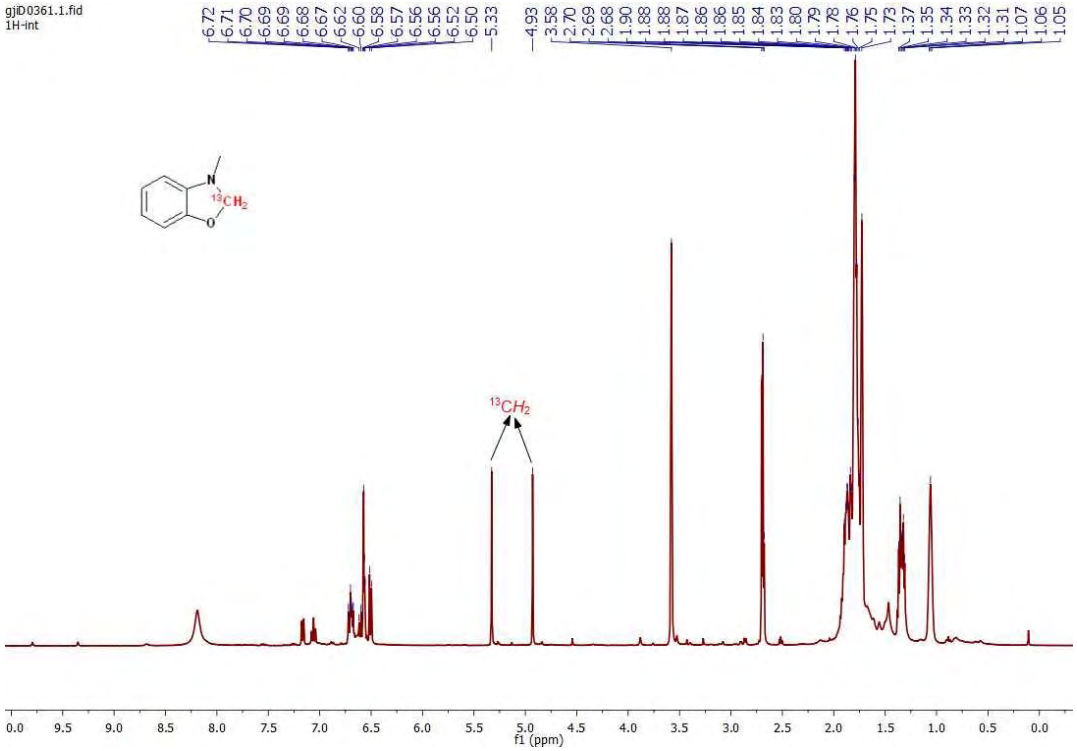

Figure 91. ^{1}H NMR spectrum for in situ characterization of compound **144**(^{13}C)

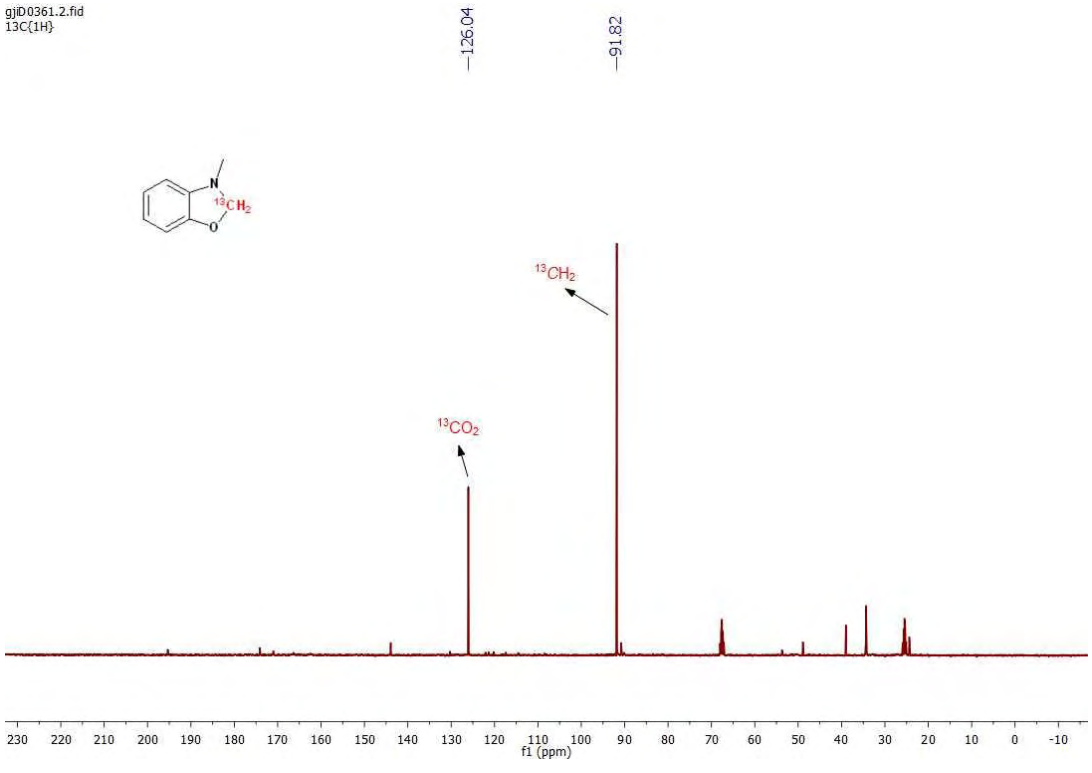

Figure 92. $^{13}C\{^{1}H\}$ NMR spectrum for in situ characterization of compound **144**(^{13}C)

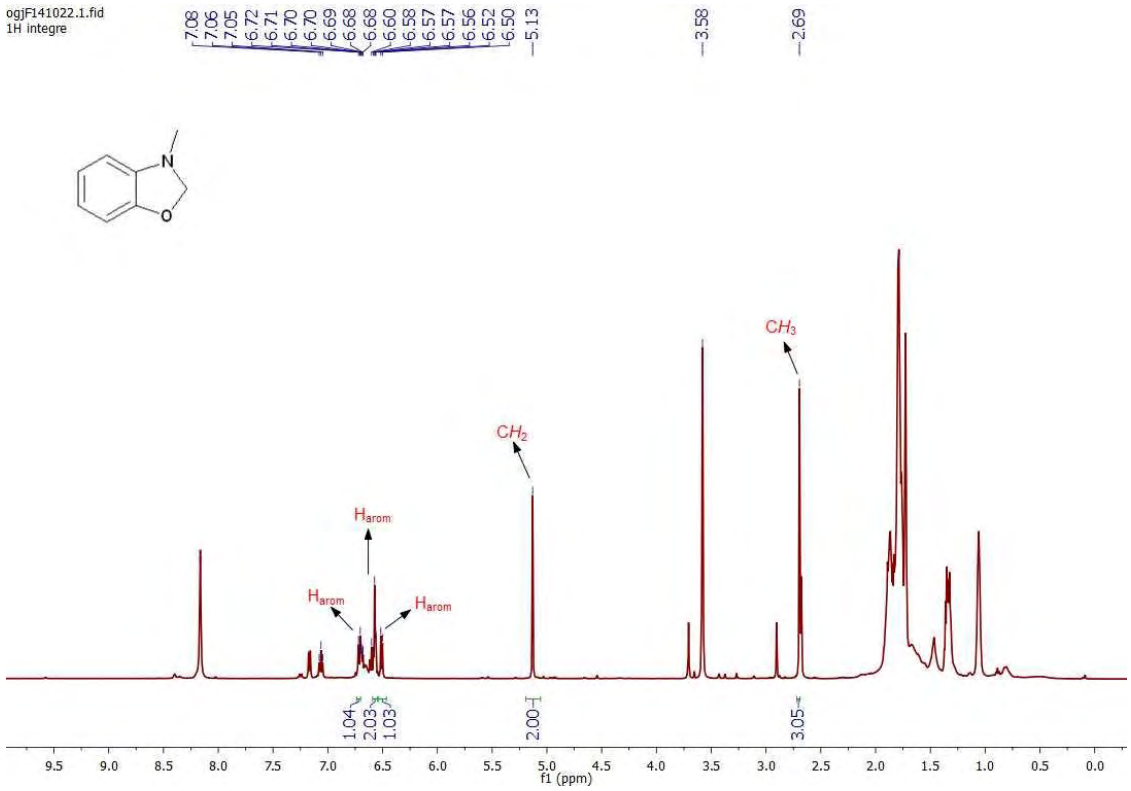

Figure 93. ^{1}H NMR spectrum for in situ characterization of compound **144**(^{12}C)

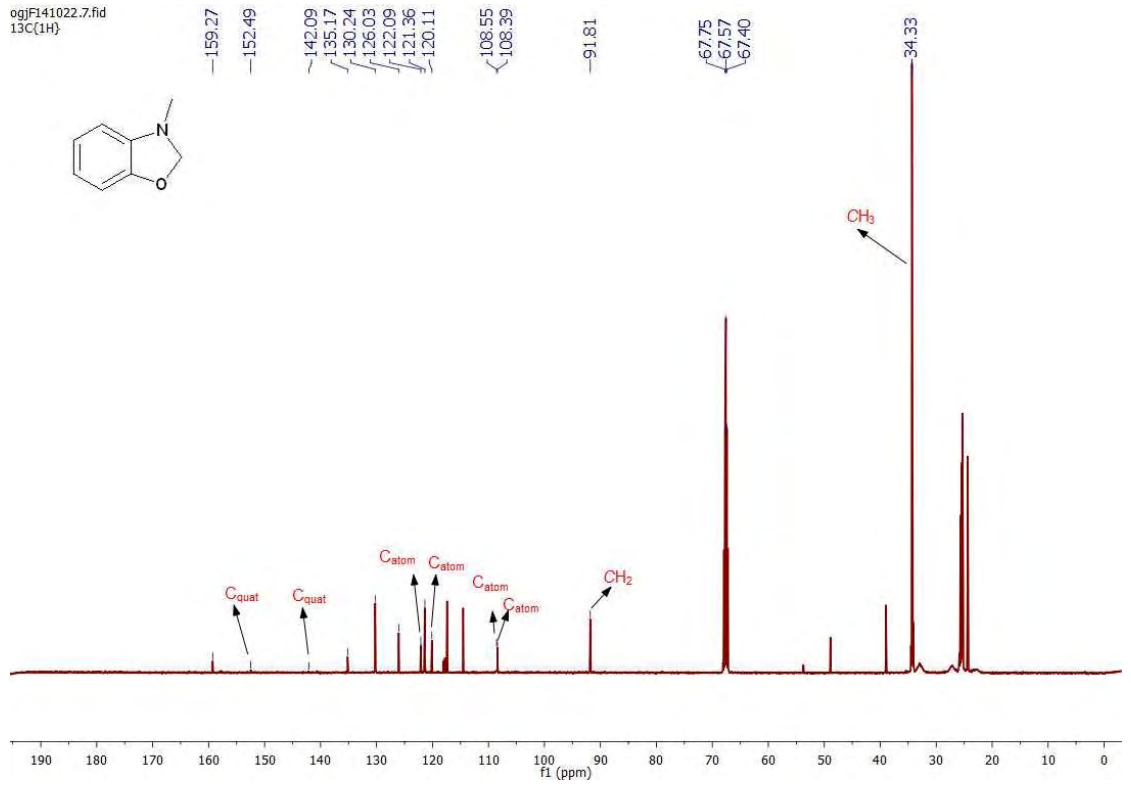

Figure 94. ^{13}C{^{1}H} NMR spectrum for in situ characterization of compound **144**(^{12}C)

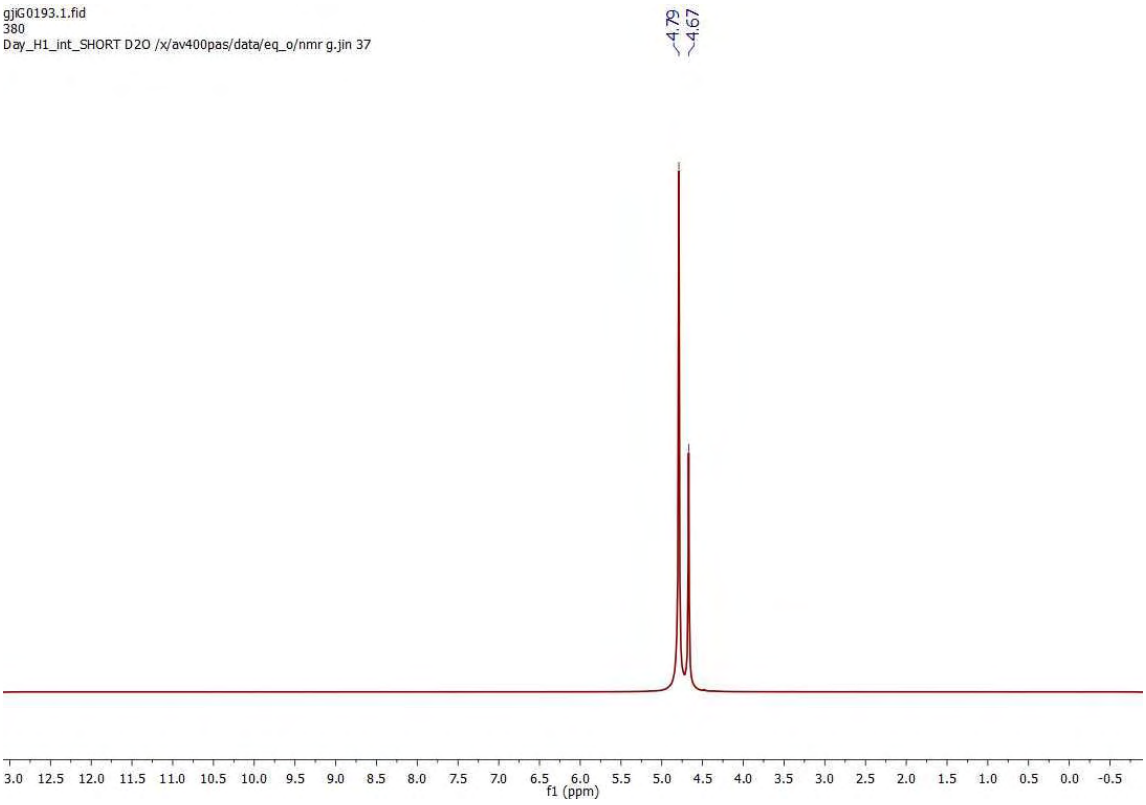

Figure 95. ^{1}H NMR spectrum of independently synthesized compound **145** (D_2O)

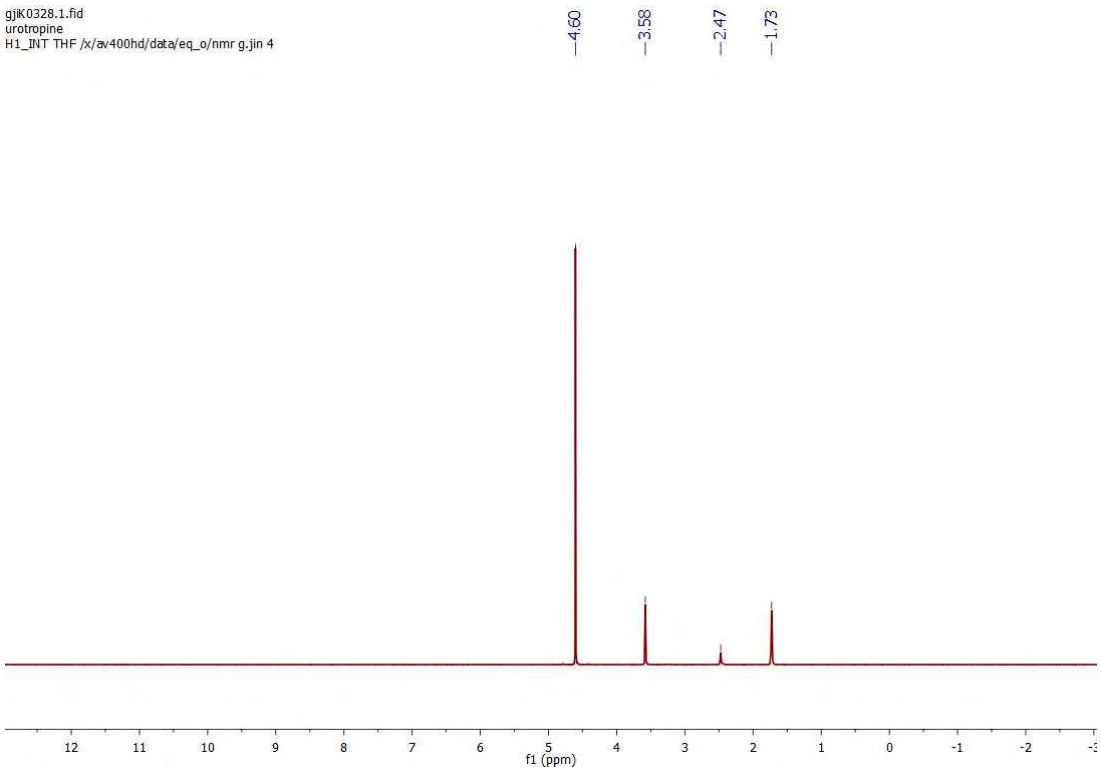

Figure 96. ^{1}H NMR spectrum of independently synthesized compound **145** (THF-D_8)

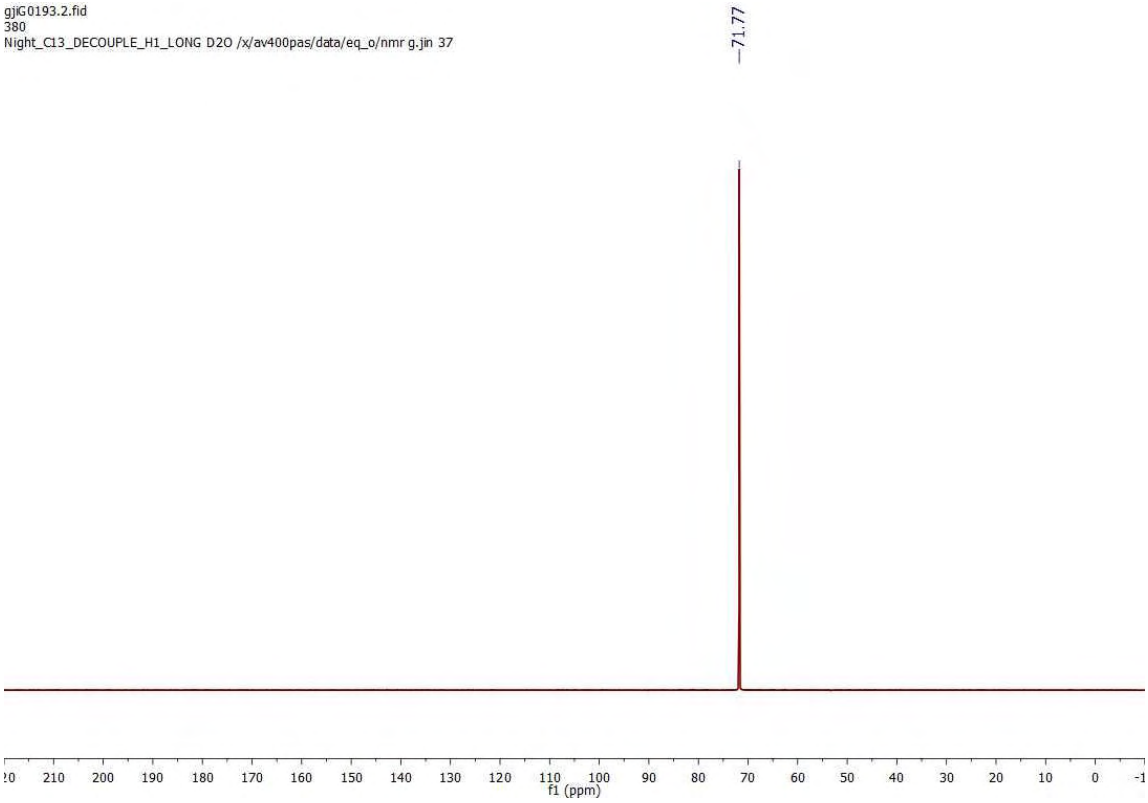

Figure 97. $^{13}C\{^{1}H\}$ NMR spectrum of independently synthesized compound **145** (D_2O)

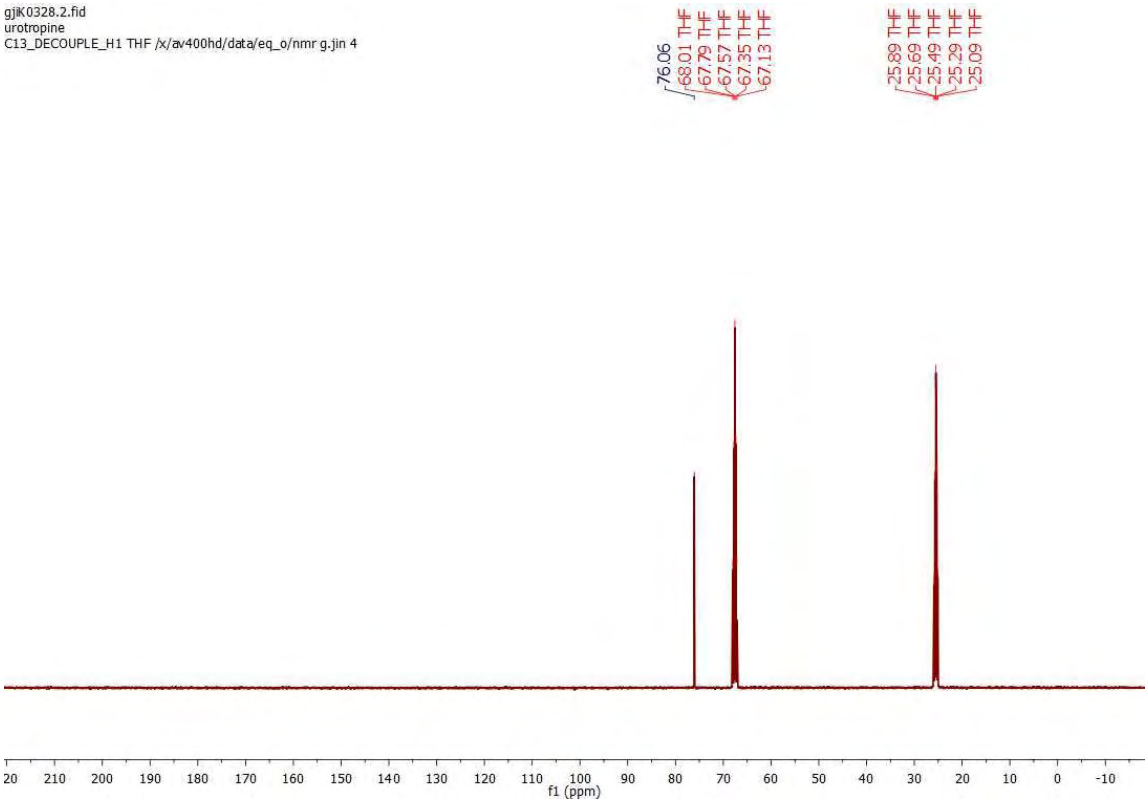

Figure 98. $^{13}C\{^{1}H\}$ NMR spectrum of independently synthesized compound **145** (THF-D_8)

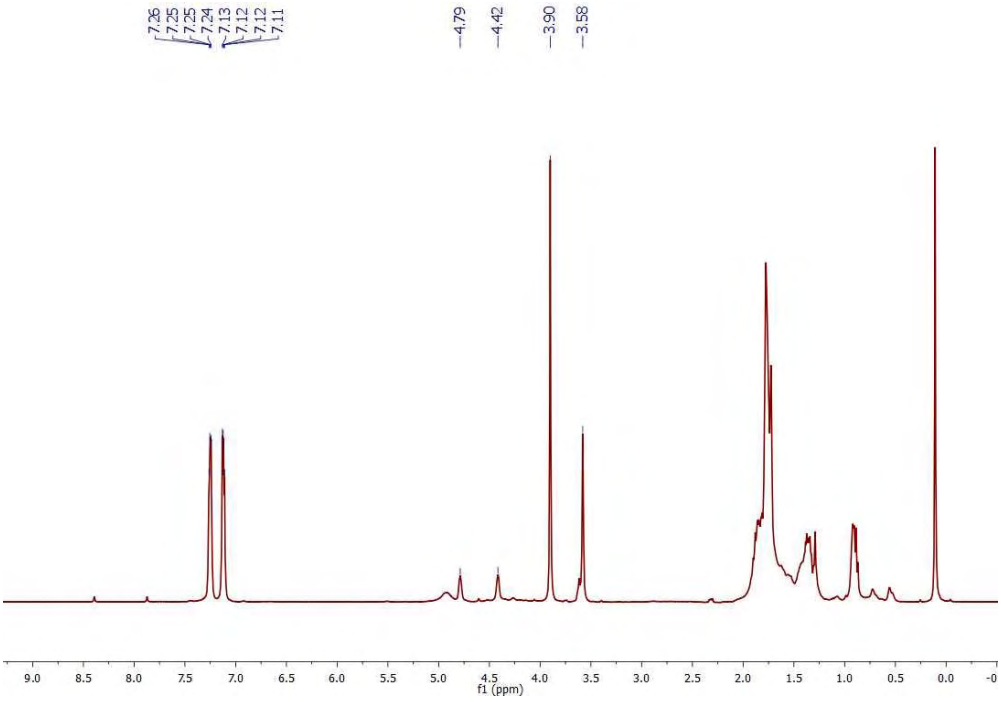

Figure 99. ^{1}H NMR spectrum for in situ characterization of compound **145**(^{13}C)

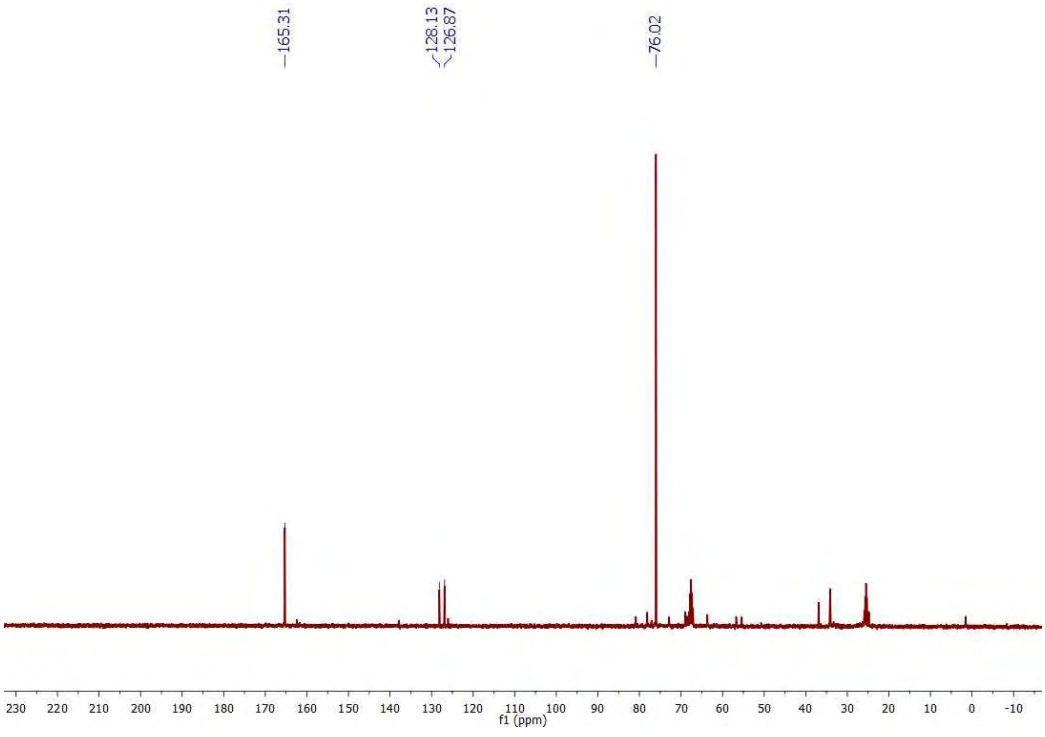

Figure 100. ^{13}C{^{1}H} NMR for in situ characterization of compound **145**(^{13}C)

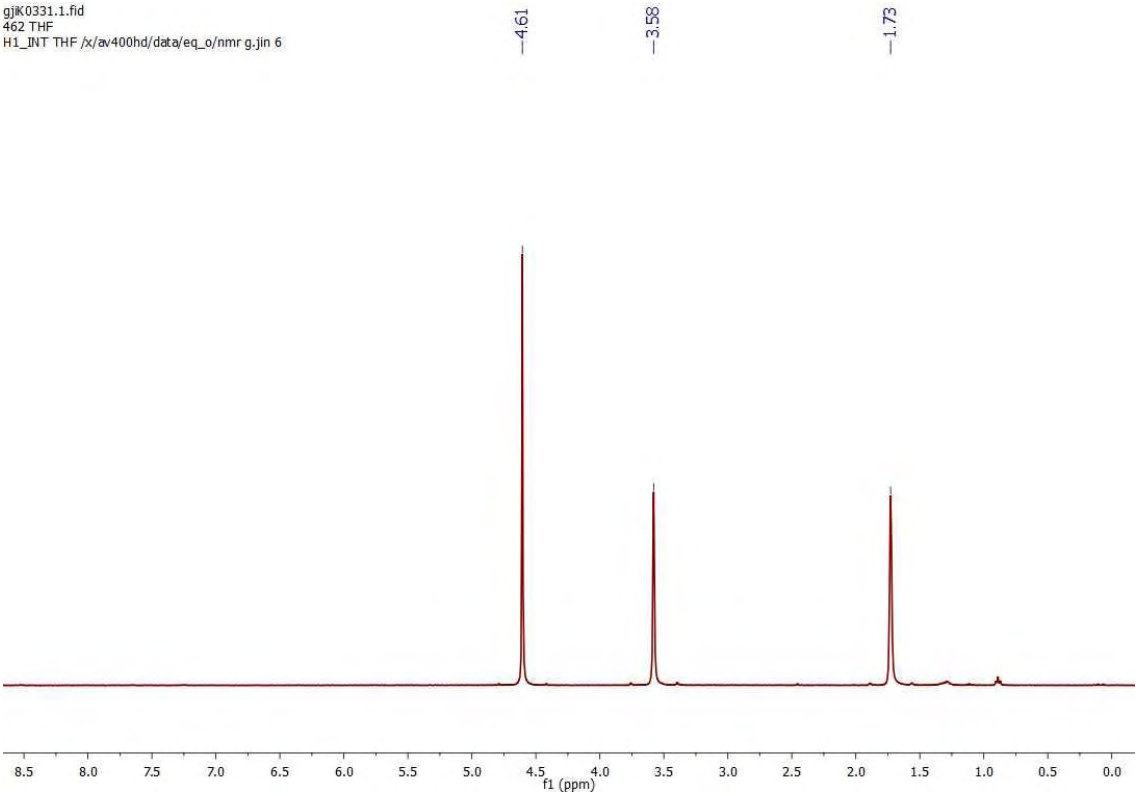

Figure 101. ^{1}H NMR spectrum for isolated compound **145**(^{12}C) (THF-D_8)

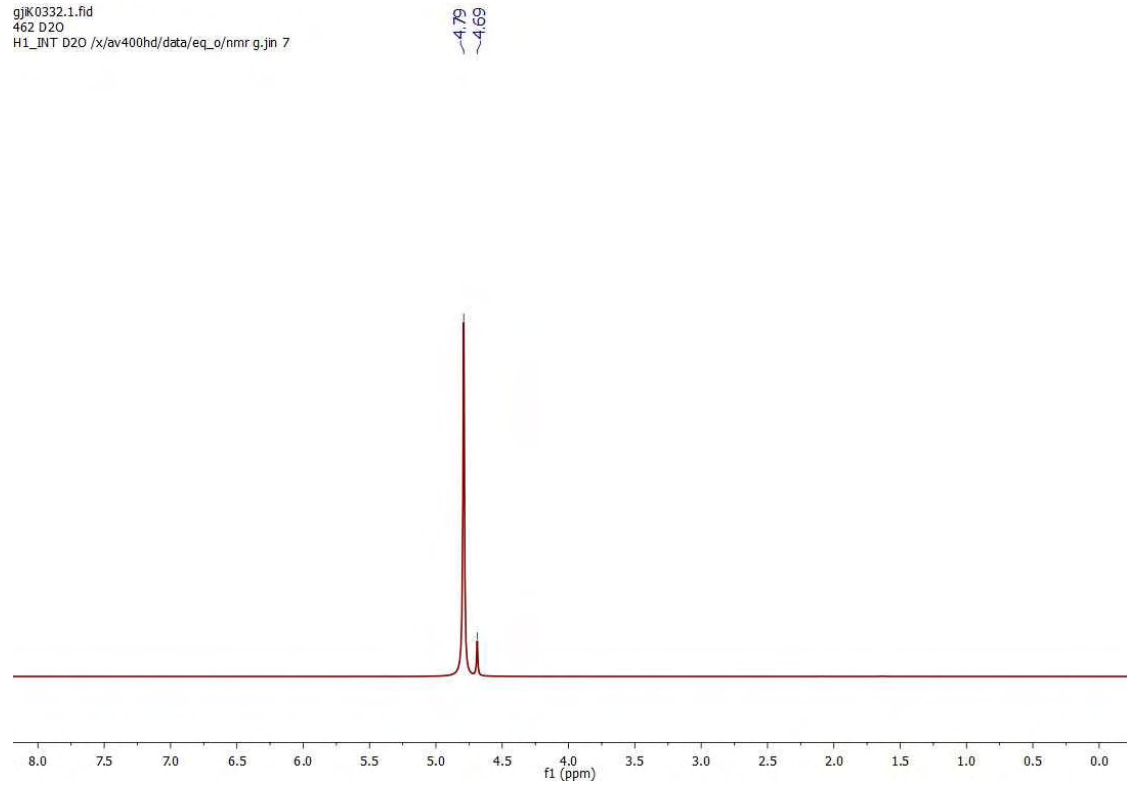

Figure 102. ^{1}H NMR spectrum for isolated compound **145**(^{12}C) (D_2O)

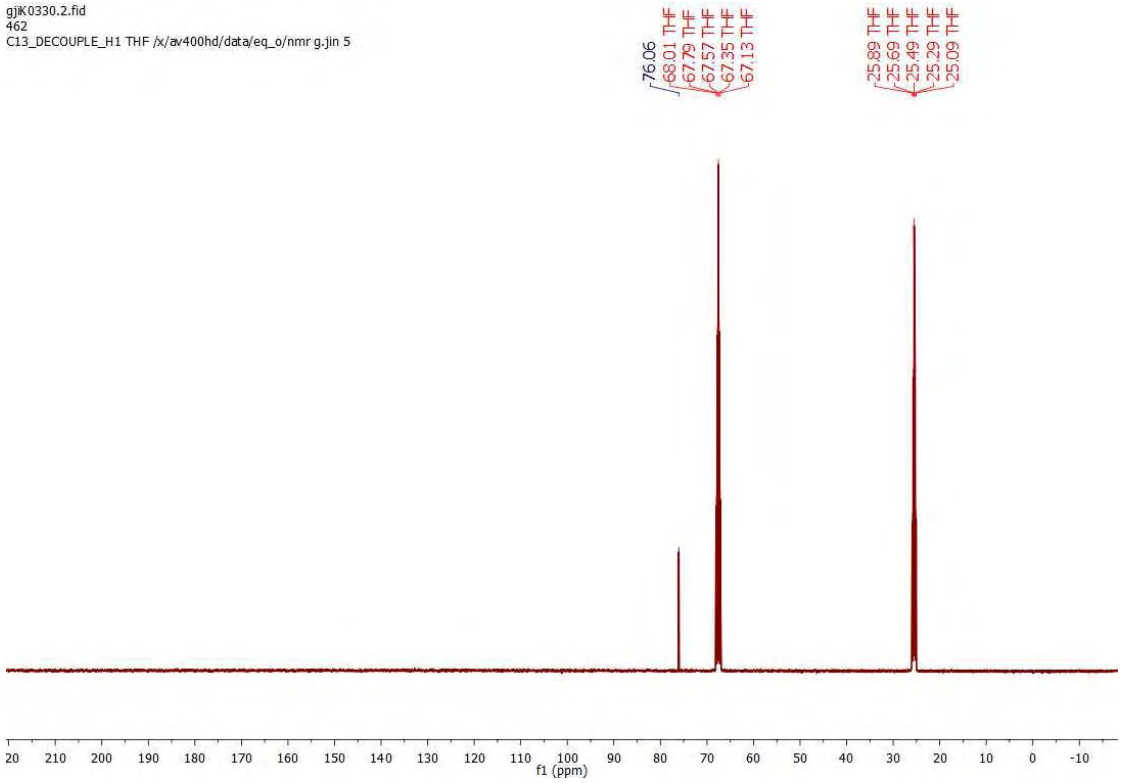

Figure 103. $^{13}C\{^{1}H\}$ NMR for isolated compound **145**(^{12}C) (THF-D_8)

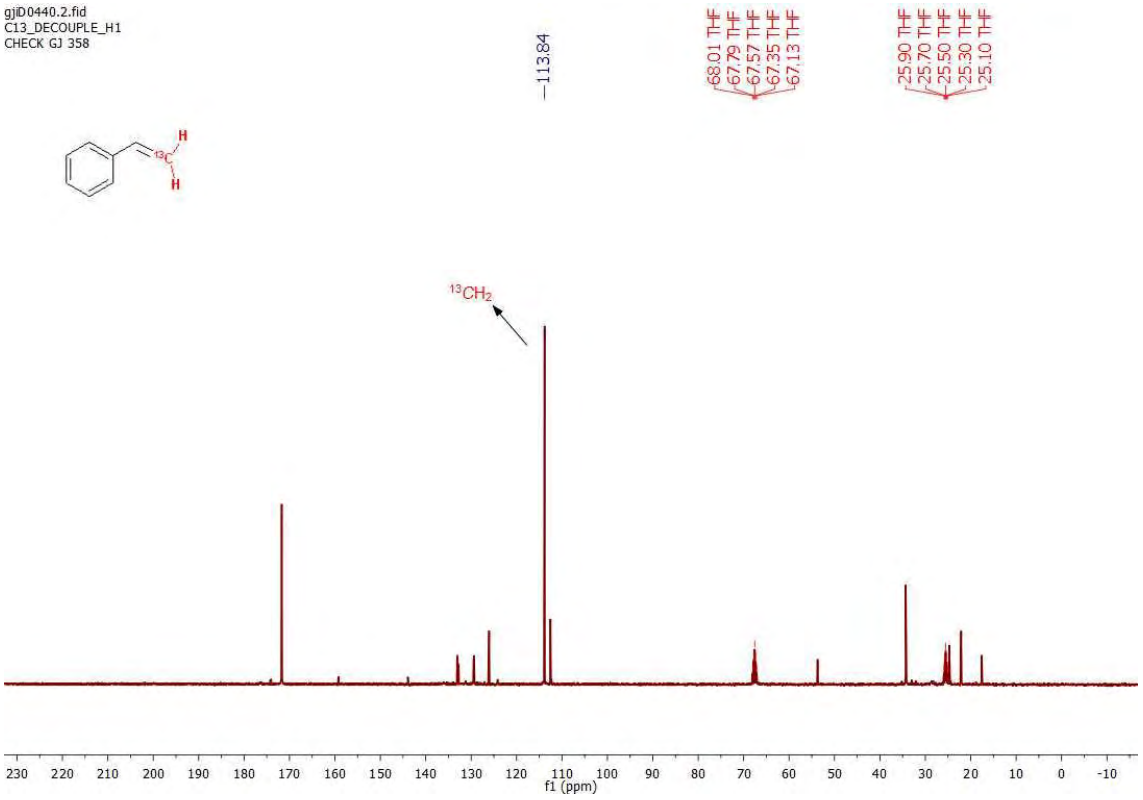

Figure 104. $^{13}C\{^{1}H\}$ NMR spectrum for in situ characterization of compound **148**(^{13}C)

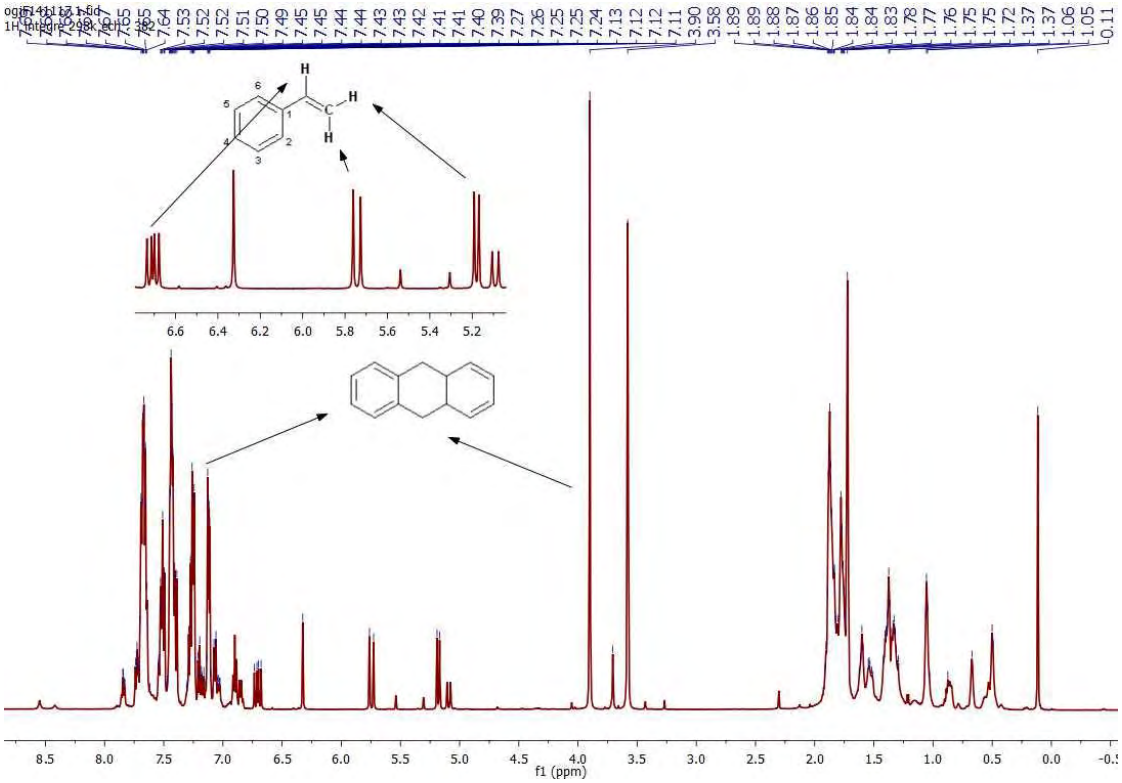

Figure 105. ^{1}H NMR spectrum for in situ characterization of compound **148**(^{12}C)

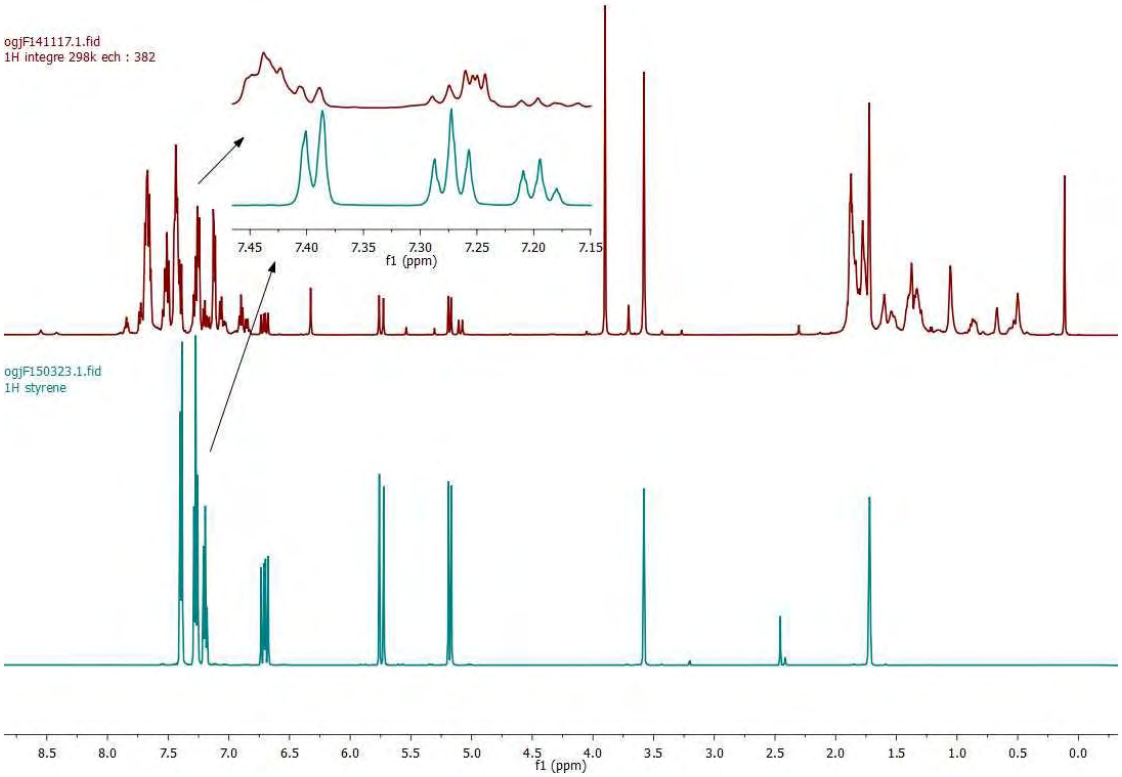

Figure 106. Stack 1H NMR spectra (top: 148(12C), below: styrene)

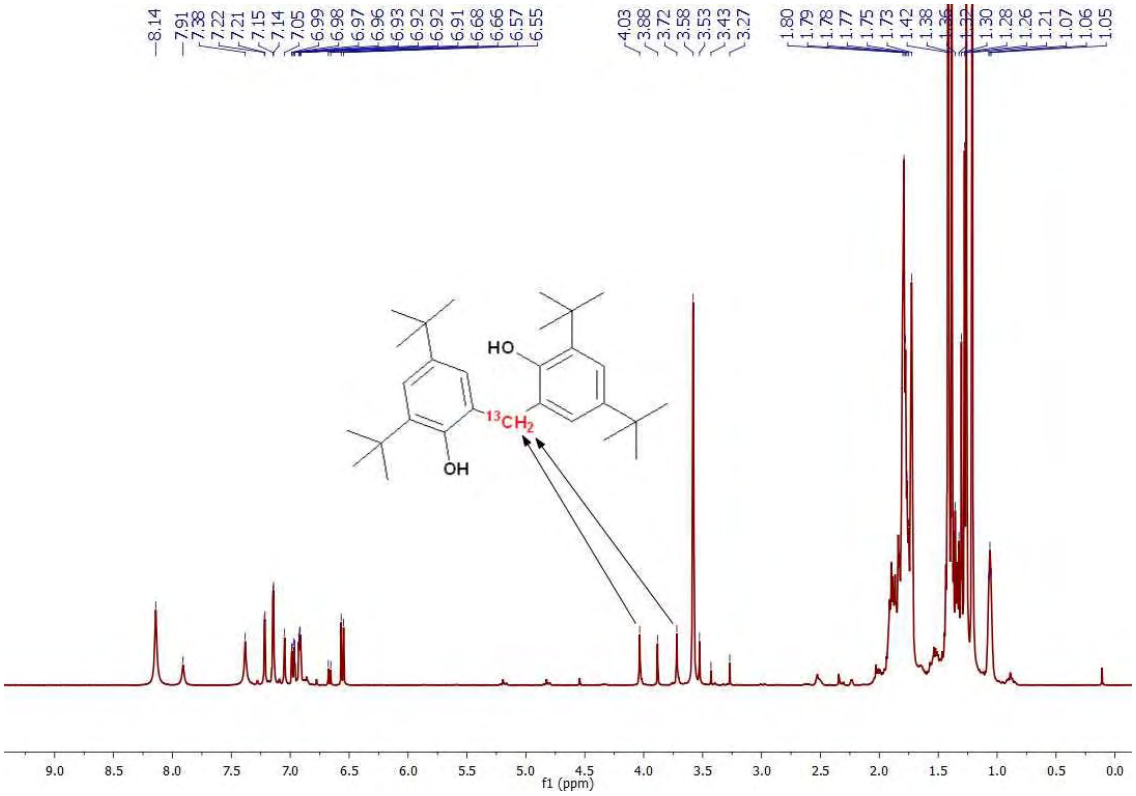

Figure 107. ^{1}H NMR spectrum for in situ characterization of compound **151**(^{13}C)

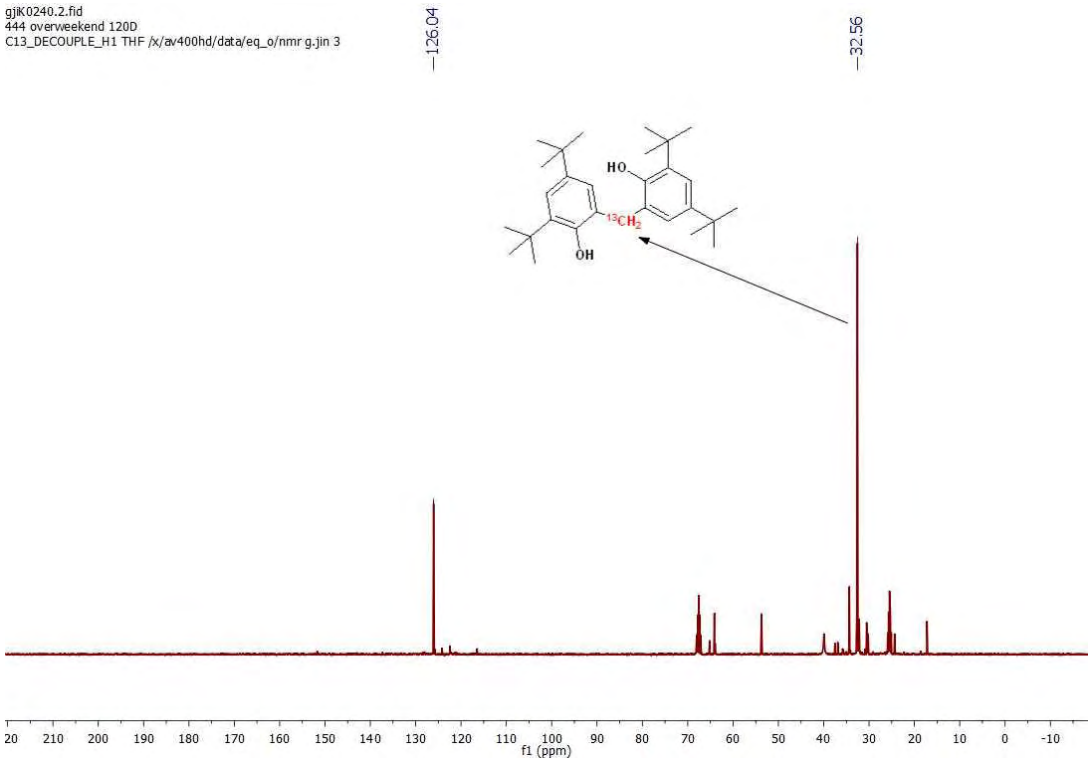

Figure 108. ^{13}C{^{1}H} NMR spectrum for in situ characterization of compound **151**(^{13}C)

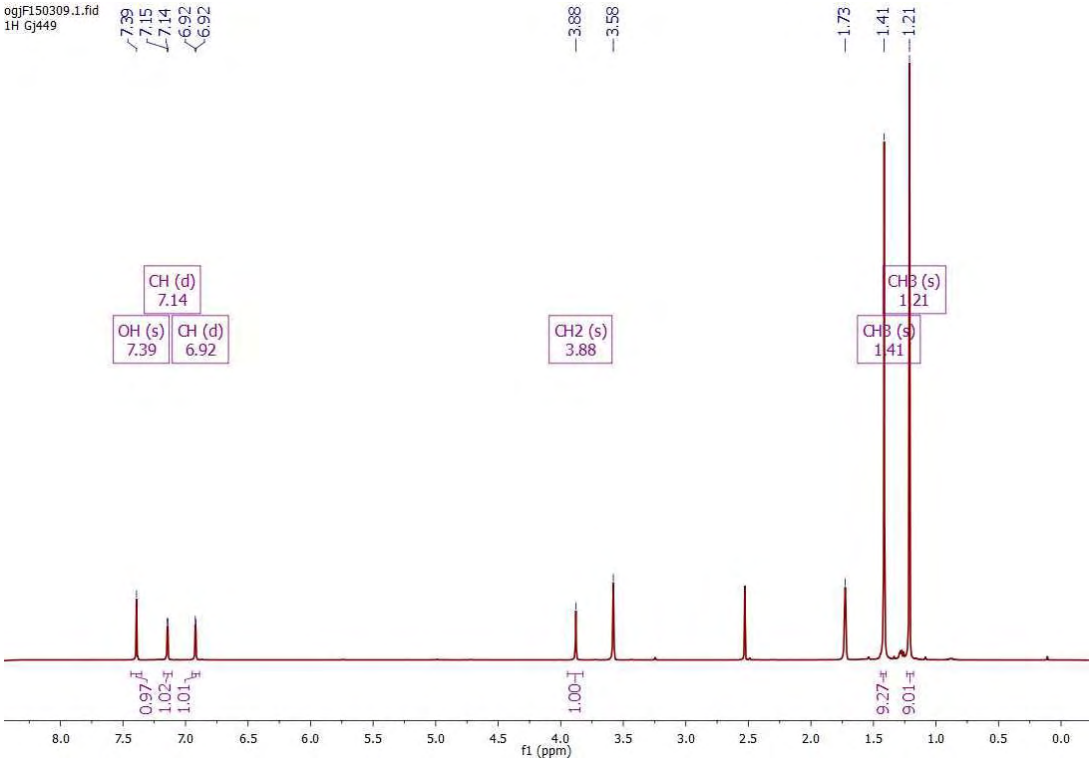

Figure 109. ^{1}H NMR spectrum of compound **151**(^{12}C)

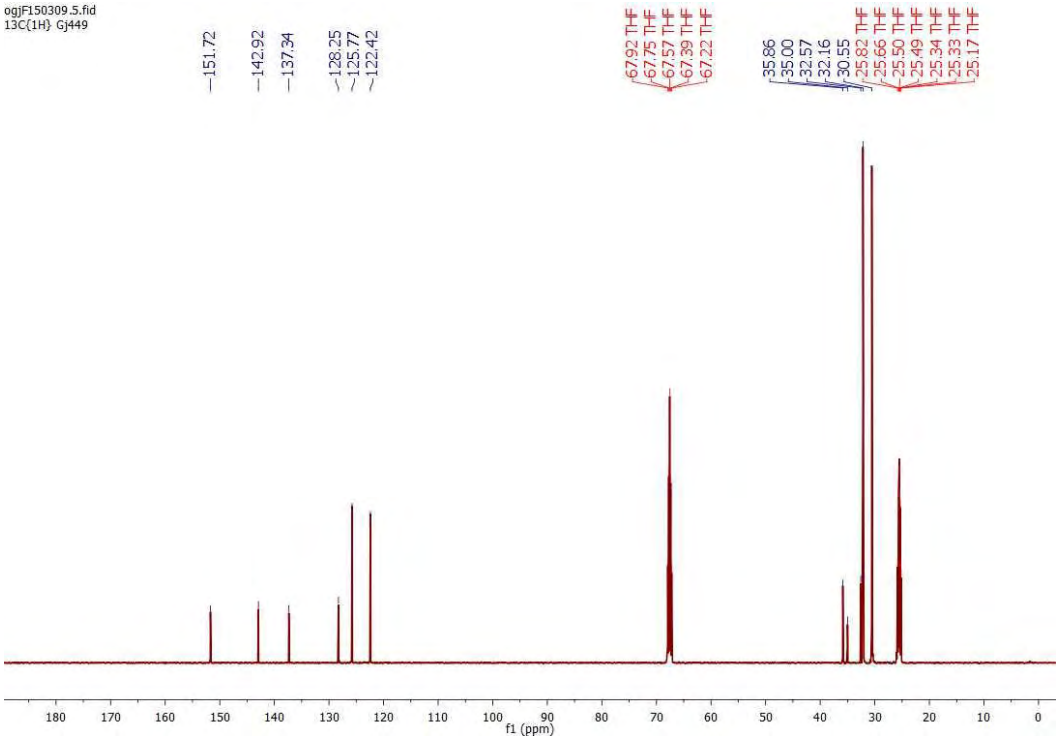

Figure 110. ^{13}C{^{1}H} NMR spectrum of compound **151**(^{12}C)

Appendix 2

Crystallographic data of [Fe(N(TMS)$_2$)$_2$($\kappa^{N,P}$-NPN)] 104

Complex	**104**
Empirical formula	$C_{30}H_{53}N_4PSi_4Fe$
Formula weight	668.94
Color, habit	yellow
Crystal size, mm^3	0.2 x 0.1 x 0.03
Crystal system	Monoclinic
Space group	*P* 1 2_1/*c* 1
a, Å	13.3755(3)
b, Å	13.1595(3)
c, Å	21.5380(5)
β, deg	99.8630(10)
V (Å^3)	3734.98(15)
Z	4
D_{calc} (g cm^{-3})	1.19
Absorption coeff., mm^{-1}	0.599
T (K)	100
F(000)	1432
Reflections collected / unique	60812 / 7632
R_{int}	0.0290
Final R indices[$I \geq 2\sigma(I)$]	*R1* = 0.0251, *wR2* = 0.0630
R indices (all data)	*R1* = 0.0314, *wR2* = 0.0670
Goodness-of-fit (GOF)	1.039
Largest difference peak/hole, e Å^{-3}	0.387 / -0.272

Crystallographic data of $[Fe(N(TMS)_2)(\mu\text{-}\kappa^{N,P}\text{:}\kappa^{N}\text{-NPN})]_2$ 105

Complex	**105**
Empirical formula	$C_{48}H_{68}N_6P_2Si_4Fe_2$
Formula weight	1015.08
Color, habit	black
Crystal size, mm^3	0.17 x 0.1 x 0.03
Crystal system	Monoclinic
Space group	$P\ 2_1/c$
a, Å	9.7251(6)
b, Å	17.9658(10)
c, Å	17.3879(11)
β, deg	104.907(2)
V ($Å^3$)	2935.8 (3)
Z	2
D_{calc} (g cm^{-3})	1.148
Absorption coeff., mm^{-1}	0.664
T (K)	100
F(000)	1072
Reflections collected / unique	40022 / 5993
R_{int}	0.0307
Final R indices[$I \geq 2\sigma(I)$]	*R1* = 0.0348, *wR2* = 0.0808
R indices (all data)	*R1* = 0.0405, *wR2* = 0.0832
Goodness-of-fit (GOF)	1.051
Largest difference peak/hole, e $Å^{-3}$	0.357 / -0.255

Crystallographic data of [Fe($\kappa^{N,P,N}$-NPN)$_2$] 106

Complex	**106**
Empirical formula	$C_{36}H_{32}N_4P_2Fe$
Formula weight	638.44
Color, habit	brown
Crystal size, mm^3	0.1 x 0.1 x 0.05
Crystal system	Monoclinic
Space group	*P* 2_1/c
a, Å	9.9744(7)
b, Å	19.7099(15)
c, Å	15.5352(12)
β, deg	93.424(2)
V (Å^3)	3048.7(4)
Z	4
D_{calc} (g cm^{-3})	1.391
Absorption coeff., mm^{-1}	0.633
T (K)	173
F(000)	1328
Reflections collected / unique	125687 / 6199
R_{int}	0.1467
Final R indices[$I \geq 2\sigma(I)$]	*R1* = 0.0463, *wR2* = 0.0942
R indices (all data)	*R1* = 0.0841, *wR2* = 0.1102
Goodness-of-fit (GOF)	1.027
Largest difference peak/hole, e Å^{-3}	1.224 / -0.502

Crystallographic data of [Ru(κ^P-NPN)($\kappa^{N,P}$-NPN)(COD)] 119

Complex	**119**
Empirical formula	$C_{44}H_{46}N_4P_2Ru$
Formula weight	793.86
Color, habit	Orange
Crystal size, mm^3	0.14 x 0.09 x 0.02
Crystal system	Triclinic
Space group	*P* -1
a, Å	9.6615(3)
b, Å	10.5430(3)
c, Å	19.0650(6)
α	76.6330(10)
β, deg	76.5710(10)
γ	83.6500(10)
V ($Å^3$)	1834.39(10)
Z	2
D_{calc} (g cm^{-3})	1.437
Absorption coeff., mm^{-1}	0.553
T (K)	100
F(000)	824
Reflections collected / unique	29290 / 7397
R_{int}	0.0158
Final R indices[$I \geq 2\sigma(I)$]	*R1* = 0.0202, *wR2* = 0.0482
R indices (all data)	*R1* = 0.0219, *wR2* = 0.0492
Goodness-of-fit (GOF)	1.042
Largest difference peak/hole, e $Å^{-3}$	0.499 / -0.341

Crystallographic data of [Ru($\kappa^{N,P,N}$-NPN)$_2$] 120

Complex	**120**
Empirical formula	$C_{36}H_{32}N_4P_2Ru$
Formula weight	683.67
Color, habit	Orange
Crystal size, mm^3	0.15 x 0.14 x 0.03
Crystal system	Monoclinic
Space group	$P\ 1\ 2_1/c\ 1$
a, Å	14.1039(6)
b, Å	12.4374(5)
c, Å	21.2928(9)
β, deg	107.437(2)
V (Å^3)	3563.5(3)
Z	4
D_{calc} (g cm^{-3})	1.274
Absorption coeff., mm^{-1}	0.558
T (K)	180
F(000)	1400
Reflections collected / unique	86092 / 7296
R_{int}	0.0228
Final R indices[$I \geq 2\sigma(I)$]	$R1$ = 0.0259, $wR2$ = 0.0630
R indices (all data)	$R1$ = 0.0274, $wR2$ = 0.0637
Goodness-of-fit (GOF)	1.130
Largest difference peak/hole, e Å^{-3}	0.415 / -0.561

Crystallographic data of [Ru(κ^P-NP)($\kappa^{N,P}$-NP)(COD)] 121

Complex	**121**
Empirical formula	$C_{44}H_{44}N_2P_2Ru$
Formula weight	763.82
Color, habit	Orange
Crystal size, mm^3	0.15 x 0.08 x 0.02
Crystal system	Monoclinic
Space group	*C 1 2/c 1*
a, Å	34.581(2)
b, Å	15.5161(10)
c, Å	19.9371(11)
β, deg	120.203(2)
V ($Å^3$)	9245.3(9)
Z	8
D_{calc} (g cm^{-3})	1.098
Absorption coeff., mm^{-1}	0.435
T (K)	180
F(000)	3168
Reflections collected / unique	43668 / 9380
R_{int}	0.0528
Final R indices[$I \geq 2\sigma(I)$]	*R1* = 0.0627, *wR2* = 0.1547
R indices (all data)	*R1* = 0.0760, *wR2* = 0.1605
Goodness-of-fit (GOF)	1.086
Largest difference peak/hole, e $Å^{-3}$	1.360 / -0.628

Crystallographic data of $[((C_8H_{14})(HOOC)B(OCH_2)PMe_2)_2C_2H_4]$ 130

Complex	**130**
Empirical formula	$C_{16}H_{28}BO_3P$
Formula weight	310.16
Color, habit	Colourless
Crystal size, mm^3	0.5 x 0.4 x 0.3
Crystal system	Monoclinic
Space group	*P* $2_1/n$
a, Å	7.0273(4)
b, Å	19.8843(11)
c, Å	12.3846(7)
β, deg	95.273(2)
V (Å^3)	1723.21(17)
Z	4
D_{calc} (g cm^{-3})	1.196
Absorption coeff., mm^{-1}	0.166
T (K)	173
F(000)	672
Reflections collected / unique	49429 / 3498
R_{int}	0.0293
Final R indices[$I \geq 2\sigma(I)$]	*R1* = 0.0353, *wR2* = 0.0898
R indices (all data)	*R1* = 0.0403, *wR2* = 0.0943
Goodness-of-fit (GOF)	1.121
Largest difference peak/hole, e Å^{-3}	0.427 / -0.194

Crystallographic data of [(OCO)N(Me)(C_2H_4)N(Me)(C_8H_{14})] 142

Complex	**142**
Empirical formula	$C_{13}H_{25}BN_2O_2$
Formula weight	252.16
Color, habit	Colourless
Crystal size, mm^3	0.2 x 0.04 x 0.04
Crystal system	Triclinic
Space group	*P -1*
a, Å	7.1569(8)
b, Å	9.0951(13)
c, Å	11.4551(13)
α	86.220(8)
β, deg	74.413(7)
γ	70.851(7)
V ($Å^3$)	678.28(15)
Z	2
D_{calc} (g cm^{-3})	1.235
Absorption coeff., mm^{-1}	0.081
T (K)	173
F(000)	276
Reflections collected / unique	36766 / 2747
R_{int}	0.1135
Final R indices[$I \geq 2\sigma(I)$]	*R1* = 0.0538, *wR2* = 0.1429
R indices (all data)	*R1* = 0.1036, *wR2* = 0.1729
Goodness-of-fit (GOF)	1.055
Largest difference peak/hole, e $Å^{-3}$	0.225 / -0.249

References

(1) Takashiro, M. Role of Precious Metal Catalysts. In *Role of Precious Metal Catalysts*; Yen-Hsun, S., Ed.; Noble Metals, 2012; pp 301–334.

(2) Dodson, J. R.; Parker, H. L.; García, A. M.; Hicken, A.; Asemave, K.; Farmer, T. J.; He, H.; Clark, J. H.; Hunt, A. J. Bio-Derived Materials as a Green Route for Precious & Critical Metal Recovery and Re-Use. *Green Chem.* **2015**, *17* (4), 1951–1965.

(3) Data Collection Is from Www.platinum.matthey.com and Www.indexmundi.com. Price of Precious Metals Starts from January, 2000, and Price of Iron Starts from March, 2000, While Ends in April, 2015 for Both.

(4) Enthaler, S.; Junge, K.; Beller, M. Sustainable Metal Catalysis with Iron: From Rust to a Rising Star? *Angew. Chem. Int. Ed.* **2008**, *47* (18), 3317–3321.

(5) Gaillard, S.; Renaud, J.-L. Iron-Catalyzed Hydrogenation, Hydride Transfer, and Hydrosilylation: An Alternative to Precious-Metal Complexes? *ChemSusChem* **2008**, *1* (6), 505–509.

(6) Bolm, C. A New Iron Age. *Nat. Chem.* **2009**, *1* (5), 420–420.

(7) Cammack, R. Bioinorganic Chemistry: Hydrogenase Sophistication. *Nature* **1999**, *397* (6716), 214–215.

(8) Turner, J. A. Sustainable Hydrogen Production. *Science* **2004**, *305* (5686), 972–974.

(9) Burgess, B. K.; Lowe, D. J. Mechanism of Molybdenum Nitrogenase. *Chem. Rev.* **1996**, *96* (7), 2983–3012.

(10) Eady, R. R. Structure−Function Relationships of Alternative Nitrogenases. *Chem. Rev.* **1996**, *96* (7), 3013–3030.

(11) Hoffman, B. M.; Lukoyanov, D.; Yang, Z.-Y.; Dean, D. R.; Seefeldt, L. C. Mechanism of Nitrogen Fixation by Nitrogenase: The Next Stage. *Chem. Rev.* **2014**, *114* (8), 4041–4062.

(12) Tondreau, A. M.; Atienza, C. C. H.; Weller, K. J.; Nye, S. A.; Lewis, K. M.; Delis, J. G. P.; Chirik, P. J. Iron Catalysts for Selective Anti-Markovnikov Alkene Hydrosilylation Using Tertiary Silanes. *Science* **2012**, *335* (6068), 567–570.

(13) Rodriguez, M. M.; Bill, E.; Brennessel, W. W.; Holland, P. L. N2 Reduction and Hydrogenation to Ammonia by a Molecular Iron-Potassium Complex. *Science* **2011**, *334* (6057), 780–783.

(14) Anderson, J. S.; Rittle, J.; Peters, J. C. Catalytic Conversion of Nitrogen to Ammonia by an Iron Model Complex. *Nature* **2013**, *501* (7465), 84–87.

(15) Hennessy, E. T.; Betley, T. A. Complex N-Heterocycle Synthesis via Iron-Catalyzed, Direct C–H Bond Amination. *Science* **2013**, *340* (6132), 591–595.

(16) Bolm, C.; Legros, J.; Le Paih, J.; Zani, L. Iron-Catalyzed Reactions in Organic Synthesis. *Chem. Rev.* **2004**, *104* (12), 6217–6254.

(17) Liu; Liang-Xian. Recent Uses of Iron Catalysts in Organic Reactions. *Curr. Org. Chem.* **2010**, *14* (11), 1099–1126.

(18) Sherry, B. D.; Fürstner, A. The Promise and Challenge of Iron-Catalyzed Cross Coupling. *Acc. Chem. Res.* **2008**, *41* (11), 1500–1511.

(19) Czaplik, W. M.; Mayer, M.; Cvengroš, J.; Wangelin, A. J. von. Coming of Age: Sustainable Iron-Catalyzed Cross-Coupling Reactions. *ChemSusChem* **2009**, *2* (5), 396–417.

(20) Junge, K.; Schröder, K.; Beller, M. Homogeneous Catalysis Using Iron Complexes: Recent Developments in Selective Reductions. *Chem. Commun.* **2011**, *47* (17), 4849–4859.

(21) Grützmacher, H. Cooperating Ligands in Catalysis. *Angew. Chem. Int. Ed.* **2008**, *47* (10), 1814–1818.

(22) Chirik, P. J.; Wieghardt, K. Radical Ligands Confer Nobility on Base-Metal Catalysts. *Science* **2010**, *327* (5967), 794–795.

(23) Kaim, W.; Schwederski, B. Non-Innocent Ligands in Bioinorganic chemistry—An Overview. *Coord. Chem. Rev.* **2010**, *254* (13–14), 1580–1588.

(24) van der Vlugt, J. I. Cooperative Catalysis with First-Row Late Transition Metals. *Eur. J. Inorg. Chem.* **2012**, *2012* (3), 363–375.

(25) Lyaskovskyy, V.; de Bruin, B. Redox Non-Innocent Ligands: Versatile New Tools to Control Catalytic Reactions. *ACS Catal.* **2012**, *2* (2), 270–279.

(26) Praneeth, V. K. K.; Ringenberg, M. R.; Ward, T. R. Redox-Active Ligands in Catalysis. *Angew. Chem. Int. Ed Engl.* **2012**, *51* (41), 10228–10234.

(27) Luca, O. R.; Crabtree, R. H. Redox-Active Ligands in Catalysis. *Chem. Soc. Rev.* **2013**, *42* (4), 1440–1459.

(28) Suarez, A. I. O.; Lyaskovskyy, V.; Reek, J. N. H.; van der Vlugt, J. I.; de Bruin, B. Complexes with Nitrogen-Centered Radical Ligands: Classification, Spectroscopic Features, Reactivity, and Catalytic Applications. *Angew. Chem. Int. Ed.* **2013**, *52* (48), 12510–12529.

(29) Blanchard, S.; Derat, E.; Desage-El Murr, M.; Fensterbank, L.; Malacria, M.; Mouriès-Mansuy, V. Non-Innocent Ligands: New Opportunities in Iron Catalysis. *Eur. J. Inorg. Chem.* **2012**, *2012* (3), 376–389.

(30) Zell, T.; Milko, P.; Fillman, K. L.; Diskin-Posner, Y.; Bendikov, T.; Iron, M. A.; Leitus, G.; Ben-David, Y.; Neidig, M. L.; Milstein, D. Iron Dicarbonyl Complexes Featuring Bipyridine-Based PNN Pincer Ligands with Short Interpyridine C□C Bond Lengths: Innocent or Non-Innocent Ligand? *Chem. – Eur. J.* **2014**, *20* (15), 4403–4413.

(31) Jørgensen, C. K. Differences between the Four Halide Ligands, and Discussion Remarks on Trigonal-Bipyramidal Complexes, on Oxidation States, and on Diagonal Elements of One-Electron Energy. *Coord. Chem. Rev.* **1966**, *1* (1–2), 164–178.

(32) Wanat, A.; Schneppensieper, T.; Stochel, G.; van Eldik, R.; Bill, E.; Wieghardt, K. Kinetics, Mechanism, and Spectroscopy of the Reversible Binding of Nitric Oxide to Aquated Iron(II). An Undergraduate Text Book Reaction Revisited. *Inorg. Chem.* **2002**, *41* (1), 4–10.

(33) Butin, K. P.; Beloglazkina, E. K.; Zyk, N. V. Metal Complexes with Non-Innocent Ligands. *Russ. Chem. Rev.* **2005**, *74* (6), 531.

(34) Sieh, D.; Schlimm, M.; Andernach, L.; Angersbach, F.; Nückel, S.; Schöffel, J.; Šušnjar, N.; Burger, P. Metal–Ligand Electron Transfer in 4d and 5d Group 9 Transition Metal Complexes with Pyridine, Diimine Ligands. *Eur. J. Inorg. Chem.* **2012**, *2012* (3), 444–462.

(35) Ray, K.; Petrenko, T.; Wieghardt, K.; Neese, F. Joint Spectroscopic and Theoretical Investigations of Transition Metal Complexes Involving Non-Innocent Ligands. *Dalton Trans.* **2007**, No. 16, 1552–1566.

(36) van der Vlugt, J. I.; Reek, J. N. H. Neutral Tridentate PNP Ligands and Their Hybrid Analogues: Versatile Non-Innocent Scaffolds for Homogeneous Catalysis. *Angew. Chem. Int. Ed Engl.* **2009**, *48* (47), 8832–8846.

(37) Ohkuma, T.; Ooka, H.; Ikariya, T.; Noyori, R. Preferential Hydrogenation of Aldehydes and Ketones. *J. Am. Chem. Soc.* **1995**, *117* (41), 10417–10418.

(38) Ohkuma, T.; Ooka, H.; Yamakawa, M.; Ikariya, T.; Noyori, R. Stereoselective Hydrogenation of Simple Ketones Catalyzed by Ruthenium(II) Complexes. *J. Org. Chem.* **1996**, *61* (15), 4872–4873.

(39) Ryoji, N.; Masatoshi, K.; Dai, I.; Takeshi, O. Asymmetric Hydrogenation via Architectural and Functional Molecular Engineering. *Pure Appl. Chem.* **2001**, *73* (2), 227–232.

(40) Gunanathan, C.; Milstein, D. Metal–Ligand Cooperation by Aromatization–Dearomatization: A New Paradigm in Bond Activation and “Green” Catalysis. *Acc. Chem. Res.* **2011**, *44* (8), 588–602.

(41) Kohl, S. W.; Weiner, L.; Schwartsburd, L.; Konstantinovski, L.; Shimon, L. J. W.; Ben-David, Y.; Iron, M. A.; Milstein, D. Consecutive Thermal H2 and Light-Induced O2 Evolution from Water Promoted by a Metal Complex. *Science* **2009**, *324* (5923), 74–77.

(42) Hindson, K.; de Bruin, B. Cooperative & Redox Non-Innocent Ligands in Directing Organometallic Reactivity (Eur. J. Inorg. Chem. 3/2012). *Eur. J. Inorg. Chem.* **2012**, *2012* (3), 340–342.

(43) Boyer, J. L.; Rochford, J.; Tsai, M.-K.; Muckerman, J. T.; Fujita, E. Ruthenium Complexes with Non-Innocent Ligands: Electron Distribution and Implications for Catalysis. *Coord. Chem. Rev.* **2010**, *254* (3–4), 309–330.

(44) Chirik, P. J. Preface: Forum on Redox-Active Ligands. *Inorg. Chem.* **2011**, *50* (20), 9737–9740.

(45) Bauer, G.; Kirchner, K. A. Well-Defined Bifunctional Iron Catalysts for the Hydrogenation of Ketones: Iron, the New Ruthenium. *Angew. Chem. Int. Ed.* **2011**, *50* (26), 5798–5800.

(46) Zanello, P.; Corsini, M. Homoleptic, Mononuclear Transition Metal Complexes of 1,2-Dioxolenes: Updating Their Electrochemical-to-Structural (X-Ray) Properties. *Coord. Chem. Rev.* **2006**, *250* (15–16), 2000–2022.

(47) Papavassiliou, G. C.; Anyfantis, G. C.; Mousdis, G. A. Neutral Metal 1,2-Dithiolenes: Preparations, Properties and Possible Applications of Unsymmetrical in Comparison to the Symmetrical. *Crystals* **2012**, *2* (3), 762–811.

(48) Broere, D. L. J.; de Bruin, B.; Reek, J. N. H.; Lutz, M.; Dechert, S.; van der Vlugt, J. I. Intramolecular Redox-Active Ligand-to-Substrate Single-Electron Transfer: Radical Reactivity with a Palladium(II) Complex. *J. Am. Chem. Soc.* **2014**, *136* (33), 11574–11577.

(49) Bowman, A. C.; England, J.; Sproules, S.; Weyhermüller, T.; Wieghardt, K. Electronic Structures of Homoleptic [Tris(2,2′-bipyridine)M]n Complexes of the Early Transition Metals (M = Sc, Y, Ti, Zr, Hf, V, Nb, Ta; N = 1+, 0, 1–, 2–, 3−): An Experimental and Density Functional Theoretical Study. *Inorg. Chem.* **2013**, *52* (4), 2242–2256.

(50) Gluyas, J. B. G.; Boden, A. J.; Eaves, S. G.; Yu, H.; Low, P. J. Long Range Charge Transfer in Trimetallic Mixed-Valence Iron Complexes Mediated by Redox Non-Innocent Cyanoacetylide Ligands. *Dalton Trans.* **2014**, *43* (17), 6291–6294.

(51) Bart, S. C.; Chłopek, K.; Bill, E.; Bouwkamp, M. W.; Lobkovsky, E.; Neese, F.; Wieghardt, K.; Chirik, P. J. Electronic Structure of Bis(imino)pyridine Iron Dichloride, Monochloride, and Neutral Ligand Complexes: A Combined Structural, Spectroscopic, and Computational Study. *J. Am. Chem. Soc.* **2006**, *128* (42), 13901–13912.

(52) Lu, C. C.; Bill, E.; Weyhermüller, T.; Bothe, E.; Wieghardt, K. Neutral Bis(α-Iminopyridine)metal Complexes of the First-Row Transition Ions (Cr, Mn, Fe, Co, Ni, Zn) and Their Monocationic Analogues: Mixed Valency Involving a Redox Noninnocent Ligand System. *J. Am. Chem. Soc.* **2008**, *130* (10), 3181–3197.

(53) Volpe, E. C.; Wolczanski, P. T.; Darmon, J. M.; Lobkovsky, E. B. Syntheses and Characterizations of α-Iminopyridine Compounds (alkylNCHpy)2Fe(L/Xn), and an Assessment of Redox Non-Innocence. *Polyhedron* **2013**, *52*, 406–415.

(54) Caulton, K. G. Systematics and Future Projections Concerning Redox-Noninnocent Amide/Imine Ligands. *Eur. J. Inorg. Chem.* **2012**, *2012* (3), 435–443.

(55) Russell, S. K.; Milsmann, C.; Lobkovsky, E.; Weyhermüller, T.; Chirik, P. J. Synthesis, Electronic Structure, and Catalytic Activity of Reduced Bis(aldimino)pyridine Iron Compounds: Experimental Evidence for Ligand Participation. *Inorg. Chem.* **2011**, *50* (7), 3159–3169.

(56) Small, B. L.; Brookhart, M.; Bennett, A. M. A. Highly Active Iron and Cobalt Catalysts for the Polymerization of Ethylene. *J. Am. Chem. Soc.* **1998**, *120* (16), 4049–4050.

(57) Small, B. L.; Brookhart, M. Iron-Based Catalysts with Exceptionally High Activities and Selectivities for Oligomerization of Ethylene to Linear α-Olefins. *J. Am. Chem. Soc.* **1998**, *120* (28), 7143–7144.

(58) Britovsek, G. J. P.; Gibson, V. C.; McTavish, S. J.; Solan, G. A.; White, A. J. P.; Williams, D. J.; Britovsek, G. J. P.; Kimberley, B. S.; Maddox, P. J. Novel Olefin Polymerization Catalysts Based on Iron and Cobalt. *Chem. Commun.* **1998**, No. 7, 849–850.

(59) Britovsek, G. J. P.; Bruce, M.; Gibson, V. C.; Kimberley, B. S.; Maddox, P. J.; Mastroianni, S.; McTavish, S. J.; Redshaw, C.; Solan, G. A.; Strömberg, S.; et al. Iron and Cobalt Ethylene Polymerization Catalysts Bearing 2,6-Bis(Imino)Pyridyl Ligands: Synthesis, Structures, and Polymerization Studies. *J. Am. Chem. Soc.* **1999**, *121* (38), 8728–8740.

(60) Bouwkamp, M. W.; Lobkovsky, E.; Chirik, P. J. Bis(imino)pyridine Iron(II) Alkyl Cations for Olefin Polymerization. *J. Am. Chem. Soc.* **2005**, *127* (27), 9660–9661.

(61) Tondreau, A. M.; Milsmann, C.; Patrick, A. D.; Hoyt, H. M.; Lobkovsky, E.; Wieghardt, K.; Chirik, P. J. Synthesis and Electronic Structure of Cationic, Neutral, and Anionic Bis(imino)pyridine Iron Alkyl Complexes: Evaluation of Redox Activity in Single-Component Ethylene Polymerization Catalysts. *J. Am. Chem. Soc.* **2010**, *132* (42), 15046–15059.

(62) Bouwkamp, M. W.; Bowman, A. C.; Lobkovsky, E.; Chirik, P. J. Iron-Catalyzed [2π + 2π] Cycloaddition of α,ω-Dienes: The Importance of Redox-Active Supporting Ligands. *J. Am. Chem. Soc.* **2006**, *128* (41), 13340–13341.

(63) Sylvester, K. T.; Chirik, P. J. Iron-Catalyzed, Hydrogen-Mediated Reductive Cyclization of 1,6-Enynes and Diynes: Evidence for Bis(imino)pyridine Ligand Participation. *J. Am. Chem. Soc.* **2009**, *131* (25), 8772–8774.

(64) Russell, S. K.; Lobkovsky, E.; Chirik, P. J. Iron-Catalyzed Intermolecular [2π + 2π] Cycloaddition. *J. Am. Chem. Soc.* **2011**, *133* (23), 8858–8861.

(65) Hoyt, J. M.; Sylvester, K. T.; Semproni, S. P.; Chirik, P. J. Synthesis and Electronic Structure of Bis(imino)pyridine Iron Metallacyclic Intermediates in Iron-Catalyzed Cyclization Reactions. *J. Am. Chem. Soc.* **2013**, *135* (12), 4862–4877.

(66) Moreau, B.; Wu, J. Y.; Ritter, T. Iron-Catalyzed 1,4-Addition of α-Olefins to Dienes. *Org. Lett.* **2009**, *11* (2), 337–339.

(67) Raynaud, J.; Wu, J. Y.; Ritter, T. Iron-Catalyzed Polymerization of Isoprene and Other 1,3-Dienes. *Angew. Chem. Int. Ed.* **2012**, *51* (47), 11805–11808.

(68) Bart, S. C.; Lobkovsky, E.; Chirik, P. J. Preparation and Molecular and Electronic Structures of Iron(0) Dinitrogen and Silane Complexes and Their Application to Catalytic Hydrogenation and Hydrosilation. *J. Am. Chem. Soc.* **2004**, *126* (42), 13794–13807.

(69) Trovitch, R. J.; Lobkovsky, E.; Bill, E.; Chirik, P. J. Functional Group Tolerance and Substrate Scope in Bis(imino)pyridine Iron Catalyzed Alkene Hydrogenation. *Organometallics* **2008**, *27* (7), 1470–1478.

(70) Tondreau, A. M.; Lobkovsky, E.; Chirik, P. J. Bis(imino)pyridine Iron Complexes for Aldehyde and Ketone Hydrosilylation. *Org. Lett.* **2008**, *10* (13), 2789–2792.

(71) Tondreau, A. M.; Darmon, J. M.; Wile, B. M.; Floyd, S. K.; Lobkovsky, E.; Chirik, P. J. Enantiopure Pyridine Bis(oxazoline) “Pybox” and Bis(oxazoline) “Box” Iron Dialkyl

Complexes: Comparison to Bis(imino)pyridine Compounds and Application to Catalytic Hydrosilylation of Ketones. *Organometallics* **2009**, *28* (13), 3928–3940.

(72) Salanouve, E.; Bouzemame, G.; Blanchard, S.; Derat, E.; Desage-El Murr, M.; Fensterbank, L. Tandem C□H Activation/Arylation Catalyzed by Low-Valent Iron Complexes with Bisiminopyridine Ligands. *Chem. – Eur. J.* **2014**, *20* (16), 4754–4761.

(73) Russell, S. K.; Darmon, J. M.; Lobkovsky, E.; Chirik, P. J. Synthesis of Aryl-Substituted Bis(imino)pyridine Iron Dinitrogen Complexes. *Inorg. Chem.* **2010**, *49* (6), 2782–2792.

(74) Wu, J. Y.; Moreau, B.; Ritter, T. Iron-Catalyzed 1,4-Hydroboration of 1,3-Dienes. *J. Am. Chem. Soc.* **2009**, *131* (36), 12915–12917.

(75) Wu, J. Y.; Stanzl, B. N.; Ritter, T. A Strategy for the Synthesis of Well-Defined Iron Catalysts and Application to Regioselective Diene Hydrosilylation. *J. Am. Chem. Soc.* **2010**, *132* (38), 13214–13216.

(76) Umehara, K.; Kuwata, S.; Ikariya, T. N–N Bond Cleavage of Hydrazines with a Multiproton-Responsive Pincer-Type Iron Complex. *J. Am. Chem. Soc.* **2013**, *135* (18), 6754–6757.

(77) Kim, Y.-E.; Oh, S.; Kim, S.; Kim, O.; Kim, J.; Han, S. W.; Lee, Y. Phosphinite-Ni(0) Mediated Formation of a Phosphide-Ni(II)-OCOOMe Species via Uncommon Metal–Ligand Cooperation. *J. Am. Chem. Soc.* **2015**, *137* (13), 4280–4283.

(78) Poverenov, E.; Milstein, D. Noninnocent Behavior of PCP and PCN Pincer Ligands of Late Metal Complexes. In *Organometallic Pincer Chemistry*; van Koten, G., Milstein, D., Eds.; Topics in Organometallic Chemistry; Springer Berlin Heidelberg, 2013; pp 21–47.

(79) Srimani, D.; Diskin-Posner, Y.; Ben-David, Y.; Milstein, D. Iron Pincer Complex Catalyzed, Environmentally Benign, E-Selective Semi-Hydrogenation of Alkynes. *Angew. Chem. Int. Ed.* **2013**, *52* (52), 14131–14134.

(80) Sues, P. E.; Demmans, K. Z.; Morris, R. H. Rational Development of Iron Catalysts for Asymmetric Transfer Hydrogenation. *Dalton Trans.* **2014**, *43* (21), 7650–7667.

(81) Sui-Seng, C.; Freutel, F.; Lough, A. J.; Morris, R. H. Highly Efficient Catalyst Systems Using Iron Complexes with a Tetradentate PNNP Ligand for the Asymmetric Hydrogenation of Polar Bonds. *Angew. Chem. Int. Ed.* **2008**, *47* (5), 940–943.

(82) Sui-Seng, C.; Haque, F. N.; Hadzovic, A.; Pütz, A.-M.; Reuss, V.; Meyer, N.; Lough, A. J.; Zimmer-De Iuliis, M.; Morris, R. H. Synthesis and Characterization of Iron(II) Complexes with Tetradentate Diiminodiphosphine or Diaminodiphosphine Ligands as Precatalysts for the Hydrogenation of Acetophenone. *Inorg. Chem.* **2009**, *48* (2), 735–743.

(83) Zuo, W.; Tauer, S.; Prokopchuk, D. E.; Morris, R. H. Iron Catalysts Containing Amine(imine)diphosphine P-NH-N-P Ligands Catalyze Both the Asymmetric Hydrogenation and Asymmetric Transfer Hydrogenation of Ketones. *Organometallics* **2014**, *33* (20), 5791–5801.

(84) Meyer, N.; Lough, A. J.; Morris, R. H. Iron(II) Complexes for the Efficient Catalytic Asymmetric Transfer Hydrogenation of Ketones. *Chem. – Eur. J.* **2009**, *15* (22), 5605–5610.

(85) Mikhailine, A.; Lough, A. J.; Morris, R. H. Efficient Asymmetric Transfer Hydrogenation of Ketones Catalyzed by an Iron Complex Containing a P−N−N−P Tetradentate Ligand Formed by Template Synthesis. *J. Am. Chem. Soc.* **2009**, *131* (4), 1394–1395.

(86) Mikhailine, A. A.; Morris, R. H. Effect of the Structure of the Diamine Backbone of P−N−N−P Ligands in Iron(II) Complexes on Catalytic Activity in the Transfer Hydrogenation of Acetophenone. *Inorg. Chem.* **2010**, *49* (23), 11039–11044.

(87) Lagaditis, P. O.; Lough, A. J.; Morris, R. H. Low-Valent Ene–Amido Iron Complexes for the Asymmetric Transfer Hydrogenation of Acetophenone without Base. *J. Am. Chem. Soc.* **2011**, *133* (25), 9662–9665.

(88) Zuo, W.; Lough, A. J.; Li, Y. F.; Morris, R. H. Amine(imine)diphosphine Iron Catalysts for Asymmetric Transfer Hydrogenation of Ketones and Imines. *Science* **2013**, *342* (6162), 1080–1083.

(89) Mikhailine, A. A.; Maishan, M. I.; Morris, R. H. Asymmetric Transfer Hydrogenation of Ketimines Using Well-Defined Iron(II)-Based Precatalysts Containing a PNNP Ligand. *Org. Lett.* **2012**, *14* (17), 4638–4641.

(90) Lagaditis, P. O.; Lough, A. J.; Morris, R. H. Iron Complexes for the Catalytic Transfer Hydrogenation of Acetophenone: Steric and Electronic Effects Imposed by Alkyl Substituents at Phosphorus. *Inorg. Chem.* **2010**, *49* (21), 10057–10066.

(91) Prokopchuk, D. E.; Sonnenberg, J. F.; Meyer, N.; Zimmer-De Iuliis, M.; Lough, A. J.; Morris, R. H. Spectroscopic and DFT Study of Ferraaziridine Complexes Formed in the Transfer Hydrogenation of Acetophenone Catalyzed Using Trans-[Fe(CO)(NCMe)(PPh2C6H4CH═NCH2−)2-κ4P,N,N,P](BF4)2. *Organometallics* **2012**, *31* (8), 3056–3064.

(92) Prokopchuk, D. E.; Morris, R. H. Inner-Sphere Activation, Outer-Sphere Catalysis: Theoretical Study on the Mechanism of Transfer Hydrogenation of Ketones Using Iron(II) PNNP Eneamido Complexes. *Organometallics* **2012**, *31* (21), 7375–7385.

(93) Mikhailine, A. A.; Maishan, M. I.; Lough, A. J.; Morris, R. H. The Mechanism of Efficient Asymmetric Transfer Hydrogenation of Acetophenone Using an Iron(II) Complex Containing an (S,S)-Ph2PCH2CH═NCHPhCHPhN═CHCH2PPh2 Ligand: Partial Ligand Reduction Is the Key. *J. Am. Chem. Soc.* **2012**, *134* (29), 12266–12280.

(94) Casey, C. P.; Guan, H. An Efficient and Chemoselective Iron Catalyst for the Hydrogenation of Ketones. *J. Am. Chem. Soc.* **2007**, *129* (18), 5816–5817.

(95) Casey, C. P.; Guan, H. Cyclopentadienone Iron Alcohol Complexes: Synthesis, Reactivity, and Implications for the Mechanism of Iron-Catalyzed Hydrogenation of Aldehydes. *J. Am. Chem. Soc.* **2009**, *131* (7), 2499–2507.

(96) Pagnoux-Ozherelyeva, A.; Pannetier, N.; Mbaye, M. D.; Gaillard, S.; Renaud, J.-L. Knölker's Iron Complex: An Efficient In Situ Generated Catalyst for Reductive Amination of Alkyl

Aldehydes and Amines. *Angew. Chem. Int. Ed.* **2012**, *51* (20), 4976–4980.

(97) Zhu, F.; Zhu-Ge, L.; Yang, G.; Zhou, S. Iron-Catalyzed Hydrogenation of Bicarbonates and Carbon Dioxide to Formates. *ChemSusChem* **2015**, *8* (4), 609–612.

(98) Moulin, S.; Dentel, H.; Pagnoux-Ozherelyeva, A.; Gaillard, S.; Poater, A.; Cavallo, L.; Lohier, J.-F.; Renaud, J.-L. Bifunctional (Cyclopentadienone)Iron–Tricarbonyl Complexes: Synthesis, Computational Studies and Application in Reductive Amination. *Chem. – Eur. J.* **2013**, *19* (52), 17881–17890.

(99) Gunanathan, C.; Ben-David, Y.; Milstein, D. Direct Synthesis of Amides from Alcohols and Amines with Liberation of H2. *Science* **2007**, *317* (5839), 790–792.

(100) Zell, T.; Langer, R.; Iron, M. A.; Konstantinovski, L.; Shimon, L. J. W.; Diskin-Posner, Y.; Leitus, G.; Balaraman, E.; Ben-David, Y.; Milstein, D. Synthesis, Structures, and Dearomatization by Deprotonation of Iron Complexes Featuring Bipyridine-Based PNN Pincer Ligands. *Inorg. Chem.* **2013**, *52* (16), 9636–9649.

(101) Butschke, B.; Fillman, K. L.; Bendikov, T.; Shimon, L. J. W.; Diskin-Posner, Y.; Leitus, G.; Gorelsky, S. I.; Neidig, M. L.; Milstein, D. How Innocent Are Potentially Redox Non-Innocent Ligands? Electronic Structure and Metal Oxidation States in Iron-PNN Complexes as a Representative Case Study. *Inorg. Chem.* **2015**.

(102) Zhang, J.; Gandelman, M.; Herrman, D.; Leitus, G.; Shimon, L. J. W.; Ben-David, Y.; Milstein, D. Iron(II) Complexes Based on Electron-Rich, Bulky PNN- and PNP-Type Ligands. *Inorganica Chim. Acta* **2006**, *359* (6), 1955–1960.

(103) Trovitch, R. J.; Lobkovsky, E.; Chirik, P. J. Bis(diisopropylphosphino)pyridine Iron Dicarbonyl, Dihydride, and Silyl Hydride Complexes. *Inorg. Chem.* **2006**, *45* (18), 7252–7260.

(104) Pelczar, E. M.; Emge, T. J.; Krogh-Jespersen, K.; Goldman, A. S. Unusual Structural and Spectroscopic Features of Some PNP-Pincer Complexes of Iron. *Organometallics* **2008**, *27* (22), 5759–5767.

(105) Langer, R.; Diskin-Posner, Y.; Leitus, G.; Shimon, L. J. W.; Ben-David, Y.; Milstein, D. Low-Pressure Hydrogenation of Carbon Dioxide Catalyzed by an Iron Pincer Complex Exhibiting Noble Metal Activity. *Angew. Chem. Int. Ed.* **2011**, *50* (42), 9948–9952.

(106) Langer, R.; Leitus, G.; Ben-David, Y.; Milstein, D. Efficient Hydrogenation of Ketones Catalyzed by an Iron Pincer Complex. *Angew. Chem. Int. Ed.* **2011**, *50* (9), 2120–2124.

(107) Langer, R.; Iron, M. A.; Konstantinovski, L.; Diskin-Posner, Y.; Leitus, G.; Ben-David, Y.; Milstein, D. Iron Borohydride Pincer Complexes for the Efficient Hydrogenation of Ketones under Mild, Base-Free Conditions: Synthesis and Mechanistic Insight. *Chem. – Eur. J.* **2012**, *18* (23), 7196–7209.

(108) Zell, T.; Ben-David, Y.; Milstein, D. Unprecedented Iron-Catalyzed Ester Hydrogenation. Mild, Selective, and Efficient Hydrogenation of Trifluoroacetic Esters to Alcohols Catalyzed by an Iron Pincer Complex. *Angew. Chem. Int. Ed.* **2014**, *53* (18), 4685–4689.

(109) Zell, T.; Ben-David, Y.; Milstein, D. Highly Efficient, General Hydrogenation of Aldehydes Catalyzed by PNP Iron Pincer Complexes. *Catal. Sci. Technol.* **2015**, *5* (2), 822–826.

(110) Milko, P.; Iron, M. A. On the Innocence of Bipyridine Ligands: How Well Do DFT Functionals Fare for These Challenging Spin Systems? *J. Chem. Theory Comput.* **2014**, *10* (1), 220–235.

(111) Zhang, L.; Peng, D.; Leng, X.; Huang, Z. Iron-Catalyzed, Atom-Economical, Chemo- and Regioselective Alkene Hydroboration with Pinacolborane. *Angew. Chem. Int. Ed.* **2013**, *52* (13), 3676–3680.

(112) Aresta, M.; Dibenedetto, A.; Angelini, A. Catalysis for the Valorization of Exhaust Carbon: From CO2 to Chemicals, Materials, and Fuels. Technological Use of CO2. *Chem. Rev.* **2014**, *114* (3), 1709–1742.

(113) Aresta, M.; Dibenedetto, A. Utilisation of CO2 as a Chemical Feedstock: Opportunities and Challenges. *Dalton Trans.* **2007**, No. 28, 2975–2992.

(114) Riduan, S. N.; Zhang, Y. Recent Developments in Carbon Dioxide Utilization under Mild Conditions. *Dalton Trans.* **2010**, *39* (14), 3347–3357.

(115) Omae, I. Recent Developments in Carbon Dioxide Utilization for the Production of Organic Chemicals. *Coord. Chem. Rev.* **2012**, *256* (13–14), 1384–1405.

(116) Huang, C.-H.; Tan, C.-S. A Review: CO2 Utilization. *Aerosol Air Qual. Res.* **2014**, *14*, 480–499.

(117) Cokoja, M.; Bruckmeier, C.; Rieger, B.; Herrmann, W. A.; Kühn, F. E. Transformation of Carbon Dioxide with Homogeneous Transition-Metal Catalysts: A Molecular Solution to a Global Challenge? *Angew. Chem. Int. Ed.* **2011**, *50* (37), 8510–8537.

(118) Pinaka, A.; Vougioukalakis, G. C. Using Sustainable Metals to Carry out “green” Transformations: Fe- and Cu-Catalyzed CO2 Monetization. *Coord. Chem. Rev.* **2015**, *288*, 69–97.

(119) Komiya, S.; Akita, M.; Kasuga, N.; Hirano, M.; Fukuoka, A. Synthesis, Structure and Reactions of a Carbon Dioxide Complex of iron(0) Containing 1,2-Bis(diethylphosphino)ethane Ligands. *J. Chem. Soc. Chem. Commun.* **1994**, No. 9, 1115–1116.

(120) Huang, K.; Sun, C.-L.; Shi, Z.-J. Transition-Metal-Catalyzed C–C Bond Formation through the Fixation of Carbon Dioxide. *Chem. Soc. Rev.* **2011**, *40* (5), 2435–2452.

(121) Palmer, D. A.; Van Eldik, R. The Chemistry of Metal Carbonato and Carbon Dioxide Complexes. *Chem. Rev.* **1983**, *83* (6), 651–731.

(122) Behr, A. Carbon Dioxide as an Alternative C1 Synthetic Unit: Activation by Transition-Metal Complexes. *Angew. Chem. Int. Ed. Engl.* **1988**, *27* (5), 661–678.

(123) Leitner, W. The Coordination Chemistry of Carbon Dioxide and Its Relevance for Catalysis: A Critical Survey. *Coord. Chem. Rev.* **1996**, *153*, 257–284.

(124) Mascetti, J.; Galan, F.; Pàpai, I. Carbon Dioxide Interaction with Metal Atoms: Matrix Isolation Spectroscopic Study and DFT Calculations. *Coord. Chem. Rev.* **1999**, *190–192*, 557–576.

(125) Gibson, D. H. Carbon Dioxide Coordination Chemistry: Metal Complexes and Surface-Bound Species. What Relationships? *Coord. Chem. Rev.* **1999**, *185–186*, 335–355.

(126) Hans Heinz, K. Trimethylphosphine Iron Complexes. *Inorg Synth* **1980**, *20*, 69.

(127) Rosi, M.; Sgamellotti, A.; Tarantelli, F.; Floriani, C. Study of the Interaction between iron(0) and Carbon Dioxide, Carbonyl Sulphide and Carbon Disulphide: “ab Initio” Calculations on the Model Compounds Fe(CO)2(PH3)2(η2-CO2), Fe(CO)2(PH3)2(η2-COS), Fe(CO)2(PH3)2(η2-CS2), and Fe(PH3)4(η2-CO2). *J. Organomet. Chem.* **1987**, *332* (1–2), 153–164.

(128) Gibson, D. H.; Ye, M.; Richardson, J. F. Synthesis and Characterization of .mu.2-.eta.2- and .mu.2-.eta.3-CO2 Complexes of Iron and Rhenium. *J. Am. Chem. Soc.* **1992**, *114* (24), 9716–9717.

(129) Gibson, D. H.; Ye, M.; Richardson, J. F.; Mashuta, M. S. Synthesis, Characterization, and Reactions of Carbon Dioxide Bridged Iron-Rhenium Complexes. *Organometallics* **1994**, *13* (11), 4559–4569.

(130) Hirano, M.; Akita, M.; Tani, K.; Kumagai, K.; Kasuga, N. C.; Fukuoka, A.; Komiya, S. Activation of Coordinated Carbon Dioxide in Fe(CO2)(depe)2 by Group 14 Electrophiles. *Organometallics* **1997**, *16* (19), 4206–4213.

(131) Gibson, D. H. The Organometallic Chemistry of Carbon Dioxide. *Chem. Rev.* **1996**, *96* (6), 2063–2096.

(132) Jessop, P. G.; Ikariya, T.; Noyori, R. Homogeneous Hydrogenation of Carbon Dioxide. *Chem. Rev.* **1995**, *95* (2), 259–272.

(133) Leitner, W. Carbon Dioxide as a Raw Material: The Synthesis of Formic Acid and Its Derivatives from CO2. *Angew. Chem. Int. Ed. Engl.* **1995**, *34* (20), 2207–2221.

(134) Correa, A.; Martín, R. Metal-Catalyzed Carboxylation of Organometallic Reagents with Carbon Dioxide. *Angew. Chem. Int. Ed.* **2009**, *48* (34), 6201–6204.

(135) Darensbourg, D. J.; Grotsch, G. Stereochemical Studies of the Carbon Dioxide Insertion Reactions into the Tungsten-Alkyl Bond. *J. Am. Chem. Soc.* **1985**, *107* (25), 7473–7476.

(136) Allen, O. R.; Dalgarno, S. J.; Field, L. D.; Jensen, P.; Willis, A. C. Insertion of CO2 into the Ru−C Bonds of Cis- and Trans-Ru(dmpe)2Me2 (dmpe = Me2PCH2CH2PMe2). *Organometallics* **2009**, *28* (8), 2385–2390.

(137) Johnson, M. T.; Johansson, R.; Kondrashov, M. V.; Steyl, G.; Ahlquist, M. S. G.; Roodt, A.; Wendt, O. F. Mechanisms of the CO2 Insertion into (PCP) Palladium Allyl and Methyl σ-

Bonds. A Kinetic and Computational Study. *Organometallics* **2010**, *29* (16), 3521–3529.

(138) Ostapowicz, T. G.; Hölscher, M.; Leitner, W. CO2 Insertion into Metal–Carbon Bonds: A Computational Study of RhI Pincer Complexes. *Chem. – Eur. J.* **2011**, *17* (37), 10329–10338.

(139) Schmeier, T. J.; Hazari, N.; Incarvito, C. D.; Raskatov, J. A. Exploring the Reactions of CO2 with PCP Supported Nickel Complexes. *Chem. Commun.* **2011**, *47* (6), 1824–1826.

(140) Fan, T.; Chen, X.; Lin, Z. Theoretical Studies of Reactions of Carbon Dioxide Mediated and Catalysed by Transition Metal Complexes. *Chem. Commun.* **2012**, *48* (88), 10808–10828.

(141) Field, L. D.; Lawrenz, E. T.; Shaw, W. J.; Turner, P. Insertion of CO2, CS2, and COS into Iron(II)−Hydride Bonds. *Inorg. Chem.* **2000**, *39* (25), 5632–5638.

(142) Allen, O. R.; Dalgarno, S. J.; Field, L. D.; Jensen, P.; Turnbull, A. J.; Willis, A. C. Addition of CO2 to Alkyl Iron Complexes, Fe(PP)2Me2. *Organometallics* **2008**, *27* (9), 2092–2098.

(143) Lu, C. C.; Saouma, C. T.; Day, M. W.; Peters, J. C. Fe(I)-Mediated Reductive Cleavage and Coupling of CO2: An FeII(μ-O,μ-CO)FeII Core. *J. Am. Chem. Soc.* **2007**, *129* (1), 4–5.

(144) Saouma, C. T.; Lu, C. C.; Day, M. W.; Peters, J. C. CO2 Reduction by Fe(I): Solvent Control of C–O Cleavage versus C–C Coupling. *Chem. Sci.* **2013**, *4* (10), 4042–4051.

(145) Sadique, A. R.; Brennessel, W. W.; Holland, P. L. A Diketiminate-Bound Diiron Complex with a Bridging Carbonate Ligand. *Acta Crystallogr. Sect. C* **2009**, *65* (5), m174–m176.

(146) Sadique, A. R.; Brennessel, W. W.; Holland, P. L. Reduction of CO2 to CO Using Low-Coordinate Iron: Formation of a Four-Coordinate Iron Dicarbonyl Complex and a Bridging Carbonate Complex. *Inorg. Chem.* **2008**, *47* (3), 784–786.

(147) Eckert, N. A.; Stoian, S.; Smith, J. M.; Bominaar, E. L.; Münck, E.; Holland, P. L. Synthesis, Structure, and Spectroscopy of an Oxodiiron(II) Complex. *J. Am. Chem. Soc.* **2005**, *127* (26), 9344–9345.

(148) Allen, O. R.; Dalgarno, S. J.; Field, L. D. Reductive Disproportionation of Carbon Dioxide at an Iron(II) Center. *Organometallics* **2008**, *27* (14), 3328–3330.

(149) Karsch, H. H. Funktionelle Trimethylphosphinderivate, III. Ambivalentes Verhalten von Tetrakis(trimethylphosphin)eisen : Reaktion Mit CO2. *Chem. Ber.* **1977**, *110* (6), 2213–2221.

(150) Herskovitz, T.; Guggenberger, L. J. Carbon Dioxide Coordination Chemistry. The Structure and Some Chemistry of the Novel Carbon Dioxide Addition Product Chlorobis(carbon Dioxide)tris(trimethylphosphine)iridium. *J. Am. Chem. Soc.* **1976**, *98* (6), 1615–1616.

(151) Field, L. D.; Shaw, W. J.; Turner, P. Functionalisation of Carbon Dioxide by an iron(II) Complex. *Chem. Commun.* **2002**, No. 1, 46–47.

(152) Hoberg, H.; Jenni, K.; Krüger, C.; Raabe, E. CC-Coupling of CO2 and Butadiene on Iron(0) Complexes—A Novel Route to α,ω-Dicarboxylic Acids. *Angew. Chem. Int. Ed. Engl.* **1986**, *25* (9), 810–811.

(153) Hoberg, H.; Jenni, K.; Angermund, K.; Krüger, C. CC-Linkages of Ethene with CO2 on an Iron(0) Complex—Synthesis and Crystal Structure Analysis of [(PEt3)2Fe(C2H4)2]. *Angew. Chem. Int. Ed. Engl.* **1987**, *26* (2), 153–155.

(154) Hoberg, H.; Jenni, K. CC-Kupplungen von CO2 Mit 1,3-Dienen an eisen(0)-Komplexen; Carboxylatbildung Und Folgereaktionen. *J. Organomet. Chem.* **1987**, *322* (2), 193–201.

(155) Inoue, S.; Koinuma, H.; Tsuruta, T. Copolymerization of Carbon Dioxide and Epoxide. *J. Polym. Sci. [B]* **1969**, *7* (4), 287–292.

(156) Darensbourg, D. J.; Holtcamp, M. W. Catalysts for the Reactions of Epoxides and Carbon Dioxide. *Coord. Chem. Rev.* **1996**, *153*, 155–174.

(157) Sakakura, T.; Choi, J.-C.; Yasuda, H. Transformation of Carbon Dioxide. *Chem. Rev.* **2007**, *107* (6), 2365–2387.

(158) Kisch, H.; Millini, R.; Wang, I.-J. Bifunktionelle Katalysatoren Zur Synthese Cyclischer Carbonate Aus Oxiranen Und Kohlendioxid. *Chem. Ber.* **1986**, *119* (3), 1090–1094.

(159) Buchard, A.; Kember, M. R.; Sandeman, K. G.; Williams, C. K. A Bimetallic iron(III) Catalyst for CO2/epoxide Coupling. *Chem. Commun.* **2011**, *47* (1), 212–214.

(160) Nakano, K.; Kobayashi, K.; Ohkawara, T.; Imoto, H.; Nozaki, K. Copolymerization of Epoxides with Carbon Dioxide Catalyzed by Iron–Corrole Complexes: Synthesis of a Crystalline Copolymer. *J. Am. Chem. Soc.* **2013**, *135* (23), 8456–8459.

(161) Dengler, J. E.; Lehenmeier, M. W.; Klaus, S.; Anderson, C. E.; Herdtweck, E.; Rieger, B. A One-Component Iron Catalyst for Cyclic Propylene Carbonate Synthesis. *Eur. J. Inorg. Chem.* **2011**, *2011* (3), 336–343.

(162) Sheng, X.; Qiao, L.; Qin, Y.; Wang, X.; Wang, F. Highly Efficient and Quantitative Synthesis of a Cyclic Carbonate by Iron Complex Catalysts. *Polyhedron* **2014**, *74*, 129–133.

(163) Fuchs, M. A.; Zevaco, T. A.; Ember, E.; Walter, O.; Held, I.; Dinjus, E.; Döring, M. Synthesis of Cyclic Carbonates from Epoxides and Carbon Dioxide Catalyzed by an Easy-to-Handle Ionic iron(III) Complex. *Dalton Trans.* **2013**, *42* (15), 5322–5329.

(164) Adolph, M.; Zevaco, T. A.; Altesleben, C.; Walter, O.; Dinjus, E. New Cobalt, Iron and Chromium Catalysts Based on Easy-to-Handle N4-Chelating Ligands for the Coupling Reaction of Epoxides with CO2. *Dalton Trans.* **2014**, *43* (8), 3285–3296.

(165) Whiteoak, C. J.; Martin, E.; Belmonte, M. M.; Benet-Buchholz, J.; Kleij, A. W. An Efficient Iron Catalyst for the Synthesis of Five- and Six-Membered Organic Carbonates under Mild Conditions. *Adv. Synth. Catal.* **2012**, *354* (2-3), 469–476.

(166) Whiteoak, C. J.; Gjoka, B.; Martin, E.; Belmonte, M. M.; Escudero-Adán, E. C.; Zonta, C.; Licini, G.; Kleij, A. W. Reactivity Control in Iron(III) Amino Triphenolate Complexes: Comparison of Monomeric and Dimeric Complexes. *Inorg. Chem.* **2012**, *51* (20), 10639–10649.

(167) Taherimehr, M.; Amsyar, S. M. Al-; Whiteoak, C. J.; Kleij, A. W.; Pescarmona, P. P. High Activity and Switchable Selectivity in the Synthesis of Cyclic and Polymeric Cyclohexene Carbonates with Iron Amino Triphenolate Catalysts. *Green Chem.* **2013**, *15* (11), 3083–3090.

(168) Sunjuk, M.; Abu-Surrah, A. S.; Ramahi, E. Al-; Qaroush, A. K.; Saleh, A. Selective Coupling of Carbon Dioxide and Epoxystyrene via Salicylaldimine-, Thiophenaldimine-, and Quinolinaldimine-iron(II), iron(III), chromium(III), and cobalt(III)/Lewis Base Catalysts. *Transit. Met. Chem.* **2013**, *38* (3), 253–257.

(169) Buonerba, A.; Nisi, A. D.; Grassi, A.; Milione, S.; Capacchione, C.; Vagin, S.; Rieger, B. Novel iron(III) Catalyst for the Efficient and Selective Coupling of Carbon Dioxide and Epoxides to Form Cyclic Carbonates. *Catal. Sci. Technol.* **2015**, *5* (1), 118–123.

(170) Inoue, Y.; Sasaki, Y.; Hashimoto, H. Synthesis of Formates from Alcohols, Carbon Dioxide, and Hydrogen Catalysed by a Combination of Group VIII Transition-Metal Complexes and Tertiary Amines. *J. Chem. Soc. Chem. Commun.* **1975**, No. 17, 718–719.

(171) Evans, G. O.; Newell, C. J. Conversion of CO2, H2, and Alcohols into Formate Esters Using Anionic Iron Carbonyl Hydrides. *Inorganica Chim. Acta* **1978**, *31*, L387–L389.

(172) Tai, C.-C.; Chang, T.; Roller, B.; Jessop, P. G. High-Pressure Combinatorial Screening of Homogeneous Catalysts: Hydrogenation of Carbon Dioxide. *Inorg. Chem.* **2003**, *42* (23), 7340–7341.

(173) Federsel, C.; Boddien, A.; Jackstell, R.; Jennerjahn, R.; Dyson, P. J.; Scopelliti, R.; Laurenczy, G.; Beller, M. A Well-Defined Iron Catalyst for the Reduction of Bicarbonates and Carbon Dioxide to Formates, Alkyl Formates, and Formamides. *Angew. Chem. Int. Ed.* **2010**, *49* (50), 9777–9780.

(174) Ziebart, C.; Federsel, C.; Anbarasan, P.; Jackstell, R.; Baumann, W.; Spannenberg, A.; Beller, M. Well-Defined Iron Catalyst for Improved Hydrogenation of Carbon Dioxide and Bicarbonate. *J. Am. Chem. Soc.* **2012**, *134* (51), 20701–20704.

(175) Elek, J.; Nádasdi, L.; Papp, G.; Laurenczy, G.; Joó, F. Homogeneous Hydrogenation of Carbon Dioxide and Bicarbonate in Aqueous Solution Catalyzed by Water-Soluble ruthenium(II) Phosphine Complexes. *Appl. Catal. Gen.* **2003**, *255* (1), 59–67.

(176) Himeda, Y.; Onozawa-Komatsuzaki, N.; Sugihara, H.; Arakawa, H.; Kasuga, K. Half-Sandwich Complexes with 4,7-Dihydroxy-1,10-Phenanthroline: Water-Soluble, Highly Efficient Catalysts for Hydrogenation of Bicarbonate Attributable to the Generation of an Oxyanion on the Catalyst Ligand. *Organometallics* **2004**, *23* (7), 1480–1483.

(177) Himeda, Y.; Onozawa-Komatsuzaki, N.; Sugihara, H.; Kasuga, K. Simultaneous Tuning of Activity and Water Solubility of Complex Catalysts by Acid−Base Equilibrium of Ligands for Conversion of Carbon Dioxide. *Organometallics* **2007**, *26* (3), 702–712.

(178) Schmeier, T. J.; Dobereiner, G. E.; Crabtree, R. H.; Hazari, N. Secondary Coordination Sphere Interactions Facilitate the Insertion Step in an Iridium(III) CO2 Reduction Catalyst. *J. Am. Chem. Soc.* **2011**, *133* (24), 9274–9277.

(179) Yang, X. Hydrogenation of Carbon Dioxide Catalyzed by PNP Pincer Iridium, Iron, and Cobalt Complexes: A Computational Design of Base Metal Catalysts. *ACS Catal.* **2011**, *1* (8), 849–854.

(180) Knölker, H.-J.; Baum, E.; Goesmann, H.; Klauss, R. Demetalation of Tricarbonyl(cyclopentadienone)iron Complexes Initiated by a Ligand Exchange Reaction with NaOH—X-Ray Analysis of a Complex with Nearly Square-Planar Coordinated Sodium. *Angew. Chem. Int. Ed.* **1999**, *38* (13-14), 2064–2066.

(181) Greenhalgh, M. D.; Thomas, S. P. Iron-Catalyzed, Highly Regioselective Synthesis of α-Aryl Carboxylic Acids from Styrene Derivatives and CO2. *J. Am. Chem. Soc.* **2012**, *134* (29), 11900–11903.

(182) Kim, T.-J.; Kwon, K.-H.; Kwon, S.-C.; Baeg, J.-O.; Shim, S.-C.; Lee, D.-H. Iron Complexes of 1,1'-Bis(diphenylphosphino)ferrocene (BPPF) as Efficient Catalysts in the Synthesis of Carbamates. X-Ray Crystal Structure of (BPPF)Fe(CO)3. *J. Organomet. Chem.* **1990**, *389* (2), 205–217.

(183) Frogneux, X.; Jacquet, O.; Cantat, T. Iron-Catalyzed Hydrosilylation of CO2: CO2 Conversion to Formamides and Methylamines. *Catal. Sci. Technol.* **2014**, *4* (6), 1529–1533.

(184) Kermagoret, A.; Tomicki, F.; Braunstein, P. Nickel and Iron Complexes with N,P,N-Type Ligands: Synthesis, Structure and Catalytic Oligomerization of Ethylene. *Dalton Trans.* **2008**, No. 22, 2945–2955.

(185) Objartel, I.; Pott, N. A.; John, M.; Stalke, D. Coordination Site Selective Janus Head Ligands. *Organometallics* **2010**, *29* (21), 5670–5675.

(186) Hung-Low, F.; Renz, A.; Klausmeyer, K. K. The Variable Binding Modes of Phenylbis(pyrid-2-Ylmethyl)phosphane and Bis(pyrid-2-Ylmethyl) Phenylphosphonite with AgI and CuI. *Eur. J. Inorg. Chem.* **2009**, *2009* (20), 2994–3002.

(187) Liu, S.; Peloso, R.; Braunstein, P. Palladium and Iridium Complexes with a N,P,N-Bis(pyridine)phenylphosphine Ligand. *Dalton Trans.* **2010**, *39* (10), 2563–2572.

(188) Liu, S.; Peloso, R.; Pattacini, R.; Braunstein, P. Electrophilic Activation and the Formation of an Unusual Tl+/Cr3+ Tetranuclear Ion-Complex Adduct. *Dalton Trans.* **2010**, *39* (34), 7881–7883.

(189) Liu, S.; Pattacini, R.; Braunstein, P. Reactions between an Ethylene Oligomerization Chromium(III) Precatalyst and Aluminum-Based Activators: Alkyl and Cationic Complexes with a Tridentate NPN Ligand. *Organometallics* **2011**, *30* (13), 3549–3558.

(190) Murso, A.; Stalke, D. Electronic Response of a (P,N)-Based Ligand on Metal coordinationElectronic Supplementary Information (ESI) Available: Full Crystallographic Data of 1?3. See http://www.rsc.org/suppdata/dt/b4/b405680a/. *Dalton Trans.* **2004**, No. 16, 2563.

(191) Ott, H.; Pieper, U.; Leusser, D.; Flierler, U.; Henn, J.; Stalke, D. Carbanion or Amide? First Charge Density Study of Parent 2-Picolyllithium. *Angew. Chem. Int. Ed.* **2009**, *48* (16),

2978–2982.

(192) Andersen, R. A.; Faegri, K.; Green, J. C.; Haaland, A.; Lappert, M. F.; Leung, W. P.; Rypdal, K. Synthesis of bis[bis(trimethylsilyl)amido]iron(II). Structure and Bonding in M[N(SiMe3)2]2 (M = Manganese, Iron, Cobalt): Two-Coordinate Transition-Metal Amides. *Inorg. Chem.* **1988**, *27* (10), 1782–1786.

(193) Olmstead, M. M.; Power, P. P.; Shoner, S. C. Three-Coordinate Iron Complexes: X-Ray Structural Characterization of the Iron Amide-Bridged Dimers [Fe(NR2)2]2 (R = SiMe3, C6H5) and the Adduct Fe[N(SiMe3)2]2(THF) and Determination of the Association Energy of the Monomer Fe{N(SiMe3)2}2 in Solution. *Inorg. Chem.* **1991**, *30* (11), 2547–2551.

(194) Hung-Low, F.; Klausmeyer, K. K. Silver Coordination Complexes of 2-(diphenylphosphinomethyl)pyridine and Their Bipyridine Derivatives. *Inorganica Chim. Acta* **2008**, *361* (5), 1298–1310.

(195) Braunstein, P.; Fryzuk, M. D.; Naud, F.; Rettig, S. J. Catalytic Transfer Hydrogenation of Ketones by the Use of Ruthenium Complexes Incorporating the New Tridentate Ligand, bis(2-Oxazolin-2-Ylmethyl)phenylphosphine. *J. Chem. Soc. Dalton Trans.* **1999**, No. 4, 589–594.

(196) Evans, D. F. 400. The Determination of the Paramagnetic Susceptibility of Substances in Solution by Nuclear Magnetic Resonance. *J. Chem. Soc. Resumed* **1959**, No. 0, 2003–2005.

(197) Ernest M., S. Utilizing the Evans Method with a Superconducting NMR Spectrometer in the Undergraduate Laboratory. *J. Chem. Educ. 69* (1), 62.

(198) Cracknell, J. A.; Vincent, K. A.; Armstrong, F. A. Enzymes as Working or Inspirational Electrocatalysts for Fuel Cells and Electrolysis. *Chem. Rev.* **2008**, *108* (7), 2439–2461.

(199) Tard, C.; Pickett, C. J. Structural and Functional Analogues of the Active Sites of the [Fe]-, [NiFe]-, and [FeFe]-Hydrogenases. *Chem. Rev.* **2009**, *109* (6), 2245–2274.

(200) Berggren, G.; Adamska, A.; Lambertz, C.; Simmons, T. R.; Esselborn, J.; Atta, M.; Gambarelli, S.; Mouesca, J.-M.; Reijerse, E.; Lubitz, W.; et al. Biomimetic Assembly and Activation of [FeFe]-Hydrogenases. *Nature* **2013**, *499* (7456), 66–69.

(201) Gütlich, P.; Goodwin, H. A. Spin Crossover—An Overall Perspective. In *Spin Crossover in Transition Metal Compounds I*; Gütlich, P., Goodwin, H. A., Eds.; Topics in Current Chemistry; Springer Berlin Heidelberg, 2004; pp 1–47.

(202) Rao, C. N. R.; Seikh, M. M.; Narayana, C. Spin-State Transition in LaCoO3 and Related Materials. In *Spin Crossover in Transition Metal Compounds II*; Topics in Current Chemistry; Springer Berlin Heidelberg, 2004; pp 1–21.

(203) Brady, C.; McGarvey, J. J.; McCusker, J. K.; Toftlund, H.; Hendrickson, D. N. Time-Resolved Relaxation Studies of Spin Crossover Systems in Solution. In *Spin Crossover in Transition Metal Compounds III*; Topics in Current Chemistry; Springer Berlin Heidelberg, 2004; pp 1–22.

(204) Zhang, J.; Leitus, G.; Ben-David, Y.; Milstein, D. Efficient Homogeneous Catalytic Hydrogenation of Esters to Alcohols. *Angew. Chem. Int. Ed.* **2006**, *45* (7), 1113–1115.

(205) Vogt, M.; Gargir, M.; Iron, M. A.; Diskin-Posner, Y.; Ben-David, Y.; Milstein, D. A New Mode of Activation of CO2 by Metal–Ligand Cooperation with Reversible C□C and M□O Bond Formation at Ambient Temperature. *Chem. – Eur. J.* **2012**, *18* (30), 9194–9197.

(206) Vogt, M.; Rivada-Wheelaghan, O.; Iron, M. A.; Leitus, G.; Diskin-Posner, Y.; Shimon, L. J. W.; Ben-David, Y.; Milstein, D. Anionic Nickel(II) Complexes with Doubly Deprotonated PNP Pincer-Type Ligands and Their Reactivity toward CO2. *Organometallics* **2012**, *32* (1), 300–308.

(207) Sita, L. R.; Babcock, J. R.; Xi, R. Facile Metathetical Exchange between Carbon Dioxide and the Divalent Group 14 Bisamides M[N(SiMe3)2]2 (M = Ge and Sn). *J. Am. Chem. Soc.* **1996**, *118* (44), 10912–10913.

(208) Dickie, D. A.; Parkes, M. V.; Kemp, R. A. Insertion of Carbon Dioxide into Main-Group Complexes: Formation of the [N(CO2)3]3− Ligand. *Angew. Chem. Int. Ed.* **2008**, *47* (51), 9955–9957.

(209) Sattler, W.; Parkin, G. Synthesis, Structure, and Reactivity of a Mononuclear Organozinc Hydride Complex: Facile Insertion of CO2 into a Zn–H Bond and CO2-Promoted Displacement of Siloxide Ligands. *J. Am. Chem. Soc.* **2011**, *133* (25), 9708–9711.

(210) Whited, M. T.; Kosanovich, A. J.; Janzen, D. E. Synthesis and Reactivity of Three-Coordinate (dtbpe)Rh Silylamides: CO2 Bond Cleavage by a Rhodium(I) Disilylamide. *Organometallics* **2014**, *33* (6), 1416–1422.

(211) Phull, H.; Alberti, D.; Korobkov, I.; Gambarotta, S.; Budzelaar, P. H. M. Fixation of CO2 by Magnesium Cations: A Reinterpretation. *Angew. Chem. Int. Ed.* **2006**, *45* (32), 5331–5334.

(212) Plietker, B. *Iron Catalysis: Fundamentals and Applications*, Bernd Plietker.; Springer Heidelberg Dordrecht London New York, 2011; Vol. 33.

(213) Ni, C.; Ellis, B. D.; Stich, T. A.; Fettinger, J. C.; Long, G. J.; Britt, R. D.; Power, P. P. Reduction of Terphenyl iron(II) or cobalt(II) Halides in the Presence of Trimethylphosphine: An Unusual Triple Dehydrogenation of an Alkyl Group. *Dalton Trans.* **2009**, No. 27, 5401–5405.

(214) Blom, B.; Tan, G.; Enthaler, S.; Inoue, S.; Epping, J. D.; Driess, M. Bis-N-Heterocyclic Carbene (NHC) Stabilized η6-Arene Iron(0) Complexes: Synthesis, Structure, Reactivity, and Catalytic Activity. *J. Am. Chem. Soc.* **2013**, *135* (48), 18108–18120.

(215) Lin, C.-Y.; Fettinger, J. C.; Grandjean, F.; Long, G. J.; Power, P. P. Synthesis, Structure, and Magnetic and Electrochemical Properties of Quasi-Linear and Linear Iron(I), Cobalt(I), and Nickel(I) Amido Complexes. *Inorg. Chem.* **2014**, *53* (17), 9400–9406.

(216) Mo, Z.; Ouyang, Z.; Wang, L.; Fillman, K. L.; Neidig, M. L.; Deng, L. Two- and Three-Coordinate Formal iron(I) Compounds Featuring Monodentate Aminocarbene Ligands. *Org. Chem.* **2014**, *1* (9), 1040–1044.

(217) Werncke, C. G.; Bunting, P. C.; Duhayon, C.; Long, J. R.; Bontemps, S.; Sabo-Etienne, S. Two-Coordinate Iron(I) Complex [Fe{N(SiMe3)2}2]−: Synthesis, Properties, and Redox Activity. *Angew. Chem.* **2015**, *127* (1), 247–250.

(218) Shintani, R.; Nozaki, K. Copper-Catalyzed Hydroboration of Carbon Dioxide. *Organometallics* **2013**, *32* (8), 2459–2462.

(219) Bontemps, S.; Vendier, L.; Sabo-Etienne, S. Borane-Mediated Carbon Dioxide Reduction at Ruthenium: Formation of C1 and C2 Compounds. *Angew. Chem. Int. Ed.* **2012**, *51* (7), 1671–1674.

(220) Bontemps, S.; Sabo-Etienne, S. Trapping Formaldehyde in the Homogeneous Catalytic Reduction of Carbon Dioxide. *Angew. Chem. Int. Ed.* **2013**, *52* (39), 10253–10255.

(221) Bontemps, S.; Vendier, L.; Sabo-Etienne, S. Ruthenium-Catalyzed Reduction of Carbon Dioxide to Formaldehyde. *J. Am. Chem. Soc.* **2014**, *136* (11), 4419–4425.

(222) Benson, E. E.; Kubiak, C. P.; Sathrum, A. J.; Smieja, J. M. Electrocatalytic and Homogeneous Approaches to Conversion of CO2 to Liquid Fuels. *Chem. Soc. Rev.* **2008**, *38* (1), 89–99.

(223) Costentin, C.; Robert, M.; Savéant, J.-M. Catalysis of the Electrochemical Reduction of Carbon Dioxide. *Chem. Soc. Rev.* **2013**, *42* (6), 2423–2436.

(224) Appel, A. M.; Bercaw, J. E.; Bocarsly, A. B.; Dobbek, H.; DuBois, D. L.; Dupuis, M.; Ferry, J. G.; Fujita, E.; Hille, R.; Kenis, P. J. A.; et al. Frontiers, Opportunities, and Challenges in Biochemical and Chemical Catalysis of CO2 Fixation. *Chem. Rev.* **2013**, *113* (8), 6621–6658.

(225) Fontaine, F.-G.; Courtemanche, M.-A.; Légaré, M.-A. Transition-Metal-Free Catalytic Reduction of Carbon Dioxide. *Chem. – Eur. J.* **2014**, *20* (11), 2990–2996.

(226) Yang, Z.-Z.; He, L.-N.; Gao, J.; Liu, A.-H.; Yu, B. Carbon Dioxide Utilization with C–N Bond Formation: Carbon Dioxide Capture and Subsequent Conversion. *Energy Environ. Sci.* **2012**, *5* (5), 6602–6639.

(227) Centi, G.; Perathoner, S. Opportunities and Prospects in the Chemical Recycling of Carbon Dioxide to Fuels. *Catal. Today* **2009**, *148* (3–4), 191–205.

(228) Peters, M.; Köhler, B.; Kuckshinrichs, W.; Leitner, W.; Markewitz, P.; Müller, T. E. Chemical Technologies for Exploiting and Recycling Carbon Dioxide into the Value Chain. *ChemSusChem* **2011**, *4* (9), 1216–1240.

(229) Quadrelli, E. A.; Centi, G.; Duplan, J.-L.; Perathoner, S. Carbon Dioxide Recycling: Emerging Large-Scale Technologies with Industrial Potential. *ChemSusChem* **2011**, *4* (9), 1194–1215.

(230) Jessop, P. G.; Joó, F.; Tai, C.-C. Recent Advances in the Homogeneous Hydrogenation of Carbon Dioxide. *Coord. Chem. Rev.* **2004**, *248* (21–24), 2425–2442.

(231) Wang, W.; Wang, S.; Ma, X.; Gong, J. Recent Advances in Catalytic Hydrogenation of Carbon Dioxide. *Chem. Soc. Rev.* **2011**, *40* (7), 3703–3727.

(232) Fernández-Alvarez, F. J.; Aitani, A. M.; Oro, L. A. Homogeneous Catalytic Reduction of CO2 with Hydrosilanes. *Catal. Sci. Technol.* **2014**, *4* (3), 611–624.

(233) Chong, C. C.; Kinjo, R. Catalytic Hydroboration of Carbonyl Derivatives, Imines, and Carbon Dioxide. *ACS Catal.* **2015**, *5* (6), 3238–3259.

(234) Bontemps, S. Boron-Mediated Activation of Carbon Dioxide. *Coord. Chem. Rev.*

(235) Dorner, R. W.; Hardy, D. R.; Williams, F. W.; Willauer, H. D. Heterogeneous Catalytic CO2 Conversion to Value-Added Hydrocarbons. *Energy Environ. Sci.* **2010**, *3* (7), 884–890.

(236) MacDowell, N.; Florin, N.; Buchard, A.; Hallett, J.; Galindo, A.; Jackson, G.; Adjiman, C. S.; Williams, C. K.; Shah, N.; Fennell, P. An Overview of CO2 Capture Technologies. *Energy Environ. Sci.* **2010**, *3* (11), 1645–1669.

(237) Balaraman, E.; Gunanathan, C.; Zhang, J.; Shimon, L. J. W.; Milstein, D. Efficient Hydrogenation of Organic Carbonates, Carbamates and Formates Indicates Alternative Routes to Methanol Based on CO2 and CO. *Nat. Chem.* **2011**, *3* (8), 609–614.

(238) Markewitz, P.; Kuckshinrichs, W.; Leitner, W.; Linssen, J.; Zapp, P.; Bongartz, R.; Schreiber, A.; Müller, T. E. Worldwide Innovations in the Development of Carbon Capture Technologies and the Utilization of CO2. *Energy Environ. Sci.* **2012**, *5* (6), 7281–7305.

(239) Nielsen, M.; Alberico, E.; Baumann, W.; Drexler, H.-J.; Junge, H.; Gladiali, S.; Beller, M. Low-Temperature Aqueous-Phase Methanol Dehydrogenation to Hydrogen and Carbon Dioxide. *Nature* **2013**, *495* (7439), 85–89.

(240) Rodríguez-Lugo, R. E.; Trincado, M.; Vogt, M.; Tewes, F.; Santiso-Quinones, G.; Grützmacher, H. A Homogeneous Transition Metal Complex for Clean Hydrogen Production from Methanol–water Mixtures. *Nat. Chem.* **2013**, *5* (4), 342–347.

(241) Huff, C. A.; Sanford, M. S. Cascade Catalysis for the Homogeneous Hydrogenation of CO2 to Methanol. *J. Am. Chem. Soc.* **2011**, *133* (45), 18122–18125.

(242) Wesselbaum, S.; Stein, T. vom; Klankermayer, J.; Leitner, W. Hydrogenation of Carbon Dioxide to Methanol by Using a Homogeneous Ruthenium–Phosphine Catalyst. *Angew. Chem. Int. Ed.* **2012**, *51* (30), 7499–7502.

(243) Wesselbaum, S.; Moha, V.; Meuresch, M.; Brosinski, S.; Thenert, K. M.; Kothe, J.; Stein, T. vom; Englert, U.; Hölscher, M.; Klankermayer, J.; et al. Hydrogenation of Carbon Dioxide to Methanol Using a Homogeneous ruthenium–Triphos Catalyst: From Mechanistic Investigations to Multiphase Catalysis. *Chem. Sci.* **2014**, *6* (1), 693–704.

(244) Rezayee, N. M.; Huff, C. A.; Sanford, M. S. Tandem Amine and Ruthenium-Catalyzed Hydrogenation of CO2 to Methanol. *J. Am. Chem. Soc.* **2015**, *137* (3), 1028–1031.

(245) Zhang, L.; Han, Z.; Zhao, X.; Wang, Z.; Ding, K. Highly Efficient Ruthenium-Catalyzed N-Formylation of Amines with H2 and CO2. *Angew. Chem. Int. Ed.* **2015**, *54* (21), 6186–6189.

(246) Yu, B.; Zhang, H.; Zhao, Y.; Chen, S.; Xu, J.; Huang, C.; Liu, Z. Cyclization of O-Phenylenediamines by CO2 in the Presence of H2 for the Synthesis of Benzimidazoles. *Green Chem.* **2012**, *15* (1), 95–99.

(247) Beydoun, K.; Stein, T. vom; Klankermayer, J.; Leitner, W. Ruthenium-Catalyzed Direct Methylation of Primary and Secondary Aromatic Amines Using Carbon Dioxide and Molecular Hydrogen. *Angew. Chem. Int. Ed.* **2013**, *52* (36), 9554–9557.

(248) Li, Y.; Sorribes, I.; Yan, T.; Junge, K.; Beller, M. Selective Methylation of Amines with Carbon Dioxide and H2. *Angew. Chem. Int. Ed.* **2013**, *52* (46), 12156–12160.

(249) Cui, X.; Dai, X.; Zhang, Y.; Deng, Y.; Shi, F. Methylation of Amines, Nitrobenzenes and Aromatic Nitriles with Carbon Dioxide and Molecular Hydrogen. *Chem. Sci.* **2013**, *5* (2), 649–655.

(250) Beydoun, K.; Ghattas, G.; Thenert, K.; Klankermayer, J.; Leitner, W. Ruthenium-Catalyzed Reductive Methylation of Imines Using Carbon Dioxide and Molecular Hydrogen. *Angew. Chem. Int. Ed.* **2014**, *53* (41), 11010–11014.

(251) Tlili, A.; Frogneux, X.; Blondiaux, E.; Cantat, T. Creating Added Value with a Waste: Methylation of Amines with CO2 and H2. *Angew. Chem. Int. Ed.* **2014**, *53* (10), 2543–2545.

(252) Tominaga, K.; Sasaki, Y. Ruthenium Complex-Catalyzed Hydroformylation of Alkenes with Carbon Dioxide. *Catal. Commun.* **2000**, *1* (1–4), 1–3.

(253) Liu, Q.; Wu, L.; Fleischer, I.; Selent, D.; Franke, R.; Jackstell, R.; Beller, M. Development of a Ruthenium/Phosphite Catalyst System for Domino Hydroformylation–Reduction of Olefins with Carbon Dioxide. *Chem. – Eur. J.* **2014**, *20* (23), 6888–6894.

(254) Riduan, S. N.; Zhang, Y.; Ying, J. Y. Conversion of Carbon Dioxide into Methanol with Silanes over N-Heterocyclic Carbene Catalysts. *Angew. Chem. Int. Ed.* **2009**, *48* (18), 3322–3325.

(255) Neves Gomes, C. Das; Jacquet, O.; Villiers, C.; Thuéry, P.; Ephritikhine, M.; Cantat, T. A Diagonal Approach to Chemical Recycling of Carbon Dioxide: Organocatalytic Transformation for the Reductive Functionalization of CO2. *Angew. Chem. Int. Ed.* **2012**, *51* (1), 187–190.

(256) Jacquet, O.; Neves Gomes, C. Das; Ephritikhine, M.; Cantat, T. Recycling of Carbon and Silicon Wastes: Room Temperature Formylation of N–H Bonds Using Carbon Dioxide and Polymethylhydrosiloxane. *J. Am. Chem. Soc.* **2012**, *134* (6), 2934–2937.

(257) Jacquet, O.; Neves Gomes, C. Das; Ephritikhine, M.; Cantat, T. Complete Catalytic Deoxygenation of CO2 into Formamidine Derivatives. *ChemCatChem* **2013**, *5* (1), 117–120.

(258) Jacquet, O.; Frogneux, X.; Gomes, C. D. N.; Cantat, T. CO2 as a C1-Building Block for the Catalytic Methylation of Amines. *Chem. Sci.* **2013**, *4* (5), 2127–2131.

(259) Motokura, K.; Takahashi, N.; Kashiwame, D.; Yamaguchi, S.; Miyaji, A.; Baba, T. Copper-Diphosphine Complex Catalysts for N-Formylation of Amines under 1 Atm of Carbon Dioxide with Polymethylhydrosiloxane. *Catal. Sci. Technol.* **2013**, *3* (9), 2392–2396.

(260) González-Sebastián, L.; Flores-Alamo, M.; García, J. J. Nickel-Catalyzed Hydrosilylation of CO2 in the Presence of Et3B for the Synthesis of Formic Acid and Related Formates. *Organometallics* **2013**, *32* (23), 7186–7194.

(261) Itagaki, S.; Yamaguchi, K.; Mizuno, N. Catalytic Synthesis of Silyl Formates with 1 Atm of CO2 and Their Utilization for Synthesis of Formyl Compounds and Formic Acid. *J. Mol. Catal. Chem.* **2013**, *366*, 347–352.

(262) Chakraborty, S.; Zhang, J.; Krause, J. A.; Guan, H. An Efficient Nickel Catalyst for the Reduction of Carbon Dioxide with a Borane. *J. Am. Chem. Soc.* **2010**, *132* (26), 8872–8873.

(263) Neves Gomes, C. Das; Blondiaux, E.; Thuéry, P.; Cantat, T. Metal-Free Reduction of CO2 with Hydroboranes: Two Efficient Pathways at Play for the Reduction of CO2 to Methanol. *Chem. – Eur. J.* **2014**, *20* (23), 7098–7106.

(264) Blondiaux, E.; Pouessel, J.; Cantat, T. Carbon Dioxide Reduction to Methylamines under Metal-Free Conditions. *Angew. Chem.* **2014**, *126* (45), 12382–12386.

(265) Park, S.; Bézier, D.; Brookhart, M. An Efficient Iridium Catalyst for Reduction of Carbon Dioxide to Methane with Trialkylsilanes. *J. Am. Chem. Soc.* **2012**, *134* (28), 11404–11407.

(266) Wang, T.; Stephan, D. W. Phosphine Catalyzed Reduction of CO2 with Boranes. *Chem. Commun.* **2014**, *50* (53), 7007–7010.

(267) Courtemanche, M.-A.; Pulis, A. P.; Rochette, É.; Légaré, M.-A.; Stephan, D. W.; Fontaine, F.-G. Intramolecular B/N Frustrated Lewis Pairs and the Hydrogenation of Carbon Dioxide. *Chem. Commun.* **2015**, *51* (48), 9797–9800.

(268) Whittlesey, M. K.; Mawby, R. J.; Osman, R.; Perutz, R. N.; Field, L. D.; Wilkinson, M. P.; George, M. W. Transient and Matrix Photochemistry of Fe(dmpe)2H2 (dmpe = Me2PCH2CH2Me2): Dynamics of C-H and H-H Activation. *J. Am. Chem. Soc.* **1993**, *115* (19), 8627–8637.

(269) Dombray, T.; Werncke, C. G.; Jiang, S.; Grellier, M.; Vendier, L.; Bontemps, S.; Sortais, J.-B.; Sabo-Etienne, S.; Darcel, C. Iron-Catalyzed C–H Borylation of Arenes. *J. Am. Chem. Soc.* **2015**, *137* (12), 4062–4065.

(270) Baker, M. V.; Field, L. D.; Young, D. J. Synthesis and Properties of Bis(dialkylphosphino)ethane Iron Dihydrides. *Appl. Organomet. Chem.* **1990**, *4* (5), 551–556.

(271) Coto, B.; Peschla, R.; Kreiter, C.; Maurer, G. Reaction Kinetics in Liquid Mixtures of Formaldehyde and 1-Butanol from 13C NMR Spectroscopy. *Ind. Eng. Chem. Res.* **2003**, *42* (13), 2934–2939.

(272) Maiwald, M.; Fischer, H. H.; Kim, Y.-K.; Albert, K.; Hasse, H. Quantitative High-Resolution on-Line NMR Spectroscopy in Reaction and Process Monitoring. *J. Magn. Reson.* **2004**, *166*

(2), 135–146.

(273) Azofra, L. M.; Alkorta, I.; Elguero, J.; Toro-Labbé, A. Mechanisms of Formation of Hemiacetals: Intrinsic Reactivity Analysis. *J. Phys. Chem. A* **2012**, *116* (31), 8250–8259.

(274) Kathryn Helen, B. Kinetic Studies on the Reaction of Formaldehyde with Amines in the Presence of Sulfite. Ph. D thesis, University of Durham, Chemistry Department, 1999.

(275) Zhu, X.-Q.; Zhang, M.-T.; Yu, A.; Wang, C.-H.; Cheng, J.-P. Hydride, Hydrogen Atom, Proton, and Electron Transfer Driving Forces of Various Five-Membered Heterocyclic Organic Hydrides and Their Reaction Intermediates in Acetonitrile. *J. Am. Chem. Soc.* **2008**, *130* (8), 2501–2516.

(276) Benhamou, L.; Chardon, E.; Lavigne, G.; Bellemin-Laponnaz, S.; César, V. Synthetic Routes to N-Heterocyclic Carbene Precursors. *Chem. Rev.* **2011**, *111* (4), 2705–2733.

(277) Poyatos, M.; Prades, A.; Gonell, S.; Gusev, D. G.; Peris, E. Imidazolidines as Hydride Sources for the Formation of Late Transition-Metal Monohydrides. *Chem. Sci.* **2012**, *3* (4), 1300–1303.

(278) Richmond, H. H.; Myers, G. S.; Wright, G. F. The Reaction between Formaldehyde and Ammonia. *J. Am. Chem. Soc.* **1948**, *70* (11), 3659–3664.

(279) Nielsen, A. T.; Moore, D. W.; Ogan, M. D.; Atkins, R. L. Structure and Chemistry of the Aldehyde Ammonias. 3. Formaldehyde-Ammonia Reaction. 1,3,5-Hexahydrotriazine. *J. Org. Chem.* **1979**, *44* (10), 1678–1684.

(280) Kaur, N.; Kishore, D. An Insight into Hexamethylenetetramine: A Versatile Reagent in Organic Synthesis. *J. Iran. Chem. Soc.* **2013**, *10* (6), 1193–1228.

(281) Allenmark, S. G.; Andersson, M. A. Chloroperoxidase-Catalyzed Asymmetric Synthesis of Series of Aromatic Cyclic Sulfoxides. *Tetrahedron Asymmetry* **1996**, *7* (4), 1089–1094.

(282) Hoppmann, A.; Weyerstahl, P.; Zummack, W. Terpene Und Terpen-Derivate, VI. Reaktionen von α, β-Ungesättigten Ketonen Mit Dithiolen Und 13C-NMR-Spektren von 1,3-Dithianen Und 1,3-Dithiolanen. *Justus Liebigs Ann. Chem.* **1977**, *1977* (9), 1547–1556.

(283) Cao, Y.-J.; Lai, Y.-Y.; Cao, H.; Xing, X.-N.; Wang, X.; Xiao, W.-J. A Highly Efficient Carbon–sulfur Bond Formation Reaction via Microwave-Assisted Nucleophilic Substitution of Thiols to Polychloroalkanes without a Transition-Metal Catalyst. *Can. J. Chem.* **2006**, *84* (11), 1529–1533.

(284) Wittig, G.; Haag, W. Über Triphenyl-Phosphinmethylene Als Olefinbildende Reagenzien (II. Mitteil.1)). *Chem. Ber.* **1955**, *88* (11), 1654–1666.

(285) Vedejs, E.; Meier, G. P.; Snoble, K. A. J. Low-Temperature Characterization of the Intermediates in the Wittig Reaction. *J. Am. Chem. Soc.* **1981**, *103* (10), 2823–2831.

(286) Skatova, A. A.; Fedushkin, I. L.; Maslova, O. V.; Hummert, M.; Schumann, H. Synthesis and Structures of New Conformationally Rigid 1-Aza-1,3-Dienes of the Acenaphthene

Series. *Russ. Chem. Bull.* **2007**, *56* (11), 2284–2289.

(287) Arend, M.; Westermann, B.; Risch, N. Modern Variants of the Mannich Reaction. *Angew. Chem. Int. Ed.* **1998**, *37* (8), 1044–1070.

(288) Evans, D. A.; Johnson, J. S. Diels-Alder Reactions. *Compr. Asymmetric Catal.* **1999**, *3*, 1177.

(289) Mannich, C.; Krösche, W. Ueber Ein Kondensationsprodukt Aus Formaldehyd, Ammoniak Und Antipyrin. *Arch. Pharm. (Weinheim)* **1912**, *250* (1), 647–667.

(290) CUMMINGS, T. F.; SHELTON, J. R. Mannich Reaction Mechanisms. *J. Org. Chem.* **1960**, *25* (3), 419–423.

(291) Frogneux, X.; Blondiaux, E.; Thuéry, P.; Cantat, T. Bridging Amines with CO2: Organocatalyzed Reduction of CO2 to Aminals. *ACS Catal.* **2015**, 3983–3987.

(292) Fulmer, G. R.; Miller, A. J. M.; Sherden, N. H.; Gottlieb, H. E.; Nudelman, A.; Stoltz, B. M.; Bercaw, J. E.; Goldberg, K. I. NMR Chemical Shifts of Trace Impurities: Common Laboratory Solvents, Organics, and Gases in Deuterated Solvents Relevant to the Organometallic Chemist. *Organometallics* **2010**, *29* (9), 2176–2179.

Résumé Français

Résumé : Ce texte est un résumé en français de la thèse de Guanghua Jin écrite en anglais.

Trois modes de coordination du composé bis(2-picolyl)phénylphosphine au fer: isolation d'un complexe dinucléaire de fer présentant un fragment pyridinique déaromatisé.

Un intérêt croissant dans la chimie du fer découle de la volonté de remplacer les métaux nobles dans les réactions catalytiques. Les propriétés catalytiques des enzymes incorporant un fer dans le site actif soit comme unités monomères ou dimères peuvent être une source d'inspiration. Il y a donc un effort dans la communauté inorganique pour synthétiser de nouveaux complexes de fer, et quelques systèmes ont récemment montré des propriétés catalytiques très intéressant Dans la dernière décennie, Milstein *et al.* ont développés une famille de ligands pince PNL déprotonables comportant un fragment picolyle qui peut se déaromatiser / aromatiser par déprotonation / protonation en position benzylique (figure 1). L'utilisation de systèmes de ruthénium principalement, a permis de décrire des propriétés catalytiques très intéressants et plus récemment, le même type de coopération métal / ligand a été appliquée avec succès au fer. En comparaison, le composé bis(2-picolyl)phénylphosphine (NPN) a été beaucoup moins étudiés en chimie de coordination. Si Stalke *et al.* ont démontré que ce ligand pouvait présenter un comportement Janus avec deux carbones benzyliques déprotonés à un centre Sn, le ligand NPN n'a jamais été engagé

dans un processus de déaromatisation lorsqu'il est coordonné à un centre de métal de transition, malgré la présence de deux fragment picolyle (Figure 1).

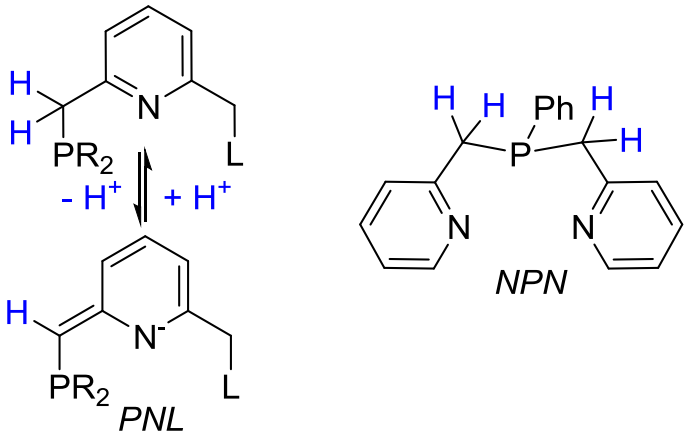

Figure 1. PNL and NPN ligands

Dans le cadre de notre enquête en cours sur la chimie de [Fe{N(SiMe$_3$)$_2$}$_2$] comme précurseur pour générer et isoler des complexes de fer réactifs, nous avons sondé sa réactivité avec NPN. Nous tenons à signaler ici, l'isolation et la caractérisation des complexes **1**-**3** incorporant un ou deux ligands NPN adoptant trois modes de coordination différents (Schéma 1). Dans les complexes **2** et **3**, la déprotonation du ligand NPN est observée, ce qui permet la stabilisation d'une structure dimère dans le cas de **2**, avec deux ligands NPN reliant les deux centres métalliques.

Schéma 1: Synthèse des complexes 1-3

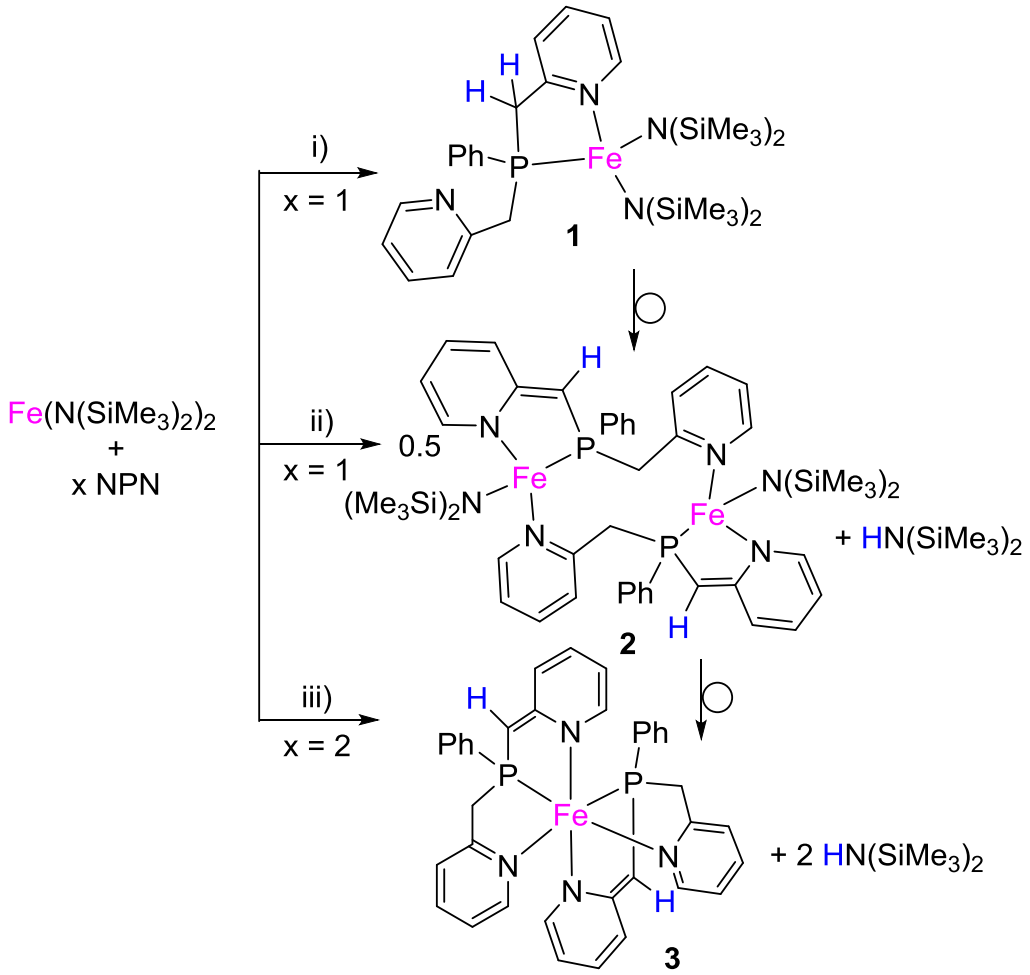

Conditions: i) pentane, mélange à -78 ° C et agitation à -30 ° C pendant 90 min; ii) pentane, mélange à -78 ° C, sous agitation à -30 ° C pendant 3 h et à température ambiante pendant 45 min; iii) pentane, mélange à -78 ° C, agitation à -30 ° C pendant 3 heures, puis à température ambiante pendant 36h.

En raison de la forte réactivité du précurseur de fer [Fe{N(SiMe$_3$)$_2$}$_2$], la coordination a été effectuée avec une attention particulière aux paramètres de température et de temps. Après le mélange du ligand NPN avec le précurseur de fer à -78 ° C, la solution de pentane a été réchauffée à -30 ° C et agitée à cette température pendant 90 min. Un précipité jaune a

été observé et le complexe **1** a pu être isolé après filtration avec 28% de rendement (schéma 1). Le complexe **1** présente des signaux paramagnétiques larges dans le spectre RMN ^{1}H allant de 130 à −30 ppm. Des cristaux pour l'analyse par diffraction des X-Ray ont été obtenus en mélangeant le précurseur de fer avec le ligand NPN à −30 ° C dans une solution de pentane / toluène. L'analyse révèle la coordination du ligand au précurseur de fer dans un mode NP-bidenté, un bras de picolyl restant pendant (Figure 2). Les deux ligands amido complétent la sphère de coordination du centre métallique qui adopte une géométrie de tétraédrique déformée. Le complexe **1** n'est pas stable à la salle température, et conduit à la formation du complexe dimère **2**, qui a été isolé dans un bon rendement (81%) (schéma 1). Le complexe **2** présente également de larges signaux paramagnétiques dans le spectre RMN ^{1}H allant de + 175 à −30 ppm (Figure S7). L'analyse par diffraction des rayons X sur monocristaux a révélé une structure dimère avec un centre d'inversion (Figure 2). Les centres métalliques présentent une géométrie tétraédrique déformée et les ligands NPN relient les deux centres métalliques dans un mode NP-bidenté pour le premier mode de fer et N-monodenté pour le deuxième fer. La sphère de coordination est ensuite complétée par un ligand amido sur chaque métal. L'espaceur méthylène de la fraction NP-bidenté a été déprotoné. La charge anionique est donc formellement délocalisée sur une double liaison C5=C6 et un centre pyridinique déaromatisé. Comme prévu, la distance C5=C6 de 1.389(3) Å est plus courte que la liaison simple C−C (dC17−C18 = 1.502(2) Å) de l'autre fragment picolyl sur le même ligand ou de la liaison C−C adjacente dans le composé **1** (1.500 (2) Å). En outre la distance Fe−N de l'anneau pyridinique déaromatisé (dFe−N1 = 2.0654(15) Å) est plus courte que la distance Fe−N de l'anneau pyridinique aromatique (dFe−N2 = 2,1548(15) Å).

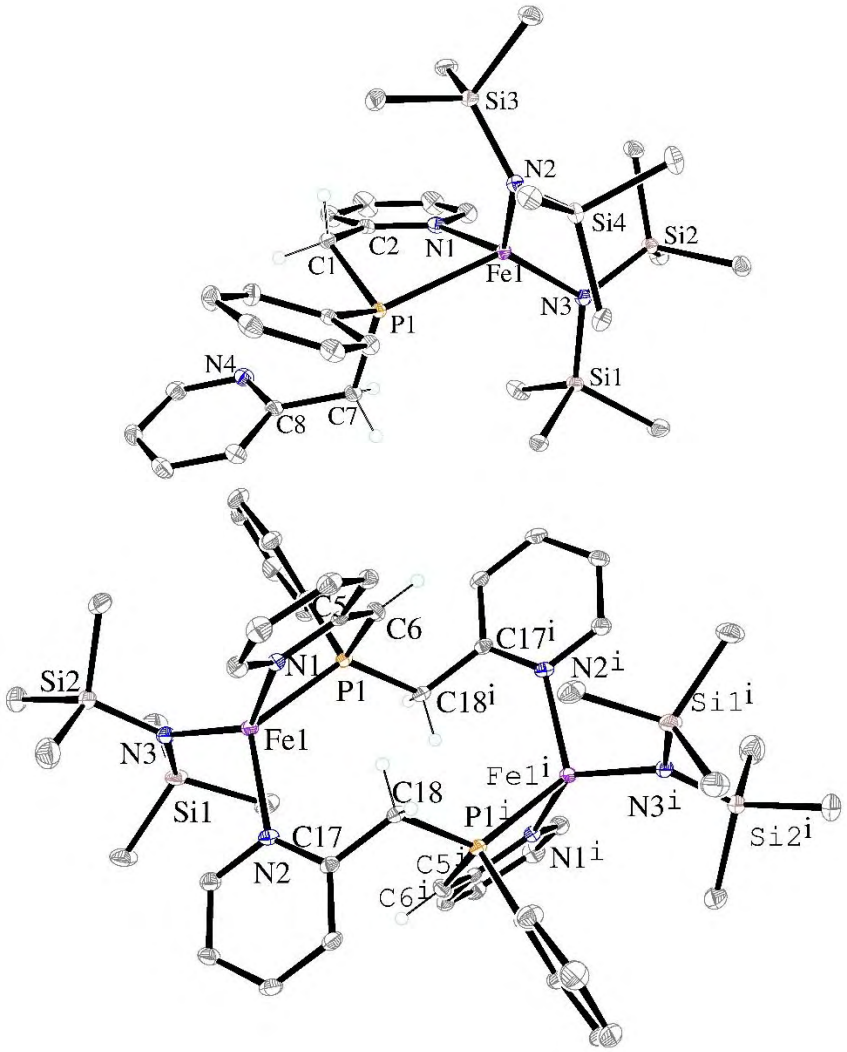

Figure 2. Structures moléculaires des complexes 1 (en haut) et 2 (en bas). Les atomes d'hydrogène ont été omis pour plus de clarté à l'exception des fragments CH et CH_2 entre les atomes de phosphore et les cycles pyridiniques.

Tableau 1: Données structurales principales pour les complexes **1**, **2** et **3.**

Complexe **1**			
Fe(1)-N(1)	2.2236(12)	Fe(1)-N(2)	1.9663(11)
Fe(1)-N(3)	1.9799(11)	Fe(1)-P(1)	2.5579(4)
C(1)-C(2)	1.500(2)	C(7-C(8)	1.498(2)
N(1)-Fe(1)-N(2)	122.52(5)	N(1)-Fe(1)-N(3)	99.66(5)

N(1)-Fe(1)-P(1)	75.03(3)	N(2)-Fe(1)-N(3)	124.28(5)
N(2)-Fe(1)-P(1)	100.73(3)	N(3)-Fe(1)-P(1)	125.98(4)
C(2)-C(1)-P(1)	109.04(10)	C(8)-C(7)-P(1)	116.36(10)
Complexe **2**			
Fe(1)-N(1)	2.0654(15)	Fe(1)-N(2)	2.1548(15)
Fe(1)-N(3)	1.9499(15)	Fe(1)-P(1)	2.4387(5)
C(5)-C(6)	1.389(3)	C(6)-P(1)	1.7524(19)
C(17)-C(18)	1.502(2)	C(18)-P(1)$^{\#1}$	1.8530(18)
N(1)-Fe(1)-N(2)	101.50(6)	N(1)-Fe(1)-N(3)	132.71(6)
N(1)-Fe(1)-P(1)	82.49(4)	N(2)-Fe(1)-N(3)	105.72(6)
N(2)-Fe(1)-P(1)	121.53(4)	N(3)-Fe(1)-P(1)	113.30(5)
C(5)-C(6)-P(1)	119.47(14)	C(17)-C(18)-P(1)$^{\#1}$	113.51(12)
Complexe **3**			
Fe(1)-P(1)	2.1564(9)	P(2)-Fe(1)	2.1547(9)
N(1)-Fe(1)	2.046(2)	N(2)-Fe(1)	2.011(2)
N(3)-Fe(1)	2.013(2)	N(4)-Fe(1)	2.058(2)
C(1)-C(2)	1.499(4)	C(7)-C(8)	1.396(4)
C(19)-C(20)	1.399(4)	C(25)-C(26)	1.491(4)
P(2)-Fe(1)-P(1)	96.80(3)	N(1)-Fe(1)-P(1)	82.28(7)
N(2)-Fe(1)-P(1)	84.75(7)	N(3)-Fe(1)-P(1)	93.34(8)
N(4)-Fe(1)-P(1)	177.73(8)	N(1)-Fe(1)-P(2)	179.07(8)
N(2)-Fe(1)-P(2)	93.50(7)	N(3)-Fe(1)-P(2)	85.12(8)
N(4)-Fe(1)-P(2)	81.13(7)	N(2)-Fe(1)-N(1)	86.27(10)
N(3)-Fe(1)-N(1)	95.07(10)	N(1)-Fe(1)-N(4)	99.79(10)
N(2)-Fe(1)-N(3)	177.51(10)	N(2)-Fe(1)-N(4)	96.30(10)
N(3)-Fe(1)-N(4)	85.56(10)		

[a] Codes de symétrie: #1 –x+1, -y, -z

Les composés **1** et **2** ont été caractérisés comme contenant un atome de fer à haut spin (II) en ^{57}Fe Mössbauer spectroscopie (Figure 3). A 80 K, l'analyse révèle des doublets quadrupolaires pour **1** (δ = 0,7676 (18) mm s-1 et ε = 0,9572 (35) mm s-1) et **2** (δ = 0,7164

(12) mm s -1 = 2,1553 et ε (23) mm s-1) avec un plus grand splitting quadripolaire pour le complexe dinucléaire.

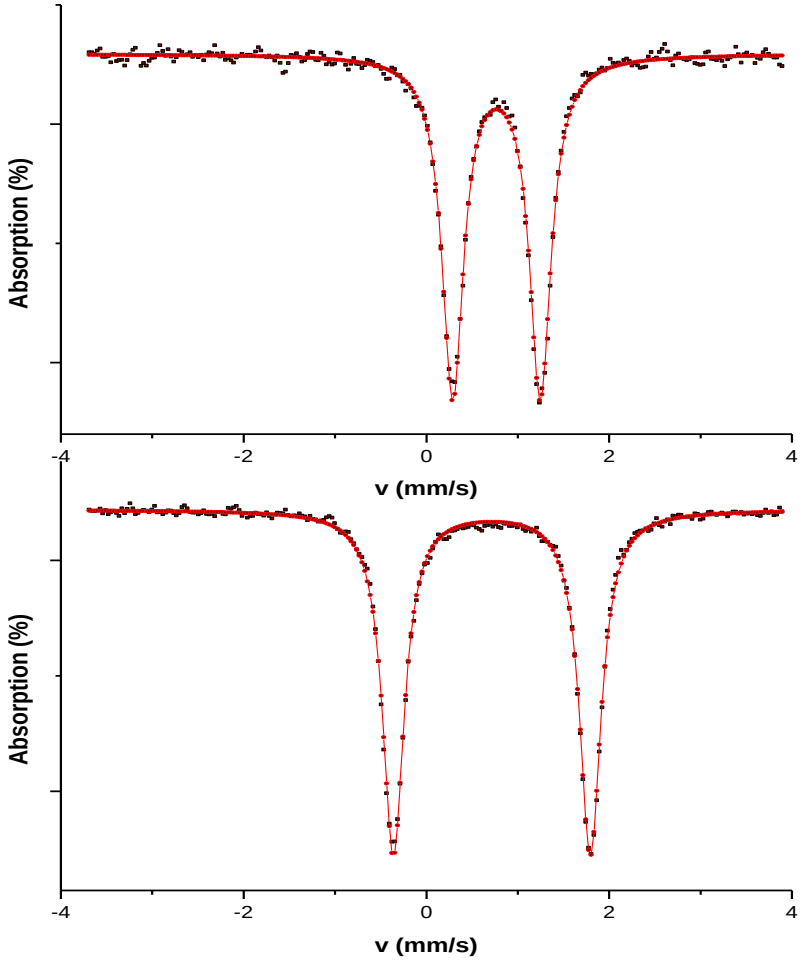

Figure 3. Spectre Mössbauer des complexes 1 (haut) and 2 (bas) at 80 K.

Une caractérisation supplémentaire pour les composés **1** et **2** à l'état solide a été obtenue par analyses RMN. Les signaux de l'état solide RMN ^{31}P est difficile à observer, le phosphore étant à proximité des centres de fer: pour les deux complexes, les signaux détectés sont très larges, δ = 39 ($w_{1/2}$ = 13,7 kHz) et 41 ($w_{1/2}$ = 13,0 KHz), pour **1** et **2** respectivement. En outre, en raison de la sensibilité des deux composés, leur décompositions ont été observées lors des analyses et des signaux RMN ^{31}P du ligand libre NPN et d'un nouveau complexe **3** (voir ci-dessous) ont été observés; masquant partiellement le signal de composés **1** et **2**. (Figure 4).

Plus intéressant encore, les spectres RMN ^{13}C présentent des signatures RMN spécifiques pour **1** et **2**, avec des signaux allant de 600 à −100 ppm.

En solutions les deux complexes sont instables à température ambiante donnant lieu à des composés complexes non caractérisées et au complexe **3**. Complexe **3** a pu être directement isolé sous forme d'une poudre brune avec un rendement de 55% par réaction de $[Fe\{N(SiMe_3)_2\}_2]$ avec deux équivalents du ligand NPN, après 36 h à température ambiante. Les analyses RMN indiquent la formation d'un composé diamagnétique en accord avec un complexe à bas spin de fer (II). Le spectre RMN ^{31}P montre une résonance à 87,0 ppm indiquant deux ligands NPN équivalents en solution. Le spectre RMN ^{1}H montre trois signaux dans la région aliphatique de 3 à 4,5 ppm. Les signaux à δ 4,06 et δ 3.14 correspondent aux protons inéquivalents des espaceurs méthylène présentant un motif AB en RMN ^{31}P ($^{2}J_{HH}$ = 15,5 Hz), tandis que le troisième signal à δ 3.50 apparaît comme un singulet et correspond aux fragments PCH.

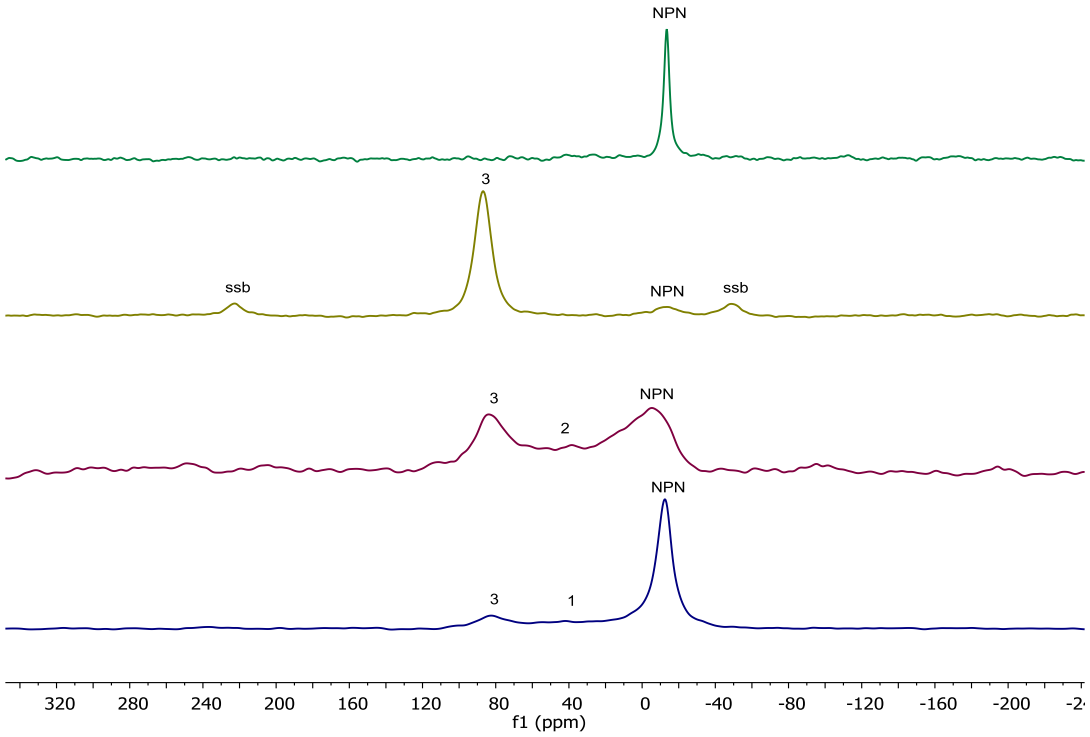

Figure 4: Spectres MAS RMN ^{31}P du ligand NPN, complexe **3**, **2** et **1** d'en haut vers le bas à l'état solide.

La structure aux rayons X de **3** confirme la coordination des deux ligands NPN à un centre de fer dans un mode de coordination tridentate avec une unité pyridinique déaromatisation sur chaque ligand NPN (Figure 6). Les atomes d'azote des anneaux déaromatisés sont en position trans lun de l'autre et occupent les positions axiales. Les deux atomes de phosphore sont en position cis dans le plan équatorial et trans aux atomes d'azote des cycles pyridine. Les doubles liaisons C=C (d(C7–C8 = 1,396(4) Å, d(C19–C20) = 1.399(4) Å) sont plus courtes que les liaisons simples C-C (d(C1–C2) = 1.499 (4) Å et d(C25–C26) = 1.491 Å) et les distances Fe-N de cycles pyridiniques déaromatisés (d(Fe–N2) = 2.011(2) Å, d(Fe–N3) = 2.013(2) Å) sont légèrement plus courtes que les distances Fe–N des cycles pyridiniques aromatiques (d(Fe–N1) = 2,046(2) Å, d(Fe–N4) = 2,058(2) Å).

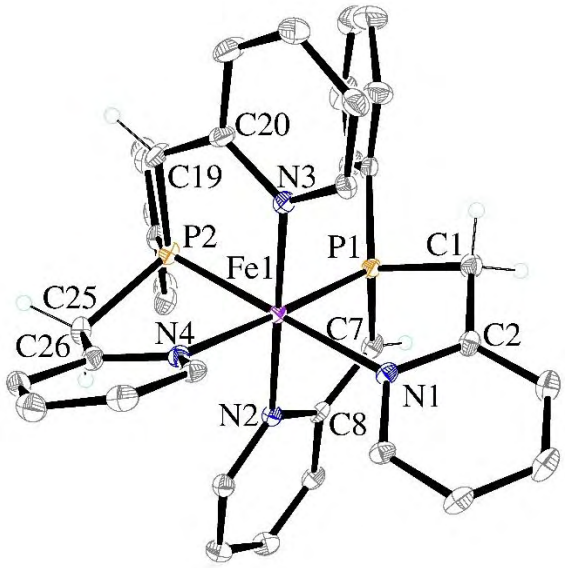

Figure 6. Structure moléculaire du complexe **3**. Les atomes d'hydrogène sont omis pour plus de clarté à l'exception des fragments CH et CH_2 entre les atomes de phosphore et les cycles pyridiniques.

En résumé, nous avons démontré que le composé bis(2-picolyle)phénylphosphine agit comme un ligand polyvalent NPN vers le précurseur de fer [Fe{N(SiMe$_3$)$_2$}$_2$], offrant un accès aux différents modes de coordination. Nous avons pu isoler les complexes **1**-**3**, grâce à un contrôle fin des conditions expérimentales. Ces composés paramagnétiques et diamagnétiques ont été caractérisés des analyses par diffraction des rayons X ainsi que par spectroscopie RMN à la fois en solution et à l'état solide. Lors de la coordination, la déprotonation du ligand NPN a été observée donnant lieu à la déaromatisation d'un anneau pyridinique dans les composés **2** et **3**. C'est la première fois qu'un tel comportement est signalé pour ce ligand. En outre, sa flexibilité permet la formation d'un dimère original, complexe **2**. Nous souhaitons maintenant exploiter ce type de structure dimérique avec un ligand activé pour l'activation des petites molécules, et les enquêtes en cours visent à résoudre les problèmes de stabilité rencontrés dans cette étude.

Réduction fonctionnalisante du CO_2 catalysée par un complexe de fer : formation de nouvelles liaisons C-N, C-O, et C-C.

Le dioxyde de carbone est une source de carbone très abondante, et non toxique par comparaison aux autres sources C1 employées par l'industrie chimique. Son utilisation a donc suscité un intérêt dans différents domaines de la chimie, malgré sa grande stabilité thermodynamique intrinsèque. Dans les procédés les plus avancés de transformation du CO_2, l'unité OCO est maintenue, comme dans les synthèses de l'acide salicylique et / ou l'atome de carbone reste à l'état d'oxydation +4 comme dans les dérivés de l'urée. Toutefois, pour utiliser pleinement le CO_2 comme source de carbone, on a besoin d'arracher un ou les deux atomes d'oxygène et d'avoir accès à la gamme complète des états d'oxydation du carbone. En conséquence, la catalyse homogène de réduction du CO_2 avec abstraction concomitante d'oxygène a été étudiée avec du dihydrogène, des silanes et des boranes comme agents réducteurs. Quel que soit le réducteur, le champ d'application de produits résultant de la re-réduction de CO_2 est encore assez limité. L'utilisation de dihydrogène comme réducteur a donné lieu à du méthanol, tandis que l'addition d'amines, d'imines ou d'oléfines au processus d'hydrogénation ont conduit à la formation de formamides, méthylamines et d'alcools aliphatiques, générant ainsi de nouvelles liaisons C-N et C-C. Bien que l'hydrogénation du CO_2 apparaisse comme la réaction idéale en termes d'économie d'atome, une source durable de dihydrogène « décarbonée » et des conditions de réaction

plus douces restent à découvrir. L'utilisation de silanes et de boranes comme réducteurs a permis d'utiliser des conditions opératoires nettement plus douces, et de développer différents types de catalyseurs pour obtenir la liste complète des composés C1 (CO, CH_2O, CH_3OH et de CH_4). Des mécanismes clés ont été découverts et jusqu'à quatre réactions hydro-fonctionnalisation consécutives ont été décrite (Figure 1) conduisant aux composés formoxy A, à l'acétal B et / ou au formaldéhyde, au méthoxy C, et finalement au méthane, ce dernier étant obtenu seulement dans le cas d'hydrosilanes. Nos études sur la catalyse au ruthénium d'hydroboration du CO_2 nous a permis de faire la lumière sur la deuxième étape de réduction du CO_2 avec la première preuve de expérimentale de la formation d'un composé bis(boryle)acétal B, et de formaldéhyde. Pour augmenter la complexité moléculaire, Cantat et al. et d'autres ont décrit la réduction du CO_2 au niveau formoxy A, suivit de sa fonctionnalisation par une amine pour donner des formamides, ou après une réduction supplémentaire de générer des méthylamines (Figure 1).

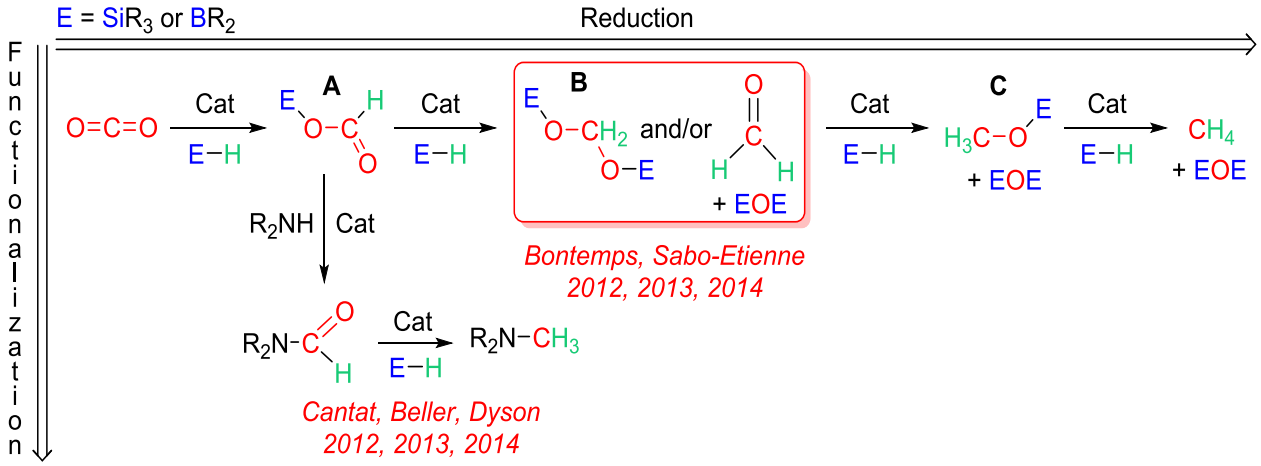

Figure 1: Schéma général pour la réduction et la fonctionnalisation du CO_2.

Dans ce contexte, nous avons cherché à élargir encore la quantité des composés carbonés accessibles à partir de la transformation du CO_2. Nous avons postulé que la synthèse sélective du bis(boryl)acétal B serait possible et que ce composé serait une source

réactive et polyvalente de méthylène. En outre, nous avons cherché des systèmes catalytiques à base de métaux abondants et visé des complexes de fer définis comportant des ligands hydrures afin de transférer notre expertise sur les complexes polyhydrures de ruthénium. L'utilisation de catalyseurs à base de fer pour la transformation homogène du CO_2 est rare et les études récentes se sont concentrées sur la formation d'acide formique et de ses dérivés. Il a également été rapporté que, en présence de ligands multidentés de phosphine, le précurseur de fer $Fe(acac)_2$ a été capable de catalyser la réduction fonctionnalisante du CO_2 pour donner des formamides et des méthylamines. Nous avons choisis le complexe dihydrure de fer $Fe(H)_2(DMPE)_2$ (**1**) en tant que précurseur catalytique, car il a été démontré par Field et al. qu'il réagissait avec le CO_2, et par nous qu'il catalysait la borylation déshydrogénante d'arenes. Nous décrivons ici la réduction sélective du CO_2 en bis(boryl)acétal catalysée par un complexe de fer et son utilisation ultérieure en tant qu'agent de transfert de méthylène réactif et polyvalent pour former non seulement de nouvelles liaisons C-N, mais aussi, C-O, C-C, C=N, et C=C en employant une stratégie en un pot et deux étapes.

L'hydroboration catalytique du CO_2 a été effectué avec 5% molaire de catalyseur en présence de trois hydroboranes différents: catécholborane (HBCat), pinacolborane (HBpin) et 9-borabicyclo [3.3.1] nonane (9-BBN) (schéma 1, Tableau 1). Les réactions ont d'abord été menées dans C_6D_6 à température ambiante sous 1 atm de CO_2 dans un tube RMN et les rendements des deux principaux produits observés, le bis(boryl)acétal et le méthoxyborane, ont été déterminés par intégrations RMN ^1H à conversion complète de l'hydroborane correspondant. Avec HBCat, la conversion complète a été observée après les 3 heures et seul le méthoxyborane est obtenu avec un rendement de 59%. Dans le cas de HBpin et 9-BBN,

conversion complète est observée en 5h et le bis(boryl)acétal est favorisé (30% et 46%, respectivement) sur le méthoxyborane (18% et 27%, respectivement).

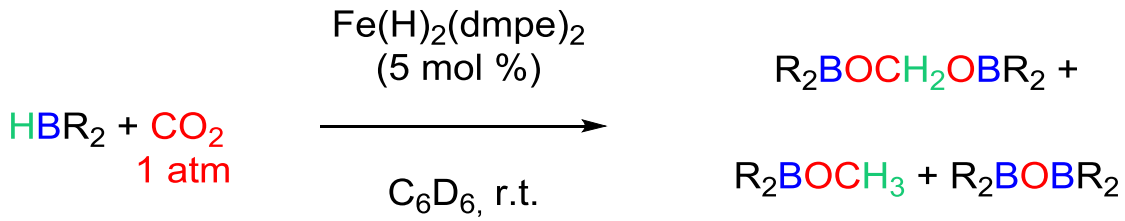

Schéma 1: Hydroboration du CO_2 avec HBcat, HBpin et 9-BBN

Tableau 1 : Hydroboration du CO_2 avec HBcat, HBpin et 9-BBN

HBR_2	Time (h)	Rendement de $R_2BOCH_2OBR_2$ (%)	Rendement de R_2BOCH_3 (%)
HBCat	1	0	41
	3[a]	0	59
HBpin	1	4	6
	3	21	10
	5[a]	30	18
9-BBN	1	36	3
	3	56	15
	5[a]	46	27

Nous avons donc choisis le 9-BBN pour une synthèse sélective du bis(boryl)acétal et optimisé les conditions expérimentales. Parmi les différents paramètres testés, le solvant a eu l'impact le plus important, puisque l'utilisation de THF a favorisé la formation du bis(boryl)acétal **2** en termes de vitesse et de sélectivité (Tableau 2). Après 47 min, une conversion complète 9-BBN, un rendement de 8% en méthoxyborane et 85% dans le composé **2** a été déterminé par intégration RMN ^1H par rapport à un étalon interne. Il convient de noter que, avant la réduction complète en méthoxyborane, l'accumulation transitoire du bis(boryl)acétal a été récemment rapportée dans un système utilisant des bases fortes comme

catalyseur et également le 9-BBN comme réducteur. Dans notre système, **2** n'a pas été réduit plus avant, puisque, après 15 h, 52% d'acétal et seulement 11% de méthoxyborane ont été observés. Des produits non identifiés comportant des fragments méthylène et méthoxy ont été observés dans le spectre RMN ^{1}H qui pourrait expliquer la diminution de la quantité de **2**.

Tableau 2: Optimisation des conditions opératoires avec 9-BBN et réaction témoins (entrées 16 et 17)

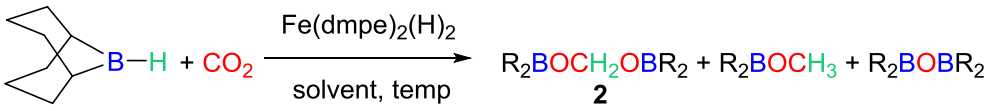

#	mol %	$P(CO_2)$	T °C	Time (min.)	Conv. of 9-BBN (%)	relative ratio **2:R_2BOCH_3**	Solvent
1	5	1	25	170	95	5.6 : 1	C_6D_6
2[a]	5	1	25	225	93	1.9 : 1	C_6D_6
3	10	1	25	145	98	3.4 : 1	C_6D_6
4	10	3	25	165	89	0.6 : 1	C_6D_6
5	1	1	25	180	95	2.4 : 1	C_6D_6
6	5	3	25	135	93	1.1 : 1	C_6D_6
7	5	3	10	455	64	0.6 : 1	C_6D_6
8	5	1	45	47	> 99	8.8 : 1	C_6D_6
9	5	1	50	20	> 99	12.6 : 1	C_6D_6
10	5	1	60	10	> 99	13.4 : 1	C_6D_6
11	5	1	25	30	> 99	18.2 : 1	THF-D_8
12	1	1	25	47	> 99	19.9 : 1	THF-D_8
13	1	3	25	47	> 99	11.2 : 1	THF-D_8
14	0.1	1	25	53	> 99	12.3 : 1	THF-D_8
15	5	1	25	150	> 99	2.1 : 1	Tol-D_8
16[b]	2	1	60	47	4[c]	3.5:1	THF-D_8
17[d]	---	3	50	2 weeks	0	0	THF-D_8

[a]: 0.26 mmol de 9-BBN et 5 mol% catalyst; [b]: dmpe comme catalyseur; [c]: réaction de 9-BBN avec dmpe n'est pas prise en compte dans la conversion de 9-BBN; [d]: sans catalyseur, jusqu'à 50 °C pendant 2 semaines.

Nous avons alors testé la capacité de **2** à transférer le fragment méthylène. Comme décrit dans le schéma 2, la réduction sélective du CO_2 en **2** a été effectuée, suivi par l'addition de 0,4 équiv. de méthanol ou de diisopropylaniline par rapport à la quantité de 9-BBN ajoutée. Ce mode opératoire en un pot, deux étapes conduit respectivement à l'hémiacétal **3** et la méthyleneaniline **4** en 89% (72%) et 83% (66%) de rendement RMN, par rapport à l'agent de piégeage correspondant (et au 9-BBN).

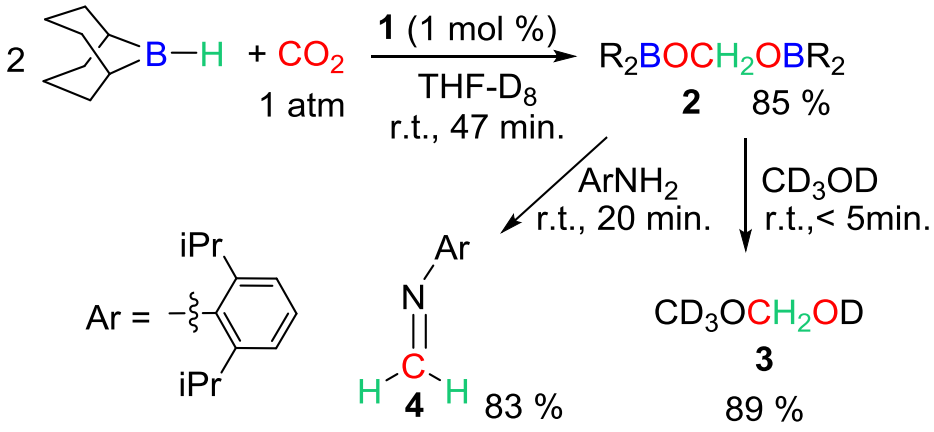

Schéma 2: par Réduction sélective de CO_2 catalysée par le complexe de fer 1 en bis(boryl)acetal **2** et sa fonctionnalisation en composés **3** et **4**.

Nous avons ensuite étudié la réactivité du composé **2** comme ersatz de formaldéhyde dans quelques réactions représentatives qui ont d'abord été menées dans des tubes RMN (schéma 3). Sauf indication contraire, les rendements sont basés sur l'agent de piégeage pour rendre compte de l'efficacité de la réaction de piégeage. Le composé **2** généré in-situ a été mis à réagir à température ambiante avec le 2-méthylaminophénol ou le N,N-diméthyl-1,2-benzènediamine pour donner les composés hémiaminal et aminal cycliques **5** (1 heure, 67% de rendement) et **6** (3 h, 77% de rendement), respectivement. Les aminals cycliques sont notamment utilisés en tant que donneurs d'hydrures organiques ou en tant que précurseurs de carbène N-hétérocycliques. L'aminal acyclique **7** a été aisément obtenu avec un rendement de 92% après 1 h à température ambiante par la réaction de deux équivalents

de l'amine secondaire correspondante. L'ammoniac est un synthon de construction important, mais sa réactivité est difficile à contrôler. Cependant, la réaction de l'ammoniac avec formaldéhyde est une condensation réversible connue qui conduit au composé cage hexaméthylènetétramine **8**, réactif organique polyvalent. Le composé 2 généré in-situ a été exposé à une solution d'ammoniaque et conduit après 16 h, à température ambiante au composé **8** avec un rendement de 84% par rapport au 9-BBN. Ce composé présente six groupements méthylènes résultant de la réduction du CO_2. La caractérisation de **3**-**8** complète la liste des composés accessibles à partir de la fonctionnalisation réductive du CO_2 avec des amines avec la génération des liaisons C-N et C-O. Avec l'objectif de former des liaisons C-C, nous avons porté notre attention sur les réactifs de phénol. Le formaldéhyde est en effet utilisé à l'échelle industrielle dans les résines phénoliques, par réaction de condensation générant ainsi des liaisons C-C. Comme preuve de concept, nous avons choisis d'utiliser un phénol protégé t-Bu en positions 2 et 4. A titre de comparaison et pour obtenir sa signature RMN dans le THF, **9** a d'abord été généré avec un rendement in situ mesurée de 48%, à partir de la réaction de para-formaldéhyde avec le composé phénol substitué en présence de KOH en 16 h à 120 °C. Lorsque le composé **2** généré in situ a été utilisé à la place du para-formaldéhyde, la réaction a lieu avec la production de **9** avec un rendement de 46% après 36 heures à 120 °C sans ajouter de KOH. Encouragé par la génération de ces liaisons C-C à partir de CO_2, nous avons ensuite exposés le composé **2** à un ylure de phosphore et observé le résultat attendu d'une réaction de Wittig avec la formation de styrène **10** avec un très bon rendement de 72%.

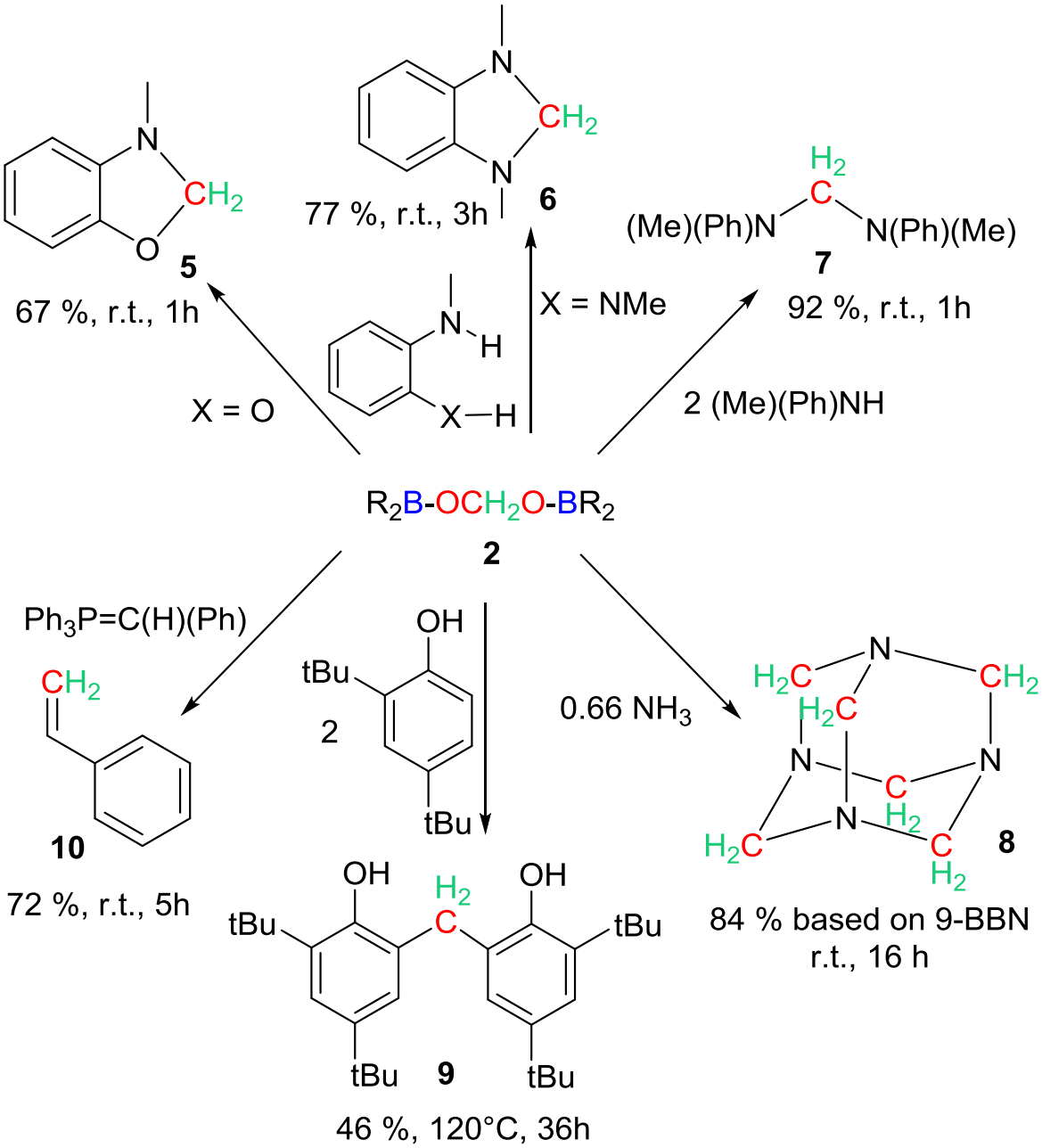

Schéma 3: Réactions de **2** généré in-situ conduisant aux composés **5**-**10**.

Nous avons utilisé le $^{13}CO_2$ et $^{12}CO_2$ pour confirmer par RMN et HRMS que l'atome de carbone du méthylène dans les composés **3**-**10** résultait de la réduction du CO_2. Les données RMN pour le bis(boryl)acétal **2** et pour les composés résultants **3**-**10** sont fournis dans le tableau 3. Les variations importantes de déplacements chimiques en RMN ^{13}C et ^{1}H (de $\delta(^{13}C)$ = 32,6 et $\delta(^{1}H)$ = 3,88 pour le composé **9** à $\delta(^{13}C)$ = 156,5 et $\delta(^{1}H)$ = 7,73 pour le

composé [4]), indiquant les différents types de méthylène obtenus, mettent en évidence la réactivité extrêmement polyvalente du composé **2**.

Tableau 3 : Caractérisation RMN des groupements méthylènes dans les composés **2**-**10** dans le THF-d^8

	$\delta^{13}C(CH_2)$	$\delta^{1}H(CH_2)$	$^{1}J_{H-C}$ (Hz)
2	87.0	5.54	165.2
3	91.0	4.54	160
4	156.5	7.73 7.30	150.9 132.0
5	91.8	5.31	160.1
6	81.3	4.24	148.0
7	71.0	4.77	146.3
8	76.0	4.61	149.0
9	32.6	3.88	126.1
10	113.8	5.75 5.18	154.4 159.7

Les expériences réalisées dans des tubes RMN a permis le suivi pratique. Dans une étape suivante, nous avons cherché à isoler des produits et les composés **8** et **9** ont été sélectionnés. Sur une synthèse à l'échelle fois10, le composé **2** a été généré de manière sélective à 60 ° C en 10 min, puis piégé pour donner les composés **8** et **9** à 98 et 37% des rendements isolés sur la base de l'agent de piégeage, respectivement. Une échelle de fois 100 a conduit à **8** en 2 jours à température ambiante avec un rendement isolé de 70% (106,2 mg) sur la base de 9-BBN.

En conclusion, nous avons rapporté ici l'utilisation d'un complexe dihydrure de fer dans la réduction de CO_2 soit en bis(boryl)acétal ou en méthoxyborane selon l'hydroborane utilisé comme agent réducteur. La réduction sélective du CO_2 au niveau acétal et la

fonctionnalisation ultérieure en un seul pot et en deux étapes, a permis de transformer le CO_2 en méthylène et d'élargir considérablement le type de fonctions accessibles en générant de nouvelles liaison C-N, mais aussi C-O et C-C. Nos résultats soulignent en outre l'importance des complexes d'hydrures de métal dans la transformation contrôlée de CO_2. Nous menons actuellement une enquête mécanistique pour comprendre et améliorer le système catalytique et poursuivre la recherche sur la réactivité spécifique des composés bis(boryl) et / ou bis(silyl)acétal.

Chimie de Coordination et Catalyse au Fer. Ligands Non-Innocents et Transformation du CO_2

L'utilisation du fer en chimie de coordination et en catalyse suscite un intérêt croissant de par son abondance et sa faible toxicité. Dans le premier chapitre, une étude bibliographique présente deux domaines d'applications du fer : i) l'utilisation de complexes de fer comportant des ligands « non innocent » pour différentes applications en catalyse, et ii) l'utilisation de complexes de fer pour des transformations stœchiométriques et catalytiques du CO_2.

Dans le chapitre 2, la synthèse et la caractérisation de complexes de fer portant un ligand coopératif non-innocent sont présentées. Le composé hautement réactif $[Fe(N(TMS)_2)_2]$ a été choisi comme précurseur pour l'étude de la coordination du ligand bis(picolyl)phosphine dans des conditions douces. Une famille de complexes mono- et di-nucléaires de fer a été isolée et le comportement « non-innocent » du ligand a été mis en évidence. La combinaison de plusieurs techniques : diffraction des rayons X, RMN (en solution et à l'état solide), RPE, Mössbauer et spectroscopie infrarouge a permis de complètement caractériser à la fois les complexes diamagnétiques mais aussi paramagnétiques.

Le chapitre 3 se concentre sur la transformation de CO_2 par un système catalytique efficace au fer. Les complexes dihydrure de fer $[Fe(H)_2(diphosphine)_2]$ catalysent la fonctionnalisation réductrice du CO_2 dans des conditions douces. Dans ce système, la première étape concerne la réduction catalytique du CO_2 par des hydroboranes donnant un composé bis(boryl)acetal. Via une stratégie « un pot, deux étapes » l'intermédiaire acétal est ensuite utilisé comme source de méthylène et est fonctionnalisé pour donner une série de composés organiques contenant non seulement des liaisons C-N mais aussi des liaisons C-O, C-S et C-C avec de bons à très bons rendements.

Coordination Chemistry and Catalysis at Iron: From Non-Innocent Ligands to CO_2 Transformation

There is an increasing interest in the use of iron in coordination chemistry and catalysis because it is an earth abundant metal which exhibits a low toxicity. The first chapter is a bibliographic study concerning two areas of applications for iron: the combination of iron with non-innocent ligands leading to highly active catalysts, and the use of iron complexes for CO_2 transformations at the stoichiometric and catalytic levels.

In chapter 2, the synthesis and characterization of iron complexes bearing a cooperative non-innocent ligand are presented. The highly reactive compound $[Fe(N(TMS)_2)_2]$ has been chosen as a precursor for the study of the coordination of the bis(picolyl)phosphine ligand under mild conditions. As a result, a family of mono- and di-meric iron complexes has been isolated and the non-innocent behavior of the ligand has been observed. The combination of several techniques: X-ray diffraction, NMR (in solution and in the solid state), EPR, Mössbauer and infrared spectroscopy allows to clearly characterize both diamagnetic and paramagnetic complexes.

Chapter 3 focuses on the transformation of CO_2 catalyzed by an efficient iron-based system. In this system, iron hydride complexes $[Fe(H)_2(diphosphine)_2]$ have been chosen to catalyze the reductive functionalization of CO_2 through a one-pot two steps strategy under mild conditions. The first step concerns the iron-catalyzed reduction of CO_2 by hydroboranes affording a bis(boryl)acetal compound. This intermediate is then used as a source of methylene in functionalization reactions, leading to a series of organic compounds containing not only C-N but also C-O, C-S, and C-C bonds in good yields.